2017

Performance Evaluation and Characterization of Encapsulated Calcium Nitrate for Self-Healing Concrete Applications

Jose Eduardo Milla
Louisiana State University and Agricultural and Mechanical College

PERFORMANCE EVALUATION AND CHARACTERIZATION OF ENCAPSULATED CALCIUM NITRATE FOR SELF-HEALING CONCRETE APPLICATIONS

A Dissertation

Submitted to the Graduate Faculty of the
Louisiana State University and
Agricultural and Mechanical College
in partial fulfillment of the
Requirements for the degree of
Doctorate of Philosophy

in

The Interdepartmental Program in Engineering Science

by
Jose E. Milla
B.S., University of New Orleans, May 2013
M.S., Louisiana State University, December 2015
May 2017

TABLE OF CONTENTS

ACKNOWLEDGEMENTS

First and foremost, the author would like to express his gratitude to his major professor, Dr. Marwa Hassan, for her invaluable guidance, support, and mentoring since the project's inception. Her wealth of experience and encouragement proved to be fundamental for the development of this project. The author would also like to recognize the assistance and recommendations provided by the supervisory committee members Dr. Ayman Okeil, Dr. Sherif Ishak, the Dean's representative Dr. William Grimes, as well as the invaluable expertise from Dr. William Daly, Dr. Tyson Rupnow, Dr. Clayton Loehn, and Dr. Ioan Negulescu. The author would also like to express his gratitude to the Department of Construction Management, the Socolofsky Microscopy Center, and the Louisiana Department of Transportation Research Center.

Special thanks are given to his colleagues and friends, including but not limited to Gabriel Arce, Max Aguirre, Luis Bonilla, and Sharareh Shirzad for their advice and support. Finally, special thanks are given to the author's friends and family who have constantly encouraged and supported him, particularly during the most challenging aspects throughout this journey.

ABSTRACT

Self-healing concrete through microencapsulated calcium nitrate is a novel approach to enhance durability and decrease the costs associated with maintenance and repairs. However, to fully assess the potential of this technology, there are many questions to be answered, ranging from identifying the microcapsule properties that are successfully carry the healing agent, to the effect of the microcapsule size, concentration (by weight of cement), and morphology have on the intrinsic concrete material properties and self-healing potential. Hence, the objectives of this study were to: (a) Develop a microencapsulation procedure for calcium nitrate as the healing agent; (b) Measure the short-term healing efficiency of the developed microcapsules in concrete; (c) Measure the long-term healing efficiency of such microcapsules in concrete.

To achieve objective A, the effect of the production parameters was quantified with respect to the microcapsule size and morphology. The results indicated that the agitation rate, emulsifier type, and emulsifier concentration affected the mean microcapsule diameter. The morphology of the microcapsule did not vary significantly between the tested production parameters. Objectives B and C measured the healing performance of concrete with embedded microcapsules. For the short-term healing period, the microcapsules proved to be significantly detrimental to the intrinsic concrete properties as the air content in the cement paste was substantially increased. Hence, factors contributing to the concrete strength deficiencies were addressed and corrected with modifications to the mix design and encapsulation procedures to evaluate the long-term healing period with respect to the mechanical properties and crack-sealing of concrete with embedded microcapsules.

CHAPTER 1
INTRODUCTION

Concrete is the most widely used construction material in the world. Given the high demand for concrete, the cement industry produces 2.8 billion tons a year, accounting up to 5% of the world's man-made carbon dioxide emissions (EPA 2010) (IEA 2009). However, a significant portion of public infrastructure built with concrete is deteriorating. In the United States, the associated repair and maintenance costs are estimated between 18 to 21 billion dollars (International Concrete Repair Institute 2006). Similarly, half of Europe's annual construction budget is estimated to be spent on rehabilitation and repair of the existing structures, thereby highlighting a global demand for an infrastructure upgrade (Schlangen and Sangadji 2013).

Concrete cracking is inevitable, and will affect the structure's durability if not controlled or reduced significantly. Cracking is a major problem particularly for steel reinforced concrete structures, as the cracks would expose the reinforcement to corrosion. To address this problem, continuous inspections and maintenance repairs would be needed, thus making this approach unfeasible to implement due to the large amounts of labor and funds required. In addition, crack repair can also be very difficult to achieve when the cracks are internal and/or inaccessible.

A proposed alternative is to engineer concrete materials for higher quality and durability to extend the service life of the given structure. Such an approach would tackle the problem from its roots, and promote sustainability since a lower demand for concrete production would result from this strategy. Therefore, a low-maintenance concrete material would be ideal, and can be achieved through self-healing technology.

Self-healing concrete is a state-of-the-art material that is capable of autonomously sealing cracks in fractured concrete. Several studies have indicated that self-healing of cracks in

cementitious materials can be achieved by: a) formation of calcium carbonate or calcium hydroxide; b) blocking cracks with the impurities in the water and loose concrete particles resulting from crack spalling; and c) further hydration of unreacted cement or cementitious materials, d) expansion of the hydrated cementitious matrix in the cracks, i.e., swelling of Calcium Silicate Hydrate (C–S–H) (Wu et al. 2012). Through these mechanisms, researchers have developed techniques to make self-healing concrete a reality.

Current self-healing technologies in concrete function through either bacterial mineral precipitation, microencapsulation of a chemical healing agent, or through Engineered Cementitious Composites (ECCs). Biologically-based healing is activated by bacterial spores in concrete with water to enable precipitation of calcium carbonate, which seals the cracks. Therefore, this technique is useful for infrastructure that is exposed to wet environments.

Engineering Cementitious Composites is another approach to self-healing, where the concrete material is fiber reinforced and exhibits high ductility properties, which allow more uniform distribution of micro-cracks. Such micro-crack control facilitates autogenous repair, and requires water to promote continued hydration and pozzolanic activities.

Microencapsulation techniques aim to enclose the healing agent with an inert shell material, in order to enable the interaction of the healing agent with concrete only when the stresses are sufficiently high to propagate cracks and to rupture the capsules. Therefore, a successful application of this technique requires that the microcapsule shell must be strong enough to be properly embedded in the concrete matrix, without compromising its ability to rupture when the cracks form. The main encapsulation methods are achieved by either mechanical means, coacervation, or polymerization. It has been reported that sodium silicate is a suitable chemical healing agent to repair cracks because it reacts with portlandite to form C-S-H

gel, and thus enhances the sealed surface's properties with decreased permeability, increased hardness, and overall increased durability (Pelletier et al. 2010) (La Rosa Thompson et al. 1997).

With the continual deterioration of infrastructure, and thus increasing costs in repairs, the construction industry will highly benefit by designing structures with self-healing concrete due to its low-maintenance and capacity to increase durability. Such extension of a structure's service life would bring important economic and environmental benefits, as it is an ideal long-term strategy for reducing maintenance costs and concrete's environmental footprint on carbon dioxide emissions respectively.

1.1 Problem Statement

Self-healing concrete through microencapsulated healing agents is a promising technology that can address concrete infrastructure durability. A suitable self-healing agent should: (a) be easily encapsulated; (b) remain stable and reactive over the service life of the concrete structure under various environmental conditions; and (c) respond quickly to repair damage (Wu et al. 2008). By this healing mechanism, it is possible to enable a concrete structure to repair both its internal and external micro-cracks without human intervention.

Besides sodium silicate, other microencapsulated healing agents have been studied such as polyurethane, cyanoacrylates, and epoxy (Dry 2001) (Van Tittelboom et al. 2011). Other healing agents may require a catalyst embedded in concrete as well, such as the methylmethacrylate monomer and triethylborane system (Yang et al. 2011). However, there is little information on how other common concrete admixtures such as calcium nitrate would perform as an encapsulated healing agent. Calcium nitrate is a suitable prospect as it is widely used as an accelerator for early strength development of concrete. In addition, it has been found

to be a corrosion inhibitor, and is often the preferred admixture to counteract concrete's slow strength development in cold environments (Justnes 2010).

The main limitation to this self-healing strategy is its functionality once the healing agent itself is consumed in the process. Further research can be aimed at establishing the longevity of these microcapsules with respect to the amount of self-healing action that takes place. Other limitations include the potential effects the microencapsulated particles may have on the intrinsic material properties of concrete. Therefore, a high concentration of microcapsules may negatively affect the compressive strength of concrete.

1.2 Objectives

To address the problem statement, the objectives of this study are to:

1. Develop a microencapsulation procedure for calcium nitrate as the healing agent.
    - Quantify the optimum production parameters that control microcapsule size and morphology;
2. Measure the short term self-healing efficiency of the developed microcapsules, and compare it to a control sample with no microcapsules added;
    - Quantify the best microcapsule size for self-healing action through modulus of elasticity (ASTM C469) and surface resistivity tests.
3. Measure the long term self-healing efficiency of the developed microcapsules
    - Quantify the best microcapsule size for self-healing action through modulus of elasticity (ASTM C469)
    - Identify the potential healing products forming near the cracked surfaces

- Determine if there are any correlations between the microcapsule size and crack width repair.

This study therefore aims to evaluate calcium nitrate's crack-repair potential based on its healing efficiency, and its effects on the strength of the healed specimen. The selected chemical process to encapsulate calcium nitrate is in-situ polymerization with a poly (urea-formaldehyde) shell due to its simplicity and low cost. There are many questions to be answered on what factors control the microcapsule size and morphology, the potential crack width limitations for self-healing, and whether the microcapsule size has any effect on the healing process and efficiency.

This study will develop a framework for quantifying the performance before and after self-healing action in concrete and will determine if calcium nitrate is a suitable healing agent to enhance durability.

1.3 Research Approach

Proposed research activities will be organized into three phases and eight tasks as detailed in the following section.

Objective 1: Microcapsule Synthesis and Characterization

Task 1: Development of the Microencapsulation Procedure

The procedure has been developed by combining the methods from two patents on microencapsulation. The first patent was developed by Dietrich et al. defining the procedure for an in situ encapsulation of water-immiscible liquids by urea-formaldehyde polymer at an acidic pH (Dietrich et al. 1989). The second patent was developed by Rodson et al. where it outlines a procedure for the encapsulation of water-soluble materials through a water-in-oil emulsion (Rodson and Scher 2000).

The proportions of the chemicals that will react to form urea-formaldehyde microcapsules was adapted from the first patent, and the second patent was used to form a water-in-oil emulsion with a sulfonic acid surfactant/catalyst since calcium nitrate is a water-soluble material. A total of 30 samples of microcapsules were produced at varying production parameters, which include: temperature, time of heating, agitation rate, and amount of sulfonic acid catalyst used. The amounts of calcium nitrate will be held constant at 10 grams during these experiments. The experimental matrix shown in Table 1.1 was applied for microcapsules produced at agitation rates of 450, 800, and 1500 rpm.

Table 1.1 Experimental matrix for microcapsule production

Temperature (°C)	Heating Time (h)	Sulfonic acid (g)
40	1	0.6
40	1.5	0.6
40	3	0.6
45	1	0.6
45	1.5	0.6
50	1	0.6
50	1	0.3
50	1	1.0
50	1.5	0.6
50	3	0.6

Task 2: Microcapsule Characterization

Characterization of microcapsules will be conducted using Energy Dispersive Spectroscopy (EDS) and Scanning Electron Microscopy (SEM) to analyze the effects of the production parameters on the size and morphology. Based on the results, the ideal microcapsule production parameters will be determined for use in concrete applications.

Task 3: Microcapsule Production

Based on the work of Task 2, for the cases in which the sulfonic acid was varied, the quantities of both 0.60g and 1.00g produced positive results. Experiments made with 0.30g sulfonic acid did not seem to form a stable suspension at low agitations. With respect to the heating time, all three levels yielded high quality results, and did not have a significant effect in the morphology nor the yield of the microcapsules.

Temperatures of either 40 °C or 45 °C were preferred, since higher temperatures are close to the boiling point of hexane, and this would interfere with the encapsulation process. No significant differences in morphology were observed between those experiments made at temperatures of 45 °C and 40 °C, although it was noted that the shell thickness was slightly larger for the 40 °C case. Based on these results, the selected parameters were: (a) Temperature: 40 °C; (b) Heating time: 1.5 hours; (c) Sulfonic acid quantity: 0.60g.

Table 1.2. Details of the production levels of the microcapsules used for concrete

Agitation Rate (rpm)	Temperature (°C)	Heating Time (h)	Sulfonic acid (g)
450	40	1.5	0.6
800	40	1.5	0.6
1500	40	1.5	0.6

Task 4: Concrete Cylinder Production

Five types of concrete cylinders were prepared: (a) Control specimens, (b) Cylinders with 0.25% microcapsule concentration (by weight of cement), (c) Cylinders with 0.50% of microcapsule concentration, (d) Cylinders with 1.00% of microcapsule concentration, and

(e) Cylinders with 2.0% of microcapsule concentration. Three sizes of microcapsules were added for each concentration level, given that the agitation rate controls the microcapsule diameter.

Mix Design

The mix design used has an expected compressive strength of 41 MPa and a water-cement ratio of 0.48; the selected mix was based on a typical mix used in Louisiana for road applications. Limestone was used as the coarse aggregate, where the maximum aggregate size was 19 mm. For the fine aggregates, the sand had a maximum particle size of 4.76 mm.

The mixing sequence involved three minutes of mixing coarse aggregates with two thirds of the water content, to ensure saturation. Next, the cement, fine aggregate, and one third of the water mixed with the microcapsules were added and mixed for three minutes. A resting period of three minutes followed and finally the contents were mixed again for three more minutes before pouring. Once the mixing process was complete, slump and air entrainment tests were performed, and the concrete cylinders were cast according to ASTM C31.

Objective 2: Laboratory testing of concrete cylinders for short-term healing

Task 5: Material testing of concrete cylinders

In order to measure the short-term self-healing action of the produced microcapsules, the following tests will be conducted: Modulus of elasticity (ASTM C469), compression strength (ASTM C39), 80% strain (a modification of the ASTM C469 to induce internal

cracks), and the surface resistivity test TR 233-11 in lieu of the apparent chlorine ion penetration (ASTM C1202). Each test will have three replicas to control variability, and control samples with no added microcapsules will be used to compare results with specimens containing microcapsules.

A set of 150 mm x 300 mm cylinders with and without microcapsules were used to monitor the potential self-healing effects with respect to material strength. Every specimen group is subject to the compressive strength tests to determine the 40% strain mark that will be used for the modulus of elasticity test. Once the modulus of elasticity test has been conducted, all specimens will be subject to the modified modulus of elasticity test to induce internal micro-cracks at the 80% strain level. The damaged samples will then be left to heal by water immersion. Retests for modulus of elasticity will be conducted after 14 days and after 55 days to evaluate the samples' strength recovery.

Task 6: Quantification of the self-healing concrete's surface resistivity

A set of 100 mm x 200 mm cylinders with and without microcapsules were also used to have an indication of the concrete's ability to resist chlorine ions. Readings will be taken before and after the samples are damaged at a load that corresponds to 80% of the ultimate load. Control specimens and cylinders containing microcapsules were tested at various concentrations (0.25%, 0.50%, 1.0%, 2.0% by wt. cement), and were left to cure under water immersion after being damaged. Retests were taken after 14 days, 28 days, and 42 days after damage to assess the potential healing effects.

Task 7: Evaluation of Self-Healing Processes

A comprehensive analysis on the material testing results was done for each specimen group. A comparison will be made with the test results of the control specimens to determine the self-healing effect. The samples that showed the highest modulus of elasticity recovery without compromising much of the compressive strength were selected as optimal.

A selection of microcapsule containing samples that were broken due to the compressive strength tests were prepared for observation under the SEM at Backscattered Electron (BSE) imaging mode to inspect the morphology of the polished concrete microstructure.

Objective 3: Laboratory testing of concrete cylinders for long-term healing

Task 8: Modification of microencapsulation procedure

The encapsulation procedure developed microcapsules that were found to have traces of sulfonic acid in the surface, thus acidifying the concrete mixing water. This could have been the reason for the strength deficiencies observed for the samples that had embedded microcapsules. Therefore, a proposed solution to this problem was to develop a new encapsulation procedure that required (a) a DI water bath to rinse off or neutralize the sulfonic acid in the microcapsule shell; and (b) minimize the amount of sulfonic acid catalyst used by adding a secondary lipophilic surfactant to maintain a stable emulsion or suspension.

Task 9: Production of Microcapsules

Based on the findings of Task 8, the microcapsules were produced at three different agitation rates to evaluate the effect of the microcapsule size on the self-healing efficiency. These agitation rates were: 450 rpm, 800 rpm, and 1500 rpm. In addition, the microcapsules were synthesized with a procedure near identical to that developed in Task 3, with the following modifications: (a) Temperature was set at 45 °C; (b) 1 hour of heating time to enable the polymerization reaction; (c) Decreased the sulfonic acid amount from 0.6g to 0.1g; (d) The introduction of 0.8g of Span 60 surfactant to maintain a stable emulsion; (e) The introduction of a DI water bath to rinse the microcapsules and neutralized the sulfonic acid present in the microcapsule surface.

Task 10: Concrete Cylinder Production

Prepare four types of concrete cylinders. a) Control specimens, b) Cylinders with 0.25% microcapsule concentration (by weight of cement), c) Cylinders with 0.50% of microcapsule concentration, d) Cylinders with 1.00% of microcapsule concentration. There will be three types of microcapsules added for each concentration level, given that the agitation rate controls the microcapsule size.

Based on the results from objective 2, another potential cause for the decrease in the compressive strength was the concrete mix design. The presence of a super plasticizer admixture in conjunction of the microcapsules added may have had an undesired reaction, where the air content was significantly increased. To address this issue, the proposed new mix design needed to have a plasticizer admixture that is compatible with the microcapsules, and a defoaming agent will be used to counter the increases in air

content that were caused by the introduction of microcapsules. In addition, a lower water-cement ratio was explored.

Mix Design

Through trial-and-error, the mix design used in this task was selected with a lower water-cement ratio of 0.40. Limestone was used as the coarse aggregate, where the maximum aggregate size will be 19 mm. For the fine aggregates, the sand had a maximum particle size of 4.76 mm. A high range water reducer and a defoaming agent were used as admixtures, in addition to the microcapsules. Two control groups were used for this task: the first control group does not include a defoaming agent in its mix design, while the second control group does include the same defoaming agent dosage that the microcapsule concrete specimens had. The mixing sequence used was the same as that outlined in Task 4.

Task 11: Material testing of concrete cylinders

The concrete cylinders were measured for their long-term self-healing action by measuring the modulus of elasticity over time, before and after healing per ASTM C469. Therefore, the samples that were used for this purpose are three 100 mm x 200 mm cylinders from all specimen groups. The curing regime was set as wet-dry cycles of tap water immersion followed by three days of oven drying at 60 °C.

With respect to the compressive strengths, three replicas of 150 mm x 300 mm cylinders, and three replicas of 100 mm x 200 mm cylinders were used and tested per ASTM C39. The results of this test determined the ultimate strength for each specimen group. After the curing period ended, the healed samples were subjected to compressive

strength tests to evaluate whether they surpassed their original compressive strength after damage.

Sequence of Testing

After the ultimate strength of each specimen group was determined from the compressive strength tests, the modulus of elasticity (ASTM C469) tests were carried out for all 4”x8” virgin samples (before damage). To induce damage on the concrete samples, a series of four load cycles were made at the 80%, 90%, and 95% of the sample’s ultimate strength. Next, the modulus of elasticity was measured after damage. The samples were then submerged in water to enable healing for a period of 21 days. At the 21st day, the samples were placed in an oven to dry at 60 degrees Celsius for a period of three days. Once the samples were dry, a new modulus of elasticity reading was taken to measure the potential self-healing effects. The sample was then left to cure under water submersion and was retested for modulus of elasticity. The retests were therefore set at days 21, 42, and 84 (after damage). At the end of the testing period, the samples were subjected to compressive strength tests to evaluate the effect of the microcapsules after healing.

Task 12: Characterization of Self-Healing Processes

A comprehensive characterization analysis was done for a selection of specimen groups. This task essentially followed the steps outlined in Task 7. After the healing period, a selection of samples that were broken from the compressive strength tests were prepared for observation under the SEM at backscattered electron mode. The samples were epoxy impregnated and polished to inspect the morphology of the concrete microstructure. This

was useful for comparing the microstructure of the current samples with those samples inspected in Task 7.

Task 13: Production of Concrete Beams

A new study was necessary to evaluate how effective encapsulated calcium nitrate is to autonomously heal cracks. For this reason, concrete beams of 100 mm x 100 mm x 350 mm were poured. Two different types of microcapsules were used in this study: (a) the microcapsules that were first synthesized in Task 3 (referred as the OG microcapsules); and (b) the microcapsules that were synthesized in Task 9 (referred as the SP microcapsules.

The production parameters used for all microcapsules were: (a) two levels of agitation rates, 800 rpm and 1500 rpm, respectively; (b) Temperature of 45 C; (c) Heating time of 1 hour; and (d) a DI water bath to rinse microcapsules before admixing in concrete. The difference between the OG microcapsules and the SP microcapsules was the amount of sulfonic acid catalyst added during synthesis. Hence, the OG capsules had 0.6g of sulfonic acid, while the SP capsules had 0.1g of sulfonic acid and 0.8g of Span 60 surfactant.

<u>Mix Design</u>

The concrete mix design was the same as the one outlined in Task 10, with one notable addition: the introduction of 25 mm steel fibers to add ductility to the concrete beams. The microcapsule concentrations investigated were 0.50%, and 0.75% by weight of cement. The size of microcapsules used in concrete were controlled by two levels of

agitation rates during synthesis: 800 rpm, and 1500 rpm. In addition, two control groups were used for this task: the first control group did not include a defoaming agent in its mix design, while the second control group did include the same defoaming agent dosage that the microcapsule concrete specimens had. The mixing sequence followed the steps outlined in Task 4.

Task 14: Inducing cracks

Given that concrete is a brittle material, it was essential to ensure that the concrete beams were damaged to a point where cracks were induced without breaking the beams. For this reason, 25 mm steel fibers were used to add ductility. A third-point loading test set-up was used to induce cracks through a strain-controlled test, performed at a low rate to ensure the test is stopped once cracking begins to prevent sudden failure.

Task 15: Monitoring Self-Healing Processes

Once the concrete beams were cracked, the samples were then viewed under an optical microscope to observe and take images of the cracks. The cracks were then monitored periodically at days 7, 21, and 42 (after damage). The crack widths were then measured over time to evaluate the microcapsules' efficiency for crack sealing. The curing regime was composed of wet-dry cycles where specimens were immersed under tap water, followed by three days of oven drying at 60 °C.

Task 16: Characterization of Healing Products

At the end of the healing period, a comparison was made with the microcapsule-containing specimens and the control specimens to determine the impact of the microcapsules on healing, where SEM and EDS was used to identify any potential release of the healing agent, and analyzed the morphology and composition of the concrete matrix. An atomic ratio plot of the Silicon/Calcium and Aluminum/Calcium ratios was used to identify whether the healing products are composed of calcium-rich crystals or of particles comparable to Calcium-Silicate-Hydrate gels.

1.4 References

Abdel-Jawad, Y., and Haddad, R. (1992). "Effect of early overloading of concrete on strength at later ages." *Cement and Concrete Research*, 22(5), 927–936.

Abdelrazig, B. E. ., Bonner, D. ., Nowell, D. ., Dransfield, J. ., and Egan, P. . (1999). "The solution chemistry and early hydration of ordinary portland cement pastes with and without admixtures." *Thermochimica Acta*, 340-341, 417–430.

Aggoun, S., Cheikh-Zouaoui, M., Chikh, N., and Duval, R. (2008). "Effect of some admixtures on the setting time and strength evolution of cement pastes at early ages." *Construction and Building Materials*, 22(2), 106–110.

Al-Amoudi, O. S. B., Maslehuddin, M., Lashari, A. N., and Almusallam, A. A. (2003). "Effectiveness of corrosion inhibitors in contaminated concrete." *Cement and Concrete Composites*, 25(4-5 SPEC), 439–449.

Aldea, C., Song, W., Popovics, J., and Shah, S. (2000). "Extent of Healing of Cracked Normal Strength Concrete." *Journal of Materials in Civil Engineering*, American Society of Civil Engineers, 12(1), 92–96.

Alshamsi, A. M., and Imran, H. D. A. (2002). "Development of a permeability apparatus for concrete and mortar." *Cement and Concrete Research*, 32(6), 923–929.

Bang, S. S., Galinat, J. K., and Ramakrishnan, V. (2001). "Calcite precipitation induced by polyurethane-immobilized Bacillus pasteurii." *Enzyme and Microbial Technology*, 28(4-5), 404–409.

Becker, J., Jacobs, L., and Qu, J. (2003). "Characterization of Cement-Based Materials Using Diffuse Ultrasound." *Journal of Engineering Mechanics*, American Society of Civil Engineers, 129(12), 1478–1484.

Brown, E. N. (2004). "Microcapsule induced toughening in a self-healing polymer composite." 9, 1703–1710.

Cabrera, J. G., and Lynsdale, C. J. (1988). "A new gas permeameter for measuring the permeability of mortar and concrete." *Magazine of Concrete Research*, 40(144), 177–182.

Cernica, J. N. (1982). *Geotechnical Engineering*. Holt, Reinhart and Winston, New York.

Dietrich, K., Bonatz, E., Geistlinger, H., Herma, H., Nastke, R., Purz, H. -J., Schlawne, M., and Teige, W. (1989). "Amino resin microcapsules. II. Preparation and morphology." *Acta Polymerica*, Akademie Verlag GmbH, 40(5), 325–331.

Dry, C. M. (1994). "Smart multiphase composite materials that repair themselves by a release of liquids that become solids." 62–70.

Dry, C. M. (2001). “Design of self-growing, self-sensing, and self-repairing materials for engineering applications.” *Proc. SPIE*.

EPA. (2010). *Available and Emerging Technologies for Reducing Greenhouse Gas Emissions from the Portland Cement Industry*.

Fan, C., and Zhou, X. (2011). “Effect of emulsifier on poly(urea-formaldehyde) microencapsulation of tetrachloroethylene.” *Polymer Bulletin*, 67(1), 15–27.

Ghosh, S. K. (2006). “Functional Coatings and Microencapsulation: A General Perspective.” *Functional Coatings*, Wiley-VCH Verlag GmbH & Co. KGaA, 1–28.

Hammes, F., and Verstraete, W. (2002). “Key roles of pH and calcium metabolism in microbial carbonate precipitation.” *Reviews in Environmental Science and Biotechnology*, 1(1), 3–7.

Hearn, N. (1998). “Self-sealing, autogenous healing and continued hydration: What is the difference?” *Materials and Structures*, 31(8), 563–567.

Hilloulin, B., Tittelboom, K. Van, Gruyaert, E., Belie, N. De, and Loukili, A. (2015). “Cement & Concrete Composites Design of polymeric capsules for self-healing concrete.” *Cement and Concrete Composites*, Elsevier Ltd, 55, 298–307.

Hoseini, M., Bindiganavile, V., and Banthia, N. (2009). “The effect of mechanical stress on permeability of concrete: A review.” *Cement and Concrete Composites*, 31(4), 213–220.

IEA. (2009). *Cement Technology Roadmap 2009: Carbon emissions reductions up to 2050*.

In, C. W., Kim, J.-Y., Jacobs, L. L., and Kurtis, K. (2012). “Crack depth measurement in concrete using diffuse ultrasound.” *AIP Conference Proceedings*, 1430(1).

The Strategic Development Council (SDC) (2006). “Vision 2020: A vision for the concrete repair protection and strengthening industry” (http://www.concretesdc.org/_pdfs/vision2020-version1.0_%20may2006.pdf) (November 10, 2015).

Jacobsen, S., Marchland, J., and Boisvert, L. (1996). “Effect of cracking and healing on chloride transport in OPC concrete.” United States.

Jonkers, H. M., Thijssen, A., Muyzer, G., Copuroglu, O., and Schlangen, E. (2010). “Application of bacteria as self-healing agent for the development of sustainable concrete.” *Ecological Engineering*, 36(2), 230–235.

Justnes, H. (2010). “Calcium nitrate as a multi-functional concrete admixture.” *Concrete (London)*, 44(1), 34–36.

Justnes, H., and Nygaard, E. C. (1993). “Technical Nitrate as Set Accelerator for Cement.” *Nordic Concrete Research*, 13(2), 70–87.

Justnes, H., and Nygaard, E. C. (1995). “Technical calcium nitrate as set accelerator for cement at low temperatures.” *Cement and Concrete Research*, 25(8), 1766–1774.

Kan, L. L., and Shi, H. S. (2012). “Investigation of self-healing behavior of Engineered Cementitious Composites (ECC) materials.” *Construction and Building Materials*, Elsevier Ltd, 29, 348–356.

Li, V. C. (2003). “On engineered cementitious composites (ECC). A review of the material and its applications.” *Journal of Advanced Concrete Technology*, 1(3), 215–230.

Li, V. C., and Herbert, E. (2012). “Robust Self-Healing Concrete for Sustainable Infrastructure.” *Journal of Advanced Concrete Technology*, 10(6), 207–218.

De Muynck, W., Cox, K., Belie, N. De, and Verstraete, W. (2008a). “Bacterial carbonate precipitation as an alternative surface treatment for concrete.” *Construction and Building Materials*, 22(5), 875–885.

De Muynck, W., Debrouwer, D., De Belie, N., and Verstraete, W. (2008b). “Bacterial carbonate precipitation improves the durability of cementitious materials.” *Cement and Concrete Research*, 38(7), 1005–1014.

Pelletier, M. M., Brown, R., Shukla, A., and Bose, A. (2010). “Self-healing concrete with a microencapsulated healing agent.” *University of Rhode Island, Kingston,USA*, (C).

Picandet, V., Khelidj, A., and Bellegou, H. (2009). “Crack effects on gas and water permeability of concretes.” *Cement and Concrete Research*, 39(6), 537–547.

Punurai, W., Jarzynski, J., Qu, J., Kurtis, K. E., and Jacobs, L. J. (2007). “Characterization of dissipation losses in cement paste with diffuse ultrasound.” *Mechanics Research Communications*, 34(3), 289–294.

Ramakrishnan, V. (2007). “Performance characteristic of bacterial concrete - a smart biomaterial.” *First International Conference on Recent Advances in Concrete Technology*, 67–78.

Ramamoorthy, S. K., Kane, Y., and Turner, J. A. (2004). “Ultrasound Diffusion for Crack Depth Determination in Concrete.” *Acoustical Imaging*, W. Arnold and S. Hirsekorn, eds., Springer Netherlands, Dordrecht, 121–128.

Rodson, M., and Scher, H. B. (2000). “Water-in-oil microencapsulation process and microcapsules produced thereby.” Google Patents.

Roig-Flores, M., Moscato, S., Serna, P., and Ferrara, L. (2015). “Self-healing capability of concrete with crystalline admixtures in different environments.” *Construction and Building Materials*, Elsevier Ltd, 86, 1–11.

La Rosa Thompson, J. ., Silsbee, M. R., Gill, P. M., and Scheetz, B. E. (1997). “Characterization of silicate sealers on concrete.” *Cement and Concrete Research*, 27(10), 1561–1567.

Rule, J. D., Sottos, N. R., and White, S. R. (2007). “Effect of microcapsule size on the performance of self-healing polymers.” *Polymer*, 48(12), 3520–3529.

Rupnow, T., and Icenogle, P. (2012). “Surface Resistivity Measurements Evaluated as Alternative to Rapid Chloride Permeability Test for Quality Assurance and Acceptance.” *Transportation Research Record: Journal of the Transportation Research Board*, Transportation Research Board, 2290, 30–37.

Saihi, D., Vroman, I., Giraud, S., and Bourbigot, S. (2006). “Microencapsulation of ammonium phosphate with a polyurethane shell. Part II. Interfacial polymerization technique.” *Reactive and Functional Polymers*, 66(10), 1118–1125.

Schlangen, E., and Sangadji, S. (2013). “Addressing infrastructure durability and sustainability by self healing mechanisms - Recent advances in self healing concrete and asphalt.” *Procedia Engineering*, Elsevier B.V., 54, 39–57.

Schlegel, H., Zaborosch, C., and Kogut, M. (1993). *General Microbiology*. Cambridge University Press.

Schurr, D. P., Kim, J. Y., Sabra, K. G., and Jacobs, L. J. (2011). “Damage detection in concrete using coda wave interferometry.” *NDT and E International*, Elsevier, 44(8), 728–735.

Seher, M., In, C.-W., Kim, J.-Y., Kurtis, K. E., and Jacobs, L. J. (2013). “Numerical and Experimental Study of Crack Depth Measurement in Concrete Using Diffuse Ultrasound.” *Journal of Nondestructive Evaluation*, 32(1), 81–92.

Sun, G., and Zhang, Z. (2002). “Mechanical strength of microcapsules made of different wall materials.” *International Journal of Pharmaceutics*, 242(1-2), 307–311.

Van Tittelboom, K., and De Belie, N. (2013). *Self-healing in cementitious materials-a review*. *Materials*.

Van Tittelboom, K., De Belie, N., Van Loo, D., and Jacobs, P. (2011). “Self-healing efficiency of cementitious materials containing tubular capsules filled with healing agent.” *Cement and Concrete Composites*, Elsevier Ltd, 33(4), 497–505.

Van Tittelboom, K., Gruyaert, E., Rahier, H., and De Belie, N. (2012). “Influence of mix composition on the extent of autogenous crack healing by continued hydration or calcium carbonate formation.” *Construction and Building Materials*, Elsevier Ltd, 37, 349–359.

Wang, J., Van Tittelboom, K., De Belie, N., and Verstraete, W. (2012). “Use of silica gel or polyurethane immobilized bacteria for self-healing concrete.” *Construction and Building Materials*, Elsevier Ltd, 26(1), 532–540.

Wang, J. Y., Soens, H., Verstraete, W., and De Belie, N. (2014). “Self-healing concrete by use of microencapsulated bacterial spores.” *Cement and Concrete Research*, Elsevier Ltd, 56, 139–152.

Wang, K., Jansen, D. C., Shah, S. P., and F.KArr, A. (1997). “Permeability study of cracked concrete.” *Cement and Concrete Research*, 27(3), 381–393.

White, S. R., Sottos, N. R., Geubelle, P. H., Moore, J. S., Kessler, M. R., Sriram, S. R., Brown, E. N., and Viswanathan, S. (2001). “Autonomic healing of polymer composites.” *Nature*, Macmillian Magazines Ltd., 409(6822), 794–797.

Wu, D. Y., Meure, S., and Solomon, D. (2008). “Self-healing polymeric materials: A review of recent developments.” *Progress in Polymer Science*, 33(5), 479–522.

Wu, M., Johannesson, B., and Geiker, M. (2012). “A review : Self-healing in cementitious materials and engineered cementitious composite as a self-healing material.” *Construction and Building Materials*, Elsevier Ltd, 28(1), 571–583.

Yang, Y., Lepech, M. D., Yang, E. H., and Li, V. C. (2009). “Autogenous healing of engineered cementitious composites under wet-dry cycles.” *Cement and Concrete Research*, Elsevier Ltd, 39(5), 382–390.

Yang, Z., Hollar, J., He, X., and Shi, X. (2011). “A self-healing cementitious composite using oil core/silica gel shell microcapsules.” *Cement and Concrete Composites*, Elsevier Ltd, 33(4), 506–512.

Zhong, W., and Yao, W. (2008). “Influence of damage degree on self-healing of concrete.” *Construction and Building Materials*, 22(6), 1137–1142.

CHAPTER 2

LITERATURE REVIEW

2.1 Introduction

The current state of public infrastructure such as bridges, roads, and buildings is deteriorating. Concrete cracks will occur inevitably, and so it is extremely importance to control and minimize the crack propagation. Reinforced concrete structures are the most vulnerable to cracks as they can expose the steel reinforcement to water and therefore corrosion. For this reason, research on self-healing materials has gained significant attention over the past years as a promising solution to extend the service life and safety of infrastructure. Studies focused on self-healing polymers, concrete, and asphalt have reported promising results on their crack-repair potential. The ideal self-healing material should be capable of responding directly to the damaged area throughout its intended lifetime (Wu et al. 2008).

Several studies have indicated that self-healing of cracks in cementitious materials can be caused by: a) formation of calcium carbonate or calcium hydroxide by the autogenous healing mechanism, b) blocking cracks by impurities in the water and loose concrete particles resulting from crack spalling, c) further hydration of unreacted cement or cementitious materials, d) Expansion of the hydrated cementitious matrix in the cracks, i.e. swelling of Calcium Silicate Hydrate (C–S–H) (Wu et al. 2012).

Researchers have investigated ways to maximize the autogenous healing mechanism of concrete by adding chemical admixtures or adding fiber reinforcement into the mix design to limit the crack width. Other studies focus on embedding a healing agent (and catalyst, if required) in the concrete matrix, usually by microcapsules, to enable a localized response to

fractures if capsules are uniformly dispersed inside the matrix. In essence, such a healing mechanism is triggered by mechanical stresses that induce cracks, and subsequently rupture microcapsules for the release of the healing agent. Depending on the sealing strategy selected, the healing agent would then react with the cementitious matrix, or initiate a polymerization reaction to seal the newly formed cracks (Van Tittelboom and De Belie 2013).

If microcapsules are to be embedded in cementitious materials, it is imperative that the microcapsule shell is strong enough to withstand the concrete mixing process. It has been reported that urea-formaldehyde or melamine-formaldehyde resins are suitable shell materials for self-healing applications (Wang et al. 2014) (White et al. 2001). In addition, the selection of the healing agent will determine the crack sealing efficiency. Calcium nitrate has been a commonly used admixture by the concrete industry due to its capabilities as a set accelerator and its long-term strength contribution (of concrete aged 28 days or older). Hence, the functions of calcium nitrate as an admixture, and its effect on the cement hydration chemistry will serve as an indication of its healing potential.

2.2 Self-healing Concrete

For the self-healing of cementitious materials to occur, it is important to provide the necessary conditions and reactants to the damaged area. For this reason, several experimental studies been conducted on this subject to develop state-of-the-art techniques that result in autonomic crack-repair.

2.2.1 Self-Healing, Autogenous Healing, and Continued Hydration of Concrete

The perceived effect of self-healing in concrete is often measured with permeability tests, and it can be caused by a number of factors. Hence, if there is any reported decrease in permeability flow, such variation in flow can be attributed to either continuing hydration, autogenous healing,

and/or the self-sealing effect. The term Self-Sealing Effect (SSE) has been commonly used to refer to both autogenous healing and continuous hydration. While there is a significant interdependence between these three distinct phenomena, it is important to differentiate these terms because these three reactions occur under different conditions.

The potential self-sealing mechanisms are summarized below (Hearn 1998).

1. Air in the Hardened Cement Paste (HCP) matrix
    a. Incomplete saturation of the test specimen
    b. dissolution of air under pressure, into permeating water
2. Swelling of HCP caused by the expansion of Calcium-Silicate-Hydrate (CSH) gel layers.
3. Chemical interaction of water and HCP:
    a. continued hydration of residual clinker
    b. dissolution and deposition of soluble hydrates along the flow path
    c. carbonation of dissolved calcium hydroxide
4. Osmotic pressure, caused by a dissolution of alkalis by the permeating water
5. Physical clogging caused by downstream movement of a loose particles in the HCP matrix in a process analogous to sediment transport

The Self-Sealing Effect

The self-sealing effect makes a permanent modification to the microstructure of the concrete specimen, because it results from an interaction between the hardened cement matrix and the permeating fluid. It has been reported that cycles of drying and re-saturation contribute to an increase in SSE. This is because after a drying phase, shrinkage cracks expose segments of unhydrated cement paste that were previously not accessible by the permeating water. Hence, when the concrete specimen is re-saturated, water reacts with the unhydrated cement particles,

causing a dissolution and re-deposition of hydration products, which result in a lower permeability (Hearn 1998).

A non-permanent SSE includes air in the HCP matrix and swelling of the hydration layers and osmotic pressure. Therefore, an incomplete saturation of the concrete specimen might cause one to misinterpret the lower permeability test results and attribute them to SSE.

Autogenous Healing

Autogenous healing is a term that describes the ability of cement to re-seal cracks in fractured concrete. This can be due to a reaction between calcium hydrogen carbonate from water and calcium hydroxide from concrete. It could also occur due to the carbonation of calcium hydroxide when exposed to the Earth's atmosphere. Hence, the sealing material has been found to be calcium carbonate crystals with calcium hydroxide deposits. The rate of healing is dependent on the initial crack width, where a smaller crack is able to heal faster than larger cracks (Hearn 1998).

The major differences between autogenous healing and SSE are that major cracks are not required to observe SSE, and that SSE occurs in a system that is not exposed to carbon dioxide. Hence, carbonation of dissolved calcium hydroxide cannot happen under the self-sealing effect.

Continuous Hydration

The reaction of a continuing cement hydration will decrease the permeability of the concrete specimen. There are significant differences between the permeability of a young cement paste, and the permeability of an advanced cement hydration. This is because the hydration reaction will continue as long as the water content is still sufficient to react with unhydrated cement paste, and if there is space for the deposition of the subsequent hydration products. It is important to

note that, unlike SSE and autogenous healing, continued hydration does not require a flow of permeating water. In other words, hydration can still take place under stagnant conditions (Hearn 1998).

The following figure illustrates the effect of the cement hydration on permeability. The decrease in permeability can be observed to be in several orders of magnitude, depending on the water-cement ratio and the curing time which corresponds to the level of cement hydration. Once the concrete specimen matures, the effect of continued hydration becomes minimal when subjected to permeability tests.

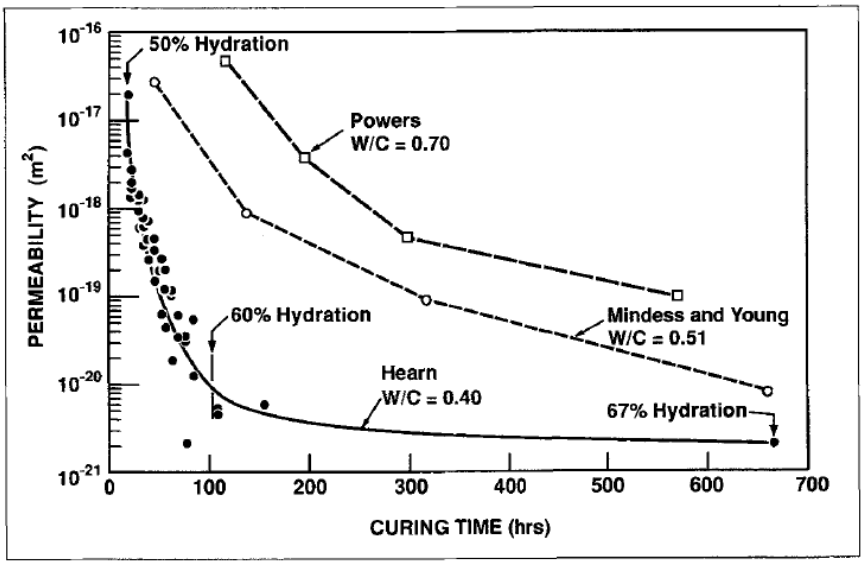

Figure 2.1. Permeability vs extent of hydration (Hearn 1998)

2.2.2 Self-Healing Concrete with Crystalline Admixtures

Roig-Flores et al. studied the effects of crystalline admixtures on the autogenous healing mechanism of concrete. Due to the limitations of the autogenous healing of normal concrete, research efforts have been focused on maximizing the crack-repair potential of concrete. Crystalline admixtures (CA), which are classified as permeability reducer admixtures, are

hydrophilic chemicals that form water insoluble precipitates, thereby increasing the density of calcium-silicate-hydrate (CSH) in cement. In the presence of water, these crystalline admixtures react with tricalcium silicate and form new hydration products that are capable of sealing concrete crack (Roig-Flores et al. 2015).

A study was conducted to determine the influence of the environment on the crystalline admixture's healing efficiency, through water permeability tests and microscopic observations of the crack evolutions. The results indicated that the presence of water had a direct impact on the self-healing effect of both control and crystalline-admixed samples. Indeed, the samples that were fully immersed in water, or had water contact exhibited a high level of surface crack-repair. In contrast, those samples that were not in contact with water (i.e. exposed to the humidity chamber or the laboratory room conditions) did not exhibit any degree of healing on surface cracks. The following figure illustrates the evolution of the surface cracks before and after healing for each specimen type. The control samples achieved a relatively high degree of autogenous healing when water was present, ranging from 60-75%, while those samples containing crystalline admixtures completely sealed the cracks. Hence, it is evident that the crystalline admixtures significantly improve the autogenous healing of concrete (Roig-Flores, 2015).

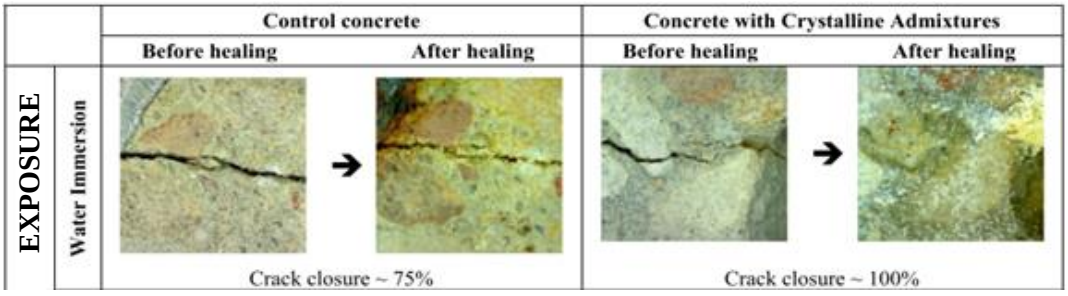

Figure 2.2. Crack evolution with respect to the environmental exposure (Roig-Flores, 2015) *(Continued)*

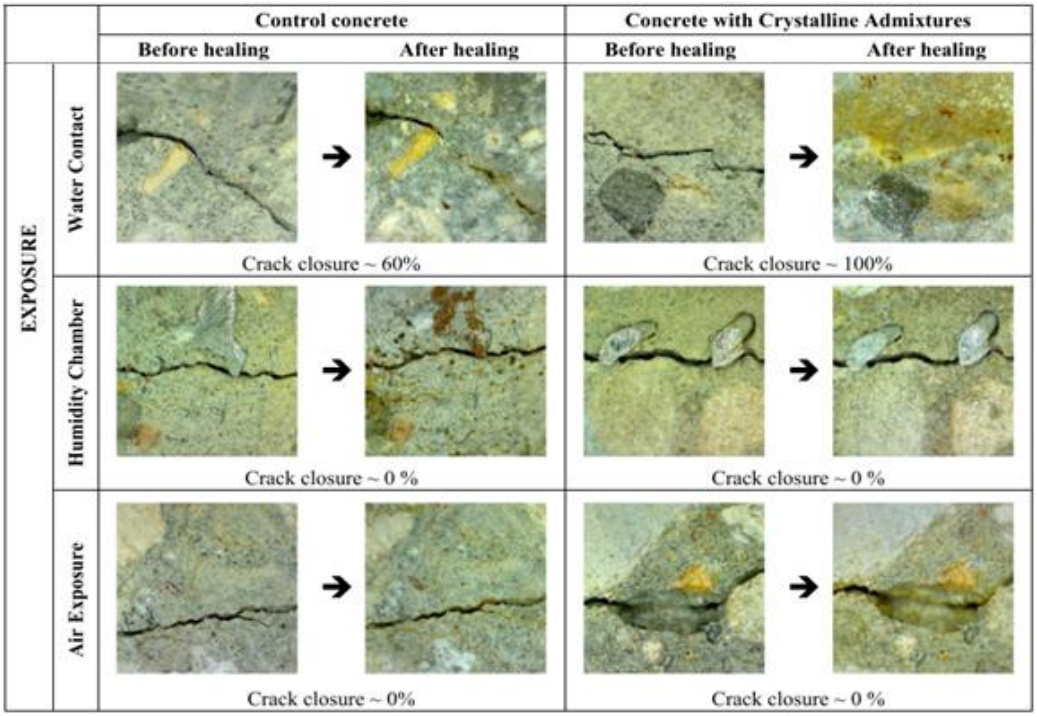

Figure 2.2. *(Continued)* Crack evolution with respect to the environmental exposure (Roig-Flores, 2015)

The self-healing efficiency with respect to the water permeability was calculated as the difference between one and the ratio of the final flow (recorded after 42 days) over the initial flow. Therefore, if the final flow were negligible, the healing efficiency would be 1, and if the final flow was virtually the same as the initial flow, the self-healing efficiency would be 0. With such defined parameter, it was easier to compare the influence of the environmental conditions on each sample group.

By order of decreasing average permeability healing rate, it was reported that full water immersion was optimal, followed by water contact, 95% relative humidity, and air exposure, respectively. The least ideal environmental exposure for healing was found in the laboratory conditions due to the low relative humidity. It was observed that the final flow was higher than

the initial flow, thus indicating that after 42 days the cracks grew wider. This is likely due to the shrinkage cracks of the control specimens due to a loss of moisture that was not properly compensated under a low humidity atmosphere. Nevertheless, the crystalline admixture was able to compensate for the loss of humidity and therefore exhibited a much favorable healing rate under the same laboratory environment (Roig-Flores et al. 2015).

2.2.3 Engineering Cementitious Composites.

Engineered Cementitious Composite (ECC) is a new type of cement-based material that features high ductility and that substantially limits the crack width propagation (Li 2003; Yang et al. 2009) (Li and Herbert 2012). These mechanical properties make ECCs a highly desirable construction material as its ultimate strain capacity of 3 to 5% is 300 times greater than that of traditional concrete. This is achieved by adding fiber reinforcement in the mix design that adds tensile strength and provides a more uniform distribution of micro-cracks. As a result, the autogenous repair mechanism of concrete is facilitated as there is a greater possibility to seal the cracks completely when they are small enough.

Autogenous Healing under Wet-Dry Cycles

In general, the self-healing capacity of concrete materials is mainly limited to the crack width. Macro-cracks greater than 1 mm are usually difficult, if not impossible to heal. However, Engineered Cementitious Composites (ECCs) are capable of limiting crack widths even at a high tensile strain. For this reason, ECCs have great potential to completely seal such cracks in the presence of moisture by the autogenous healing of concrete. The study analyzed the self-healing potential of ECCs that were loaded to five different tensile strain values to induce various damage levels. These were recorded in the table below. After cracking the ECCs, the samples were left to heal under two curing conditions.

Table 2.1. Microcracks obtained with respect to the tensile strain load (Yang et al. 2009)

Tensile strain (%)	Number of cracks	Maximum crack widths (μm)
3	39	90
2	27	60
1	15	60
0.5	7	70
0.3	5	50

The ECCs were subject to a non-destructive test method known as resonant frequency (RF) to indicate to what extent the specimens were damaged and potentially recovered. The study found that in general, the ECCs required 4 to 5 wet-dry cycles to achieve a self-healing effect. Indeed, the specimen's degree of damage and therefore, the size of the crack width determined the self-healing efficiency. For crack widths smaller than 50 microns, a full recovery was attainable after 10 wet-dry cycles according to the resonant frequency measurements. However, if the crack width was larger than 150 microns there was no observed recovery as the RF measurements remained the same after the damaged sample was subjected to the wet-dry cycles.

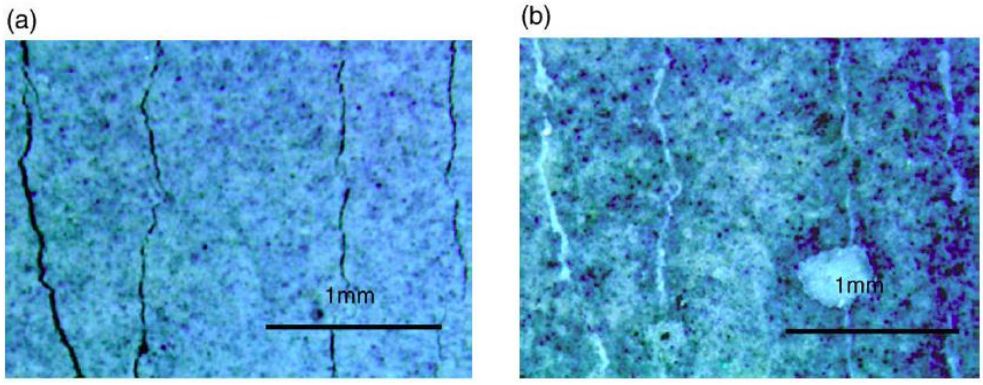

Figure 2.3. Microcracks in ECC were observed under a microscope before and after self-healing (Yang et al. 2009)

With respect to the healing efficiency, the results were highly dependent on the curing regime (Yang et al. 2009). Resonant frequency tests indicated that a higher recovery ratio (87%-100%) was attainable under the wet-dry cycles at a constant temperature of 20 °C, rather than in wet-dry cycles that include high temperatures of 55 °C (77%-90%). The healed samples were then loaded to their respective tensile strain tests, and the results indicated a significant stiffness recovery in both types of curing regimes. Hence, the ECC specimens were able to maintain their high ductility properties after healing. However, no significant recovery was found for those samples that were not exposed to a curing regime.

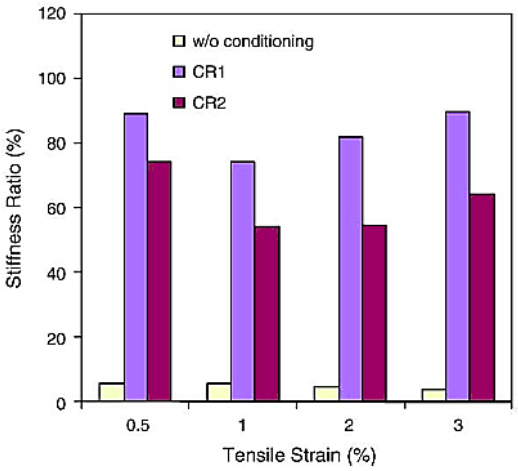

Figure 2.4. Influence of the curing regime on stiffness recovery (Yang et al. 2009)

The healed cracks were observed under energy dispersive spectroscopy (EDS) to analyze the chemical components of the sealing material. The results determined that calcium carbonate crystals were formed as a product of autogenous healing. Indeed, when water is present in the cracked surfaces, any unhydrated cement particles will continue the hydration reaction. Nevertheless, calcium hydroxide crystals that are exposed by the crack surfaces will also leach out due to their high solubility in water. Therefore, if carbon dioxide is available in the crack site

as well, a carbonation reaction will take place with the dissolved calcium hydroxide particles, which explains why calcium carbonate was found as the main healing product (Yang et al. 2009).

Table 2.2. EDS analysis of self-healing products (Kan and Shi 2012).

Element	Product A (%) – "Fiber-like"	Product B (%) – "Stone-like"
Carbon	0	9.6 ± 0.9
Oxygen	72.9 ± 0.8	62.5 ± 0.3
Magnesium	10.3 ± 0.4	5.1 ± 0.4
Aluminum	2.8 ± 0.1	2.1 ± 0.1
Silicon	4.4 ± 0.3	2.7 ± 0.1
Calcium	9.1 ± 0.6	17.3 ± 0.8

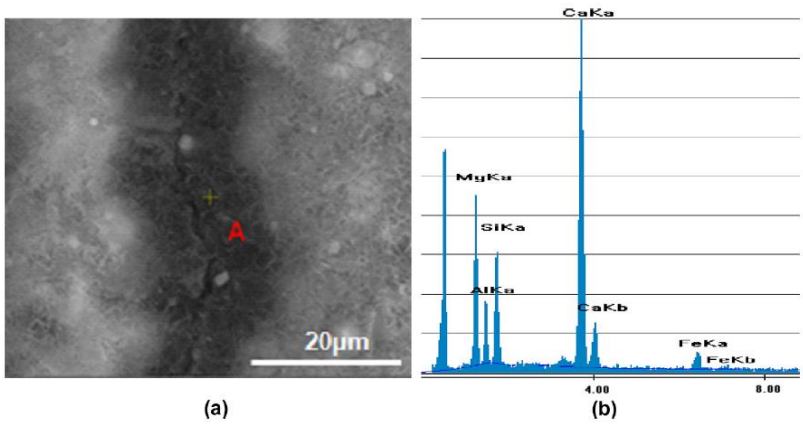

Figure 2.5. ESEM image and EDS spectrum of self-healing product A (Kan and Shi 2012).

Kan et al. investigated the self-healing products of ECCs, using an environmental scanning electron microscope (ESEM) at 30 keV accelerating voltage, and energy dispersive spectroscopy (EDS). Two main healing products were observed, which were classified by the authors either as a "fiber-like" or "stone-like" product. Based on the table below, the Calcium-Silicon ratio of the 'fiber-like' product is 2.07, and the Oxygen-Calcium ratio of the 'stone-like' product is approximately 3.62. Based on these results, it was determined that the 'fiber-like'

material could be calcium-silicate-hydrate gel and the ‘stone-like’ material could be calcium carbonate (Kan and Shi 2012).

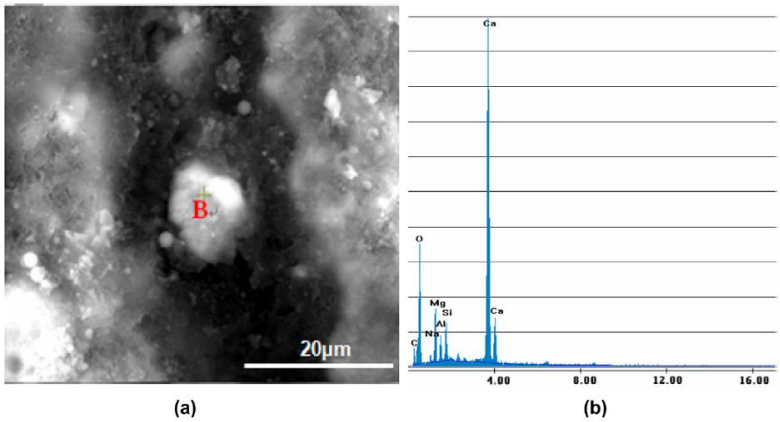

Figure 2.6. ESEM image and EDS spectrum of self-healing product B (Kan and Shi 2012).

Influence of Supplementary Cementitious Materials on Self-Healing

Tittelboom et al. conducted a study to determine the effects of Supplementary Cementitious Materials (SCM) on the self-healing effect of Engineered Cementitious Composites (ECC). A total of 9 different mix designs were made, in which different percentages of cement and SCMs were used. Most of the mix designs maintained a constant water-cement ratio of 0.4. The only sample that had a higher water-cement ratio of 0.5 was included in the experimental matrix since a higher ratio allows more cement particles to hydrate (Van Tittelboom et al. 2012). The details of each mix design are summarized in Table 2.3.

All the samples were cracked and then submerged in water to enable the autogenous healing mechanism of concrete. Specimens were left submerged in water in different time intervals of: 1 day, 4 days, 7 days, 14 days, 21 days, and 42 days. After the prescribed healing periods, the samples were dried and the evolution of the crack repair was monitored under a scanning electron microscope. The observed results indicate that all of the specimens had cracks

filled with calcium carbonate crystals. It is possible that during the drying process of the samples, carbon dioxide reacted with the dissolved calcium hydroxide particles to yield calcium carbonate. In addition, cracks of up to 200 microns were sealed after being submerged for 42 days. However, cracks larger than 200 microns were not fully healed.

Table 2.3. Mix design for each specimen studied (Van Tittelboom et al. 2012).

Type	Water-cement Ratio	% Portland Cement	% SCM	Type of SCM
CEM I	0.4	100	0	N/A
CEM II	0.4	65-79%	21–35%	Blast furnace slag, fly ash, and limestone
CEM III	0.4	20–34%	66–80%	Blast furnace slag
50 BFS	0.4	50%	50%	Blast furnace slag
70 BFS	0.4	30%	70%	Blast furnace slag
85 BFS	0.4	15%	85%	Blast furnace slag
30 FA	0.4	70%	30%	Fly ash
50 FA	0.4	50%	50%	Fly ash
CEM I	0.5	100%	0%	N/A

All the samples were cracked and then submerged in water to enable the autogenous healing mechanism of concrete. Specimens were left submerged in water in different time intervals of: 1 day, 4 days, 7 days, 14 days, 21 days, and 42 days. After the prescribed healing periods, the samples were dried and the evolution of the crack repair was monitored under a scanning electron microscope. The observed results indicate that all of the specimens had cracks filled with calcium carbonate crystals. It is possible that during the drying process of the samples, carbon dioxide reacted with the dissolved calcium hydroxide particles to yield calcium carbonate. In addition, cracks of up to 200 microns were sealed after being submerged for 42 days. However, cracks larger than 200 microns were not fully healed (Van Tittelboom et al. 2012).

The mix design also had an influence in the healing efficiency of surface cracks. Those specimens that had higher contents of SCMs, either with blast furnace slag or fly ash, produced less calcium carbonate precipitates. This is because of the pozzolan activity that takes place with slag or fly ash, as they consume calcium hydroxide to produce more calcium-silicate-hydrate. As a result, the available carbon dioxide from the atmosphere had less calcium hydroxide to react with and therefore produced less calcium carbonate crystals in the crack surfaces. For this reason, the CEM I mix design had the highest healing efficiency on surface cracks (Van Tittelboom et al. 2012).

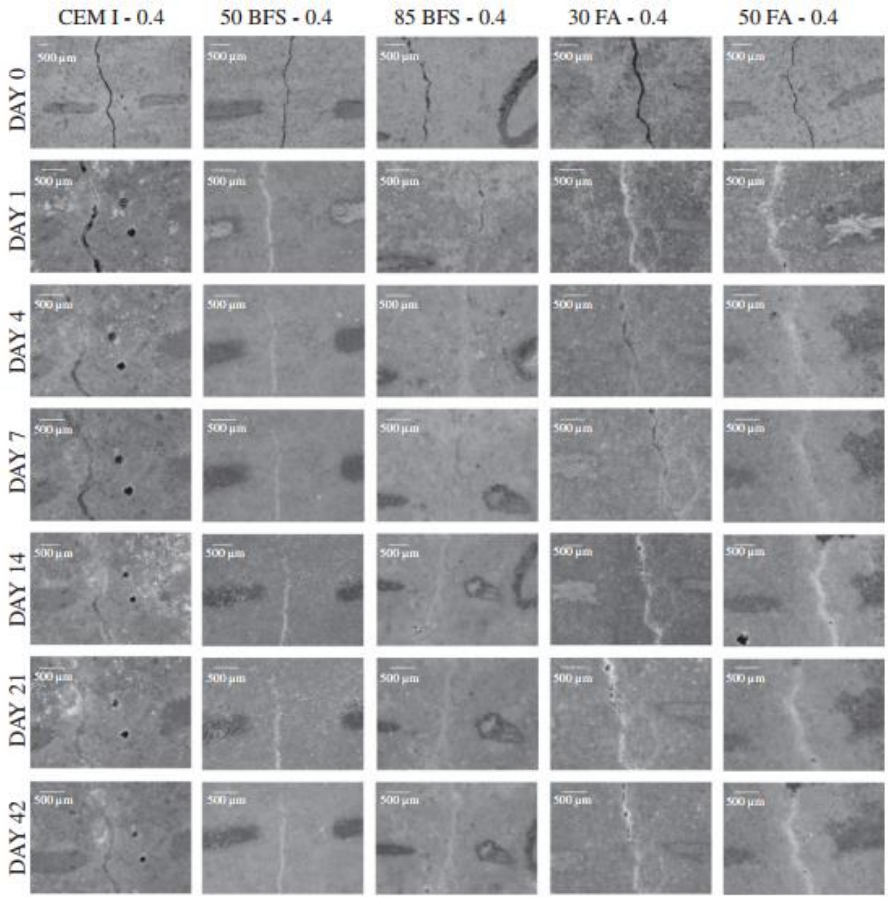

Figure 2.7. Scanning electron microscope images showing the progress of autogenous self-healing over time (Van Tittelboom et al. 2012).

Water permeability tests were also conducted on all of the mix designs from the experimental matrix. Because the samples were submerged in water to test their water absorption, there was a substantial reduction in the available carbon dioxide and therefore resulted in minimal precipitation of calcium carbonate crystals in the cracked surfaces. Therefore, if the carbonation effect is negligible, the water permeability was mainly affected by the continued hydration of unreacted cementitious particles. Those specimens containing higher amounts of SCMs, particularly the blast furnace slag showed higher healing efficiencies with respect to permeability. In addition, the higher water-cement ratio of 0.5 lead to a lower degree of continued hydration and therefore resulted in a lower healing efficiency (Van Tittelboom et al. 2012).

2.3.4 Bacteria-based Healing

Ureolytic Bacteria

Extensive research has been done in recent years on concrete with bacteria as the self-healing agent. The first biological agent investigated was an ureolytic bacteria of the genus Bacillus which is able to produce calcium carbonate-based crystals. The healing mechanism for such bacteria works through an enzymatic hydrolysis of urea to ammonia and carbon dioxide. The subsequent precipitation of calcium carbonate is therefore dependent on the concentration of dissolved inorganic carbon, the pH, the concentration of calcium ions, and the available nucleation sites. The first three of these factors are controlled by the bacteria's metabolism, and the nucleation sites are provided by the bacteria's cell walls (Hammes and Verstraete 2002). In principle, smaller bacterial specimens would yield larger specific surface areas from the cell walls to act as nucleation sites, thus potentially speeding the precipitation reaction.

The concrete specimens containing the ureolytic bacteria were tested for both permeability and compressive strength, and the results were promising. After cracking the samples, there were evident signs of self-repair as there was a strength recovery and the permeability was decreased (Bang et al. 2001) (Ramakrishnan 2007). However, with such approach the bacterial healing agent had to be applied externally on the cracks of the concrete specimens. Therefore, the main limitation is that this approach is not truly autonomic as it requires human intervention. Thorough structural inspection is required before the healing agent is applied on the surface cracks, but if the cracks are inaccessible (i.e. internal cracks), it would not be possible to apply such crack-repair technique.

Bacterial Spores

Jonkers et al. proposed an alternative approach that addresses the need for an autonomic self-healing concrete with a bacterial agent. This was achieved by embedding the bacterial agent inside the concrete matrix. For this healing mechanism to work, the type of bacteria selected needs to be able to withstand the mixing process of concrete, as well as the high alkali environment that is due to the hydration products of cement such as calcium hydroxide and calcium-silicate-hydrate. Hence, bacterial spores that belong to the genus Bacillus have been identified as suitable healing agents (Jonkers et al. 2010). These species have an expected life of 200 years in highly alkaline environments under dry conditions (Schlegel et al. 1993).

Concrete samples were mixed with two species, Bacillus pseudofirmus DSM 8715 and B. cohnii DSM 6307, to form a mix of vegetative cells and bacterial spores. The survival rate of the bacteria cultures in concrete is a crucial parameter that will determine whether the healing mechanism is feasible. It was determined that after 135 days, there were no bacteria cultures detected and therefore their life expectancy in concrete is under 4 months (Jonkers et al. 2010).

The main role of bacteria is to act as a catalyst in the formation of calcium carbonate crystals to reduce the permeability of the concrete. With the addition of appropriate organic nutrients in the concrete matrix, the production of calcium carbonate-based minerals can occur automatically. For this reason, four organic compounds were selected as the potential precursors for bacteria based healing. These compounds were yeast extract, peptone, calcium acetate, and calcium lactate, and were embedded in the concrete at a concentration of 1% by weight of cement to determine the potential impacts on the material's compressive strength. The results indicate that only calcium lactate did not negatively affect the compressive strength. The rest of the organic precursors substantially weakened the compressive strength of concrete (Jonkers et al. 2010).

Healing Capacity

Concrete samples embedded with calcium lactate (0.50% by weight of cement) and bacterial spores ($1x10^8$ of B. cohnii per cubic centimeter of concrete) were compared with control specimens with no embedded bacteria after damage. The study reported that the control specimens produced particles within the range of 1 to 5 microns on crack surfaces. The bacteria-containing specimens, however, produced large amounts of crystals ranging from 20 to 80 microns in size. However, the key observation was that the vast majority of these crystals that were formed at the crack surfaces were only formed in samples aged at 7 days. For the concrete specimens with 28 days of age (both control and bacteria-based), there was no noticeable difference between those samples aged at 7 days (Jonkers et al. 2010).

From these observations, it can be concluded that the self-healing mechanism functioned well, although its capacity is mainly limited by the size of the crystals that are formed by the bacterial cultures. Hence, this self-healing approach is suitable for healing micro-cracks rather

than macro-cracks. Another drawback to this approach is that the bacterial activity is limited to the number of nutrients or precursor available to produce calcium carbonate. The life expectancy of the bacterial spores was also shorter than expected, so the self-healing mechanism has an expiration date.

De Muynck et al. explored the microstructure of mortar specimens with varying porosity that were subjected to a biodeposition treatment (De Muynck et al. 2008a; b). In essence, such mortar specimens were immersed in a culture of bacteria known as Bacillus sphaericus LMG 225 57 that was one day old. After the biodeposition treatment, the specimens were then submerged in either calcium chloride solution, calcium lactate solution, or no calcium-based solution. The electron microscope images revealed that those specimens subjected to both bacteria and calcium solutions successfully produced carbonate crystals in the surfaces of the cement matrix.

Most of the calcium carbonate crystals that were produced by bacteria were usually in the range of 10 to 40 microns. However, crystals of up to 110 microns were found in the micrographs as well. The first set of images shown below correspond to the specimens that had a water cement ratio of 0.5, while the second set of images corresponds to a water cement ratio of 0.7. Therefore, image 2.8A represents the untreated surface, and images 2.8B and 2.8C illustrates the specimen's surface when submerged with calcium chloride solution or calcium lactate solution, respectively. Similarly, the image 2.9A represents the untreated surface, while images 2.9B and 2.9C illustrates the specimen's surface when submerged with calcium chloride solution or calcium lactate solution, respectively. The type of calcium source directly affected the morphology of the crystals. The chloride ions gave the crystals a rhombohedral shape, while the acetate ions produced spherical crystals (De Muynck et al. 2008a; b).

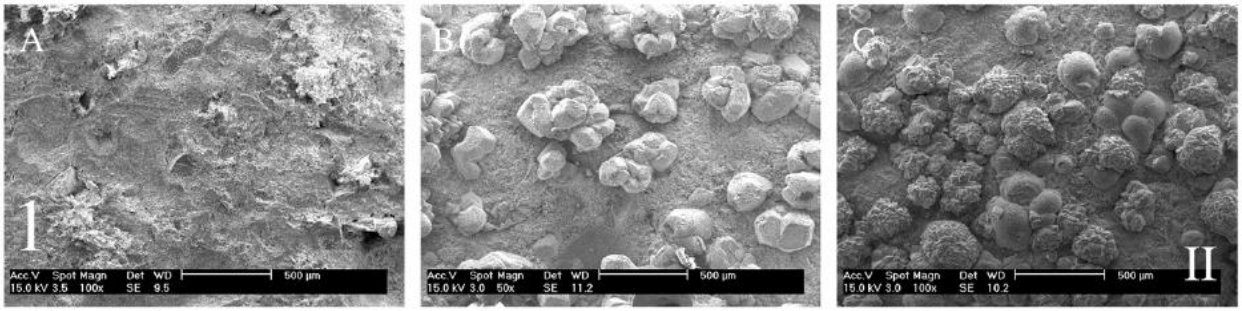

Figure 2.8. Microstructure of concrete specimens with water-cement ratio of 0.5. From left to right, A) control specimen, B) exposed to calcium chloride solution, C) Exposed to calcium lactate solution (De Muynck et al. 2008b).

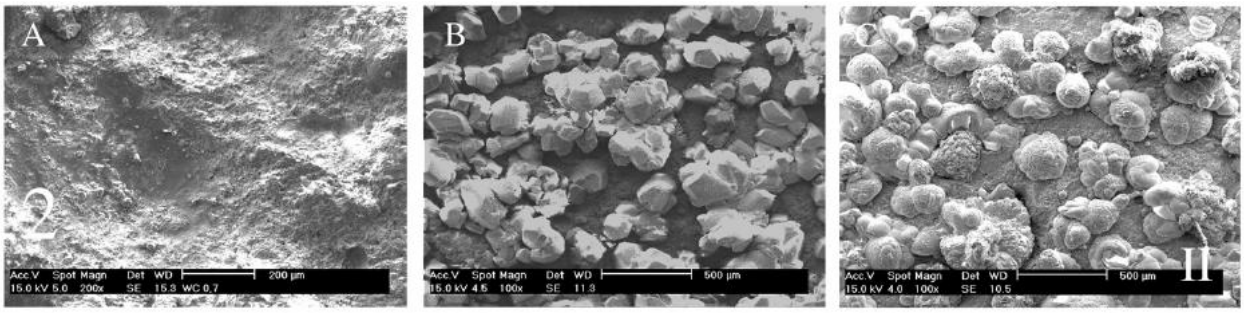

Figure 2.9. Microstructure of concrete specimens with water-cement ratio of 0.7. From left to right, A) control specimen, B) exposed to calcium chloride solution, C) Exposed to calcium lactate solution (De Muynck et al. 2008b).

2.3 Concrete Admixed with Calcium Nitrate

Calcium has been classified as a "multifunctional concrete admixture" by Justnes, as it found it was a useful to control several properties in concrete. Calcium nitrate has been regarded as an economical chloride-free set accelerator for its capability to decrease both the initial and final setting times of concrete in small concentrations, ranging from 0.2 to 1.0% by weight of cement. The performance of calcium nitrate is not temperature dependent as it functions very well with cement mixed at low temperatures. Rather, what governs the accelerator reaction is the chemical composition of the cement used (Justnes 2010).

Calcium nitrate has also functioned well as a corrosion inhibitor for steel reinforced concrete specimens, and it has the capability to increase the long term compressive strength. Additional uses include its ability to perform as an anti-freeze admixture, and its capacity to counteract the retardation effect made by plasticizers while maintaining workability (Justnes and Nygaard 1995; Justnes 2010). The exact mechanism by which calcium nitrate affects concrete's properties has not yet been fully understood due to the complexities of cement chemistry. Nevertheless, several studies have been conducted to identify the effects that such admixture may have on cement hydration.

2.3.1 Chemistry of Hydration

Chemical admixtures comprising of either organic or inorganic compounds have been used widely to accelerate the stiffening and strength development of Portland cement. Calcium chloride used to be the preferred cement accelerator for decades, as it was effective and economical. However, building codes have now prohibited admixtures containing chloride ions due to the corrosion effect on steel reinforced concrete. Since then, the concrete industry began to explore alternatives.

A study by Abdelrazig et al. focused on the solution chemistry and early hydration (i.e. the first 3 hours of hydration) to understand the influence of admixtures such as calcium nitrate, calcium thiocyanate, calcium chloride on two cement matrices: a type I Portland cement system and a type I Portland cement system with sucrose as a retarder. These three chemical admixtures are commercially available and have different effects on the setting and strength development of cement. By comparing these three salts, the effect of the cation variability can be discarded in the test results (Abdelrazig et al. 1999).

The Control System

The results for the control system without admixtures are shown below, for the concentrations of the major and minor constituents in solution during the first three hours. Most of the elements detected remained essentially constant throughout the three-hour period. The potassium concentration increased slightly for the first hour while sodium and lithium remained virtually the same after the first five minutes. Calcium was found to be around 12±15 mmol/l from start to finish. The anions present were hydroxide and sulphate, although low concentrations of chloride ions were also detected at all times.

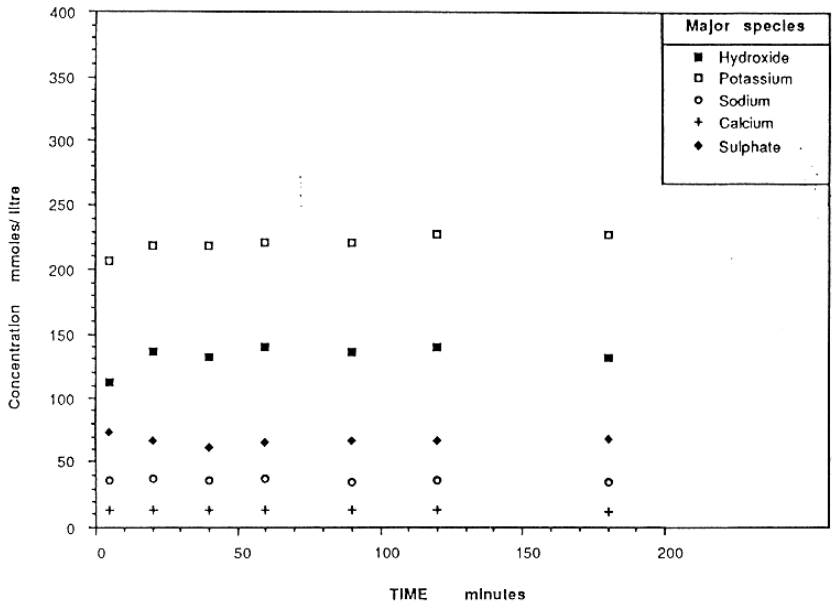

Figure 2.10. Concentrations of major species within the first 3 hours of the hydration of cement (Abdelrazig et al. 1999).

During the first hour, the hydroxide ions increased in concentration from 110 to 140 mmol/l, while the sulphate decreased from 80 to 70 mmol/l. Such observations, combined with the low amounts of calcium detected show a clear sign of the cement hydration reactions. Once the alkali sulphates and anhydrite dissolve, a removal of some sulphate from the solution as the calcium

salt, paralleled by liberation of hydroxide from continuing hydration follows. The sulphate precipitation is most likely dictated by the solubility criteria of calcium sulphate due to the supersaturation of the solution at an early stage. Other elements such as silicon, aluminum, magnesium and iron were only found in very small amounts.

Table 2.4. Concentration ranges for the minor constituents in Portland cement fluid without admixtures (Abdelrazig et al. 1999).

Ion	Silicon	Lithium	Iron	Aluminum	Magnesium	Chloride
ppm	1.7-5.3	9.7-13.9	0-0.1	4.0-7.0	0-0.07	280-475
mmol/L	0.06-0.19	1.4-2.0	$0\text{-}1.8\times10^{-3}$	0.15-0.26	$0\text{-}2.8\times10^{-3}$	7.9-13.4

Cement Admixed with Calcium Nitrate

When adding calcium nitrate, there were increases in concentrations of calcium and decreases in sulphate and hydroxide as expected. However, the initial calcium contents were slightly lower compared to those found with calcium chloride, while the initial hydroxide and sulphate components detected were slightly higher. At the end of the reaction time studied, the sulphate levels continued to decrease while the hydroxide concentration increased. The other significant difference was that the nitrate level dropped with time (from 340 mmol/l to 240 mmol/l after 3 hours) to a much greater extent than observed with the chloride ions in the calcium chloride system. These differences suggest that there may be variations in the solubility products as the nitrate replaces the chloride in the aqueous phase, leading to different proportions of calcium and the major species identified. With respect to the other ions, there was a negligible variation in the concentration and general trends when compared to the control system and the calcium chloride system.

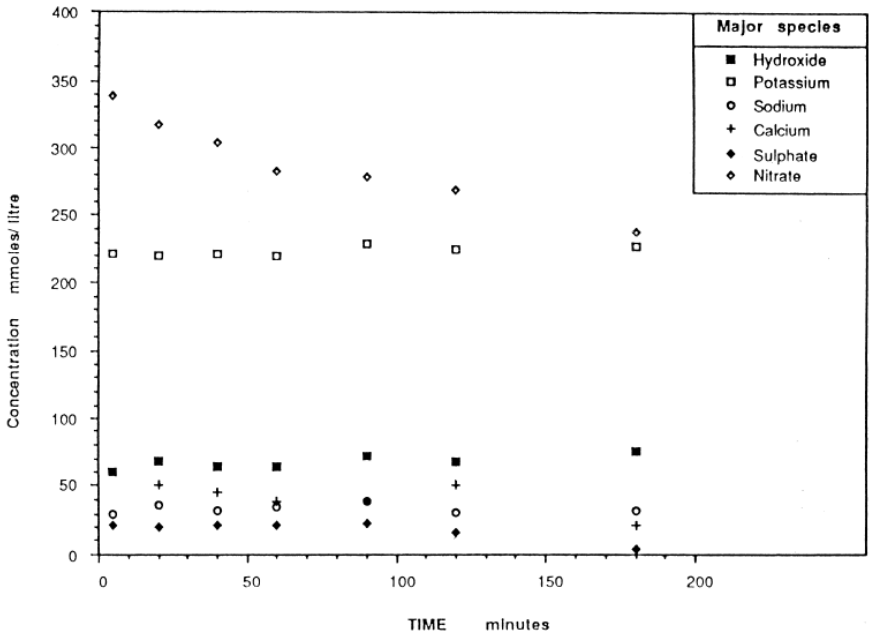

Figure 2.11. Concentrations of major species within the first 3 hours of the hydration of cement admixed with calcium nitrate (Abdelrazig et al. 1999).

Acceleration Mechanism

When ordinary Portland cement is admixed with calcium salts, it was observed that there were more gypsum and calcium hydroxide compounds formed than the control Portland cement paste. This is due to the effect that the admixtures have on the hydration reaction of cement and the solution chemistry of the liquid. Both gypsum and calcium hydroxide are major products of the hydration reaction, and when they are formed in solution (as it occurs with the admixtures investigated), they crystallize in a way that would not hinder the water access to the cement particles. Furthermore, it has been reported that gypsum contributes to the formation of ettingrite, which therefore affects the stiffening process and the amount of gypsum substitution in the calcium-silicate-hydrate gel that influences strength. In addition, the presence of more gypsum and calcium hydroxide leads to a higher release of heat energy due to their contributions in the hydration and precipitation reactions of cement. An increase in the initial temperature of the

cement paste has the potential to affect the hydration reactions significantly (Abdelrazig et al. 1999).

Nevertheless, there is an optimum amount of admixtures that can be added to cement due to its limiting reactants, which are the sulphate and hydroxyl ions. Hence, if more calcium-based admixtures were added past this optimum point, the formation of new gypsum and calcium hydroxide compounds will no longer be possible, resulting in the formation of other compounds instead. It is only at a precise concentration of admixture where the maximum degree of acceleration can be expected. The main factors that affect the hydration reaction rate are: solution equilibria, the relative degree of solvation of ionic reactants, and the presence of transition states (Abdelrazig et al. 1999).

Evaluation of the admixtures

In general, all calcium salts contributed to an increase in gypsum and calcium hydroxide formation. This is due to the addition of calcium ions that trigger a precipitation of sulphate and hydroxide, forming gypsum and calcium hydroxide from solution. However, since the amount of calcium ions added in each calcium-based admixture was the same, the anions in the calcium salts also influenced the sulphate and hydroxide solubilities. In particular, the additions of the chloride or nitrate produced approximately equal amounts of gypsum, while the thiocyanate system produced slightly more. In addition, the nitrate system was responsible for a substantial increase of ettringite formation at all ages, which indicates that the accelerator effect would be greater in this system, at least in the early ages of the cement paste (Abdelrazig et al. 1999).

For the sucrose system, the concentrations of calcium are higher than the control as well, but in this case a supersaturation occurs in order to reduce the formation of gypsum and calcium

hydroxide, thus retarding the setting time of the cement paste. For each of the cases studied, it was reported that the main differences found in both the solution and solid phases were the sulphate and hydroxyl containing components, as well as the amounts of calcium ions present. Therefore, there is significant evidence that both the anion and the cation are involved in the acceleration mechanism. Although there are some changes in concentration at later ages, it appears that the first five minutes of the hydration reaction are crucial in determining the quantities of gypsum and hydroxide to be formed through solution equilibria (Abdelrazig et al. 1999).

2.3.2 Calcium Nitrate as a Set Accelerator for Cement at Low Temperatures

Admixtures that act as set accelerators effectively reduce the initial setting for the transition of the mix from the plastic to the rigid state. Technical calcium nitrate was used by Justnes to study its effect on the set acceleration on the hydration of different types of cement. The tests were conducted at temperatures of 5-7 degrees Celsius. The applied dosages of calcium nitrate were: 0.00, 1.55, 2.32, 3.10, 3.86, and 7.73 percent of calcium nitrate by weight of cement, which thereby corresponds to 0.00, 1.00, 1.50, 2.00, 2.50, and 5.00 percent of nitrate by weight of cement, respectively.

Table 2.5. Experimental matrix of calcium nitrate dosage levels (adapted from Justnes and Nygaard 1993).

Calcium Nitrate (by % of cement weight)	
Cement Types: P30, P30-4A, SR Temperature: 7° Celsius	Cement Types: P30’93, HS65 Temperature: 5° C
0	0
1.55	1.55
3.86	2.32
7.73	3.10

The calcium nitrate admixture was tested on five different types of Portland cements, in order to cover a wide range of tricalcium aluminate in the experimental matrix. The P30 cement is an ASTM Type I Portland cement that was manufactured until 1993. The P30'93 then became the standard type I cement, thus replacing the P30 after 1993. Similarly, the P30-4A (ASTM Type II) cement is known to be of high strength that was produced until 1993, and was replaced by the HS65 cement after 1993. Lastly the SR (ASTM Type V) cement is a sulphate resistant type of cement. The water-cement ratio was held constant at 0.40 for all of the cement types.

Table 2.6. Summary of the test results at 7 °C (adapted from Justnes and Nygaard 1995).

Calcium Nitrate Dosage: 1.55%			
Temperature (°C)	Cement Type	Reduction in Initial Setting Time (%)	Reduction in Final Setting Time (%)
7	P30	22	5
7	P30-4A	58	50
7	SR	45	N/A
Calcium Nitrate Dosage: 3.86%			
Temperature (°C)	Cement Type	Reduction in Initial Setting Time (%)	Reduction in Final Setting Time (%)
7	P30	37	15
7	P30-4A	42	29
7	SR	57 (increase)	N/A
Calcium Nitrate Dosage: 7.73%			
Temperature (°C)	Cement Type	Reduction in Initial Setting Time (%)	Reduction in Final Setting Time (%)
7	P30	20 (increase)	6 (increase)
7	P30-4A	91	33
7	SR	18	N/A

The study's results indicated that the optimum calcium nitrate dosage seems to depend on the temperature and the cement type. If more than the optimal amount of calcium nitrate is added for a specific cement type, the admixture may act as a retardant. Furthermore, there is no

correlation between the tricalcium aluminate content of the cement and the accelerator effect of calcium nitrate at low temperatures, thus reflecting the results obtained with calcium nitrate at 20 °C in another study (Justnes and Nygaard 1993, 1995; Justnes 2010).

Table 2.7. Summary of the test results at 7 °C (adapted from Justnes and Nygaard 1995).

Calcium Nitrate Dosage: 1.55%			
Temperature (°C)	Cement Type	Reduction in Initial Setting Time (%)	Reduction in Final Setting Time (%)
5	P30’93	51	N/A
5	HS65	70	62
Calcium Nitrate Dosage: 2.32%			
Temperature (°C)	Cement Type	Reduction in Initial Setting Time (%)	Reduction in Final Setting Time (%)
5	P30’93	46	N/A
5	HS65	76	69
Calcium Nitrate Dosage: 3.10%			
Temperature (°C)	Cement Type	Reduction in Initial Setting Time (%)	Reduction in Final Setting Time (%)
5	P30’93	59	N/A
5	HS65	83	72

Both the SR and P30-4A cement had an optimal dosage at 1.55% of calcium nitrate, while P30 cement reached an optimum with a 3.86% dosage. It is important to note that for the SR cement paste, the final setting times were not reported because they exceeded the recording time frame. The same pattern was observed for the SR cement paste when admixed with calcium nitrate at 20 °C. In addition, a dosage of 3.86% acted as a retarder for SR, while a dosage of 7.73% retarded the P30 cement paste. However, the retardation effect for the P30 cement paste only occurs in low temperatures (Justnes and Nygaard 1995).

For the cement types tested at a temperature of 5 °C, it was found that calcium nitrate is more effective as an accelerator for the HS65 cement than the P30’93. Such effect generally increases with increasing calcium nitrate concentration, except for the cases of 2.32% and 1.55%. It is important to note that the final setting times for the P30’93 cement exceeded the recording time frame of the calorimetry study as well.

Table 2.8. Efficiency of calcium nitrate (1.55%) with respect to the belite content in cement (adapted from Justnes and Nygaard 1995).

Temperature (°C)	Cement Type	Belite content (%)	Reduction in Initial Setting Time (%)
7	P30	15	22
7	SR	18	45
5	P30’93	19	51
7	P30-4A	23	58
5	HS65	24	70

In general, the efficiency of calcium nitrate as a set accelerator appears to be greater with increasing belite content of cement. The following table illustrates this finding for the 1.55% calcium nitrate case at low temperatures. While the actual acceleration mechanism is not fully understood, it is believed that a) a supersaturation and its succeeding crystallization calcium hydroxide, and b) a depression of the sulphate solubility due to a higher calcium content due to the calcium nitrate admixture may be the key factors (Justnes and Nygaard 1995).

2.3.3 Influence of Admixtures on Cement at Early Ages

Calcium nitrate was also compared with other admixtures for its influence on the setting time of cement pastes at early ages by Aggoun et al. (2008). The experimental matrix was also expanded to include analysis on the effect of the admixtures on the hardening of the cement paste. The

three admixtures studied beside calcium nitrate were triethanolamine (TEA) and triisopropanolamine (TIPA) in two difference cement types at 20 °C. The water-cement ratio for the studied cement pastes was 0.3. The main objective of the study was to find a combination of calcium nitrate with other compounds that is capable of accelerating the setting and hardening time of cement.

The effect of the admixtures described were tested on two types of cement. The mixes used evaluated the individual effects of the three admixtures added by weight of cement: 1% Calcium nitrate, 0.05% TEA, and 0.05% TIPA. Two additional mixes were added to see the combined effect of calcium nitrate with TEA (1% and 0.05% by wt. of cement, respectively), and calcium nitrate with TIPA (1% and 0.05% by wt. of cement, respectively). The results were then compared with the control specimens that had no admixtures present. Figure 2.12 shows the effects on the strength and setting times for cement 1, and Figure 2.13 for cement 2.

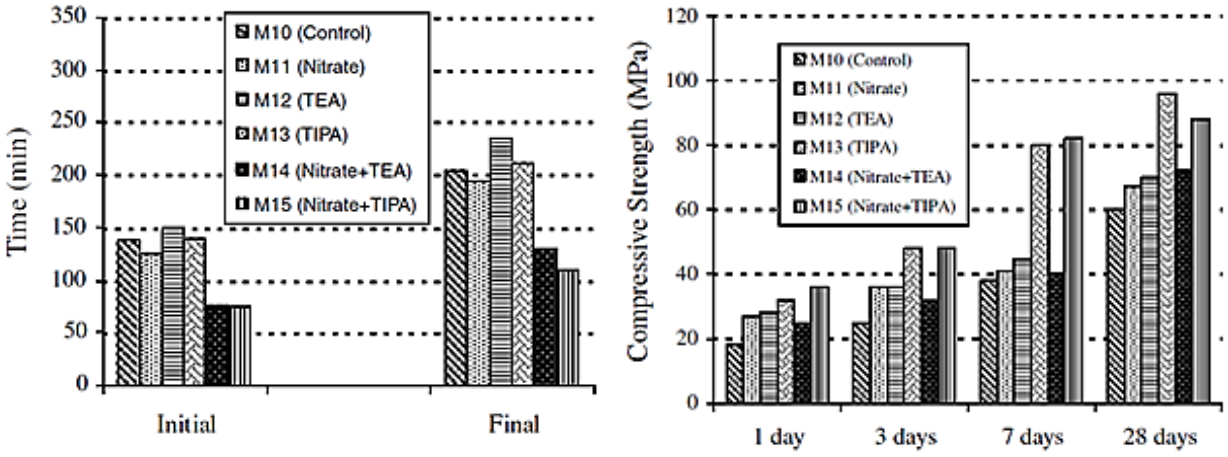

Figure 2.12. The effect of the admixtures on the setting times and compressive strength of cement C1 (Aggoun et al. 2008)

The main differences between cements C1 and C2 is that C2 has lower tricalcium aluminate contents and higher tetra-calcium aluminoferrite concentrations. For this reason, calcium nitrate on its own produced different results as a set accelerator since its performance is affected by the chemical contents of the cement it reacts with. It was also found that calcium nitrate did not act as a hardening accelerator for both cement types, although it did contribute to strength at 28 days. On the other hand, triethanolamine and triisopropanolamine were not dependent on the cement type and they both acted as hardening accelerators when examined individually. Even though both triethanolamine and triisopropanolamine were admixed at the same concentration of 0.05%, triisopropanolamine was substantially superior as a hardening accelerator (Aggoun et al. 2008).

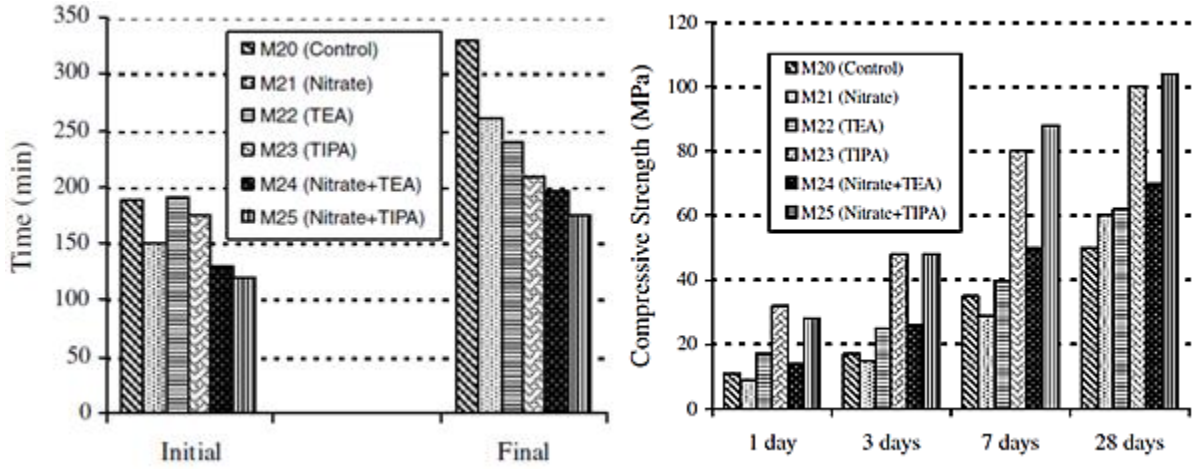

Figure 2.13. The effect of the admixtures on the setting times and compressive strength of cement C2 (Aggoun et al. 2008).

The combinations of calcium nitrate with TIPA, and calcium nitrate with TEA also produced great improvements in both setting times and strength development regardless of the cement type. The optimal combination was found with calcium nitrate and TIPA since they

exhibited great improvements in the setting time and hardening rate at the early ages on both cement types (Aggoun et al. 2008).

2.3.4 Corrosion Inhibitors in Contaminated Concrete

Reinforced concrete is a widely-used material for buildings and infrastructure, and its durability depends on the permeability of the material as it is imperative that the steel reinforcement remains pristine throughout the life of the structure. The corrosion of steel reinforcement is mainly due to chloride and carbon dioxide, and for this reason it is important to protect the steel from reacting with these hazards. Al-Amoudi et al. (2003) conducted an investigation on the efficiency of corrosion inhibitors when concrete is contaminated by chloride and sulfate ions. A corrosion inhibitor is officially defined as "a chemical admixture that is able to decrease the steel reinforcement's corrosion in hardened concrete" by ACI 116R-85.

Corrosion inhibitors work by either: 1) forming layers of protection, 2) triggering passivation of the exterior surface, 3) affecting the environment that will come in contact with the steel. Therefore, an effective corrosion inhibitor must have the following characteristics: i) compatibility with the steel and concrete matrix, ii) functionality in the temperature and pH in which it will be exposed, iii) adequate solubility, iv) strong electron acceptor or donor properties (or both), and v) able to induce polarization of the electrodes at low currents.

The four different types of corrosion inhibitors used in the study met the aforementioned criteria, and these were: calcium nitrate, calcium nitrite, and two commercial organic inhibitors referred as CI1 and CI2 respectively. These admixtures were tested in concrete specimens that were exposed in five different types of contamination, which are: 0.8% chloride, 0.8% chloride with 1.5% sulfate, seawater, brackish water, and unwashed aggregates. In particular, sea water contained 24,408 ppm of chloride and 4211 ppm of sulfate, while brackish water had 893 ppm of

chloride and 630 ppm of sulfate. The unwashed coarse aggregates had water-soluble ions that were potentially hazardous to steel, specifically with chlorine and sulfate ions with concentrations of 0.424% and 0.110% by weight of coarse aggregate, respectively.

The corrosion inhibitors studied were evaluated with respect to their ability to reduce the corrosion of the reinforcement, which was measured by corrosion potentials (ASTM C 876) and corrosion current density. In addition, a compressive strength test was made to determine the effects of these admixtures on the performance of concrete as a construction material.

With respect to the compressive strength, all specimens containing admixtures exhibited higher strengths than the control. This is a very important aspect, as other corrosion inhibitors such as sodium nitrite are known to decrease the concrete's strength. In particular, calcium nitrate produced higher strength by increasing concentration.

The corrosion levels were measured by a DC linear polarization resistance method, and the readings were categorized as: minimal corrosion, moderate, and active corrosion. The results indicated that after 122 days, the control specimens had active corrosion when concrete was contaminated by i) chloride, ii) chloride with sulfate, and iii) sea water. In fact, specimens contaminated by both chloride and sulfate took only 31 days to pass the active corrosion threshold, while specimens contaminated by chloride and seawater took 53 days and 98 days to pass the active corrosion threshold, respectively.

For all the other concrete samples, the effect of the admixtures successfully deterred the corrosion as the specimens were found to be in a passive state after 122 days of exposure. However, the performance of these admixtures was dependent on the dosage and the type of contaminant that was present. In particular, the most effective corrosion inhibitor was calcium

nitrite as it provided superior performance for specimens that were contaminated with chloride, chloride with sulfate, and seawater respectively (Al-Amoudi et al. 2003).

Table 2.9. Summary of the best corrosion inhibitors with respect to the contaminant type (Al-Amoudi et al. 2003).

Contaminant	Optimal Corrosion Inhibitor
Chloride	4% calcium nitrite or 4% calcium nitrate
Chloride and sulfate	4% calcium nitrite or 3% calcium nitrate
Sea water	4% calcium nitrite
Brackish water	2% calcium nitrite
Unwashed aggregate	4% calcium nitrite

2.4 Microcapsule Synthesis

Microencapsulation is a process by which a core material or active ingredient is enclosed by an inert shell. Depending on the desired application, microcapsules can be produced to protect the core material from the environmental conditions, or it can be used to provide a controlled release of the active ingredient to the surroundings by controlling the permeability of the shell material. In general, the size of the microcapsules can range from the millimeter to the micron level. In special cases, the production parameters may be adjusted to yield nanocapsules.

Table 2.10. Some of the most commonly used encapsulation methods sorted by production technique (Ghosh, 2006)

Chemical Processes	Physico-Chemical Processes	Physico-Mechanical Processes
In situ polymerization	Supercritical CO_2 assisted microencapsulation	Multiple nozzle spraying
Polycondensation	Layer-by-layer assembly	Spray-drying
Interfacial polymerization	Sol-gel encapsulation	Fluid-bed coating
Miniemulsion polymerization	Coacervation	Centrifugal techniques

In general, the production of microcapsules can be categorized as either chemical, physico-chemical, or physico-mechanical methods. The selection of the microencapsulation technique depends on the type of core material that is to be encapsulated, and the desired physical properties of the microcapsule. The permeability of the shell wall, the yield rates, the morphology and the particle size are all factors that need to be considered for this matter (Ghosh 2006). The table below summarizes the typical particle sizes that result from each respective encapsulation technique.

Table 2.11. Microcapsule size with respect to the production method (Ghosh, 2006)

Microencapsulation Process	Particle Size (µm)
Extrusion	250-2500
Spray-drying	5-5000
Fluid bed coating	20-1500
Rotating disk	5-1500
Coacervation	2-1200
Solvent evaporation	0.5-1000
Phase separation	0.5-1000
In situ polymerization	0.5-1000
Interfacial polymerization	0.5-1000
Miniemulsion	0.1-0.5
Sol-gel encapsulation	2-20
Layer-by-layer assembly	0.02-20

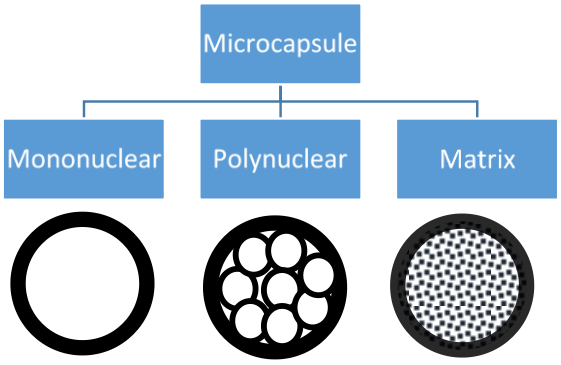

Figure 2.14. Main types of microcapsule morphologies (adapted from Ghosh, 2006)

The morphology of microcapsules is affected directly by the type of core material and the respective encapsulation method used. In general, there are three types of morphologies, as illustrated in Figure 2.14: 1) Mononuclear (core-shell) where the microcapsules form the shell wall around the core, 2) Polynuclear, where multiple cores are encapsulated within a single shell, and 3) Matrix encapsulation, where the core material is dispersed homogenously inside the shell wall. In addition, it is possible to have mononuclear microcapsules with multiple shell walls.

Several research studies have developed self-healing materials using microcapsules, where the enclosed healing agent is designed to be released when the material becomes damaged and the cracks rupture the embedded microcapsules. In this study, it is imperative to select a shell material that is sufficiently robust to be resist the mixing process in concrete, yet weak enough to rupture when cracks propagate. Hilloulin et al. determined that polymeric shell walls meet the aforementioned requirements (Hilloulin et al. 2015). For this reason, the main encapsulation techniques reviewed involve a polymerization process.

2.4.1 In Situ Polymerization

Brown et al. adapted an in situ encapsulation procedure for non-water-soluble core materials developed by Dietrich (Brown 2004; Dietrich et al. 1989). The process requires an oil-in-water emulsion that is made possible by a constant agitation rate and a surfactant such as Ethylene maleic anhydride (EMA). The emulsion will contain droplets of the core material surrounded by a water phase containing low concentrations of dissolved resorcinol, ammonium chloride, urea, and formaldehyde. In the presence of heat, the reaction of urea and formaldehyde (under a 1:1.9 molar ratio of formaldehyde to urea) is catalyzed under acidic conditions in the aqueous phase, forming a prepolymer of low molecular weight. As the reaction continues, the molecular weight of the prepolymer increases and is subsequently deposited at the oil-water interface. The urea-

formaldehyde reaction eventually becomes highly crosslinked and thereby forms a solid microcapsule shell.

The final product is a cluster of spherical microcapsules in the form of a free-flowing powder. The microcapsules subjected to agitation rates ranging from 200 to 2000 RPM resulted in average diameters 10 to 1000 microns. In addition, the average shell thickness was in the range of 160 to 220 nanometers regardless of the agitation rate used (Brown 2004). With respect to the morphology, the microcapsule shell has a smooth, impermeable internal membrane while the external surface features a rough and porous membrane. The rough porous external surface is formed by an accumulation of urea-formaldehyde nanoparticles. It has been reported that such rough surfaces provide a superior mechanical adhesion of the microcapsules when embedded in a polymer matrix, which is beneficial for self-healing purposes.

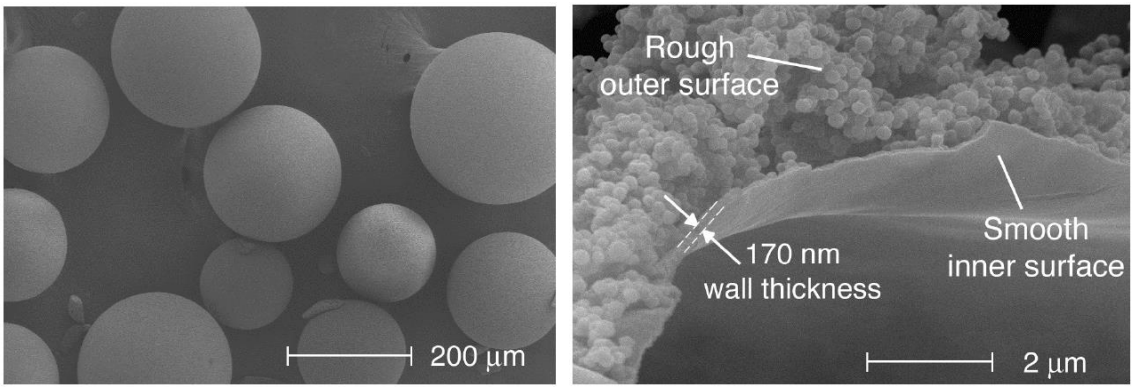

Figure 2.15. Electron microscope images of DCPD microcapsules, and their shell wall features (Brown, 2003)

The smooth impermeable wall is formed by the deposition of low molecular weight prepolymer at the oil-water interface while the prepolymer remains soluble. On the other hand, the formation of the urea-formaldehyde nanoparticles that appear on the external surface is

caused by the precipitation of higher molecular weight prepolymers in the aqueous solution, and their subsequent deposition on the capsule shell.

Effect of Operating Parameters

Brown et al. investigated the effects of the production parameters on the in situ encapsulation of dicyclopentadiene (DCPD). The agitation rate, interfacial area, and the pH were the main variables studied to examine their respective effects on the yield and surface morphology of the microcapsules. Among the findings, it was confirmed that the agitation rate has a direct correlation with the microcapsule diameter, as shown in Figure 2.16.

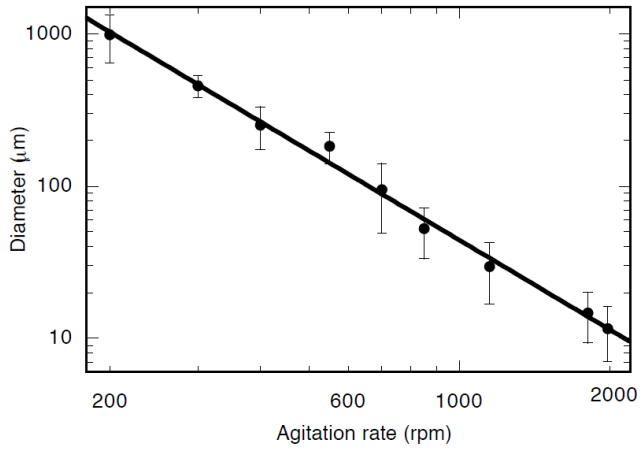

Figure 2.16. Linear Relationship between the agitation rate and the microcapsule diameter (Brown, 2003)

Indeed, a faster agitation rate forms a finer emulsion consisting of smaller droplet sizes. Once the polymerization reaction occurs, such droplets are then enclosed by a solid polymer shell. As a result, there is a linear log-log relationship between the agitation rate (in revolutions per minute) and the average microcapsule diameter. The agitation rate also affected the yield rates and the surface roughness. For instance, at an agitation of 550 RPM result in a yield rate of

79-92% and a rough external surface. However, at a significantly higher level of agitation of 1800 RPM the yield dropped to 68% and the exterior surface was smoother.

The shell wall thickness of the internal, impermeable membrane was unaffected by the production parameters investigated. The average shell thickness was found to be in the range of 160 to 220 nanometers, which is ideal for storage and self-healing applications. However, the rough and porous external surface of the microcapsule was found to be sensitive to the concentrations of ammonium chloride, resorcinol, or core material. Other factors such as an unbalanced or unaligned mixer had a significant impact on the outer shell wall as well.

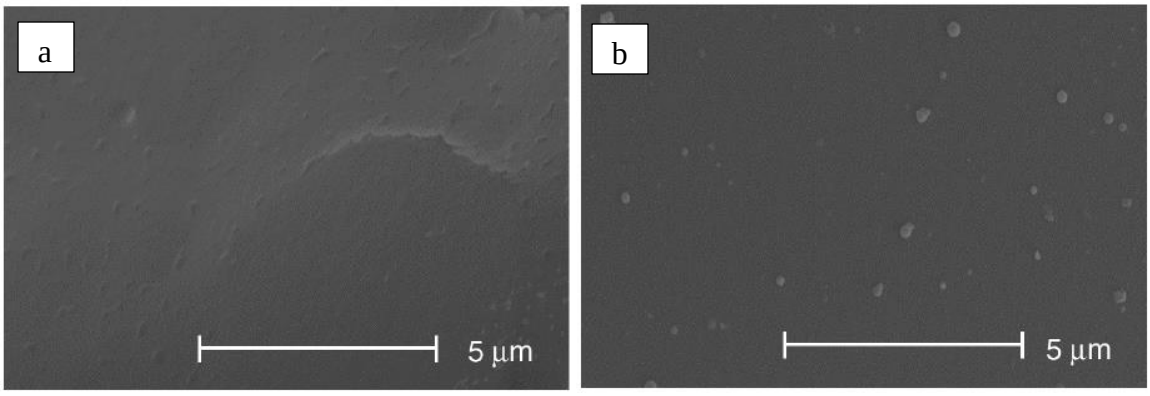

Figure 2.17. The smooth external surface morphology of (a) microcapsules produced at a constant pH level, (b) microcapsules with an increased interfacial area (Brown, 2003)

The pH had a significant effect on the yield rate and the quality of the microcapsules produced. Since it is an acid catalyst system, the pH controls the polymerization rate. When the oil-in-water emulsion is heated, the pH decreases and the viscosity increases at the oil-water interface. As a result, the droplet formation mechanism and the respective morphology of the final microcapsule is affected. When the pH was maintained at a constant level throughout the polymerization reaction, the yield rate dropped significantly and the exterior surface morphology

was smooth. This was due to the fact that the urea-formaldehyde nanoparticles remained in suspension in this system, and were not successfully deposited on the microcapsule shell. In another experiment, it was found that a lower initial pH substantially increased the thickness of the external surface membrane.

The oil-in-water emulsion ratio was also adjusted to examine its effects on the final microcapsule product. The original amount of DCPD added was of 60 ml, but in this test 180 ml were added. As a result, the emulsion transformed into a particle suspension. The formation and deposition of urea-formaldehyde nanoparticles on the external microcapsule surface was limited, which therefore produced a smooth morphology. The final product was in the form of a free-flowing powder, and the yield rates were greater than 85%.

Effect of the Emulsifier

Fan et al. studied the effect of the emulsifier on the morphology of microcapsules synthesized by an in-situ polymerization method of urea-formaldehyde. The emulsifier is an important component in the microencapsulation process, as it can form a stable emulsion between the core material and the aqueous solution. The type of emulsifier used will affect how the prepolymer is adsorbed and deposited on the surface of core material's droplets (Fan and Zhou 2011).

The emulsifiers investigated were: a) Sodium dodecylbenzene sulfuric (SDBS); b) poly(ethylene-altmaleic anhydride) (poly(E-MA)); and c) gum arabic (GA). All of these emulsifiers were tested at different concentrations in aqueous solution 0.1, 0.4, 0.1% respectively. The core material, Tetrachloroethylene (TCE), was dispersed in an oil-in-water emulsion at an initial pH of 3.5 and a constant agitation rate of 500 RPM. The emulsion was then

heated for three hours at 55 degrees Celsius, and the final product was observed under a microscope.

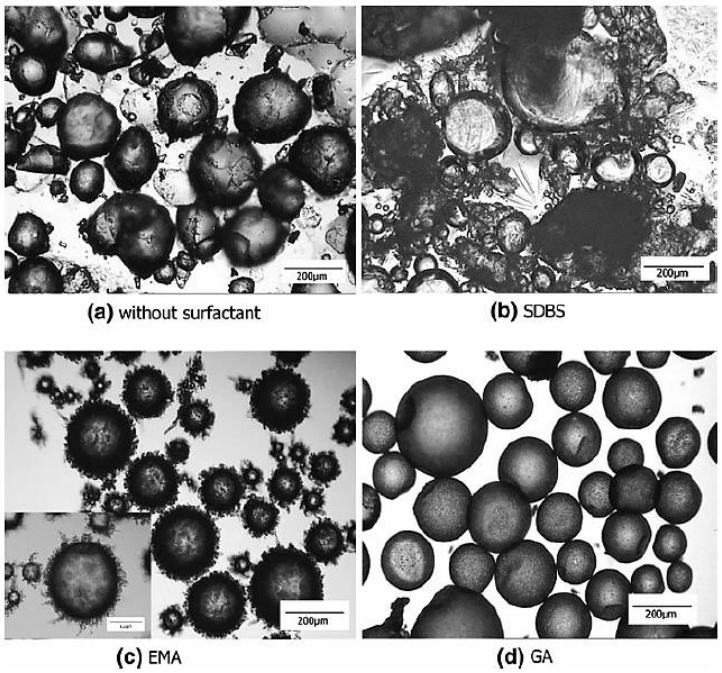

Figure 2.18. The effect of the emulsifier type on the morphology of the microcapsules (Fan and Zhou 2011).

Fan et al. reported that both EMA and GA surfactants generate large droplets with a broad size distribution, while SDBS yields small droplets with a narrow size distribution. The morphology of the microcapsules was greatly influenced by such emulsifiers, where GA produced the smoothest capsules. In the absence of a surfactant, the microcapsules have irregular shapes because the core droplets in the emulsion are not stable (Fan and Zhou 2011).

Mechanical Strength of Microcapsules

Sun et al. investigated the mechanical strength of three different shell materials for microcapsules, using a micromanipulation technique (Sun and Zhang 2002). Such technique is

able to determine the microcapsule bursting force, and the deformations at bursting by compressing individual microcapsules between two parallel surfaces. There were three shell materials explored in this study: melamine-formaldehyde resin, urea-formaldehyde resin, and gelatin-gum Arabic coacervate.

Melamine-formaldehyde (MF) and urea-formaldehyde (UF) microcapsules were synthesized by the in situ polymerization process, while the gelatin microcapsules were produced by complex coacervation. The amount of MF shell materials used were 50% of the core materials in weight, whereas UF microcapsules used 42%, and gelatin-gum arabic capsules used 50% respectively. With regard to the core materials encapsulated, MF encapsulated a 10:1 mixture of HB40 and kerosene, while UF and gelatin microcapsules stored dibutyl phthalate and dimethyl phthalate, respectively. All specimens were set to be tested mechanically after being dried.

It was reported that UF and MF microcapsules can be considered as a visco-elastic material for small deformations. However, for larger deformations, expressed as a ratio of the displacement of the microcapsule with respect to the original diameter, the UF and MF microcapsules exhibited a permanent (plastic) deformation. Such event occurred at a deformation of 39% for MF and 29% for UF microcapsules. Hence, it was concluded that the yield points for MF capsules occurred at a 19 ± 1% deformation, and for UF capsules at a 17 ± 1% deformation. With respect to the bursting point, a deformation of 68 ± 1% was needed for MF microcapsules, while UF microcapsules burst at a 35 ± 1% deformation. In addition, the bursting force and deformation at bursting for both MF and UF microcapsules was dependent on the diameter size, where larger microcapsules required larger forces to achieve the same deformations (Sun and Zhang 2002).

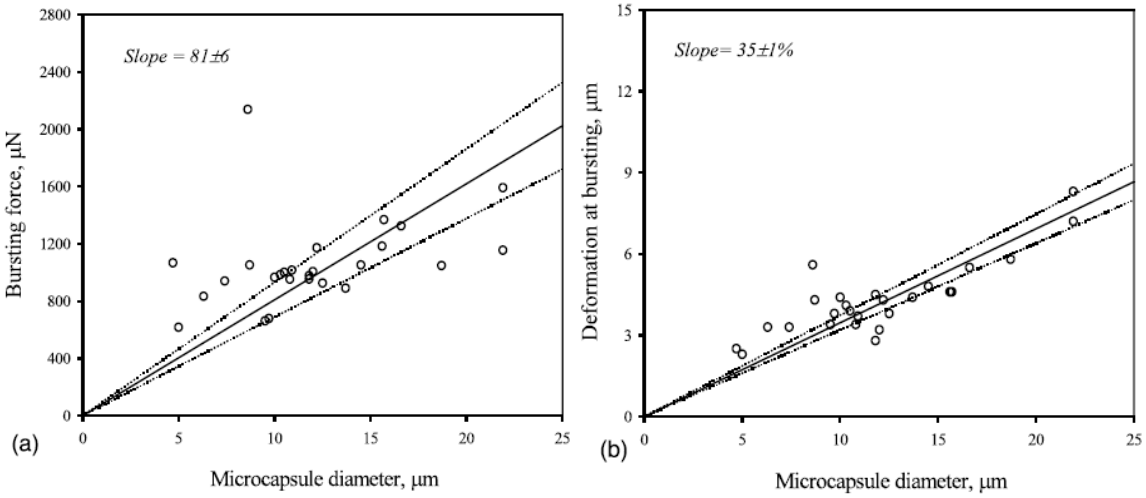

Figure 2.19. Graphs showing the relationship of the (a) bursting force and (b) deformation at bursting with respect to the diameter of the UF microcapsules (Sun and Zhang 2002).

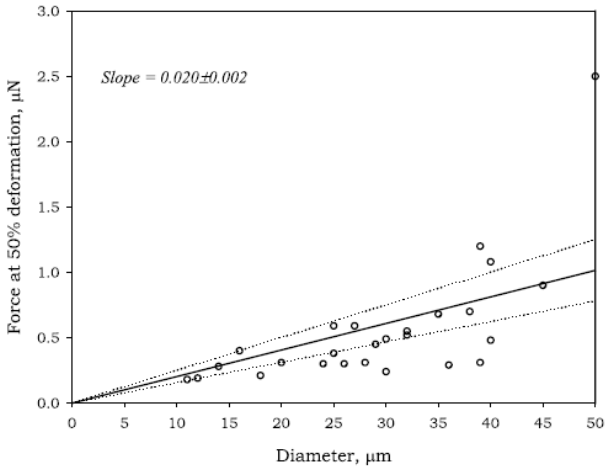

Figure 2.20. The forces required to cause a 50% deformation to the gelatin capsules with respect to their diameter (Sun and Zhang 2002).

Gelatin microcapsules exhibited a different mechanical behavior when tested in a dry state, as their walls seemed to collapse and therefore released the core material. Because such shell material is highly permeable, the capsules were tested under water suspension. The test results indicated that gelatin microcapsules behave elastically when subjected to deformations of

up to 50%. However, after this point, it was indicated that the core materials were quickly released and therefore decreased substantially the pressure inside the shell walls. In addition, it was also found that the bursting force and deformations are proportional to the microcapsule size, in the same way it was observed for UF and MF shells (Sun and Zhang 2002).

2.4.2 In Situ Self-Condensation

Rodson et al. developed a procedure for producing microcapsules that enclose a water-soluble material. The capsule shell materials are formed by a prepolymer, and it requires a water-in-oil emulsion for a successful application. Indeed, the aqueous phase would contain the desired water-soluble material –or use water itself as the core material- and the prepolymer dissolved. The suggested prepolymer materials can be made from either urea-formaldehyde resin or melamine-formaldehyde resin, as they need to be insoluble in oil but readily dissolvable in water. For the oil phase, a liquid organic solvent is required with a "surface active proton transfer catalyst" dissolved therein. Once the aqueous phase is dispersed in the oil phase, the mixture shall be agitated by a high shear stirrer to form an emulsion. In the presence of heat, the emulsion will react and form an in situ self-condensation of the prepolymer that will enclose the aqueous droplets with a solid polymer shell (Rodson and Scher 2000).

The encapsulation reaction is controlled by several production parameters: 1) The temperature at which the emulsion is heated, 2) the choice of catalyst and the respective concentration, 3) the amount of time allotted for the reaction, 4) the agitation rate, 5) the water-oil ratio, and 6) the choice of the core material. For the in situ self-condensation process to occur, the prepolymer must be inert and compatible with the core material. Otherwise, the encapsulation process will be hindered. Moreover, the organic phase must be larger than the

aqueous phase in order to maintain a water-in-oil emulsion. The recommended water-oil ratios can be around 1:3 or 1:4 by either weight or volume of water and oil.

A defining characteristic of the in situ self-condensation process is that it is a "self-terminating reaction", meaning that the reaction can be left running for an indefinite period of time until it is completed. In addition, the temperature and concentration of the catalyst are the main parameters that control the reaction rate. Indeed, the catalyst will activate the formation of the microcapsule's polymer shell. In high concentrations, the catalyst may speed up the reaction rate significantly. Similarly, a temperature of up to 100 °C would achieve the same effect (Rodson and Scher 2000).

The agitation rate has a direct influence in the droplet size of the emulsion. A faster agitation rate would result in a smaller droplet size, while a slower agitation rate yields a larger droplet size. Therefore, the final microcapsule size will depend greatly on the droplet size that was achieved according to the established agitation rate. The size of the microcapsules can range from 0.5 to 4000 microns in diameter. Once the reaction is completed and the microcapsules are successfully formed, they can be stored on their dispersed state, or filtered and left to dry (Rodson and Scher 2000).

2.4.3 Interfacial Polymerization

Saihi et al. encapsulated a water-soluble compound, di-ammonium hydrogen phosphate (DAHP), with a polyurethane-urea membrane using an interfacial polymerization method. The microcapsules are produced by an interfacial reaction of diphenyl methylene diisocyanate dissolved in the oil phase and the aqueous phase that contains the core material dispersed in the oil phase. The procedure therefore requires the dispersion of an aqueous solution containing the core in an organic phase, the addition of a solution that will react to form the shell wall of the

microcapsule, and a gentle agitation rate accompanied with heat to form the microcapsule shell over time. Once the reaction is completed, the microcapsule slurry is decanted, filtered and then allowed to dry (Saihi et al. 2006).

The results in Saihi's study revealed that the average size of the microcapsules was of 13.35 microns, where the maximum size was of 30 microns. The distribution of the microcapsule sizes revealed that 95% of the capsules were smaller than 30 microns. A wide size distribution was obtained from these microcapsules due to their sensitivity to production parameters such as agitation rate and temperature. If the average size of capsules was to be decreased, a higher agitation rate would be needed during the emulsion stage where the shell-forming solution is mixed with the dispersed aqueous phase. Elementary analysis was conducted to confirm that the core material DAHP was successfully encapsulated, and Fourier Transform Infrared spectroscopy was used to determine that the shell material of the microcapsule was formed by polyurethane.

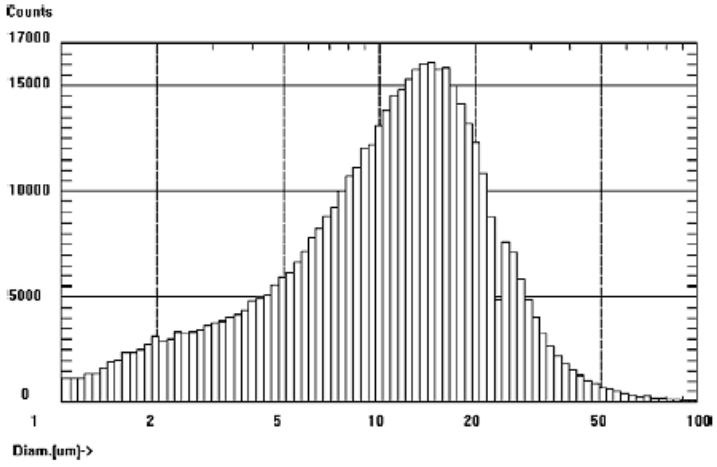

Figure 2.21. Size distribution of microcapsules containing DAHP (Saihi, 2006)

2.5 Self-healing by Microencapsulated Healing Agents

White et al. introduced the concept of self-healing materials through microencapsulation, where the healing agent is kept from any reactions with the structural material's matrix until it is needed (White et al. 2001). Hence, at a cracking event, enough microcapsules should rupture and release the healing agent to seal the newly formed cracks. However, if too many capsules are added, it can be costly to implement, and it can be detrimental to the material's strength and other fundamental properties. Therefore, a compromise has to be sought for the number of added capsules.

Materials with embedded microcapsules have the advantage of having a localized response to fractures if capsules are uniformly dispersed inside the matrix. However, the bond between the microcapsules and the matrix is crucial for a successful application. If the strength of the capsule wall is higher than the bond strength, the microcapsules would not rupture after the initiation of the cracks which means no healing agent will be released. In addition, the main disadvantage of applying particles that may further hydrate or crystallize is that their healing functionality is limited as the healing agent itself is consumed in the process.

Depending on the application, microcapsules can be designed to have a spherical or cylindrical shape. While some agents react upon contact with moisture or air or due to heating or upon contact with the cementitious matrix itself, other agents react when making contact with a second component that is present in the matrix or provided by additional capsules. In figure 2.22, the following cases are illustrated: The reaction of spherical/cylindrical encapsulated agent (dark colored inclusions) upon contact with (**A**,**B**) moisture or air or due to heating; (**C**,**D**) the cementitious matrix; (**E**,**F**) a second component present in the matrix such as a catalyst, or (**G**,**H**) a second component provided by additional capsules (big, light colored inclusions).

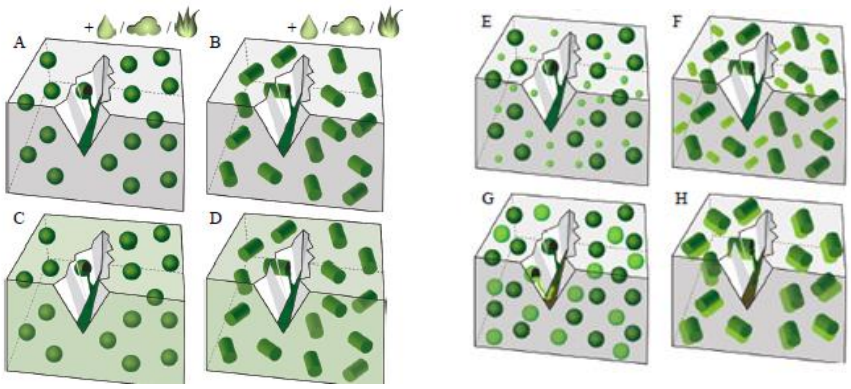

Figure 2.22. Schematic diagram for the capsule based self-healing approaches (Van Tittelboom and De Belie 2013).

In the case of embedded spherical or cylindrical capsules, there is not a 100% chance of the crack going through. However, if the capsules form weak points within the matrix, they will attract the crack and increase the probability of rupture. The main advantage of cylindrical capsules is that their probability of fracture is higher than spherical capsules due to the higher surface to volume ratio.

A key aspect of the microencapsulation strategy is the selection of the healing agent. Besides the sealing ability, viscosity is another important parameter because it controls the mobility and therefore the potential surface area it can interact with in the matrix. The viscosity should not be too high to be able to flow out of the capsules and to fill the crack. Nevertheless, if the viscosity is too low, the agent could leak out of the crack or it could disappear due to absorption by the surrounding matrix (Van Tittelboom and De Belie 2013; Wu et al. 2012). Dry et al. suggested that the viscosity of the healing agent should be between 100 and 500 cps (Dry 1994).

2.5.1 Microcapsules in Cementitious Materials

Sodium Silicate as a Concrete Sealing Agent

Pelletier et al. investigated sodium silicate as a potential healing agent for concrete. The healing agent was embedded in the concrete matrix using microcapsules with a polyurethane shell that were produced by an interfacial polymerization process adapted from Saihi (Saihi et al. 2006). When sodium silicate is released to the cementitious matrix, it reacts with the calcium hydroxide in cement and produces a calcium-silicate-hydrate (C-S-H) gel that seals the cracks (Pelletier et al. 2010). C-S-H is a hydration product of cement that decreases the permeability of the cement paste and contributes to most of concrete's strength. A secondary product formed due to the reaction of sodium silicate and cement is sodium-silicate-hydrate, which contributes to the long-term strength of concrete.

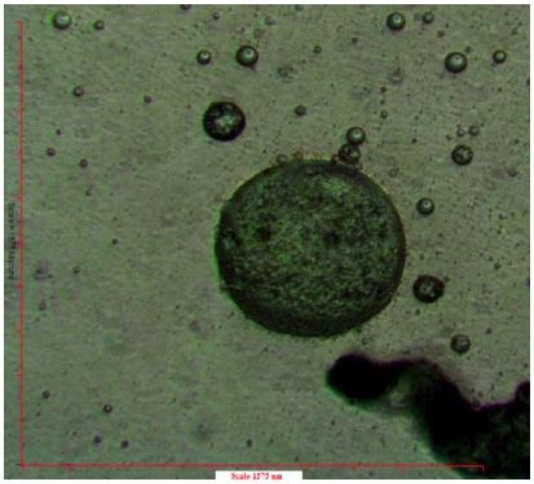

Figure 2.23. Light microscope image of polyurethane microcapsule (Pelletier et al. 2010).

Compressive strength and flexural strength tests were made for control specimens and samples containing microcapsules (2% by volume of cement). The samples were first damaged, left to heal for a week, and then retested. The results from the re-test suggested that the

microcapsules had a negligible impact on the compressive strength. With respect to the flexural tests, the results indicate that the control samples had a strength recovery of 10-14%. On the other hand, samples with microcapsules showed a superior strength recovery of 20-26%, and displayed a more ductile behavior.

Corrosion tests were also made for steel reinforced concrete samples with and without capsules by monitoring the open circuit potential of the rebar. All samples were in contact with sodium chloride until severe corrosion. Three control samples were severely corroded after being exposed for 96s, 118s, and 212s respectively. For the microcapsule containing samples, three samples reached severe corrosion after 15.6 min, 18.5 min, and 19 min respectively.

The corrosion tests can be explained by the fact that sodium silicate can form a passive layer to protect the steel reinforcement. The test results showed that those samples containing microcapsules were able to delay the severe corrosion level at the intermediate potential, unlike the control samples. In addition, it is possible that the ruptured microcapsules contributed to decreasing the permeability in the concrete matrix, and therefore decreased the chloride penetration. Overall, it was demonstrated that sodium silicate successfully triggered a self-healing mechanism in concrete, where it was found superior to the control specimens with respect to corrosion inhibition and strength recovery (Pelletier et al. 2010).

Self-Healing Using Oil Core/Silica Gel Shell Microcapsules

Yang et al. studied self-healing of mortar specimens that contain microencapsulated methylmethacrylate monomer (MMA) and triethylborane (TEB). MMA was selected as the healing agent, and was added to the mortar specimens at a concentration of 1.5% by weight of cement. TEB was selected as the catalyst, and was added at a concentration of 0.03% by wt. of

cement. The mortar specimens were reinforced with carbon microfibers for crack width control. The microcapsules were synthesized by an interfacial self-assembly process and sol–gel reaction.

The self-healing process is shown in the figure below. When the material matrix develops cracks, the microcapsules will rupture and release the healing agent and catalyst to initiate a polymerization reaction of MMA in room temperature and in the presence of air. Both the healing agent and the catalyst have a low viscosity to fill the cracks through capillary action.

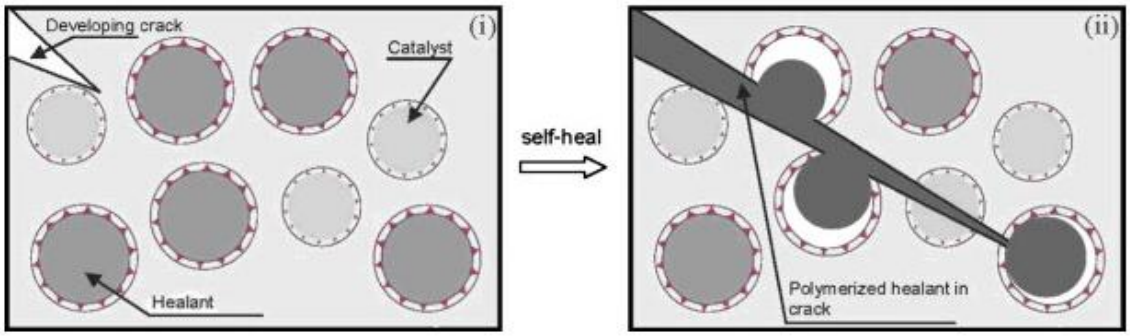

Figure 2.24. The self-healing mechanism of the microencapsulated healing agent and catalyst system (Yang et al. 2011).

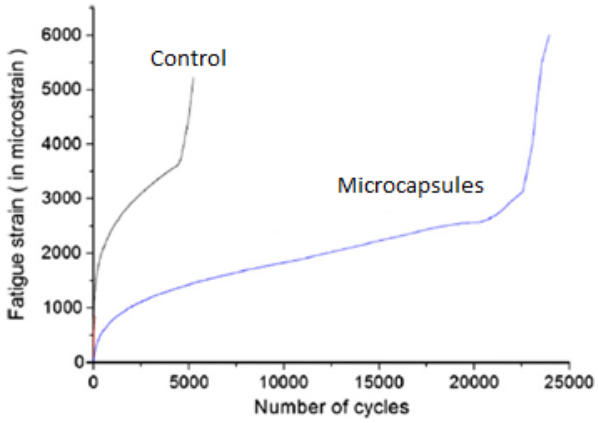

Figure 2.25. The development of fatigue strain with respect to the number of cyclic loads (Yang et al. 2011).

The permeability of the mortar specimens was measured by a gas permeability technique that uses liquid methanol as the gas source (Cabrera and Lynsdale 1988; Hoseini et al. 2009). The permeability test was conducted after the specimens were damaged and set aside to heal in laboratory conditions for 24 hours. The results indicated significant decreases in the permeability of microcapsule containing specimens. With respect to the fatigue tests, it was reported that the microcapsules improved the crack resistance and toughness of the specimens (Yang et al. 2011).

The self-healing mortar was examined under energy dispersive spectroscopy to analyze the chemical composition of the area containing surface. The results indicate that the surface of cracked area mainly consisted of Carbon, Oxygen and Silicon, suggesting that the void of the cracks was filled mainly with PMMA and some cracked silica gel shell. The Boron levels detected may come from the catalyst triethylborane (TEB). In addition, the relative elemental content of C to O in cracks (58.0 wt.% vs. 20.8 wt.%) was similar to that of PMMA (67.6 wt.% vs. 22.5 wt.%), indicating the release of healing agent and its polymerization 24 hours after the cracking event (Yang et al. 2011).

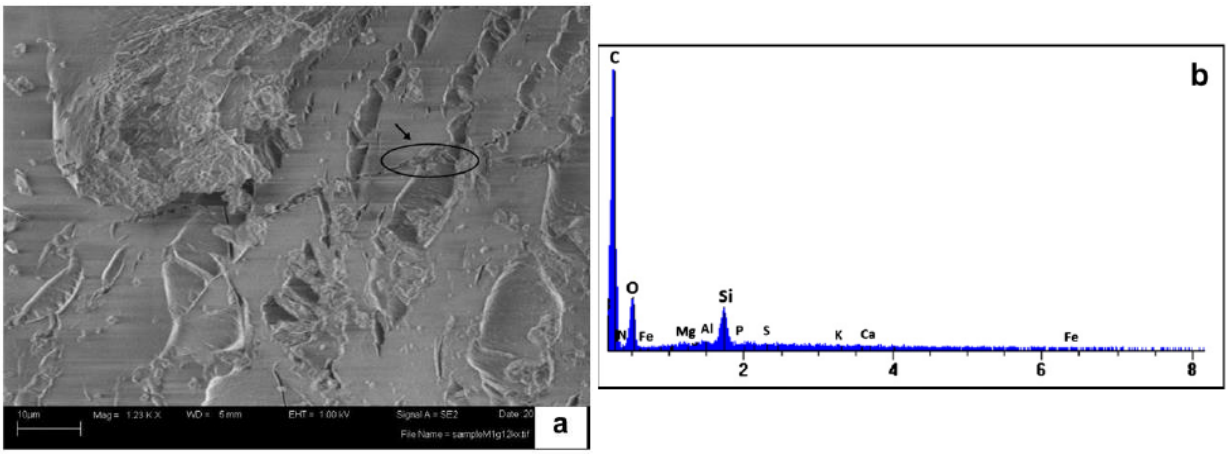

Figure 2.26. a) Electron microscope image of crack surface; b) EDS analysis at cracked surface (Yang, 2011)

Modeling Self-Healing by Further Hydration

A study conducted by Huang et al. (2012) focused on simulating self-healing concrete by providing extra water stored in microcapsules for further hydration of unhydrated cement (UHC). For most concrete specimens, a significant amount of cement particles does not react with water even after the hardening stage, particularly with high performance concrete specimens. Therefore, if a crack exposes these unhydrated cement grains to water, and the nucleation of calcite takes place, self-healing action is possible.

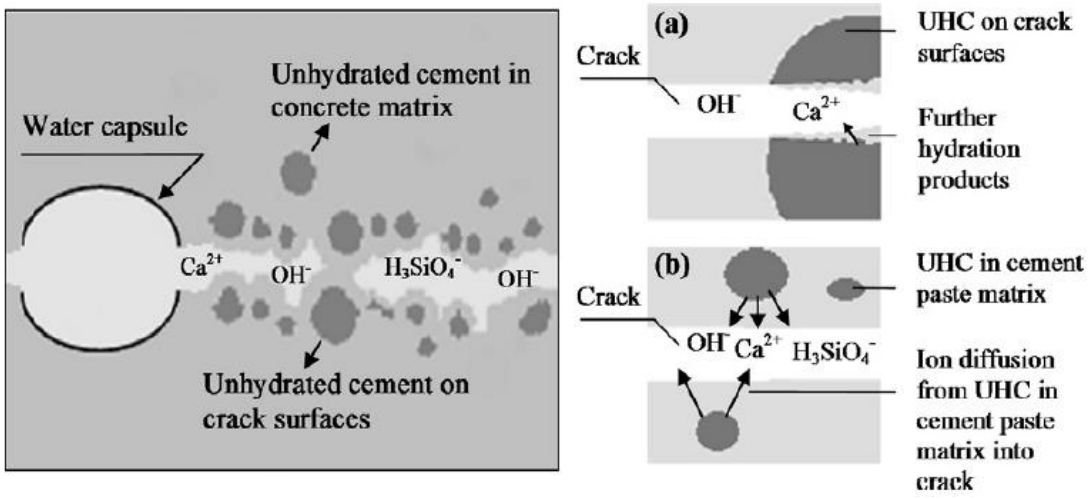

Figure 2.27. Schematic diagram of the healing mechanism of water capsules embedded in the cement matrix (Huang et al. 2012).

The self-healing mechanism is triggered by rupturing the capsules full of water through crack propagation. Once the water is released from the capsule, the unhydrated cement particles in the crack dissolve. Calcium (Ca^{2+}) ions and silicate (SiO_4^-) ions begin to diffuse out, and as a result, the concentrations of various ions in the solution increase. Once the concentrations of these ions reach a point of equilibrium, hydration products are formed by precipitation. The reaction process will therefore be governed by water transport theory, ion diffusion, and

precipitation of hydration products (Huang, 2012). Self-healing efficiency will also depend on the crack width, the amount of unhydrated cement, and the volume of water released by the ruptured capsules.

A numerical model was created by Huang et al. to simulate the effects of such factors with respect to self-healing. Self-healing efficiency was defined as the volume ratio of newly formed hydration products to the volume of the crack. Details on the cement paste, such as its water-cement ratio, age (assumed to be 1000 hours), and its chemical composition were all taken in account, and it estimated that 30% of the cement particles remained unhydrated after 1000 hours. The microcapsules were assumed to store three different volumes of water: 100 mm^3, 150 mm^3, and 200 mm^3, and the crack was assumed to be 40mm in length, 40 mm in depth, and 10 microns in width, resulting in a volume of 16 mm^3. If such crack were to remain saturated by water, the modeling results indicate that after 20 hours of further hydration, approximately 30% of the crack's volume is healed. After 20 hours, however, the rate of self-healing decreases because the transport of ions is hindered by those hydration products formed around unhydrated cement particles.

Since the amount of water is limited to the capsule's storage capacity, and the unhydrated cement grains consume water to enable the hydration reaction, the amount of time in which the crack will remain saturated is significantly shorter. If the capsules were to release 250 mm^3 of water or more, the formation of new hydration products decreases gradually after 7 hours. Huang's numerical model can be applied to any chemical healing agent, as long as the water transport parameters such as viscosity and surface tension are included.

Table 2.12. Summary of simulation results (Huang et al. 2012).

Water Provided by Capsules (mm^3)	Saturation Time (hours)	Self-healing Efficiency (%)
100	2	9.5
150	3	15.3
200	4.7	22.9

Microencapsulated Bacterial Spores

A study conducted by Wang et al. investigated the performance of bacteria for autonomous crack-repair of concrete through a microencapsulation approach (Wang et al. 2014). Through encapsulation, the bacterial agent can have a protection barrier from the unfavorable conditions inside the concrete matrix. This aspect is crucial in determining the feasibility of the bacterial concrete approach, because without encapsulation, Jonkers reported that bacteria that is known to last for 200 years in dry conditions was not able to survive in concrete for more than 4 months (Jonkers et al. 2010). If the capsules remain intact, the bacteria will stay inactive. However, when the bacterial spores are released, the healing mechanism will be activated in the presence of water, nutrients and oxygen.

The Bacillus sphaericus bacterial spores selected as the healing agent because of their ability to form calcium carbonate on crack surfaces through urease catalyzed urea hydrolysis. Such bacterial specimen was encapsulated by an interfacial polycondensation technique, where the average capsule size was approximately 5 microns and the shell materials were impermeable and melamine based. The concentration of the bacterial spores inside the microcapsules was estimated to be at 109 cells/g microcapsules (dry weight). The main advantage to these microcapsules are that they are resistant to high pH environments, and were found to withstand the concrete mixing process successfully. Along the microcapsules, some concrete specimens

were also mixed with the following nutrients: yeast extract as the precursor for the bacterial spores, and the deposition agents such as urea and calcium nitrate.

The experimental matrix contained six different samples to be tested to determine the self-healing capacity: 1) R, Control samples that had no microcapsules with bacteria nor any nutrients, 2) N, A group of samples that contained nutrients only, with no microcapsules or bacteria, 3) C, samples with microcapsules containing no bacteria nor nutrients in the concrete matrix, 4) NC, microcapsules with no bacterial spores but with nutrients embedded in the concrete matrix, 5) NCS3%, microcapsules containing bacterial spores (added at 3% of the cement weight) and nutrients, 6) NCS5%, microcapsules containing bacterial spores (added at 5% of the cement weight) and nutrients.

Table 2.13. Details of the mix designs for each group of samples (Jonkers et al. 2010).

Group	Cement (g)	Sand (g)	Water (g)	Nutrients (g)	Dry weight of Microcapsules	Bacterial Spores
R	450	1350	225	0	0	N
N	450	1350	214	57.8	0	N
C	450	1350	212.4	0	13.5	N
NC	450	1350	201.4	57.8	13.5	N
NCS3%	450	1350	192.8	57.8	13.5	Y
NCS5%	450	1350	178.7	57.8	22.5	Y

The cracked specimens were monitored for two months and after subjecting them to five different curing conditions: 1) air at 20 °C and 95% relative humidity, 2) immersion in water at 20 °C, 3) immersion in a solution of 0.2 M urea and 0.2 M calcium nitrate at 20 °C, 4) wet-dry cycles with water at 20 °C and 60% relative humidity, 5) wet-dry cycles in a solution of 0.2 M urea and 0.2 M calcium nitrate at 20 °C and 60% relative humidity. The wet-dry cycles included 16 hours of water submersion and 8 hours of air exposure.

The self-healing efficiency was calculated as a ratio between the healed crack area and the initial crack area. The results demonstrated that specimens containing microencapsulated bacterial spores produced high healing ratios ranging from 48% to 80%, while those specimens without bacteria had healing efficiencies ranging from 18-50% due to the autogenous healing mechanism of concrete. In addition, the largest crack width healed in the bacterial specimens was 970 microns, while the non-bacteria specimens healed up to 250 microns. The average coefficient of water permeability was found to be 10 times lower for specimens with encapsulated bacteria than for those without bacteria. There was a negligible difference however, on the specimens that had a concentration of 3% (by weight of cement) of microcapsules with bacteria with specimens that had 5% microcapsules with bacteria.

It is important to note that the healing capacity was highly dependent on the incubation method. There was no healing observed for any sample of any group when incubated in air at 20 °C and 95% relative humidity. Hence, water in its liquid form was a crucial component to activate the healing mechanism. This is due to the fact that bacterial spores need water to be activated, and the nutrients embedded in the concrete matrix need to be dissolved in order to be utilized by the bacteria. If water is not available where the crack was formed, there cannot be any calcium carbonate precipitate and therefore no healing.

The healing efficiency was not increased in proportion with the amount of encapsulated bacteria in concrete. In fact, for the specimens that were left to heal in wet-dry cycles, the 3% microcapsule level yielded better healing ratios than the 5% microcapsule level. Since the microcapsule shell material is impermeable, it is possible that some areas that were covered by the burst microcapsules and therefore limited the water availability in these regions. If the penetration of water is hindered in these areas, some of the necessary nutrients may not be

dissolved and therefore the bacterial spores will be limited to their capacity to precipitate calcium carbonate.

For the specimens containing encapsulated bacteria, the best healing efficiency was achieved under wet-dry cycles with water as it yielded higher healing ratios and reduced permeability. This is because bacteria need both water and oxygen to form calcium carbonate crystals at the surface cracks. Therefore, in the wet cycle, the nutrients were dissolved by water and the bacteria's function is activated. During the dry cycles, more oxygen is available for the bacteria. On the other hand, those samples that were submerged in water for the entire incubation period had less oxygen available and also had the problem of having more bacteria or nutrients leaking out from the crack surfaces to the water surrounding the specimen. The figure below shows the evolution of the crack-healing process of a specimen that was subjected to wet-dry cycles with water, containing 5% of capsules containing bacteria by weight of cement.

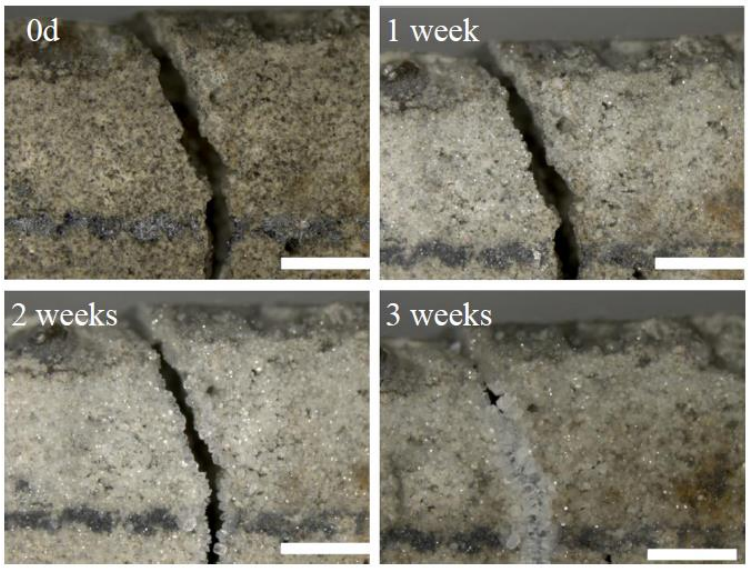

Figure 2.28. Crack-healing process of microencapsulated bacteria under wet dry cycles (Jonkers et al. 2010)

2.5.2 Microcapsules in Polymeric Materials

Polymers and structural composites are used in a variety of applications, including civil infrastructure. For this reason, it is important to minimize any microcrack propagation to protect its structural integrity. Self-healing polymers show great potential as they have the capability to recover their load transferring ability after damage. The healing mechanism can occur autonomously, or be activated by a specific stimulus (Wu et al. 2008). In this study, the literature review on polymeric materials will be focused on self-healing through microencapsulated healing agents.

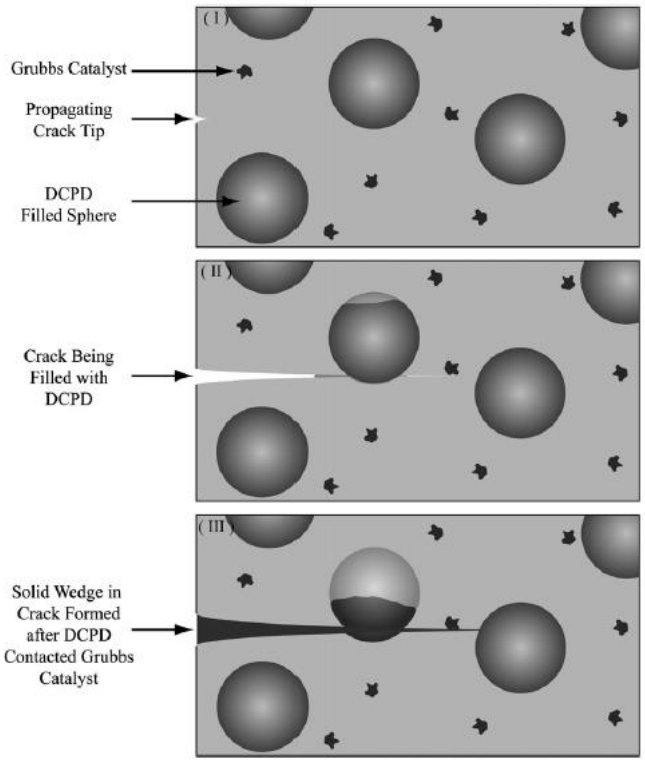

Figure 2.29. Concept of self-healing polymers by microencapsulated healing agents

The main self-healing system studied is based on a process known as living ring-opening metathesis polymerization (ROMP). The typical healing agent and catalyst used for such reaction is dicyclopentadiene (DCPD) and Grubb's catalyst, respectively. This process can be activated

autonomously by microencapsulating the healing agent and dispersing the catalyst within a polymer matrix (White et al. 2001). When the specimens are cracked, the microcapsules will rupture and release DCPD into the crack area. Once the healing agent makes contact with the catalyst, a polymerization reaction occurs to effectively seal the crack (Wu et al. 2008).

The number of microcapsules embedded in the polymer matrix will have an impact in the material's intrinsic properties. It has been observed that a high concentration of microcapsules will decrease the modulus and the ultimate strength of the polymer matrix (Brown 2004). Nevertheless, if an optimal number of capsules are added, self-healing can take place without sacrificing much of the material's strength.

White et al. introduced DCPD microcapsules in an epoxy resin containing Grubb's catalyst. The specimen was loaded to fracture, and reported a 75% recovery in toughness after healing (White et al. 2001). Once the success of the self-healing system was confirmed, Brown et al. investigated the effect of the microcapsule size and loading on the healing efficiency of the neat epoxy matrix (Brown 2004). It was reported that both the virgin and healed fracture toughness levels were affected by the size and concentration of the DCPD microcapsules added. The fracture toughness increased with microcapsule concentration until reaching a maximum value. Similarly, the healed fracture toughness increased with the microcapsule concentration until reaching a concentration of 20 vol.% (Brown 2004).

The influence of microcapsule diameter and crack size on the performance of self-healing materials was investigated by Rule et al. (Rule et al. 2007). An epoxy matrix embedded with Grubbs' catalyst particles and microencapsulated DCPD were tested. It was reported that the amount of liquid that microcapsules release to a crack surface is found to have a linear relationship with the microcapsule size for a given weight fraction of capsules. In addition, the

highest self-healing potential can only be realized if the amount of healing agent available is enough fill the crack completely. Based on these relationships, the size and weight fraction of microcapsules can be calculated to maximize the healing potential of a predetermined crack size (Rule et al. 2007).

2.6 Examination of Self-Healing Concrete

2.6.1 Curing Regimes

Roig-Flores et al. studied the influence of the environmental conditions on the crystalline admixture's healing efficiency. Four different curing conditions were investigated: full water immersion (WI), water contact where cylinders were submerged to 2 cm of water and exposed at 20 °C with 95% relative humidity (WC), humidity chamber at 20 °C and 95% relative humidity (HC), and air exposure at laboratory conditions at 17 °C and 40% relative humidity (AE). The healing period was set 42 days after damaging the samples (Roig-Flores et al. 2015).

Yang et al. investigated the healing capability after damaging the Engineering Cementitious Composites (ECC) specimens under two curing conditions. The first condition (CR1) consisted of a wet-dry cycle in which the sample was submerged in water for 24 hours at a temperature of 21 °C, and then air dried at 21 °C for 24 hours. The second condition (CR2) consisted of a wet-dry cycle in which the sample was submerged in water for 24 hours at a temperature of 20 °C, followed by oven drying at 55 °C for 22 hours, and finally cooled for 2 hours at 21 °C. These wet-dry cycles were selected to simulate the changing climate conditions that structures typically experience (Yang et al. 2009). Similarly, Kan et al. investigated ECC specimens after damage under one wet-dry cycle consisting of a full water submersion at 20 °C for 24 hours, and air drying at 20 °C with a relative humidity of 50 ± 5% for 24 hours (Kan and Shi 2012).

Tittelboom et al. submerged all cracked samples in water to enable the autogenous healing mechanism of concrete. The samples were then monitored at 1, 4, 7, 14, 21, and 42 days respectively. After such healing periods, the samples were dried and the evolution of the crack repair was monitored under a scanning electron microscope (Van Tittelboom et al. 2012). Similarly, Jonkers et al. broke up control and bacterial concrete specimens after 7 or 28 days of curing, and subsequently submerged in tap water at room temperature for 8 days for healing (Jonkers et al. 2010).

Wang et al. monitored cracked specimens subjected to five curing conditions for two months: 1) air at 20 °C and 95% relative humidity, 2) immersion in water at 20 °C, 3) immersion in a solution of 0.2 M urea and 0.2 M calcium nitrate at 20 °C, 4) wet-dry cycles with water at 20 °C and 60% relative humidity, 5) wet-dry cycles in a solution of 0.2 M urea and 0.2 M calcium nitrate at 20 °C and 60% relative humidity. The wet-dry cycles included 16 hours of water submersion and 8 hours of air exposure (Wang et al. 2014).

2.6.2 Material Tests

Cracking/Damage Strategy

Roig-Flores et al. incorporated 40 kg/m^3 of steel fibers in the concrete mix design to control the crack width when damaging the samples. Cylindrical specimens of 150 mm in diameter and 150 mm in length at the age of 2 days were damaged by a splitting tensile test set to induce controlled cracks up to 0.3 mm in width. The crack propagation was measured and controlled by a calibration ruler (Roig-Flores et al. 2015).

Yang et al. utilized a servo-hydraulic testing system was used in displacement control mode to induce cracks with a uniaxial tensile test. The loading rate used was 0.0025 mm/s to

simulate a quasi-static loading condition. Two external linear variable displacement transducers were attached to the specimen to measure the specimen deformation. Five different damage levels were induced, where the tensile loading percentage varied from 0.3, 0.5, 1.0, 2.0, and 3.0 percent strain. The nature of the ECCs controlled the crack width propagation (Yang et al. 2009).

Wang et al. cracked long reinforced concrete prisms of 30 mm x 30 mm x 360 mm after 28 days of curing using a uniaxial tensile test, where a loading rate of 0.01 mm/s was applied under stroke control. Once a crack width of 150 microns was obtained, the test was stopped. Cracking was caused by a uniaxial tensile load that generated average crack widths of 150 microns. In addition, cylinders of 78 mm in diameter and 22 mm in height were cracked by a splitting tensile test, where the crack width was controlled by the attached LVDT's measurement of the crack opening (Picandet et al. 2009; Wang et al. 2014).

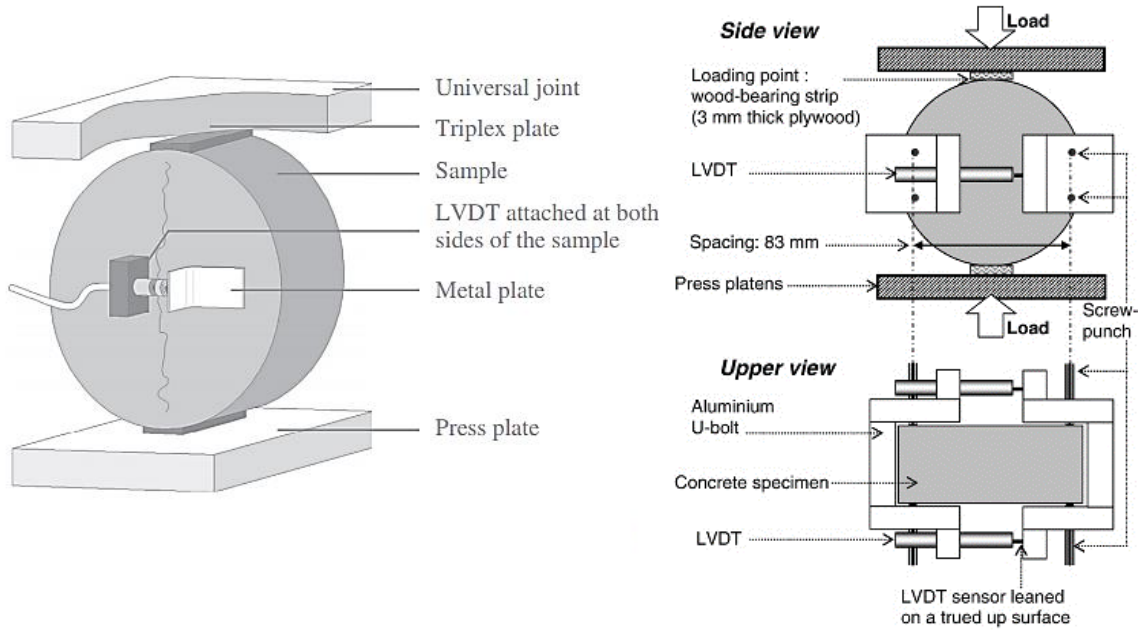

Figure 2.30. Splitting test setup to induce cracks, with and without an aluminum U-bolt apparatus (Picandet et al. 2009; Van Tittelboom et al. 2011)

Permeability

Roig-Flores et al. used adapted a permeability test per the UNE-EN 12390-8 standard, by measuring the water flow instead of the water depth penetration. The test was performed by applying a head water pressure equal to 2.00 ± 0.05 bars. The quantity of water passing through the crack was measured during a 5 min testing time. This procedure results in higher water flows for larger crack widths. In this way, if a crack closes after the healing process, the water flow should have been diminished (Roig-Flores et al. 2015).

Li et al. conducted a permeability test using a falling head test for specimens with a low permeability, and a constant head test for specimens with large crack widths (Yang et al. 2009). The falling head and constant head permeability test setups were adapted from Wang et al. and Cernica (Cernica 1982; Wang et al. 1997).

Another study slightly modified a permeability test from the low pressure water permeability test described by Wang et al. for an evaluation of self-healing in concrete (Wang et al. 1997). Tests were therefore conducted before and after the specimens were damaged. First, the cylinders were immersed in water for 3 days. Next, specimens were taken out from water and dried at room temperature. The surface dry cylinders were then mounted inside a PVC ring and vacuum saturated as described in NBN B 24-213 (NBN, 1976). After two to three hours, de-mineralized water was added into the vacuum chamber with the vacuum turned on. Once the cylinders were submerged in water, the vacuum was turned off. After leaving the cylinders submerged in water for 24 hours, they were taken out from the vacuum chamber and put into the following setup of the water permeability test (Wang et al. 2012).

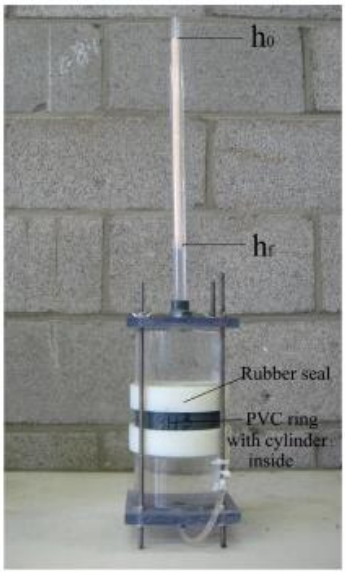

Figure 2.31. Setup of water permeability test used (Wang et al. 2012)

Yang et al. used gas permeability for concrete, where liquid methanol is the gas source. Its main advantage is that it is an easy and fast method of measuring the specimen's coefficient of permeability (Cabrera and Lynsdale 1988; Yang et al. 2011). For mortar and concrete specimens, the test setup can be adapted from a study by Alshamsi. The samples must be oven dried at 105 degrees Celsius prior to testing to eliminate moisture. Next, methanol is placed in the permeability cell, and the samples are placed at the top part of the cell and sealed with silicone rubber (shown in the figure below). The cell is then partially submerged in water, leaving the top part that holds the sample exposed in air. The rate of mass loss is recorded at different time intervals until a steady-state flow is achieved (Alshamsi and Imran 2002).

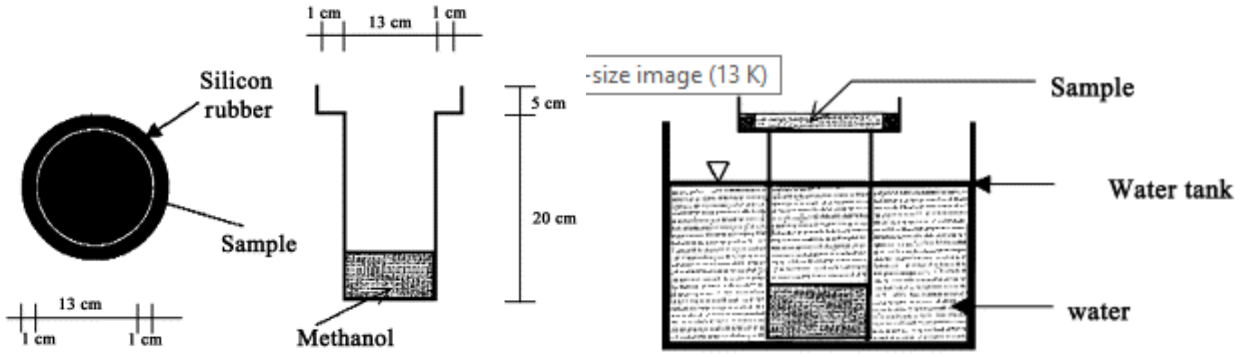

Figure 2.32. The left image shows the permeability cell, and the right image the test setup (Alshamsi and Imran 2002).

Resistance to chloride

Corrosion tests give an indication of permeability of samples containing steel reinforcement, as well as the potential corrosion inhibition of a healing agent. Pelletier et al. induced cracks of an arbitrary size on the samples and then immersed them in sodium chloride solution until severe corrosion was detected. The corrosion level was measured by the open circuit potential of the rebar. The test describes four general categories of corrosion: 1) A potential higher than -0.20 V indicates a low risk of corrosion, 2) A potential between -0.20 V and -0.35 V suggests intermediate corrosion, 3) A potential between -0.35 V and -0.50 V implies a high risk of corrosion, and 4) A potential lower than -0.50 V suggests severe corrosion (Pelletier et al. 2010).

Rupnow et al. developed a test procedure known as DOTD TR 233-11 to determine the electrical resistivity of concrete to provide a rapid indication of its resistance to the penetration of chloride ions (Rupnow and Icenogle 2012). The test method was adopted by Louisiana's Department of Transportation and Development as an approved alternative to the ASTM C1202 standard. The test method has a high correlation with the ASTM C1202 test for a variety of mix designs, and requires 28 days of moist curing prior to testing. The surface resistivity is measured

by a Wenner array probe, and requires 8 readings to be taken per sample (where each measurement is taken after rotating the specimen 90 degrees). The test is not suitable for specimens containing reinforcing or concrete admixed with calcium nitrite, however.

Pore Size Distribution

In a study of bio-concrete, Jonkers et al. measured the effect of the embedded bacteria in the pore size distribution on concrete cured at the ages of 3, 7, and 28 days. For young specimens was determined by mercury intrusion porosimetry (MIP). For aged specimens, small pieces of 0.5 cm x 0.5 cm x 0.5 cm were cut, frozen in liquid nitrogen, and subjected to cryo-vacuum evaporation for two weeks to remove any water inside the pores before subjecting them to the MIP test (Jonkers et al. 2010). Wang et al. performed the same MIP procedure to determine the influence of the microcapsules on the porosity and pore size distribution of concrete (Wang et al. 2014).

Strength Tests

Jonkers et al. performed compressive strength tests to evaluate the effects of bacteria on concrete cured at the ages of 3, 7, and 28 days. The concrete samples had dimensions of 4 cm x 4cm x 4cm, and those specimens containing bacteria had a range of 1 to 10 x 10^8 spores per cubic centimeter of concrete (Jonkers et al. 2010).

Pelletier et al. used compressive strength tests adapted from ASTM C109 for control specimens and samples containing microcapsules (2% by volume of cement). All samples were subjected to two tests. The first test involved loading the specimens to their maximum load, but not allowed to fail. Next, the samples were left to heal for one week, and retested to failure. In another experiment, two flexural strength tests were conducted per sample by an adaptation of the ASTM C348-97 standard. For the first test, the sample was loaded to its maximum load, but

stopped before failure. The samples were then allowed to heal for another week, and retested to failure (Pelletier et al. 2010).

Yang et al. performed tensile strength, strain capacity, and stiffness tests under uniaxial loading after the damaged specimens were exposed to various environments to quantify mechanical self-healing (Yang et al. 2009). In another study, fatigue tests under uniaxial compression cyclic loading were performed to measure the endurance of self-healing mortar (Yang et al. 2011).

Non-Destructive Testing

Yang et al. subjected the ECC samples to a non-destructive test method known as resonant frequency (RF) to measure the extent of the specimen's damage. Therefore, an initial scan of RF was made to the undamaged samples, and after loading another RF scan was made to measure the degree of damage. If healing was to take place, the RF scan should see a gradual recovery towards the initial RF measurements (Yang et al. 2009).

The ultrasonic phase velocity (UPV) method has been increasingly used to determine the healing capacity of cracked concrete samples (Abdel-Jawad and Haddad 1992). Jacobsen et al. found that the self-healing of microcracking can be examined by UPV and that UPV parameters correlate moderately with the actual damage levels (Jacobsen et al. 1996). Zhong et al. used the UPV method to define the ratio of damage degree to self-healing in high and normal strength concrete damaged at different ages (Zhong and Yao 2008). However, it has been found that while UPV measurements can detect the occurrence of crack healing, it is unable to provide accurate information on the depth or width of the cracks before and after healing (Aldea et al. 2000).

Diffuse ultrasonic techniques can be used to characterize microcracking and to measure the depth of large cracks in cementitious materials. It has also been confirmed that diffusivity is sensitive to microcracking and microstructural behavior (Becker et al. 2003)(Punurai et al. 2007)(Schurr et al. 2011). Other studies have numerically and experimentally shown that the diffuse ultrasonic technique can measure the depth of surface opening cracks using the arrival time of maximum energy (ATME) (Ramamoorthy et al. 2004)(In et al. 2012; Seher et al. 2013).

2.7 References

Abdel-Jawad, Y., and Haddad, R. (1992). "Effect of early overloading of concrete on strength at later ages." *Cement and Concrete Research*, 22(5), 927–936.

Abdelrazig, B. E. ., Bonner, D. ., Nowell, D. ., Dransfield, J. ., and Egan, P. . (1999). "The solution chemistry and early hydration of ordinary portland cement pastes with and without admixtures." *Thermochimica Acta*, 340-341, 417–430.

Aggoun, S., Cheikh-Zouaoui, M., Chikh, N., and Duval, R. (2008). "Effect of some admixtures on the setting time and strength evolution of cement pastes at early ages." *Construction and Building Materials*, 22(2), 106–110.

Al-Amoudi, O. S. B., Maslehuddin, M., Lashari, A. N., and Almusallam, A. A. (2003). "Effectiveness of corrosion inhibitors in contaminated concrete." *Cement and Concrete Composites*, 25(4-5 SPEC), 439–449.

Aldea, C., Song, W., Popovics, J., and Shah, S. (2000). "Extent of Healing of Cracked Normal Strength Concrete." *Journal of Materials in Civil Engineering*, American Society of Civil Engineers, 12(1), 92–96.

Alshamsi, A. M., and Imran, H. D. A. (2002). "Development of a permeability apparatus for concrete and mortar." *Cement and Concrete Research*, 32(6), 923–929.

Bang, S. S., Galinat, J. K., and Ramakrishnan, V. (2001). "Calcite precipitation induced by polyurethane-immobilized Bacillus pasteurii." *Enzyme and Microbial Technology*, 28(4-5), 404–409.

Becker, J., Jacobs, L., and Qu, J. (2003). "Characterization of Cement-Based Materials Using Diffuse Ultrasound." *Journal of Engineering Mechanics*, American Society of Civil Engineers, 129(12), 1478–1484.

Brown, E. N. (2004). "Microcapsule induced toughening in a self-healing polymer composite." 9, 1703–1710.

Cabrera, J. G., and Lynsdale, C. J. (1988). "A new gas permeameter for measuring the permeability of mortar and concrete." *Magazine of Concrete Research*, 40(144), 177–182.

Cernica, J. N. (1982). *Geotechnical Engineering*. Holt, Reinhart and Winston, New York.

Dietrich, K., Bonatz, E., Geistlinger, H., Herma, H., Nastke, R., Purz, H. -J., Schlawne, M., and Teige, W. (1989). "Amino resin microcapsules. II. Preparation and morphology." *Acta Polymerica*, Akademie Verlag GmbH, 40(5), 325–331.

Dry, C. M. (1994). "Smart multiphase composite materials that repair themselves by a release of liquids that become solids." 62–70.

Dry, C. M. (2001). "Design of self-growing, self-sensing, and self-repairing materials for

engineering applications." *Proc. SPIE*.

EPA. (2010). *Available and Emerging Technologies for Reducing Greenhouse Gas Emissions from the Portland Cement Industry*.

Fan, C., and Zhou, X. (2011). "Effect of emulsifier on poly(urea-formaldehyde) microencapsulation of tetrachloroethylene." *Polymer Bulletin*, 67(1), 15–27.

Ghosh, S. K. (2006). "Functional Coatings and Microencapsulation: A General Perspective." *Functional Coatings*, Wiley-VCH Verlag GmbH & Co. KGaA, 1–28.

Hammes, F., and Verstraete, W. (2002). "Key roles of pH and calcium metabolism in microbial carbonate precipitation." *Reviews in Environmental Science and Biotechnology*, 1(1), 3–7.

Hearn, N. (1998). "Self-sealing, autogenous healing and continued hydration: What is the difference?" *Materials and Structures*, 31(8), 563–567.

Hilloulin, B., Tittelboom, K. Van, Gruyaert, E., Belie, N. De, and Loukili, A. (2015). "Cement & Concrete Composites Design of polymeric capsules for self-healing concrete." *Cement and Concrete Composites*, Elsevier Ltd, 55, 298–307.

Hoseini, M., Bindiganavile, V., and Banthia, N. (2009). "The effect of mechanical stress on permeability of concrete: A review." *Cement and Concrete Composites*, 31(4), 213–220.

IEA. (2009). *Cement Technology Roadmap 2009: Carbon emissions reductions up to 2050*.

In, C. W., Kim, J.-Y., Jacobs, L. L., and Kurtis, K. (2012). "Crack depth measurement in concrete using diffuse ultrasound." *AIP Conference Proceedings*, 1430(1).

The Strategic Development Council (SDC) (2006). "Vision 2020: A vision for the concrete repair protection and strengthening industry" (http://www.concretesdc.org/_pdfs/vision2020-version1.0_%20may2006.pdf) (April 10, 2015).

Jacobsen, S., Marchland, J., and Boisvert, L. (1996). "Effect of cracking and healing on chloride transport in OPC concrete." United States.

Jonkers, H. M., Thijssen, A., Muyzer, G., Copuroglu, O., and Schlangen, E. (2010). "Application of bacteria as self-healing agent for the development of sustainable concrete." *Ecological Engineering*, 36(2), 230–235.

Justnes, H. (2010). "Calcium nitrate as a multi-functional concrete admixture." *Concrete (London)*, 44(1), 34–36.

Justnes, H., and Nygaard, E. C. (1993). "Technical Nitrate as Set Accelerator for Cement." *Nordic Concrete Research*, 13(2), 70–87.

Justnes, H., and Nygaard, E. C. (1995). "Technical calcium nitrate as set accelerator for cement at low temperatures." *Cement and Concrete Research*, 25(8), 1766–1774.

Kan, L. L., and Shi, H. S. (2012). “Investigation of self-healing behavior of Engineered Cementitious Composites (ECC) materials.” *Construction and Building Materials*, Elsevier Ltd, 29, 348–356.

Li, V. C. (2003). “On engineered cementitious composites (ECC). A review of the material and its applications.” *Journal of Advanced Concrete Technology*, 1(3), 215–230.

Li, V. C., and Herbert, E. (2012). “Robust Self-Healing Concrete for Sustainable Infrastructure.” *Journal of Advanced Concrete Technology*, 10(6), 207–218.

De Muynck, W., Cox, K., Belie, N. De, and Verstraete, W. (2008a). “Bacterial carbonate precipitation as an alternative surface treatment for concrete.” *Construction and Building Materials*, 22(5), 875–885.

De Muynck, W., Debrouwer, D., De Belie, N., and Verstraete, W. (2008b). “Bacterial carbonate precipitation improves the durability of cementitious materials.” *Cement and Concrete Research*, 38(7), 1005–1014.

Pelletier, M. M., Brown, R., Shukla, A., and Bose, A. (2010). “Self-healing concrete with a microencapsulated healing agent.” *University of Rhode Island, Kingston,USA*, (C).

Picandet, V., Khelidj, A., and Bellegou, H. (2009). “Crack effects on gas and water permeability of concretes.” *Cement and Concrete Research*, 39(6), 537–547.

Punurai, W., Jarzynski, J., Qu, J., Kurtis, K. E., and Jacobs, L. J. (2007). “Characterization of dissipation losses in cement paste with diffuse ultrasound.” *Mechanics Research Communications*, 34(3), 289–294.

Ramakrishnan, V. (2007). “Performance characteristic of bacterial concrete - a smart biomaterial.” *First International Conference on Recent Advances in Concrete Technology*, 67–78.

Ramamoorthy, S. K., Kane, Y., and Turner, J. A. (2004). “Ultrasound Diffusion for Crack Depth Determination in Concrete.” *Acoustical Imaging*, W. Arnold and S. Hirsekorn, eds., Springer Netherlands, Dordrecht, 121–128.

Rodson, M., and Scher, H. B. (2000). “Water-in-oil microencapsulation process and microcapsules produced thereby.” Google Patents.

Roig-Flores, M., Moscato, S., Serna, P., and Ferrara, L. (2015). “Self-healing capability of concrete with crystalline admixtures in different environments.” *Construction and Building Materials*, Elsevier Ltd, 86, 1–11.

La Rosa Thompson, J. ., Silsbee, M. R., Gill, P. M., and Scheetz, B. E. (1997). “Characterization of silicate sealers on concrete.” *Cement and Concrete Research*, 27(10), 1561–1567.

Rule, J. D., Sottos, N. R., and White, S. R. (2007). “Effect of microcapsule size on the performance of self-healing polymers.” *Polymer*, 48(12), 3520–3529.

Rupnow, T., and Icenogle, P. (2012). “Surface Resistivity Measurements Evaluated as Alternative to Rapid Chloride Permeability Test for Quality Assurance and Acceptance.” *Transportation Research Record: Journal of the Transportation Research Board*, Transportation Research Board, 2290, 30–37.

Saihi, D., Vroman, I., Giraud, S., and Bourbigot, S. (2006). “Microencapsulation of ammonium phosphate with a polyurethane shell. Part II. Interfacial polymerization technique.” *Reactive and Functional Polymers*, 66(10), 1118–1125.

Schlangen, E., and Sangadji, S. (2013). “Addressing infrastructure durability and sustainability by self healing mechanisms - Recent advances in self healing concrete and asphalt.” *Procedia Engineering*, Elsevier B.V., 54, 39–57.

Schlegel, H., Zaborosch, C., and Kogut, M. (1993). *General Microbiology*. Cambridge University Press.

Schurr, D. P., Kim, J. Y., Sabra, K. G., and Jacobs, L. J. (2011). “Damage detection in concrete using coda wave interferometry.” *NDT and E International*, Elsevier, 44(8), 728–735.

Seher, M., In, C.-W., Kim, J.-Y., Kurtis, K. E., and Jacobs, L. J. (2013). “Numerical and Experimental Study of Crack Depth Measurement in Concrete Using Diffuse Ultrasound.” *Journal of Nondestructive Evaluation*, 32(1), 81–92.

Sun, G., and Zhang, Z. (2002). “Mechanical strength of microcapsules made of different wall materials.” *International Journal of Pharmaceutics*, 242(1-2), 307–311.

Van Tittelboom, K., and De Belie, N. (2013). *Self-healing in cementitious materials-a review*. *Materials*.

Van Tittelboom, K., De Belie, N., Van Loo, D., and Jacobs, P. (2011). “Self-healing efficiency of cementitious materials containing tubular capsules filled with healing agent.” *Cement and Concrete Composites*, Elsevier Ltd, 33(4), 497–505.

Van Tittelboom, K., Gruyaert, E., Rahier, H., and De Belie, N. (2012). “Influence of mix composition on the extent of autogenous crack healing by continued hydration or calcium carbonate formation.” *Construction and Building Materials*, Elsevier Ltd, 37, 349–359.

Wang, J., Van Tittelboom, K., De Belie, N., and Verstraete, W. (2012). “Use of silica gel or polyurethane immobilized bacteria for self-healing concrete.” *Construction and Building Materials*, Elsevier Ltd, 26(1), 532–540.

Wang, J. Y., Soens, H., Verstraete, W., and De Belie, N. (2014). “Self-healing concrete by use of microencapsulated bacterial spores.” *Cement and Concrete Research*, Elsevier Ltd, 56, 139–152.

Wang, K., Jansen, D. C., Shah, S. P., and F.KArr, A. (1997). “Permeability study of cracked concrete.” *Cement and Concrete Research*, 27(3), 381–393.

White, S. R., Sottos, N. R., Geubelle, P. H., Moore, J. S., Kessler, M. R., Sriram, S. R., Brown, E. N., and Viswanathan, S. (2001). "Autonomic healing of polymer composites." *Nature*, Macmillian Magazines Ltd., 409(6822), 794–797.

Wu, D. Y., Meure, S., and Solomon, D. (2008). "Self-healing polymeric materials: A review of recent developments." *Progress in Polymer Science*, 33(5), 479–522.

Wu, M., Johannesson, B., and Geiker, M. (2012). "A review : Self-healing in cementitious materials and engineered cementitious composite as a self-healing material." *Construction and Building Materials*, Elsevier Ltd, 28(1), 571–583.

Yang, Y., Lepech, M. D., Yang, E. H., and Li, V. C. (2009). "Autogenous healing of engineered cementitious composites under wet-dry cycles." *Cement and Concrete Research*, Elsevier Ltd, 39(5), 382–390.

Yang, Z., Hollar, J., He, X., and Shi, X. (2011). "A self-healing cementitious composite using oil core/silica gel shell microcapsules." *Cement and Concrete Composites*, Elsevier Ltd, 33(4), 506–512.

Zhong, W., and Yao, W. (2008). "Influence of damage degree on self-healing of concrete." *Construction and Building Materials*, 22(6), 1137–1142.

NBN B 24-213. Belgian standard: Experiments on masonry-Water absorption under vacuum; 1976.

CHAPTER 3

MICRO-ENCAPSULATION OF CALCIUM NITRATE FOR CONCRETE APPLICATIONS

3.1 Introduction

Concrete structures exposed to natural environments are prone to cracks due to many factors such as excessive loadings, restrained shrinkage, as well as harsh environmental conditions *(1).* Cracks are detrimental to structure by either weakening its mechanical properties, or lowering its durability by creating pathways for harmful agents to enter the structure and attack the steel reinforcement and concrete (Herbert and Li 2013). Recently, many countries including the United States, Germany, and South Korea experienced extraordinary civil infrastructure deteriorations, such that the annual amount spent on repair and rehabilitation has exceeded the cost of new infrastructure construction (Li and Herbert 2012). In the United States alone, the annual economic impact related to maintenance, repair, as well as replacing the deteriorating structures is estimated to be 18 to 21 billion dollars (Li and Herbert 2012). In addition, the American Society of Civil Engineers (ASCE) stated that over the next five years, about $2.2 trillion is needed for repair and for retrofit. It is estimated that half of those concrete repairs fail and require re-repair, which raises concerns about the quality of repairing methods (Li and Herbert 2012).

The concept of self-healing has recently emerged as a promising method to repair those deteriorating infrastructures. Given the fact that cracking is the major failure mechanism leading to deteriorating structures, special attention has been given to crack repair (Li and Herbert 2012). One way to fix those cracks is inserting microcapsules into the concrete mix. Such microcapsules would store the healing agent and provide a mechanical way for the self-healing

process when damages occur. When the cracks form, the microcapsules would rupture and release the healing agent to seal the crack (White et al. 2001; Brown et al. 2003). For this mechanism to be effective, the microcapsules must have enough strength to be intact in the concrete matrix, and should only rupture when concrete is damaged. For durability, the microcapsules have to resist leakage as well as the healing agent diffusion for a long time (Brown et al. 2003).

Both microcapsule sizes and diameters affect the healing process to a great extent *(5)*. For this reason, studying microcapsules' size and diameter is critical for crack healing optimization. Many studies were conducted to determine the best size for microcapsules for an optimum self-healing process (Aïssa et al. 2012). Studies have reported that a suitable size for microcapsules is 100 μm. Although this size is suitable for crack healing in many applications, many studies attempted to decrease microcapsules' size (Aïssa et al. 2012). However, to achieve an efficient self-healing mechanism, it was proven that smaller size microcapsules have to be included in higher weight ratios. On the other hand, it was shown that at a given weight, larger microcapsules have more healing properties, since they give more healing agent per unit area. Thus, microcapsules' size selection is critical in many applications for an enhanced self-healing performance. Further, when the crack volume is small (≈ 3 μm), the self- healing process can be achieved with as little as 1.25% of microcapsules by weight of cement, or with microcapsules with diameter less than 30 μm. Hence, it is of high importance to study microcapsules properties if one were to achieve enhanced self-healing mechanism.

This study had four objectives: (1) develop the synthesis procedure for production of urea-formaldehyde microencapsulation of calcium nitrate; (2) characterize microcapsule properties such as diameter, shell thickness, and morphology; (3) relate the change in the

production parameters, such as agitation rate, heating time, and temperature to such properties; and (4) evaluate the effects of microcapsules on self-healing efficiency in concrete. Notably, this study evaluated calcium nitrate as an alternative healing agent and measured its healing potential to take advantage of the following benefits: (a) low cost; (b) ability to react with the cementitious matrix and subsequently contribute to the formation of calcium silicate hydrate; and (c) its setting accelerator benefits on unhydrated cement particles.

3.2 Background

Microcapsules are small particles that contain solid, liquid, or gas as a core material surrounded by a coating layer or shell (Samadzadeh et al. 2010). Commercial microcapsules have a diameter ranging from 6 to 800 μm and are composed of 10 to 90% of weight core material. Such microcapsules have been used in many engineering applications such as adhesives, cosmetics, as well as pharmaceutical applications (Naka et al. 1991). Many types of core materials can be encapsulated in microcapsules. Versatile core materials are used for the amelioration of long time efficiency structures, as well as stabilization against long-term degradation.

There are many existing methods for the synthesis of microcapsules such as interfacial polymerization, coacervation (Shulkin and Stöver 2002), in-situ polymerization (Brown et al. 2003), extrusion, as well as sol-gel methods. From all these methods, the in-situ polymerization method is considered the easiest and the most cost-effective method for encapsulation as it does not require high levels of technology (Samadzadeh et al. 2010). Further, the commonly used healing agent is in its liquid form because it can easily diffuse in the crack plane (Samadzadeh et al. 2010). Wide varieties of microcapsule coatings exist such as natural or synthetic polymers, depending on the desired characteristics (Lii et al. 2002; Ghosh 2006). To calculate the

conversion rate of microcapsules, the weight of the starting materials such as urea, formaldehyde, and healing agent has to be considered (Then et al. 2011). Shell wall thickness of microcapsules can be measured using confocal laser microscopy. The wall thickness depends on the ratio of the core to the shell material (Park et al. 2001).

Previous studies on particle sizes showed that there were difficulties dealing with microcapsules with an average mean diameter of 220 μm or greater (distribution sizes between 30 and 400 μm), as those particles require high coating thickness panels as well as the use of rheology modifiers to prevent sagging (Nesterova et al. 2012). If the microcapsules are too small, the content of the healing agent inside them is minimal. On the other hand, if they are too large, their mechanical properties and coating thickness will be compromised (Nesterova et al. 2012). In addition, it was reported that the change in any parameters during microcapsule preparation, affects not only one single property of the microcapsule (e.g., diameter), but also affects the overall performance of the microcapsules (Nesterova et al. 2012). Other research studies indicate that the stability of the final microcapsule is related to both the chemical structure as well as the mechanical properties of the shell (Nesterova et al. 2011). The shell thickness properties depend on "kinetics of polymerization reaction", which is influenced by the pH and temperature (Nesterova et al. 2011). The average microcapsule size is controlled by the agitation rate and the stirrer's geometry during the synthesis process (Ovez et al. 1997).

3.2.1 Microencapsulation Techniques

Depending on the desired application, microcapsules can be produced to protect the core material from the environmental conditions, or it can be used to provide a controlled release of the active ingredient to the surroundings by controlling the permeability of the shell material. In general, the production of microcapsules can be categorized as either chemical, physico-chemical, or

physico-mechanical methods (Ghosh 2006). The selection of the microencapsulation technique depends on the type of core material that is to be encapsulated, and the desired physical properties of the microcapsule. For self-healing applications, Hilloulin *et al.* determined that polymeric shell walls are sufficiently robust to resist the mixing process in concrete, yet weak enough to rupture when cracks propagate (Hillouin et al. 2015). For this reason, the main encapsulation technique reviewed involves a polymerization process.

Brown *et al.* adapted an in-situ encapsulation procedure for non-water-soluble core materials developed by Dietrich (Brown et al. 2003; Dietrich et al. 1989). The process requires an oil-in-water emulsion that is made possible by a constant agitation rate and a surfactant such as Ethylene Maleic Anhydride (EMA). The emulsion will contain droplets of the core material surrounded by a water phase containing low concentrations of dissolved resorcinol, ammonium chloride, urea, and formaldehyde. In the presence of heat, the reaction of urea and formaldehyde (under a 1:1.9 molar ratio of formaldehyde to urea) is catalyzed under acidic conditions in the aqueous phase, forming a pre-polymer of low molecular weight. As the reaction continues, the molecular weight of the pre-polymer increases and is subsequently deposited at the oil-water interface. The urea-formaldehyde reaction eventually becomes highly cross-linked and thereby forms a solid microcapsule shell.

The agitation rate, interfacial area, and the pH were the main variables studied by Brown *et al.* to examine their respective effects on the yield and surface morphology of the microcapsules (Brown et al. 2003). Among the findings, it was confirmed that the agitation rate has a direct correlation with the microcapsule diameter. Indeed, a faster agitation rate forms a finer emulsion consisting of smaller droplet sizes. The shell wall thickness of the internal, impermeable membrane was unaffected by the production parameters investigated. The average

shell thickness was found to be in the range of 160 to 220 nanometers, which is ideal for storage and self-healing applications. However, the rough and porous external surface of the microcapsule was found to be sensitive to the concentrations of ammonium chloride, resorcinol, or core material (Brown et al. 2003). Other factors such as an unbalanced or unaligned mixer had a significant impact on the outer shell wall as well. The morphology of the microcapsules is found to be greatly influenced by the type of emulsifier and its concentration. This is because the type of emulsifier used will affect how the pre-polymer is adsorbed and deposited on the surface of the core material's droplets (Fan and Zhou 2011).

The pH also has a significant effect on the yield rate and the quality of the microcapsules produced. Since it is an acid catalyst system, the pH controls the polymerization rate. When the oil-in-water emulsion is heated, the pH decreases and the viscosity increases at the oil-water interface. As a result, the droplet formation mechanism and the respective morphology of the final microcapsule is affected. When the pH was maintained at a constant level throughout the polymerization reaction, the yield rate dropped significantly and the exterior surface morphology was smooth. This was due to the fact that the urea-formaldehyde nanoparticles remained in suspension in this system, and were not successfully deposited on the microcapsule shell. In another experiment, it was found that a lower initial pH substantially increased the thickness of the external surface membrane (Brown et al. 2003).

3.3 Experimental Program

3.3.1 Scanning Electron Microscopy

The electron microscope used for this investigation was a FEI Quanta 3D FEG Dual Beam SEM/FIB. The microcapsules were sprinkled on top of a double-sided tape attached to a pin stub

specimen mount. The samples were then sputter-coated with platinum for four minutes before imaging them under secondary electron mode at an accelerating voltage of 20 kV.

3.3.2 Microcapsules Preparation

It is highly desirable to select a process that is both inexpensive and simple without compromising the quality, so that it can be readily used for manufacturing and implementation. The selected chemical process to encapsulate calcium nitrate was the in-situ polymerization process under a water-in-oil emulsion given its simplicity and low cost. The microcapsule shell material was made of urea-formaldehyde resin as it has been found suitable for self-healing applications (Brown et al. 2003).

Table 3.1. Production parameter matrix for microcapsules

Agitation Rate (RPM)	Temperature (°C)	Heating Time (hours)	Sulfonic Acid (grams)
800	40	1	0.6
800	40	1.5	0.6
800	40	3	0.6
800	45	1	0.6
800	45	1.5	0.6
800	50	1	0.6
800	50	1	0.3
800	50	1	1.0
800	50	1.5	0.6
800	50	3	0.6

The encapsulation reaction is controlled by several production parameters: (1) The temperature at which the emulsion is heated, (2) the choice of catalyst and the respective concentration, (3) the amount of time allotted for the reaction, (4) the agitation rate, (5) the water-oil ratio, and (6) the choice of the core material. In order to control the microcapsule's size and morphology, the production parameters examined were the agitation rate (in revolutions

per minute [RPM]), heating temperature (in degrees Celsius), the heating time, and the amount of acid catalyst to be used (in grams). These parameters were tested systematically according to the matrix shown in Table 3.1. In essence, each production parameter was varied while the others were kept constant. The amount of core material and the water-oil ratio was kept constant throughout the experiment.

The first successful microcapsule synthesis, shown in Figure 3.1, was achieved at an agitation rate of 800 RPM, heating at 50°C for 1 hour, and using 0.60 g of sulfonic acid catalyst. Based on these results, the aforementioned preparation procedure was developed while keeping the agitation rate constant. In addition, this preparation procedure was also applied for agitation rates of 450 RPM and 1500 RPM to evaluate if the agitation rate does influence the final microcapsule diameter.

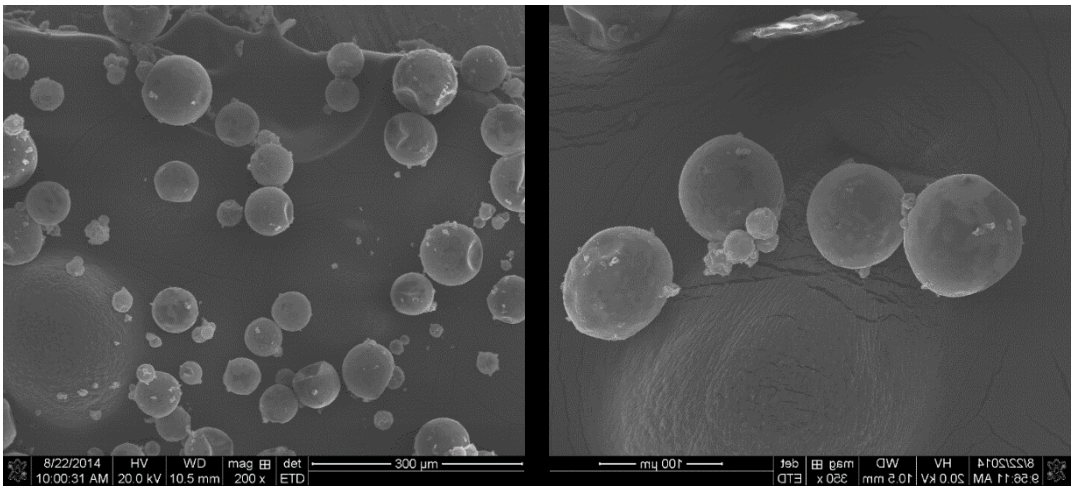

Figure 3.1. Electron Microscope Images Showing the First Successful Microcapsule Synthesis

In the developed procedure, a water-in-oil emulsion was needed to encapsulate aqueous calcium nitrate, which is the core material. For the shell material, 0.5 g of resorcinol, 5 g of urea, 0.5 g of ammonium chloride, and 12.67 g of formalin (37% solution) were used. All these

chemicals were mixed in 50 g of water to form the aqueous phase. A separate one-liter beaker was used for the oil phase, which is composed of 180 g of hexane with a small concentration of dodecylbenzenesulfonic acid, which is highly soluble in oil but insoluble in water. The sulfonic acid acts as a catalyst to the system, and its concentration has a direct impact on the rate of reaction. Hexane was selected as the oil phase because it is inexpensive and volatile. Its volatility is particularly useful when placed under a fume hood, as it facilitates the evaporation and removal of hexane to collect the microcapsules. Moreover, the ratio between the water and oil should be kept about 1:3 to ensure a water-in-oil emulsion takes place.

The oil phase was heated and agitated with a high-shear mixer, preferably to a temperature between 40 to 50°C. Because the temperature directly affects the rate of reaction, higher temperatures are not recommended as they would cause a premature formation of the shell wall (Rodson et al. 2000). Once the desired temperature was reached, the aqueous phase is added drop-wise, and the polymerization process begins. The heating time, varied between one to three hours to allow substantial completion of the in-situ condensation of urea-formaldehyde and to convert the liquid droplets in the aqueous phase to microcapsules with a solid polymer shell. Once the reaction is completed, the hexane is decanted and the microcapsule slurry filtered. The filtered microcapsules were then air-dried in the fume hood for four days (96 hours). The prepared microcapsules were then placed in the oven overnight at a temperature of 50°C to enhance durability.

3.3.3 Concrete Testing

To investigate the effect of microcapsules on concrete healing efficiency and on its surface permeability, different microcapsule sizes were incorporated into the preparation of concrete cylinders, see Table 3.2. Self-healing concrete's response to loading was evaluated in the

laboratory. Group M was used in modulus testing and Group S was used in surface resistivity testing. Group M consisted of thirty-six concrete cylinder specimens (304.8 mm in height and 152.4 mm in diameter) that were prepared using a 41.4 MPa mix design typically used in Louisiana in highway applications. Group S consisted of another 36 concrete cylinder specimens (203.2 mm in height and 101.6 mm in diameter) that were prepared using the same mix design and were used to test the concrete surface resistivity before and after damage. More information about the mix design can be found elsewhere (Milla et al. 2016). Calcium nitrate microcapsules were added to the mixing water during preparation of the cylinders at a content of 0, 0.25, 0.5, and 2.0% by weight of cement. Cylindrical concrete specimens were de-molded after 24 hours and cured in a humidity-controlled chamber for 28 days.

Table 3.2. Experimental Matrix

Agitation Rate (RPM)	Microcapsule Concentration (% by weight of cement)	
	Group M	Group S
450	0.25	0.50
450	0.50	1.00
450	2.00	2.00
800	0.25	0.50
800	0.50	1.00
800	2.00	2.00
1500	0.25	0.50
1500	0.50	1.00
1500	2.00	2.00
Control	0	0

Pristine specimens from Group M were tested based on the static modulus of elasticity approach using the ASTM C 469 standard, while Group S specimens were tested for surface resistivity. The surface resistivity was tested in accordance to Louisiana Department of Transportation and Development (LADOTD) test method for surface resistivity as an alternative

test method to the rapid chlorine permeability test (DOTD TR 233-11). Next, a modified version of ASTM C 469 was employed, where the only adjustment was the application of loads that were equivalent to 80% of the peak concrete strength, instead of the standard 40% as required in ASTM C 469. The purpose of such modified static modulus of elasticity was to induce damage in all of the concrete specimens. Immediately after damage, the surface resistivity values for the Group S specimens were recorded. All specimens were then submerged under tap water at room temperature and left to heal for 14 days.

After the healing period, Group M specimens were then retested in accordance to the traditional static modulus of elasticity per ASTM C 469 to quantify the modulus after healing. The initial tangent modulus, which is defined as the slope of the tangent to the stress-strain curve at the origin, was calculated before and after healing. Three replicates were prepared for each test condition with an average coefficient of variation (COV) of 10% for the modulus of elasticity in the reported findings. On the other hand, the surface resistivity was measured for Group S specimens after the healing period.

3.4 Results and Analysis

After completing the experimental matrix, the microcapsules were observed under an electron microscope to inspect the morphology and measure the microcapsule size and shell thickness for each production level. An elemental analysis with Energy Dispersive Spectroscopy (EDS) was also used to determine if calcium nitrate was successfully encapsulated.

3.4.1 Microcapsule Diameter

Studies have shown that there is a linear correlation between microcapsule size and the agitation rate at which it was produced, where a higher agitation rate yields smaller microcapsule sizes, and lower agitation rates yield larger microcapsules (Brown et al. 2003). This finding was

confirmed in this study where the largest microcapsules were observed at the lowest agitation rate, and the smallest microcapsules at the largest agitation rate after measuring at least 250 capsules for each case, see Table 3.3.

Table 3.3. Microcapsule diameters from the respective production matrix

Temperature (°C)	Heating Time (h)	Sulfonic Acid (g)	450 RPM		800 RPM		1500 RPM	
			Diameter (µm)	SD	Diameter (µm)	SD	Diameter (µm)	SD
40	1	0.6	106.41	34.98	60.44	25.80	50.92	23.49
40	1.5	0.6	92.92	29.99	58.73	20.32	45.22	16.02
40	3	0.6	103.33	32.81	58.93	17.80	42.97	17.32
45	1	0.6	97.07	38.54	72.08	26.31	43.46	16.86
50	1	0.6	88.02	43.49	67.34	28.68	48.59	21.62
50	1	0.3	93.90	41.58	81.06	30.17	51.07	22.35
50	1	1	95.93	40.11	52.71	25.98	41.49	21.49

For the 450 RPM case, a trend was observed that indicated that the higher the temperature, the smaller the resulting microcapsule diameter, see Figure 3.2(a). This was observed for samples that had the same heating time (1 hour) and the same amount of sulfonic acid concentration. For the other test conditions, there seemed to be no linear correlation between the production parameter investigated and the microcapsule diameter. For the 800 RPM case, a trend was observed when varying the sulfonic acid concentration, see Figure 3.2(b).

When less sulfonic acid is used, the particle size was larger, and when more sulfonic acid was used, the particle size was smaller. This seems to indicate that at such agitation rate, the sulfonic acid surfactant did have an impact on the droplet size of the emulsion, where a higher amount of surfactant resulted a finer emulsion. This differs from what was observed in the 450 RPM case. For the other experiments, there seemed to be no linear correlation between the production parameter investigated and the microcapsule diameter.

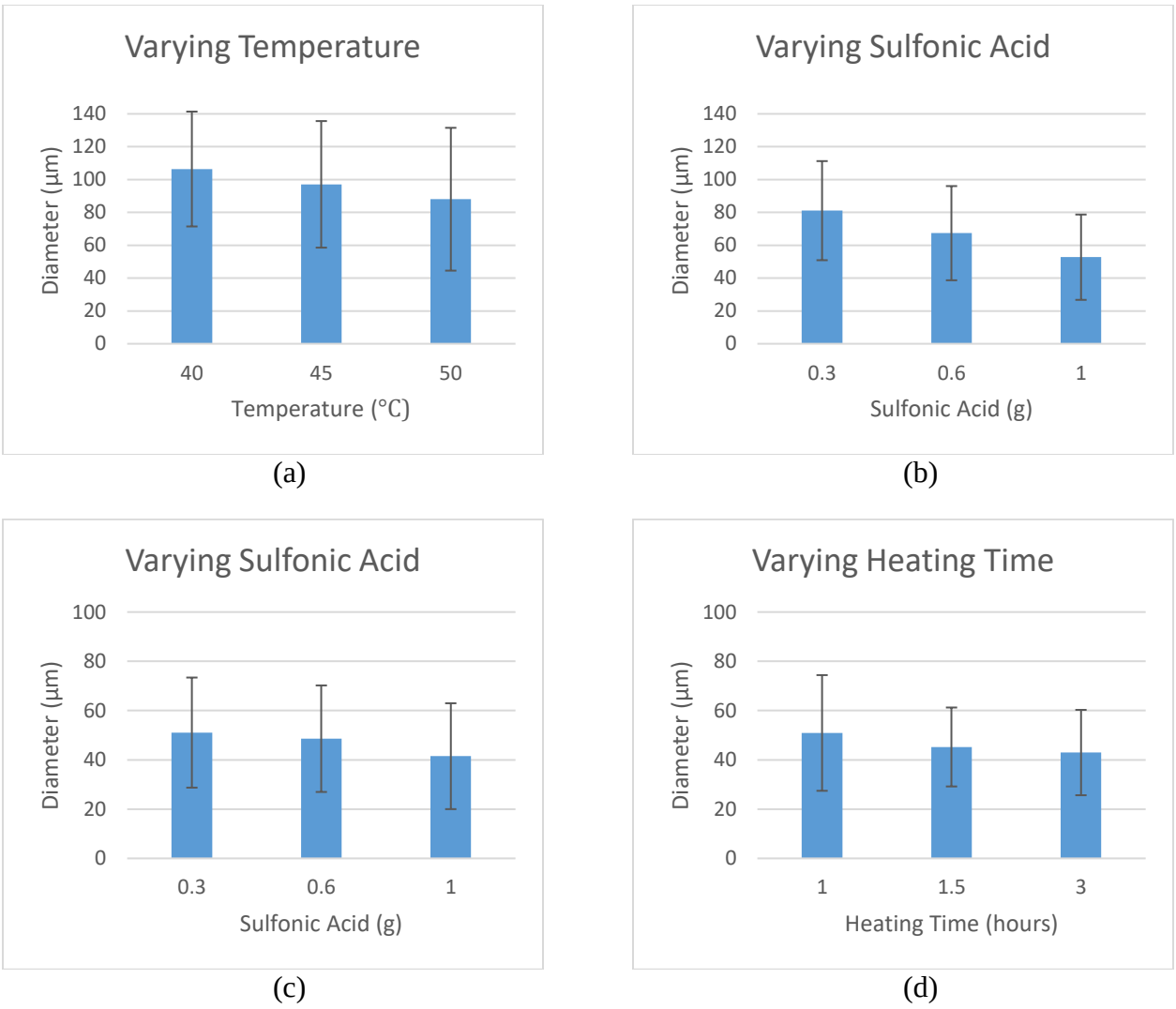

Figure 3.2. Effect of Production Parameters on the Microcapsule Diameter at (a) 450 RPM, (b) 800 RPM (c and d) 1500 RPM

For the 1500 RPM case, a similar trend was observed when varying the sulfonic acid concentration, where a higher sulfonic acid content resulted in a smaller microcapsule diameter, see Figure 3.2(c). It remains unclear why this trend was not observed for the 450 RPM case, but it is possible that at an agitation of 450 RPM, the levels of sulfonic acid used were not sufficient to control the microcapsule size. The heating time was another factor that influenced the microcapsule diameter in these findings, where a longer heating time resulted in a smaller

capsule size, see Figure 3.2(d). There was no other observable trend when varying the temperature, however.

Overall, within the same agitation rate, a lower amount of sulfonic acid resulted in larger microcapsules, while a larger amount of sulfonic acid resulted in smaller microcapsules. This may be due to the fact that a higher surfactant concentration can produce smaller droplets in the water-in-oil emulsion. The only exception was found with those samples that were synthesized at 450 RPM. There was no observable trend that indicated that any other production parameter had a potential influence on the microcapsule diameter.

3.4.2 Morphology

With respect to the morphology, all the microcapsules synthesized had a smooth exterior surface and a rough interior surface, see Figure 3.3(a). This indicates that the variations in the production parameters did not yield significant differences in the morphology. The interior of the microcapsule is believed to hold the healing agent, calcium nitrate, and an agglomeration of urea-formaldehyde nanoparticles.

All of the microcapsules produced had a spherical shape, and had a wide size distribution as shown in Figure 3.3(b). In essence, after measuring at least 250 microcapsule diameters for each case, the standard deviations for each production level were virtually the same, as shown in Table 3.2. This suggests that the production parameters investigated did not affect how a particle size would vary throughout a sample. In contrast, the microencapsulation technique and the type of surfactant used controlled the particle size distribution. This observation was supported by a study that evaluated the effect of the emulsifier on the microencapsulation process. Results

showed that the type of emulsifier used affected how the pre-polymer is adsorbed and deposited on the surface of core material's droplets (Fan and Zhou 2011).

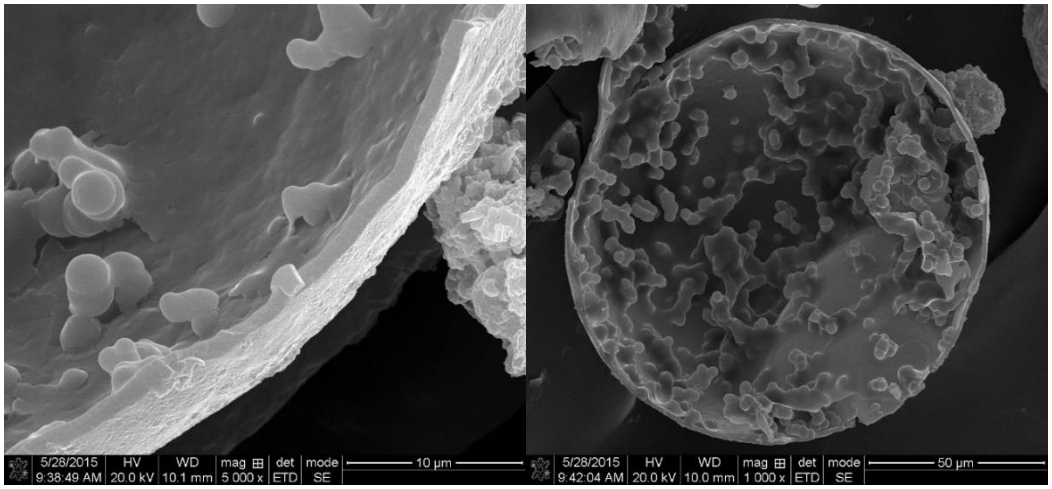

(a)

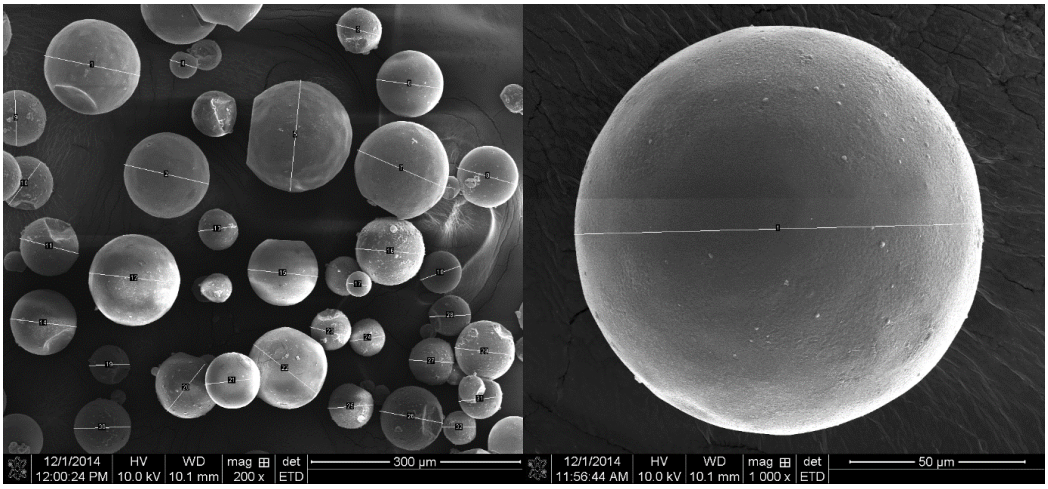

(b)

Figure 3.3. Secondary Electron (SE) microscope images showing (a) the microcapsule shell; and (b) the microcapsules produced at 450 RPM, heated at 40 °C for 1.5 hours with 0.60g of sulfonic acid

Shell Thickness

The shell thickness was not completely uniform throughout the produced microcapsules. However, there is an indication that the production parameters do control the shell thickness, as shown in Table 3.4(a).

Table 3.4. (a) Shell thickness measurements for the experimental matrix *(Continued)*

(a)

Temperature (°C)	Heating Time (h)	Sulfonic Acid (g)	450 RPM		800 RPM		1500 RPM	
			Thickness (μm)	SD	Thickness (μm)	SD	Thickness (μm)	SD
40	1	0.6	1.13	0.22	1.25	0.28	0.91	0.26
40	1.5	0.6	1.22	0.17	1.22	0.42	0.95	0.44
40	3	0.6	1.29	0.25	1.31	0.51	0.74	0.28
45	1	0.6	1.08	0.23	1.09	0.18	0.61	0.27
50	1	0.3	0.90	0.13	0.82	0.23	0.88	0.30
50	1	0.6	0.89	0.16	0.80	0.13	0.77	0.24
50	1	1.0	1.04	0.17	0.77	0.17	0.83	0.17

If only the temperature was varied while the other parameters were kept constant, there is a linear correlation between the temperature and the shell thickness. The higher the temperature, the smaller the shell thickness. This was observed at all the agitation rate levels, except at the 450 RPM case. However, in all cases, the lowest temperature produced the largest shell thickness. This may be due to the fact that at higher temperatures, there may be a more premature polymerization process since the temperature controls the rate of the reaction (Rodson et al. 2000).

Yield of Microcapsules

For each test condition, the yield was calculated according to the following equation:

$$\%\text{Yield} = \frac{\text{Weight of microcapsules}}{\text{theoretical weight of ingredients}} \text{x}100 \qquad (1)$$

Table 3.4(b) presents the average yield at different agitation rates. As shown in this table, the yields were very high approaching 100% for all cases.

Table 3.4. *(Continued)* (b) Variation in yield with agitation rate

(b)

Agitation Rate (RPM)	Average Yield (%)
450	95.3
800	98.6
1500	94.2

Optimum Production Parameters

Microcapsules were synthesized successfully at all the tested conditions and the yields were satisfactorily. With regards to the production process itself, however, it is important to note that that the hexane evaporated faster at higher temperatures or higher agitation rates, which therefore required special attention to roughly maintain the 3:1 ratio of oil-to-water by adding extra 150 ml of hexane when needed. This was also applicable for the experiments that were heated for three hours, even at the lowest temperature of 40°C. Therefore, in an attempt to make the experiment simpler and more affordable, the optimum production parameters were: heating at a temperature of 40°C for 1.5 hours, with 0.60 g of sulfonic acid. The agitation rates were still varied in the concrete experiment by evaluating three levels: 450 RPM, 800 RPM, and 1500 RPM.

Effect of Microcapsule Diameter and Content on Healing Efficiency

Figure 3.4 shows the effects of microcapsule concentration and microcapsule diameter on the ability of the concrete cylinders to heal after being submerged in water at room temperature for 14 days. The ability of the concrete to heal was measured as the increase in the modulus of elasticity after damage. Error bars showing the average variability (±10%) in the measurements are shown. As shown in this figure, the concrete modulus of elasticity increased after healing for all concrete specimens prepared with self-healing agents. The control specimens also experienced an increase in modulus possibly due to the hydration of concrete. The largest increase in the modulus was observed at an average microcapsules' diameter of 58.7 μm, which corresponds to an agitation rate of 800 RPM and a microcapsule content of 0.50%. It is also noted that the healing efficiency decreased at a microcapsule content of 2% indicating that an optimum content of microcapsules exists and that increasing the microcapsule content does not necessarily result in an improvement in healing efficiency.

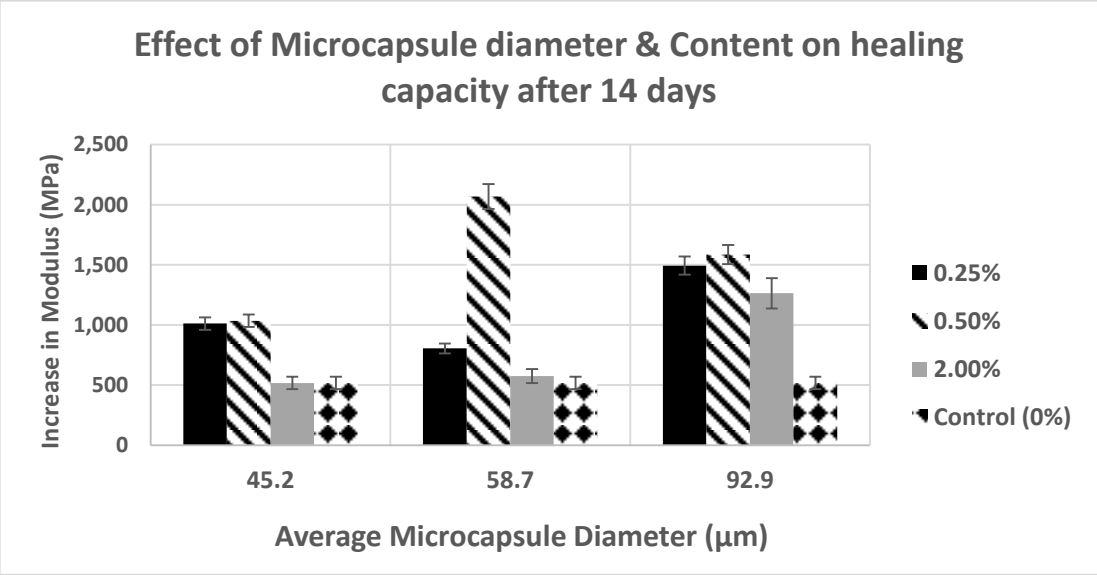

Figure 3.4. Effect of Microcapsule diameter and concentration on healing efficiency after 14 days

Effect of Microcapsules' Diameter and Content on Surface resistivity

Surface permeability was assessed based on Table 3.5, which is provided in AASHTO T 358-15 standard and DOTD TR 233-11 standard. Table 3.6 shows the concrete surface resistivity and the corresponding surface permeability for all test conditions (i.e., before damage, after damage, and after healing). As shown in this table, the concrete specimens prepared with microcapsules at all concentrations had a greater surface resistivity when compared to the control specimens. In addition, the healing process increased the surface resistivity of concrete; hence, decreasing the surface permeability of the concrete specimens prepared with microcapsules.

Table 3.5. Chloride Penetrability Classification

Surface Permeability	Resistivity Value (KΩ-cm)
High	<12
Moderate	12-21
Low	21-37
Very Low	37-254
Negligible	>254

Table 3.6. Summary of the Resistivity of the Concrete Cylinders per Microcapsule Concentration

Agitation Rate (RPM)	Microcapsule Concentration (%)	Before Damage		After Damage		After Healing	
		Resistivity (kΩ-cm)	Surface Permeability	Resistivity (kΩ-cm)	Surface Permeability	Resistivity (kΩ-cm)	Surface Permeability
Control	N/A	11.90	High	13.66	Moderate	14.03	Moderate
450	0.50%	14.18	Moderate	13.85	Moderate	14.65	Moderate
450	1.00%	14.76	Moderate	14.20	Moderate	15.61	Moderate
450	2.00%	14.86	Moderate	14.44	Moderate	15.70	Moderate
800	0.50%	14.31	Moderate	15.15	Moderate	14.63	Moderate
800	1.00%	13.83	Moderate	13.07	Moderate	14.84	Moderate
800	2.00%	15.81	Moderate	15.87	Moderate	18.59	Moderate
1500	0.50%	13.79	Moderate	13.83	Moderate	14.85	Moderate
1500	1.00%	13.57	Moderate	13.50	Moderate	14.82	Moderate
1500	2.00%	15.02	Moderate	14.83	Moderate	16.12	Moderate

Figure 3.5 shows the effect of microcapsules' concentration and diameter on the surface resistivity after healing. As shown in this figure, all concrete specimens prepared with microcapsules had a greater surface resistivity as compared to the control specimens, which is associated with a reduced surface permeability for these concrete specimens.

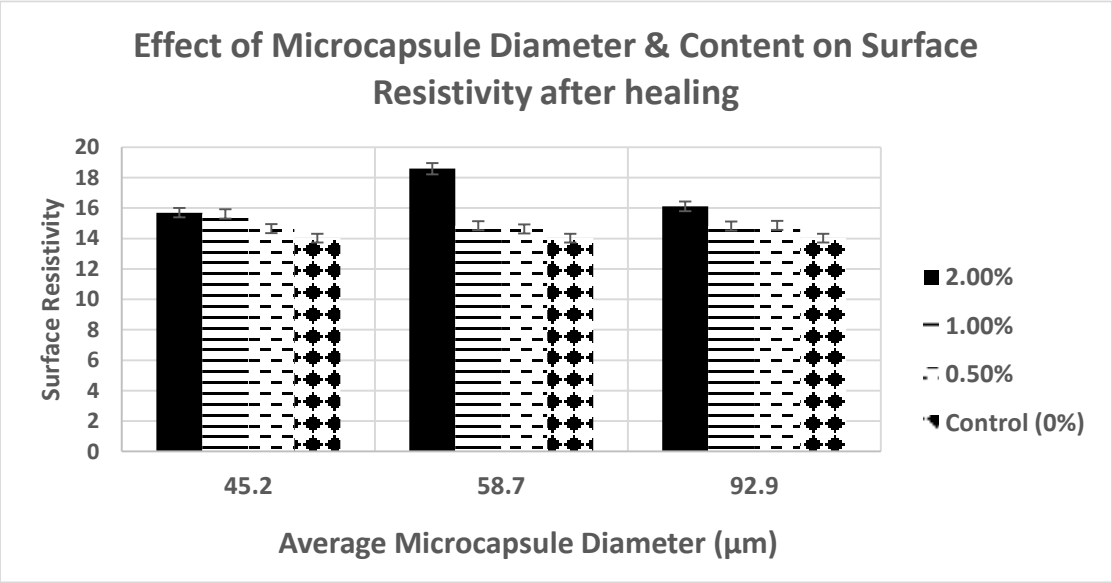

Figure 3.5. Effect of Microcapsule diameter and concentration on surface resistivity

3.5 Conclusions

The objectives of this study were to develop a synthesis procedure for the production of urea-formaldehyde microencapsulation of calcium nitrate and to characterize microcapsule properties such as diameter, shell thickness, and morphology of the prepared microcapsules. Microencapsulation of calcium nitrate was selected given its low cost and setting accelerating effect on unhydrated cement. An economic and simple microencapsulation procedure was sought, where the production parameters (i.e. agitation rate, temperature, heating time, sulfonic

acid amount) were varied to evaluate the effects on microcapsules' morphology, size, and shell thickness.

Results indicated that the agitation rate and the temperature had a linear correlation on the microcapsule diameter and shell thickness, respectively. A higher agitation rate resulted in a smaller microcapsule diameter, while a higher temperature resulted in a thinner shell thickness from the samples observed. The morphology of all of the microcapsules synthesized was virtually the same throughout the experimental matrix, which was composed of a smooth exterior surface and a rough interior surface. In addition, a broad particle size distribution was observed for all microcapsules produced. This was attributed to the type of surfactant used in the process.

With respect to the effects of microcapsules on self-healing efficiency of concrete, results showed that the concrete modulus of elasticity increased after healing for all concrete specimens prepared with self-healing agents. The largest increase in the modulus was observed at a microcapsule content of 0.50%. Results also showed that the concrete specimens incorporating microcapsules at all concentrations had greater surface resistivity when compared to the control specimens and that the healing process increased the surface resistivity; hence, decreasing the surface permeability of the concrete.

3.6 Acknowledgment

The authors would like to acknowledge the financial support through a grant from the Qatar National Research Foundation (QNRF) / National Priorities Research Program (NPRP) as well as the laboratory support from Louisiana Transportation Research Center (LTRC).

3.7 References

Herbert, E. N., and V. C. Li (2013). "Self-Healing of Microcracks in Engineered Cementitious Composites (ECC) Under a Natural Environment". *Materials*, 6(7), 2831-2845.

Li, V., and E. Herbert (2012). "Robust self-healing concrete for sustainable infrastructure. Advanced concrete technology". *Journal of Advanced Concrete Development,* 10, 207-218.

White, S. R., Sottos, N. R., Geubelle, P. H., Moore, J. S., Kessler, M. R., Sriram, S. R., Brown, E. N., and S. Viswanathan (2001). "Autonomic healing of polymer composites". *Nature*, 409, 794–797.

Brown, E. N., Kesseler, M. R., Sottos, N. R., and S. R. White (2003). "In situ poly (urea-formaldehyde) microencapsulation of dicyclopentadiene". *J. Microencapsulation*, 20, 719-730.

Aïssa, B., Therriault D., Haddad, E., and W. Jamroz (2012). "Self-Healing Materials Systems: Overview of Major Approaches and Recent Developed Technologies". *Advances in Materials Science and Engineering*, 2012

Samadzadeh, M., Hatami, S., Peikari, M., and A. Ashrafi (2010). "A review on self-healing coatings based on micro/nanocapsules". *Progress in Organic Coatings*, 68, 159-164.

Naka, Y., Kaetsu, I., Yamamoto, Y., and K. Hayashi (1991). "Preparation of microspheres by radiation-induced polymerization. I. Mechanism for the formation of monodisperse poly(diethylene glycol dimethacrylate) microspheres". *Journal of Polymer Science Part A: Polymer Chemistry*, 29, 1197-1202.

Shulkin, A., and H.D.H. Stöver (2002). "Polymer microcapsules by interfacial polyaddition between styrene–maleic anhydride copolymers and amines". *Journal of Membrane Science*, 209, 421-432.

Lii, C.Y., Liaw, S.C., Lai, V.M.F., and P. Tomasik (2002). "Xantham gum-gelatin complexes". European Polymer Journal, 38(7), 1377-1381.

Ghosh, S.K (2006). *Functional Coatings by Polymer Microencapsulation*. Wiley, Mörlenbach, Germany.

Then, S., Seng, G., and N. Abo-Kassem (2011). "Optimization of Micro-encapsulation process for Self-Healing Polymetric Material". *Sains Malysiana*, 40(7), 795-802.

Park, S.J., Shin, Y.S., and J.R. Lee (2001). "Preparation and characterization of microspheres containing lemon oil". *Journal of Colloid and Interface Science*, 241, 502-508.

Nesterova, T., Johansen, K. D., Pedersen, L., and S. Kiil (2012). "Microcapsule-based self-healing anticorrosive coatings: Capsule size, coating formulation, and exposure testing". *Progress in Organic Coatings*, 75, 309-318.

Nesterova, T., Johansen, K. D., and S. Kiil (2011). “Synthesis of durable microcapsules for self-healing anticorrosive coatings: A comparison of selected methods”. *Progress in Organic Coatings*, 70, 342-352.

Ovez, B., Citak, B., Oztemel, D., Balbas, A., Peker, S., and S. Cakir (1997). “Variation of droplet sizes during the formation of microspheres from emulsions”. *Journal of Microencapsulation*, 14, 489-499.

Hilloulin, B., Van Tittelboom, K., Gruyaert, E., De Belie, N., and A. Loukili (2015). “Design of polymeric capsules for self-healing concrete”. *Cement and Concrete Composites*, 55, 298-307.

Brown, E. N., Kessler, M. R., Sottos, N. R., and S. R. White (2003). “In situ poly(urea-formaldehyde) microencapsulation of dicyclopentadiene”. *J Microencapsul*, 20, 719–730.

Dietrich, K., Herma, H., Nastke, R., Bonatz, E., and W. Teige (1989). “Amino resin microcapsules”. *Acta Polymerica*, 40, 243–251.

Fan, C., and X. Zhou (2011). “Effect of Emulsifier on Poly(urea–formaldehyde) Microencapsulation of Tetrachloroethylene”. *Polymer Bulletin*, 67, 15-27.

Rodson, et al (2000). “Water-in-Oil Microencapsulation Process and Microcapsules Produced Thereby”. *US Patent Office, Patent No. 6113935.*

Milla, J., Hassan, M., Rupnow, T., Al-Ansari, M., and G. Arce (2016). “Effect of Self-Healing Calcium Nitrate Microcapsules on Concrete Properties”. *Journal of the Transportation Research Board*, 2577, 69-77.

CHAPTER 4

EVALUATION OF THE EFFECT OF SELF-HEALING CALCIUM NITRATE MICROCAPSULES ON CONCRETE PROPERTIES

4.1 Introduction

In recent years, it has been widely recognized that a significant portion of the concrete infrastructure is severely deteriorated. In the US, the associated repair and maintenance costs are estimated between 18 to 21 billion dollars (SDC 2006). Similarly, approximately half of Europe's annual construction budget is spent on rehabilitation and repair of existing structures, thereby, highlighting a global demand for an infrastructure upgrade (Cailleux and Pollet 2009; Schlangen et al. 2013). Concrete cracking is inevitable and it affects the structure's durability if it is not controlled or reduced significantly. Further, cracking is a major problem particularly for steel reinforced concrete structures, as the cracks would expose the reinforcement to corrosion. To address this problem, continuous inspections and maintenance repairs are needed, which is challenging to implement due to the significant funds required. In addition, crack repair can be very difficult to achieve when the cracks are internal and/or inaccessible.

A proposed alternative is to engineer concrete materials with superior quality and durability and in turn to extend the service life of concrete structures. White *et al.* introduced the concept of self-healing materials through microencapsulation, where the healing agent is kept from any reactions within the structural material's matrix until it is needed (White et al. 2001). During a cracking event, microcapsules would rupture and release the healing agent to seal the newly formed cracks. While such healing mechanism was demonstrated mainly for polymer materials, recent investigations have adapted the self-healing concept to concrete and cementitious materials.

Self-healing concrete through microencapsulated healing agents is a promising technology that can address issues with concrete infrastructure durability. A suitable self-healing agent should: (a) be easily encapsulated; (b) remain stable and reactive over the service life of the concrete structure under various environmental conditions; and (c) respond quickly to repair damage *(5)*. Through this healing mechanism, it is possible to enable a concrete structure to repair both its internal and external micro-cracks without human intervention.

Several healing agents have been explored in the literature, such as sodium silicate, polyurethane, epoxy, and cyanoacrylates (Pelletier et al. 2010; Kaes et al. 2014; Yang et al. 2011). Other healing agents require a catalyst embedded in concrete such as methylmethacrylate monomer and triethylborane system to seal cracks (Yang et al. 2011). Many of these healing agents are expensive and/or require a catalyst to trigger the self-healing mechanism. To this end, this study evaluated calcium nitrate as an alternative healing agent and measured its healing potential to take advantage of the following benefits: (a) low cost; (b) ability to react with the cementitious matrix and subsequently contribute to the formation of calcium silicate hydrate; and (c) its setting accelerator effect on unhydrated cement particles (Justnes 2003; Justnes and Nygaard 1996).

4.2 Objectives

The main objective of this study was to evaluate the use of calcium nitrate as a healing agent and to assess its effects on self-healing mechanisms for concrete materials. To achieve this objective, a laboratory experiment was conducted to measure the self-healing capacity of concrete with calcium nitrate microcapsules and to compare the results with the control specimens. Results of this study also assessed if calcium nitrate is a suitable healing agent to enhance concrete durability.

4.3 Background

4.3.1 Self-Healing Concrete

Current infrastructure repair practices are labor-intensive and costly. Depending on the structure's intended use and its damage state, there are several manual crack repair techniques. One of the most commonly used techniques involves epoxy sealers to be applied at the crack surfaces (Issa and Debs 2007). Other chemical products such as silicates, acrylates, or mortars can also be applied directly to the crack surfaces (Johnson et al. 2009). In some circumstances, it may be critical to waterproof the structure with a reinforcement wrap. However, as the current infrastructure continues to deteriorate, it becomes increasingly difficult to rehabilitate concrete structures in a timely and economic manner. In addition, it may be challenging to restore concrete structures if the damaged areas are inaccessible for human intervention. For this reason, self-healing concrete is a promising solution to address the accelerated rate of concrete deterioration.

While there are several self-healing techniques, this study focuses on applying the concept of self-healing by microencapsulation. Materials with embedded microcapsules have the advantage of having a localized response to fracture if capsules are uniformly dispersed inside the matrix. However, it is critical to find the optimum dosage of microcapsules to be added in concrete. If insufficient microcapsules are present in the concrete matrix, the healing mechanism will not be successful. On the other hand, if too many capsules are added, it can be costly to implement, and it can be detrimental to the material's strength and other fundamental properties. Therefore, a balance has to be sought for the amount of added microcapsules.

Researchers have emphasized that the bond between the microcapsules and the matrix is crucial for a successful application (Feng et al. 2008; Justnes 2003). If the strength of the

capsule wall is higher than the bond strength, the microcapsules would not rupture after the initiation of the crack, which means no healing agent will be released. In addition, the main disadvantage of applying particles, which may further hydrate or crystallize, is that their healing functionality is limited as the healing agent itself is consumed in the process (Van Tittelboom and De Belie 2013).

Depending on the application, microcapsules can be designed to have a spherical or cylindrical shape. While some agents react upon contact with moisture or air or due to heating or upon contact with the cementitious matrix itself, other agents react when making contact with a second component, which is present in the matrix or provided by additional capsules. A key aspect of the microencapsulation strategy is the selection of the healing agent. Besides the sealing ability, viscosity is another important parameter because it controls the mobility and therefore the potential surface area it can interact with in the matrix. The viscosity should not be too high, in order to be able to flow out of the capsules and to fill the crack. In contrast, if the viscosity is too low, the agent could leak out of the crack or it could disappear due to absorption by the surrounding matrix (Van Tittelboom and De Belie 2013; Wu et al. 2012). Dry *et al.* suggested that the viscosity of the healing agent should be between 100 and 500 cps (Dry 1994).

Pelletier *et al.* investigated sodium silicate as a potential healing agent for concrete (Pelletier et al. 2010). The healing agent was embedded in the concrete matrix using microcapsules with a polyurethane shell that were produced by an interfacial polymerization process adapted from Saihi (Saihi et al. 2006). When sodium silicate is released into the cementitious matrix, it reacts with the calcium hydroxide in cement and produces a calcium-silicate-hydrate (C-S-H) gel that seals the cracks (Pelletier et al. 2010). It was reported that there was a significant strength recovery and a corrosion inhibition effect when compared to those

samples that did not have microcapsules. Yang *et al.* studied self-healing of mortar specimens that contain microencapsulated methylmethacrylate monomer (MMA) as the healing agent and triethylborane (TEB) as the catalyst. Results indicated a significant decrease in the permeability of the specimens containing microcapsules after damage. Further, it was reported that the microcapsules improved the crack resistance and toughness of the specimens (Yang et al. 2011).

Calcium nitrate has been widely used as a concrete admixture that contributes to the acceleration of the hydration of cement and promotes a long-term strength gain of concrete (after 28 days). Moderate dosages of 1% to 2% by weight of cement are needed to achieve the aforementioned benefits. Yet, there is very limited information on the usage of calcium nitrate as a healing agent, and for this reason, this study aims to evaluate its suitability for self-healing applications.

4.4 Experimental Program

4.4.1 Self-Healing Microcapsules

Preparation procedure and optimization of self-healing microcapsules has been presented elsewhere (Hassan et al. 2016). Results showed that in order to make the experiment simpler and more affordable, the optimum production parameters were as follows: heating at a temperature of 40°C for 1.5 hours, with 0.60 g of sulfonic acid. The agitation rates were still varied in the concrete experiment by evaluating three levels: 450 RPM, 800 RPM, and 1500 RPM. Figure 4.1 presents an electron microscope image illustrating the characteristics of the produced microcapsules.

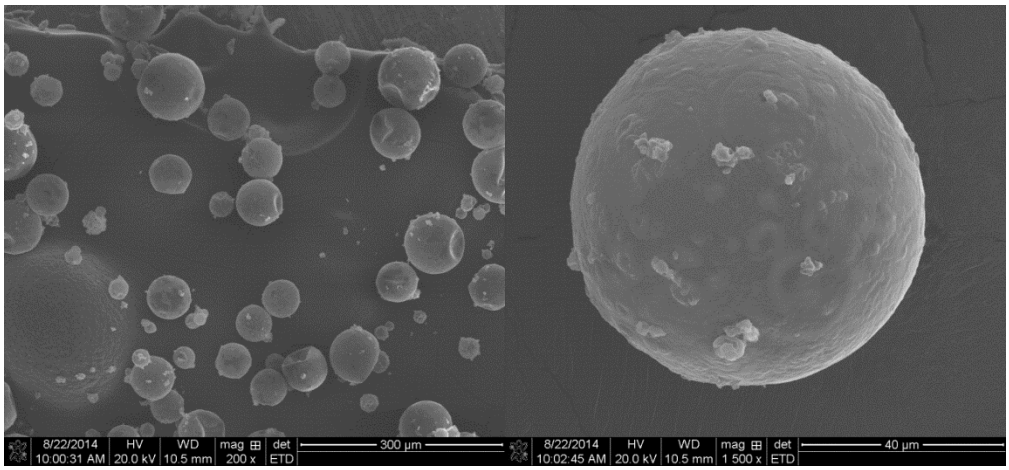

Figure 4.1. Electron Microscope Images Showing the First Successful Microcapsule Synthesis

4.4.2 Testing of Self-Healing Concrete

Microcapsules containing calcium nitrate as the healing agent were tested for their self-healing capacity in a concrete matrix. Table 4.1 shows the concrete batch size and the characteristics of the produced microcapsules. The effect of the content of microcapsules was investigated to identify the best concentration by weight of cement. The tested concentrations were 0.25%, 0.50%, 1.00%, 1.20%, and 2.0%. Laboratory evaluation of concrete specimens with and without microcapsules was based on the compressive strength test, modulus of elasticity, and surface resistivity.

The compressive strength test was conducted only for control specimens (with no microcapsules) and for specimens containing microcapsules at 0.25%, 0.50%, 1.20% and 2.00% that were synthesized at an agitation rate of 800 RPM. This test was useful in evaluating the effect the microcapsules on the compressive strength of concrete and was also used as a reference for the modulus of elasticity test. Compressive strength tests were conducted according to ASTM C 39 and the cylinders tested were of 152 mm x 305 mm and 102 mm x 203 mm in dimensions.

Table 4.1. Batch Information with Their Respective Concentrations of Microcapsules

Batch No.	Batch size (m^3)	Concentration (by weight of cement)	Agitation Rate (RPM)	Average Microcapsule Size (μm)
1	0.0424	2.00%	450	91.5
2	0.0424	1.00%	450	
3	0.0424	0.50%	450	
4	0.0424	0.25%	450	
5	0.0708	2.00%	800	58.7
6	0.0708	1.20%	800	
7	0.0424	0.50%	800	
8	0.0424	0.25%	800	
9	0.0424	2.00%	1500	45.2
10	0.0424	1.00%	1500	
11	0.0424	0.50%	1500	
12	0.0424	0.25%	1500	
13	0.0708	N/A	Control	N/A

The modulus of elasticity of concrete was conducted according to ASTM C 469. Once the ultimate strength was measured, the modulus of elasticity before damage was tested. Then, a modified modulus of elasticity was performed using 80% of the ultimate load in order to induce damage while preserving the integrity of the samples. The samples were then left to heal under water immersion, and retested for modulus of elasticity after 14 days. A comparison was then made between samples containing microcapsules and the control specimens. The surface resistivity test was used to determine the concrete's ability to resist chloride ion penetration. This test, which provides an indication of concrete's permeability, was conducted according to Louisiana Department of Transportation and Development (LADOTD) test method for surface resistivity (DOTD TR 233-11). The specimens tested were 102 mm x 203 mm in size.

4.4.3 Concrete Mix Design

The mix design used has an expected compressive strength of 41.4 MPa and a water-cement ratio of 0.48; the selected mix was based on a typical mix used in Louisiana for road applications. Limestone was used as the coarse aggregate, where the maximum aggregate size was 19 mm. For the fine aggregates, the sand had a maximum particle size of 4.76 mm. The proportions for the mix design are presented in Table 4.2.

Table 4.2. Details of the Concrete Mix Design

Material Description		Proportions (kg/m^3)
Aggregate 1	Sand, Dennis Mills, LA	789
Aggregate 2	#67 Limestone, Martin Marietta	1118
Cement	Holcim Type I	297
Water	Mixing water	141
Air (%)		5.0%
Admixtures		Dosage (ml/batch)
Air Admixture	N/A	0.00
Admixture 1	Glenium 7500	15.00
Admixture 2	Microcapsules^ (%)	0.25, 0.50, 1.22, and 2.00

* By weight of cement

The mixing sequence involved three minutes of mixing coarse aggregates with two thirds of the water content, to ensure saturation. Next, the cement, fine aggregate, and one third of the water mixed with the microcapsules were added and mixed for three minutes. A resting period of three minutes followed and finally the contents were mixed again for three more minutes before pouring. Once the mixing process was complete, slump and air entrainment tests were performed, and the concrete cylinders were cast according to ASTM C 31.

4.4.4 Scanning Electron Microscopy

The electron microscope used for this investigation was a FEI Quanta 3D FEG Dual Beam SEM/FIB. The microcapsules were sprinkled on top of a double-sided tape attached to a pin stub specimen mount. The samples were then sputter coated with platinum for 4 minutes before imaging them under secondary electron mode at an accelerating voltage of 20 kV. For the concrete specimens, the cylinders were cut by a diamond saw, and then coated with epoxy. Next, the samples were polished and then carbon coated before observing them under the backscattered electron mode at an accelerating voltage of 20 kV.

4.5 Results and Analysis

4.5.1 Concrete Properties

For all concrete batches, slump and air contents were measured, see Table 4.3. In general, the microcapsules appeared to make the concrete mix more workable than the control, even though the slumps recorded were not significantly different from the control case. However, there was a higher air content as the microcapsule concentration was higher. At the largest concentration of microcapsules, the air content was almost four times larger than the control's air content.

Table 4.3. Slump and Air Content for the Prepared Concrete Batches (*Continued)*

Batch No.	RPM	Capsule Concentration	Slump (cm)	Air Content (%)
1	450	2.00%	18.42	16
2	450	1.00%	20.96	8.5
3	450	0.50%	21.59	7.0
4	450	0.25%	22.86	4.5
5	800	2.0%	18.42	17
6	800	1.20%	17.78	8.0
7	800	0.50%	21.59	6.9
8	800	0.25%	21.59	4.0

Table 4.3. (*Continued)* Slump and Air Content for the Prepared Concrete Batches

Batch No.	RPM	Capsule Concentration	Slump (cm)	Air Content (%)
9	1500	2.00%	8.26	11.5
10	1500	1.00%	18.42	8.5
11	1500	0.50%	21.59	6.0
12	1500	0.25%	19.69	7.6
13	N/A	0.00%	22.86	4.5

4.5.2 Concrete Compressive Strength

Before Healing

After curing the samples at a humidity chamber (95% RH) for 28 days, compressive strength tests were conducted to assess the effect of the microcapsules on the intrinsic properties of concrete. The cylinders with different concentrations of microcapsules were tested and were compared to the control specimens to determine the effect that microcapsules would have on the compressive strength of concrete. All specimens were tested after allowing 28 days of curing.

Results presented in Table 4.4 indicate that the compressive strength is significantly influenced by the number of microcapsules used. At a concentration of 1.20%, the average compressive strength dropped about 13 MPa compared to the control specimens. At the higher concentration of 2.00%, the strength decrease was even more significant. Therefore, while the results indicate that a higher concentration of microcapsules does negatively affect the compressive strength of concrete, there is a possible solution to this problem. If the microcapsules were to be uniformly distributed by the aid of a dispersing agent, it is possible to reduce the amount of microcapsules used, given that the self-healing mechanism functions by having the microcapsules ready at the location of the cracks. Otherwise, more microcapsules

would be needed to overcome undesired agglomerations and lack of dispersibility in the concrete matrix.

Table 4.4. Compressive Strength Results for Samples before Healing

Agitation Rate (RPM)	Microcapsule Concentration (by wt. of cement)	Sample No.	Type Break	Compressive Strength (MPa)	Average (MPa)	Standard Deviation
800	1.20%	1	1	27.70	27.55	0.33
		2	2	27.78		
		3	1	27.18		
800	2.00%	1	3	10.40	10.72	0.29
		2	2	10.97		
		3	3	10.79		
Control	N/A	1	6	42.90	41.06	1.69
		2	6	40.69		
		3	1	39.58		

After Healing

After all specimens were damaged and left to heal under water immersion for 64 to 66 days, compressive tests were conducted. Results are presented in Figure 4.2 for the control specimens and the microcapsules prepared at different agitation rates. In general, the higher the microcapsule concentration, the lower the compressive strength, regardless of the microcapsule diameter, see Figure 4.2. The only exception was found for the 1500 RPM microcapsule case, where the 0.50% concentration yielded a higher compressive strength than the 0.25% case. This can be explained by the fact that the 0.50% case had a lower air content than the 0.25% case. However, the role of healing mechanism could also have been a contributing factor, given that the modulus recovery was slightly higher for the 0.50% case than the 0.25% case. In addition, the 1500 RPM case exhibited higher compressive strengths at higher microcapsule concentrations than the 450 RPM and 800 RPM cases.

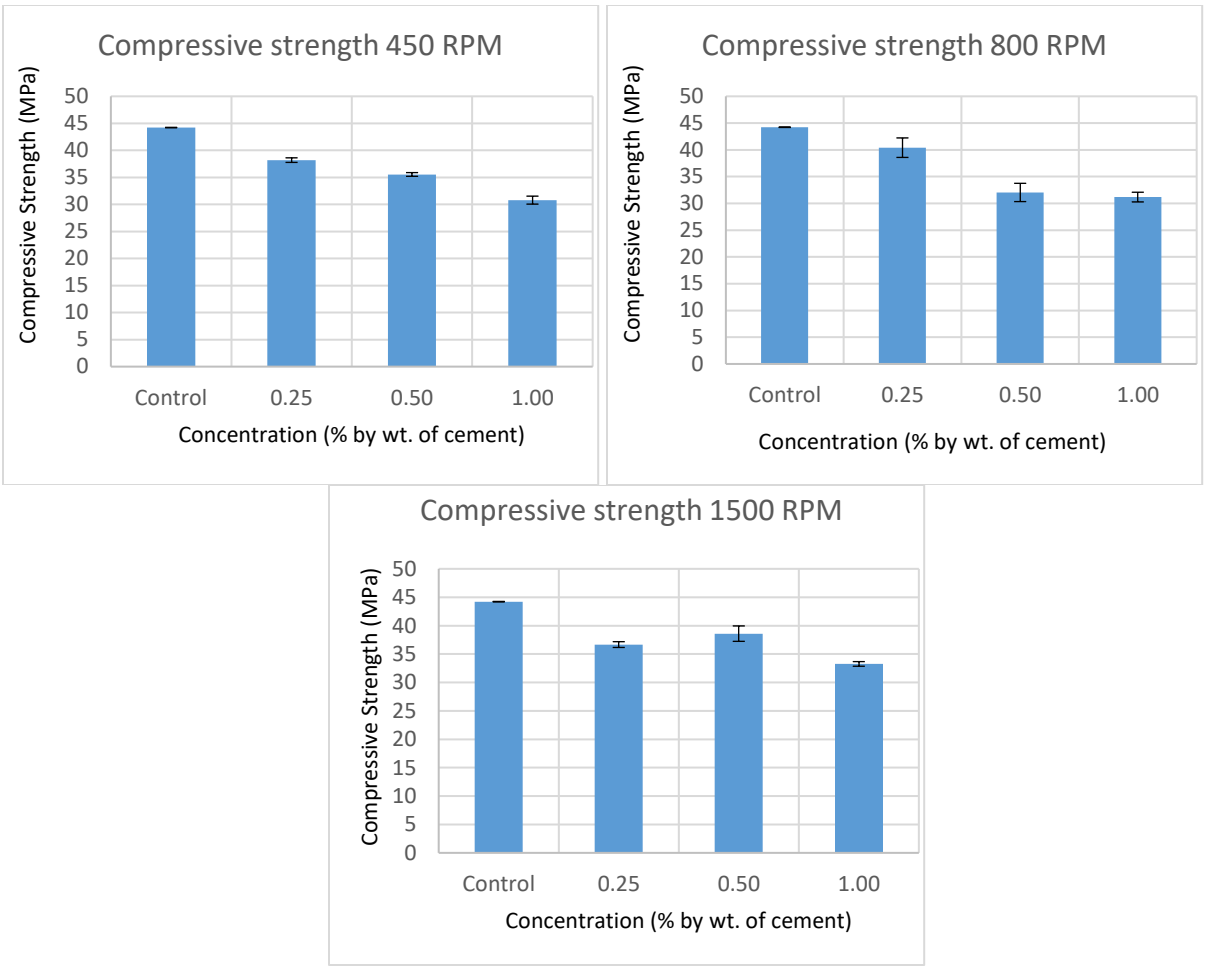

Figure 4.2. Variation in Concrete Compressive Strength with Microcapsule Concentration

Statistical analysis was conducted using the Fisher's Least Significant Difference (LSD) test to determine whether the concentration of the microcapsules had a statistical impact on the compressive strengths after healing. For the LSD test, the Type I comparison-wise error rate controls, not the experiment-wise error rate. Therefore, for a particular agitation rate, the compressive strength values from each specimen group (corresponding to the concentration of microcapsules) were used as input. This test was performed three times to evaluate all agitation rate levels, i.e. 450 RPM, 800 RPM, and 1500 RPM. The results indicated that in all of these cases, the microcapsule concentration does have a statistically significant impact on the

compressive strength of concrete. Therefore, a higher concentration of microcapsules yields weaker samples. This is mainly attributed to the increase in air content when microcapsules are used.

4.5.3 Concrete Microstructure

After the compressive tests were conducted, the samples that exhibited the best modulus of elasticity recovery were analyzed under Scanning Electron Microscopy (SEM). These samples were as follows: (1) 450 RPM, 1.00%; (2) 800 RPM, 0.50%; and (3) 1500 RPM, 1.00%. The concrete specimens were impregnated with epoxy and subsequently polished to obtain a representative sample of the microstructure. The samples were then carbon coated, and observed in the SEM using a backscattered electron imaging mode at 20 kV. The backscattered electron mode aids in the visualization of the microstructural constituents, the porosity, and the degree of hydration of the cross-section.

The microcapsules that were synthesized at an agitation of 450 RPM had the largest diameters, and has resulted in a higher concrete porosity, see Figure 4.3(a). As shown in Figure 3(a), the larger and darker spots are actual air voids in the cement matrix. On the other hand, those shallower, spherical voids that fall in the range of the average microcapsule diameter (for a particular specimen group) were assumed to be caused by the presence of microcapsules. The largest observed microcapsules were of 185 microns in diameter, and the smallest were of 15 microns, while the average was 91 microns. In these images, there are many voids within that size range, thus confirming that such voids were the result of the embedded microcapsules. Moreover, the light spots in these images represent the unhydrated cement grains. As shown in this figure, there are a very small number of white spots throughout the whole specimen, which

indicates that the degree of hydration was high, as these samples were immersed in water for 64 to 66 days prior to the SEM imaging.

The microcapsules that were synthesized at an agitation of 800 RPM had a diameter range of 101 microns to 13 microns, with an average of 59 microns. This had also an impact on the concrete's porosity. As shown in Figure 4.3(b), the darker spots and the void spaces larger than 100 microns were expected to be caused by the air voids in the cement matrix, while the shallower, spherical voids are indicative of microcapsule-induced voids. Similarly, there were a very small number of white spots throughout the whole specimen, which indicates that the degree of hydration was high, as these samples were immersed in water for 64 to 66 days prior to the SEM imaging.

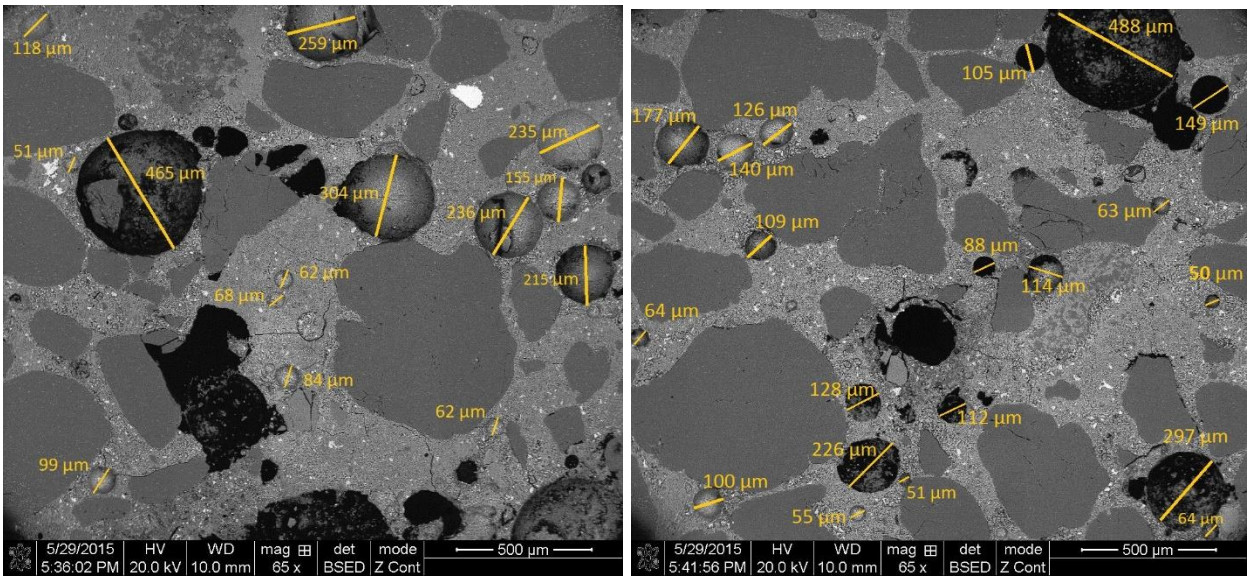

(a)

Figure 4.3. (a) Microstructure of Concrete Admixed with 450 RPM Microcapsules at a Concentration of 1.00% (*Continued*)

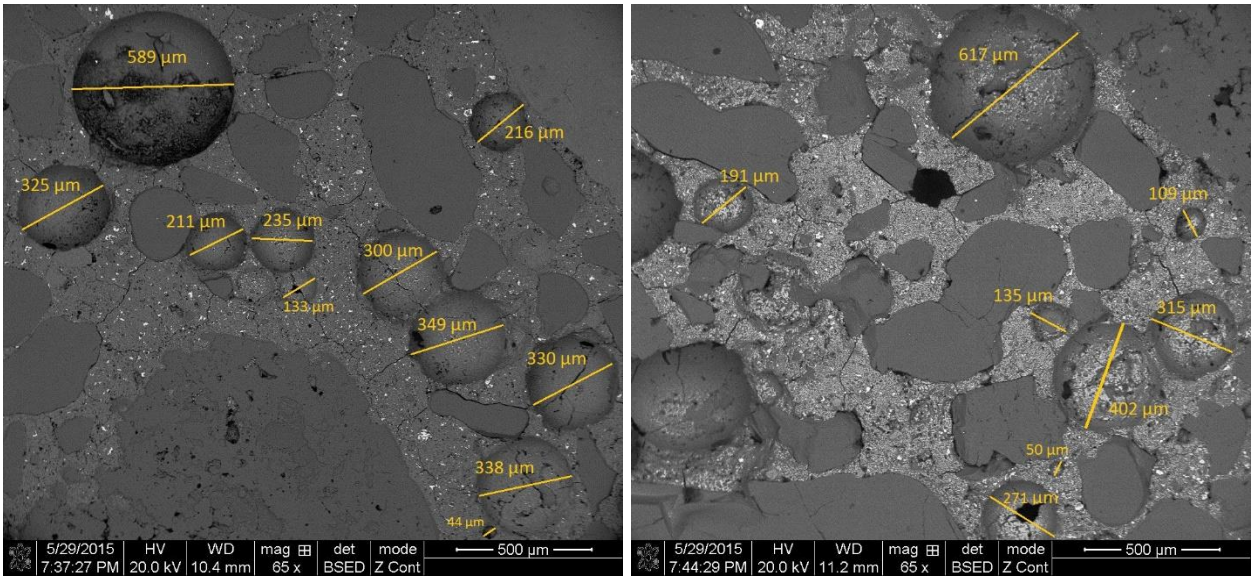

(b)

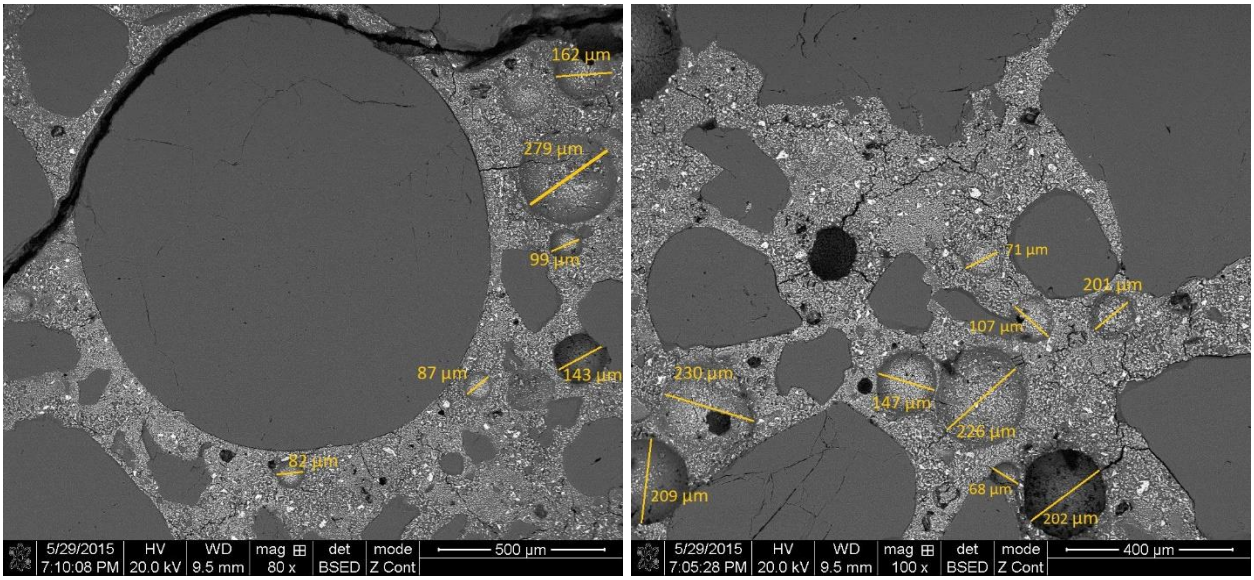

(c)

Figure 4.3. (*Continued*) (b) Microstructure of Concrete Admixed with 800 RPM Microcapsules at a Concentration of 0.50%; and (c) Microstructure of Concrete Admixed with 1500 RPM Microcapsules at a Concentration of 1.00%

The microcapsules produced at an agitation rate of 1500 RPM had a diameter range of 94 microns to 11 microns, with an average of 45 microns, Figure 4.3(c). The degree of hydration was high, and the amount of void spaces was high within the cement matrix, although it was

evident that the size of some of the voids was smaller than those observed in Figure 3 (a and b). In general, for all of the test specimens, it is important to note that the concrete failure was primarily due to the breaking at the interfacial transition zone. In addition, all of the voids, caused by either microcapsules or air inside the cement matrix, attracted most of the cracking paths.

4.5.4 Surface Penetrability

The surface resistivity test was conducted on all specimens after allowing 28 days of curing. This served as reference of the concrete specimens in their original state, and was compared with the specimens after they have been cracked and healed to evaluate the healing efficiency. Table 5, which presents the chloride penetrability classification based on the AASHTO T 358-15 standard and the DOTD TR 233-11 standard, was used to interpret the results with respect to surface permeability of the concrete specimens.

Table 4.5. Chloride Penetrability Classification

Surface Penetrability	(KΩ-cm)
High	<12
Moderate	12-21
Low	21-37
Very Low	37-254
Negligible	>254

Results presented in Table 4.6 indicated that for the vast majority of specimens, the microcapsules used were contributing to lower surface penetration, given that the control specimen had a “high” surface permeability. There were only two exceptions to this observation, particularly where the microcapsules had a low concentration (0.25%), which were synthesized

at higher agitation rates (800 RPM and 1500 RPM, respectively). The effect of the microcapsule size may have had a role in this case.

Table 4.6. Summary of the Resistivity of the Concrete Cylinders per Microcapsule Concentration

Agitation Rate (RPM)	Microcapsule Concentration (by wt. of cement)	Batch Average	
		Reading (kΩ-cm)	Surface Permeability
Control	N/A	11.90	High
450	0.25%	12.61	Moderate
450	0.50%	12.05	Moderate
450	1.00%	13.39	Moderate
800	0.25%	11.97	High
800	0.50%	12.16	Moderate
800	1.20%	12.87	Moderate
1500	0.25%	11.90	High
1500	0.50%	12.44	Moderate
1500	1.00%	13.56	Moderate

4.5.5 Modulus of Elasticity

The modulus of elasticity was used to measure the self-healing capability of concrete admixed with calcium nitrate microcapsules. Three levels of microcapsule concentration were used to observe a potential optimum concentration from the matrix. Microcapsules made with the same production parameters (i.e., temperature, heating time, and sulfonic acid) but with different agitation rates were used to investigate the effect of microcapsule size on healing as well. The largest microcapsules were made at an agitation of 450 RPM, and the smallest microcapsules were made at an agitation of 1500 RPM. For the largest microcapsules available, averaging 93 microns, the modulus of elasticity values are plotted in Figure 4.4(a). In this part of the experimental program, after damaging the concrete sample at an 80% of its ultimate load and recording its modulus of elasticity, the samples were left to heal for 14 days and retested. The

optimal concentration for this microcapsule size after 14 days of healing, based on the modulus of elasticity tests, was found to be at 1.00%. It is important to note that the higher the microcapsule concentration did not result in the highest healing potential indicating the presence of an optimal microcapsule content.

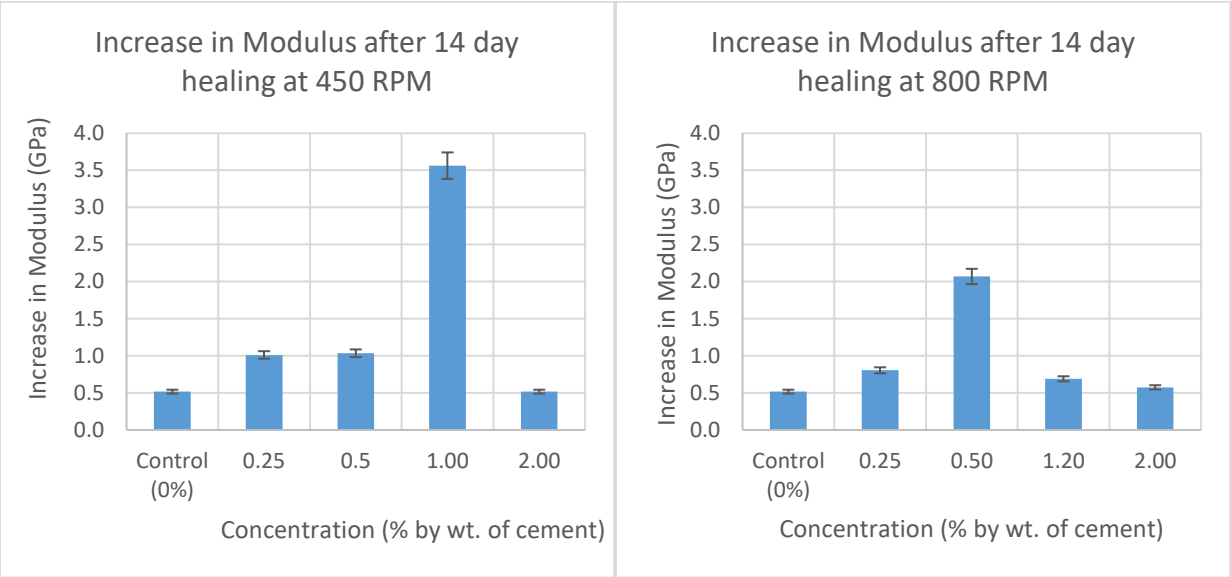

(a) (b)

Figure 4.4. Change in Modulus of Elasticity after 14 Days Healing for Concrete with and without Microcapsules Prepared at (a) 450 RPM, (b) 800 RPM (*Continued*)

For the 800 RPM case, with an average microcapsule diameter of 59 microns, the optimal concentration for healing after 14 days was 0.50% as shown in Figure 4(b). As previously noted, the higher microcapsule concentration did not yield the higher increase in modulus after healing. For the 1500 RPM case, with an average microcapsule diameter of 45 microns, the optimal concentration for healing after 14 days was 1.00% as shown in Figure 4(c).

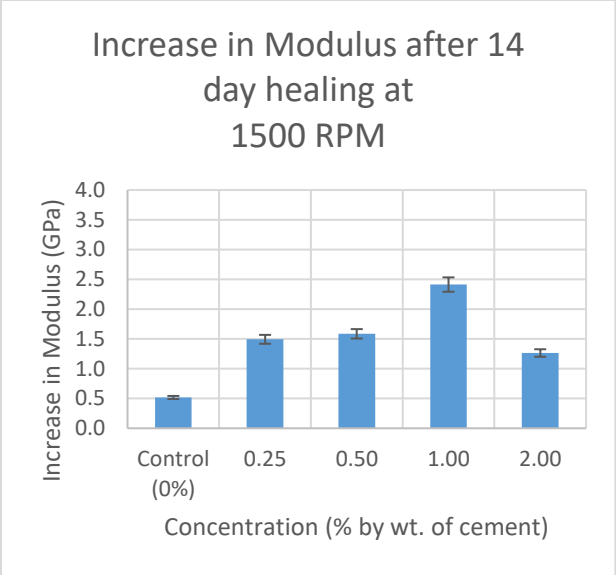

(c)

Figure 4.4. *(Continued)* Change in Modulus of Elasticity after 14 Days Healing for Concrete with and without Microcapsules Prepared at (c) 1500 RPM

From these results, it can be concluded that a 0.50% to 1.00% concentration yielded the best results. In addition, the 450 RPM case produced higher increases in modulus after 14 days, followed by the 1500 RPM case. It is also important to evaluate the differences between the modulus at a virgin state and the modulus after 14 days to have another indication of the healing efficiency. Based on this criterion, the 450 RPM case yielded a higher recovery at a concentration of 1.00%. The 800 RPM case yielded its highest recovery at 1.20%, and the 1500 RPM at 0.25%.

4.6 Conclusions

Based on the results of this study, the following conclusions are drawn:

The concentration of microcapsules added, and the size of the microcapsules had a direct impact on the compressive strength of concrete. As the concentration of the microcapsules increased,

the strength of the concrete decreased. The microcapsule size had also an impact on concrete strength. With larger microcapsules, the air content increased in the cement matrix.

The surface resistivity was virtually the same for the control and microcapsule-containing samples (moderate penetrability), except for the control samples and those admixed with 0.25% of microcapsules, which had a high surface permeability. Nevertheless, these samples were the strongest with respect to compressive strength after damage.

With respect to the modulus of elasticity recovery, the samples containing microcapsules exhibited a higher modulus increase when compared to the 80% modulus test values. The optimal concentration of microcapsules was dependent on the sizes of the microcapsules. The largest microcapsules were made at an agitation of 450 RPM, and the smallest microcapsules were made at an agitation of 1500 RPM. In general, a microcapsule concentration of 0.50% to 1.00% yielded the best results.

Overall, results of this study indicated that while microcapsules caused a decrease in concrete compressive strength, they enhanced the self-healing capability of the produced concrete. To take advantage of the benefits of microcapsules, the authors recommend that future work evaluate the use of a dispersing agent in order to reduce the amount of microcapsules needed, and therefore, minimizes the observed reduction in concrete strength.

4.7 Acknowledgments

The authors would like to acknowledge the financial support through a grant from the Qatar National Research Foundation (QNRF) / National Priorities Research Program (NPRP) as well as the laboratory support from Louisiana Transportation Research Center (LTRC).

4.8 References

The Strategic Development Council (SDC) (2006). "Vision 2020: A vision for the concrete repair protection and strengthening industry" (http://www.concretesdc.org/_pdfs/vision2020-version1.0_%20may2006.pdf) (April 10, 2015).

Cailleux, E., and V. Pollet (2009). "Investigations on the development of self-healing properties in protective coatings for concrete and repair mortars". *Proc. 2nd International Conference on Self Healing Materials*, Chicago, IL, USA.

Schlangen, E., and S. Sangadji (2013). "Addressing Infrastructure Durability and Sustainability by Self Healing Mechanisms - Recent Advances in Self Healing Concrete and Asphalt". *Procedia Engineering*, 54, 39-57.

White, S. R., Sottos, N. R., Geubelle P. H., Moore J. S., Kessler M. R., Sriram, S. R., Brown, E. N., and S. Viswanathan (2001). "Autonomic healing of polymer composites". *Nature*, 409(6822), 794-797.

Wu, D. Y., Meure, S., and D. Solomon (2008). "Self-healing polymeric materials: A review of recent developments". *Progress in Polymer Science*, 33(5), 479-522.

Pelletier, M., Brown, R., Shukla, A., and A. Bose (2010). "Self-healing concrete with a microencapsulated healing agent". (http://energetics.chm.uri.edu/system/files/Self%20healing%20concrete%20-7-11.pdf) (May 3, 2015).

Kaes, M., Van Tittelboom, K., and N. De Belie (2014). "The efficiency of self-healing cementitious materials by means of encapsulated polyurethane in chloride containing environments". *Construction and Building Materials*, 71, 528-537.

Van Tittelboom, K., De Belie, N., Van Loo, D., and P. Jacobs (2011). "Self-healing efficiency of cementitious materials containing tubular capsules filled with healing agent". *Cement and Concrete Composites*, 33, 497–505.

Yang, Z., Hollar, J., He, X., and X. Shi (2011). "A self-healing cementitious composite using oil core/silica gel shell microcapsules". *Cement and Concrete Composites*, 33, 506-512.

Issa, C. A., and P. Debs (2007). "Experimental study of epoxy repairing of cracks in concrete". *Construction and Building Materials*, 21, 157-163.

Johnson, K., Schultz, A. E., French, C., and J. Reneson (2009). *Crack and Concrete Deck Sealant Performance*. University of Minnesota, Minneapolis.

Van Tittelboom, K., and N. De Belie (2013). "Self-Healing in Cementitious Materials—A Review". *Materials*, 6(6), 2182-2217.

Wu, M., Johannesson, B., and M. Geike (2012). "A review: Self-healing in cementitious materials and engineered cementitious composite as a self-healing material". *Construction and Building Materials*, 28(1), 571-583.

Dry, C. M (1994). “Smart multiphase composite materials that repair themselves by a release of liquids that become solids”. *Proc. Symposium on Smart Structures and Materials*, Orlando, FL, USA.

Saihi, D., Vroman, I., Giraud, S., and S. Bourbigot (2006). “Microencapsulation of ammonium phosphate with a polyurethane shell. Part II. Interfacial polymerization technique”. *Reactive and Functional Polymers*, Vol. 66, 2006, 1118-1125.

Hassan, M., Milla, J., Rupnow, T., Al-Ansari, M., and B. Daly (2016). “Micro-Encapsulation of Calcium Nitrate for Concrete Applications”. *Journal of the Transportation Research Board*, 2577, 8-16.

Mihashi, H.; Kaneko, Y.; Nishiwaki, T.; Otsuka, K (2000). “Fundamental study on development of intelligent concrete characterized by self-healing capability for strength”. *Trans. Jpn Concr. Inst.*, 22, 441–450.

Feng, X.; Zhuo, N.; Ningxu, H.; Biqin, D.; Xuexiao, D.; Zhan, H.; Ming, Z (2008). “Self-healing mechanism of a novel cementitious composite using microcapsules”. *Proc. International Conference on Durability of Concrete Structures*, Hangzhou, China.

Justnes, H. (2003). “Explanation of Long-Term Compressive Strength of Concrete Cause by the Set Accelerator Calcium Nitrate”, *Proc. 11th International Congress on the Chemistry of Cement (ICCC)*, Durban, South Africa, 475-484.

Justnes, H. and Nygaard, E.C. (1996). "Calcium Nitrate - A Multifunctional Concrete Admixture", *Proc. Int. Conf. on High-Performance Concrete, and Performance and Quality of Concrete Structures*, Florianopolis, Brazil, 514-525.

CHAPTER 5

ENHANCING THE FEASIBILITY OF SELF-HEALING CONCRETE WITH MICROENCAPSULATED CALCIUM NITRATE

5.1 Introduction

In the United States, it is estimated that an annual investment of $21 billion is needed to repair and maintain highway bridge infrastructure, which marks an extra $8 billion from what is currently budgeted (ASCE 2013). Furthermore, it is estimated that half of all repaired concrete structures fail to perform at satisfactory engineering standards, and thus require additional repairs (Li and Herbert 2012). For this reason, researchers have focused on engineering self-healing concrete as an alternative, long-term solution to address this problem.

Self-healing concrete carries the potential to enhance a structure's durability and thereby substantially decrease the cost of repair and maintenance associated with the gradual deterioration of infrastructure. Several studies have focused on methods to deliver self-healing properties, whether through Engineered Cementitious Composites (ECC), crystalline admixtures, bio-concrete, or microencapsulated healing agents (Zwaag 2007; Wu et al. 2012). Depending on the method used, either the autogenous healing capacity of concrete may be enhanced, or a new product may be formed to seal the crack (Van Tittelboom and De Belie 2013).

In recent years, self-healing concrete by microencapsulated healing agents has gained significant research attention due to an ability to respond directly to the damaged areas. This is because during a cracking event, the microcapsules would rupture and release the healing agent through capillary action to seal the newly formed cracks (Hilloulin et al. 2015). The selection of a healing agent is crucial to this process as it determines the effectiveness of crack-repair mechanisms. In addition, an adequate dispersion of microcapsules throughout the concrete

matrix is key to the success of this application (Van Tittelboom and De Belie 2013). While there are certain crack-width limitations to consider, this approach has shown great potential (Maes et al. 2014; Kanellopoulos and Giannaros 2016).

A number of healing agents have been studied by researchers, including sodium silicate, polyurethane, epoxy, dicyclopentadiene (DCPD), Methylmethacrylate monomer, and cyanoacrylates (Pelletier et al. 2010; Van Tittelboom et al. 2011; Yang et al. 2011; Maes et al. 2014; Dong et al. 2016; Lv et al. 2016). Depending on the nature of the desired crack-repair mechanism, some healing agents may require a catalyst embedded in concrete to form the sealing products at room-temperature (Yang et al. 2011). Due to the fact that many of these healing agents are either expensive and/or require a catalyst to trigger the self-healing process, the authors sought to evaluate calcium nitrate tetrahydrate as an alternative healing agent (Hassan et al. 2016; Milla et al. 2016). Calcium nitrate was selected primarily due to its low cost and the ability to contribute to the formation of calcium silicate hydrate by reacting with the cementitious matrix (Justnes 2003, 2010). Previously, the authors tested concrete admixed with microcapsules (Hassan et al. 2016; Milla et al. 2016). However, the microcapsules contributed to a substantial decrease in the concrete's compressive strength, while demonstrating adequate healing capabilities.

5.2 Objectives

The main objective of this study was to evaluate the use of calcium nitrate tetrahydrate as a healing agent and to assess its effects on self-healing mechanisms for concrete materials. This investigation focused on addressing the reduction in concrete compressive strength previously reported by the authors by: (a) altering the microencapsulation procedure; (b) modifying the concrete mix design; and (c) monitoring the self-healing process over time. The results of this

study thereby assessed if there were any improvements by adapting the new encapsulation procedure and mix design with respect to mechanistic properties and performance. Furthermore, it evaluated the influence of the particle size and concentration of microcapsules by weight of cement to assess whether calcium nitrate tetrahydrate presents a suitable healing agent to enhance concrete durability.

5.3 Background

5.3.1 Self-Healing Concrete

Recently, the concept of self-healing concrete has emerged as a potential solution to enhance concrete durability while minimizing maintenance and repair costs. While concrete has an innate autogenous healing ability to seal microcracks under moisture, its natural limitations have led to the need of developing robust self-healing techniques for greater efficiency. From all the available self-healing techniques, this study focuses on self-healing through microencapsulated agents. Materials with embedded microcapsules carry the advantage of addressing a localized response to fracture, so long as the microcapsules are adequately dispersed within the material matrix. The concept of embedding microencapsulation of healing agents in a material matrix was first introduced by White et al. for an autonomous repair of polymers (White et al. 2001).

There are several parameters that must be considered when adding microcapsules; however, these may affect the material's intrinsic properties to a certain extent. Some of the key parameters are inclusive of (a) the size and morphology of the microcapsules; (b) the concentration of capsules added to the matrix; (c) the mechanical properties of the capsule's shell wall; and (d) the bond strength between the microcapsules and the host matrix (Van Tittelboom and De Belie 2013; Wang et al. 2014; Kanellopoulos and Giannaros 2016; Milla et al. 2016). With respect to the shell materials, it was shown that polymeric capsules will survive the

concrete mixing process with no protection and break upon crack appearance without human intervention (Van Tittelboom et al. 2011; Hilloulin et al. 2015).

Kanellopoulos et al. utilized spherical polymeric microcapsules, composed within a pig gelatin/gum acacia shell, for an investigation of self-healing mortars (Kanellopoulos and Giannaros 2016). Sodium silicate was selected as the healing agent for an ability to react directly with the cementitious matrix to form cement hydration products, most notably calcium-silicate-hydrate. The dosages tested ranged from 0.79% to 6% by weight of cement. Results showed that while higher concentrations of capsules resulted in a maximum of 27% reduction in the mechanical properties, the self-healing efficiency was also substantially increased. Moreover, a dosage of 6% of microcapsules achieved virtually a full crack closure of large crack widths of 0.5 mm (Kanellopoulos and Giannaros 2016).

5.4 Materials and Methods

5.4.1 Microcapsule Preparation and Characterization

Preparation procedure and optimization of self-healing microcapsules was based on a previous study (Hassan et al. 2016). However, certain parameters were modified to improve the quality of the microcapsules, as well as their compatibility with concrete materials. For instance, it was found that the previously developed microcapsules tended to acidify water, a trait which is undesirable, given that acidic environments are known to be detrimental to concrete (ACI Committee 301 1991; Zivica and Bajza 2001). For this cause, the sulfonic acid dosage was decreased six times when preparing the microcapsules, to minimize the acidic components deposited in the microcapsule shell. Span 60 was added as an emulsifier to stabilize the water-in-oil encapsulation procedure to compensate for a lower dosage of sulfonic acid. In addition,

the microcapsules were filtered with a water bath following synthesis, to neutralize the traces of sulfonic acid that were present. The finalized procedure is illustrated by the flowchart shown in Figure 5.1. The agitation rates were varied in the concrete experiment between three levels: 450 rpm, 800 rpm, and 1500 rpm, to assess the effect of the mean particle size on self-healing effectiveness.

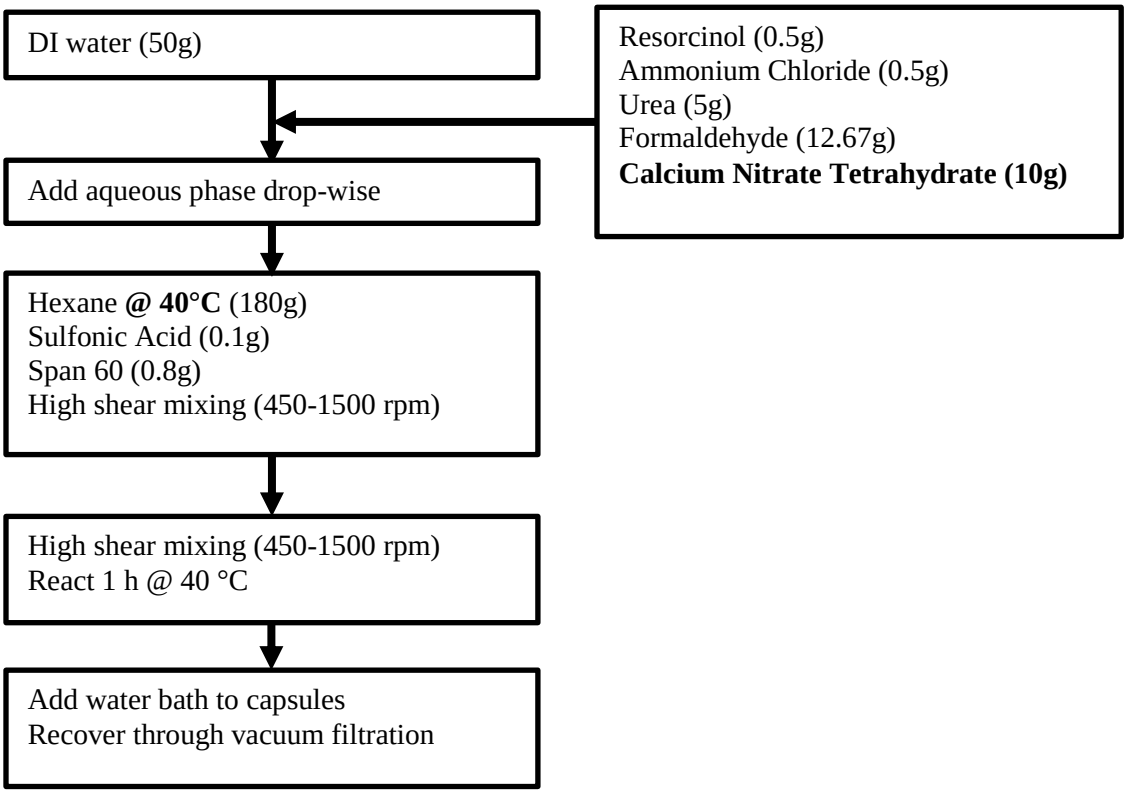

Figure 5.1. Microencapsulation Synthesis Process

The microcapsules' morphology was characterized with the electron microscope FEI Quanta 3D FEG Dual Beam SEM/FIB. The microcapsules were sprinkled on top of a double-sided tape attached to a pin stub specimen mount. Next, the samples were sputter coated with platinum for 4 minutes before observation. The electron microscope was set under a secondary electron mode at an accelerating voltage of 20 kV.

5.4.2 Concrete Mix Design

Healing Agent Selection

A calcium nitrate tetrahydrate healing agent is expected to react mainly with unhydrated cement particles (which are typically exposed on the crack surfaces), as it contains the same cations as tricalcium silicate and dicalcium silicate (Ramachandran 1996; Karagöl et al. 2013). Hence, such healing agent would accelerate the hydration reaction by nucleation of such ions and form calcium hydroxynitrate salts, which promote the densification of the cement paste and form a skeleton in which calcium hydrosilicates begin to materialize. The healing agent's functionality is not limited to its reaction with unhydrated cement particles as it can also enable the precipitation of calcium carbonate on the cementitious matrix by increasing the saturation index of calcite (Edvardsen 1999).

Mix Design

A calcium nitrate healing agent is suitable for mix designs featuring low water-cement ratios as it is expected to react with more unhydrated cement nuclei exposed in the crack surfaces and thus enhance the autogenous healing capacity in concrete to seal the microcracks. In this study, a water-cement ratio of 0.405 was used with a super plasticizer to ensure workability. In addition, a defoamer supplied by Evonik Industries was used to counter air content increase observed previously when combining microcapsules with a super plasticizer. The concrete mix design details are provided in Table 5.1.

Table 5.1. Concrete Mix Design

Material Description	Proportions (kg/m^3)
Aggregate 1: Sand, Dennis Mills, LA	791
Aggregate 2: #67 Limestone, Martin Marietta	1116
Cement: Holcim Type I	326
Water: Mixing water	132
Air (%)	5.0%
Admixture 1: Adva 195 (ml/100kg)	455
Admixture 2: Microcapsules* (%)	0.25, 0.50, and 1.00
Admixture 3: TEGO Antifoam MR 1015* (%)	0.12

* By weight of cement

Limestone was used as a coarse aggregate, where the maximum aggregate size was 19 mm. For the fine aggregates, the sand had a maximum particle size of 4.76 mm. The mixing sequence followed ASTM C 192 standard. The details of each batch produced are presented in Table 5.2. It is important to note that two different types of control specimens were used in this study. Ctrl D was admixed with a defoamer while Ctrl ND was not.

Table 5.2. Specimen Descriptions

Sample ID	Concentration (by weight of cement)	Agitation Rate (rpm)	Average Microcapsule Size (μm)
C4a	0.25%	450	109
C4b	0.50%	450	
C4c	1.00%	450	
C8a	0.25%	800	50
C8b	0.50%	800	
C8c	1.00%	800	
C15a	0.25%	1500	22
C15b	0.50%	1500	
C15c	1.00%	1500	
Ctrl D	With Defoamer	N/A	N/A
Ctrl ND	No Defoamer	N/A	N/A

5.4.3 Initial Concrete Testing

Microcapsules containing calcium nitrate as the healing agent were tested for their mechanical properties. The tested microcapsule concentrations were 0.25%, 0.50%, and 1.00%. Once the samples were cast, they were placed in a moist room with a relative humidity of 95% for 28 days. A laboratory evaluation of concrete specimens with and without microcapsules was based on the compressive strength test and static modulus of elasticity at an age of 28 days. All samples were oven-dried for 3 days at 60°C prior to testing to simulate the effect of wet-dry cycles.

Fresh Concrete Properties

The slump and air content of each mix was determined per ASTM standards C 231 and C 143, respectively.

Modulus of Elasticity

The modulus of concrete elasticity was conducted on dried specimens per ASTM C 469 for all sample groups of 100 mm x 200 mm in size. Once the ultimate strength was measured, modulus of elasticity was conducted on undamaged specimens to quantify how the variations in microcapsule size and concentrations affected the intrinsic mechanical properties of concrete.

Compressive Strength

Compressive strength test was conducted for all specimen groups per the ASTM C 39 standard, albeit in dry conditions. The cylinders tested were of 100 mm x 200 mm in dimensions. This test was useful in evaluating the effect of the microcapsules on the compressive strength of concrete and it was also utilized as a reference for the modulus of elasticity test.

5.4.4 Self-Healing Concrete Testing

Microcapsule-containing specimens were tested for their self-healing capacity in a concrete matrix. The effect of the microcapsule content was investigated to identify the best concentration by weight of cement, with respect to compressive strength and modulus of elasticity recovery after damage. The curing regime selected was a de-ionized (DI) water immersion to enable healing. All samples were oven-dried for 3 days at 60°C prior to testing to simulate the effect of wet-dry cycles.

Modulus of Elasticity

A series of cyclic loads were induced on all specimens to inflict damage. In the test sequence, four load cycles were performed at (a) 80% of the sample's ultimate strength; (b) 90% of the sample's ultimate strength; and (c) 95% of the sample's ultimate strength. Afterward, another modulus of elasticity test was conducted on all samples to record the degree of damage. Once the damage phase was concluded, the samples were left to heal, and retested for modulus of elasticity periodically. The testing sequence is therefore denoted as: (a) Day zero – Pristine; (b) Day zero – Damaged; (c) 21-Day healing; (d) 42-Day healing; and (e) 84-Day healing.

Compressive Strength

At the end of the healing period, a compressive strength test was conducted at a curing age of 86 days after damage to compare the potential strength recovery.

Concrete Microstructure

After the compressive strength tests were conducted, concrete samples were recovered for inspection under the electron microscope to evaluate the respective concrete microstructure. The samples were impregnated with epoxy, polished, and subsequently carbon coated for observation under the backscattered electron (BSE) mode at an accelerated voltage of 20 kV, using the FEI

Quanta 3D FEG Dual Beam scanning electron microscope. The samples selected for observation were both control specimens (Ctrl D and Ctrl ND) and microcapsule-containing specimens (C4a, C4b, C8a, and C15a).

5.5 Results and Analysis

5.5.1 Microcapsule Characterization

After synthesizing the microcapsules at three different agitation rates, an electron microscope was used to study the morphology and to measure the corresponding particle sizes using ImageJ image analysis software. The mean diameter and standard deviation for each test condition was determined from data sets of at least 350 measurements to be representative of the population. Figure 5.2 illustrates the correlation between the agitation rate and the capsule diameter, where lower agitation rates tend to produce larger microcapsules as reported in previous studies (Alexandridou and Kiparissides 1994; Övez et al. 1997; Brown 2003; Gilford et al. 2013).

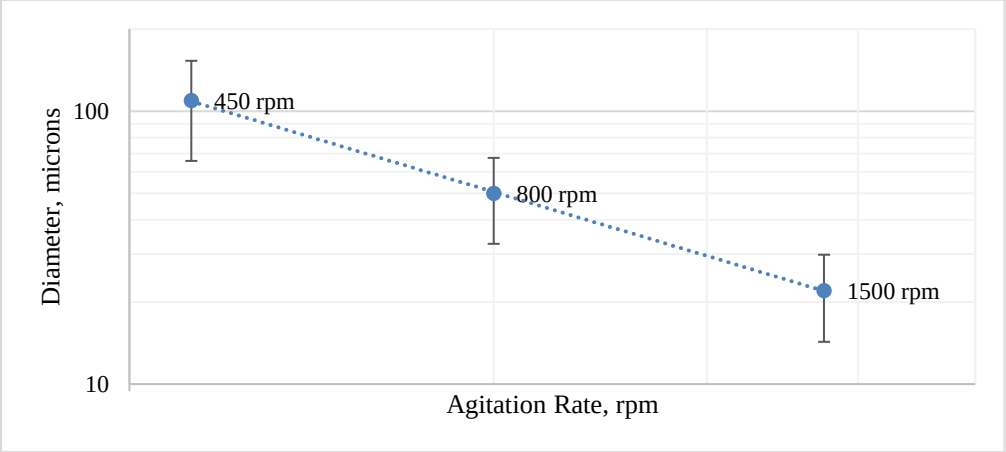

Figure 5.2. Correlation between Agitation Rate and Microcapsule Diameter

In general, all the microcapsules synthesized had a smooth exterior surface and a rough interior surface, as shown in Figure 5.3. The morphology is very similar to that from the authors'

previous study, where the emulsifier Span 60 was not introduced (Hassan et al. 2016; Milla et al. 2016), indicating that the variations in the production parameters had no significant effect on the morphology. However, at the macro scale, the particles produced at an agitation rate of 1500 rpm were prone to be clustered. This was due to the Span 60 emulsifier as it provided a hydrophobic coating on the microcapsule surface. Since larger agitation rates produce smaller microcapsules and thus larger specific surface areas, the particles would be more prone to agglomeration due to the hydrophobic attraction between the particles.

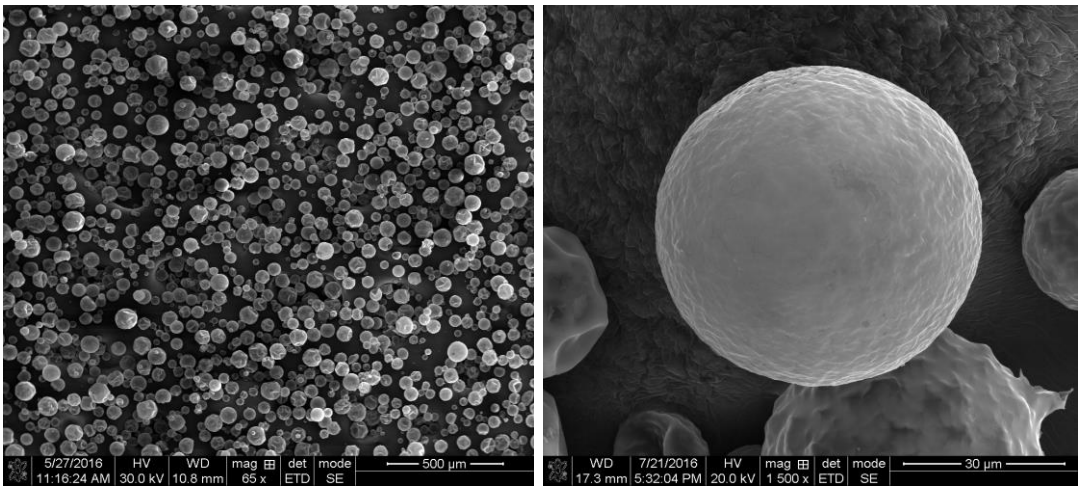

Figure 5.3. Microscopic Images of the Microcapsules Produced

5.5.2 Fresh Concrete Properties

The results from the slump and air entrainment tests are presented in Table 5.3. Overall, there was a minimal variability in the air content between the control groups and the microcapsule containing specimens. This represented a key issue in addressing the authors' previous attempts, which revealed substantial increases in air content for the microcapsule containing groups; the high air content in previous studies resulted in weaker compressive strengths (Hassan et al. 2016; Milla et al. 2016). The lowest air content corresponded to the control mix with no defoamer,

while the highest values were found for all samples admixed with 1500 rpm microcapsules, regardless of concentration. It is important to note that while the introduction of a defoaming agent did provide minimal variability in air content, there may be instances where the use of a defoamer would not be appropriate, particularly in areas where freeze-thaw conditions are common. Hence, a different mix design will be required to address cases where air entrainment is required. As to the consistency of each mix, all samples were found to be highly workable. Virtually all mixes, except for C15b, resulted in slumps higher than 100 mm.

Table 5.3. Slump and Air Content

Sample ID	Agitation Rate, rpm	Concentration (% by wt. cement)	Slump, mm	Air Content, %
Ctrl D	With Defoamer	N/A	115	1.7
Ctrl ND	No Defoamer	N/A	120	1.5
C4a	450	0.25	125	1.6
C4b	450	0.50	125	1.8
C4c	450	1.00	100	1.7
C8a	800	0.25	160	1.8
C8b	800	0.50	125	1.8
C8c	800	1.00	150	1.9
C15a	1500	0.25	150	1.9
C15b	1500	0.50	95	2.5
C15c	1500	1.00	150	2.3

5.5.3 Modulus of Elasticity

Undamaged Stage

The static modulus of elasticity test was conducted for all specimen groups using 100 mm x 200 mm cylinders. The results are illustrated in Figure 5.4. As shown in Figure 5.4, the only specimens that exhibited a higher modulus of elasticity values than the control groups were C8b and C8c. Interestingly, from the samples containing microcapsules, the lowest microcapsule

dosages yielded the lowest virgin modulus of elasticity values (except for case C4c), whereas a 0.50% concentration of microcapsules resulted in the highest modulus values for the 450 rpm and 1500 rpm agitation case.

A statistical analysis applying Fisher's Least Significant Difference (LSD) test was used to evaluate the effect of microcapsule concentrations with respect to the virgin modulus of elasticity values for all specimen groups. For the 450 rpm case, no statistical difference existed between the modulus of elasticity of both control groups and specimens C4a, C4b, and C4c. For the 800 rpm case, the mean modulus from Ctrl ND was statistically equivalent to that of specimens C8a, C8b, and C8c. C8c was the highest modulus, while Ctrl D had the lowest modulus. Lastly, for the 1500 rpm case, the modulus values from Ctrl D, Ctrl ND, C15b, and C15c displayed no statistical difference; C15a had the lowest modulus, and thus showed a significant difference.

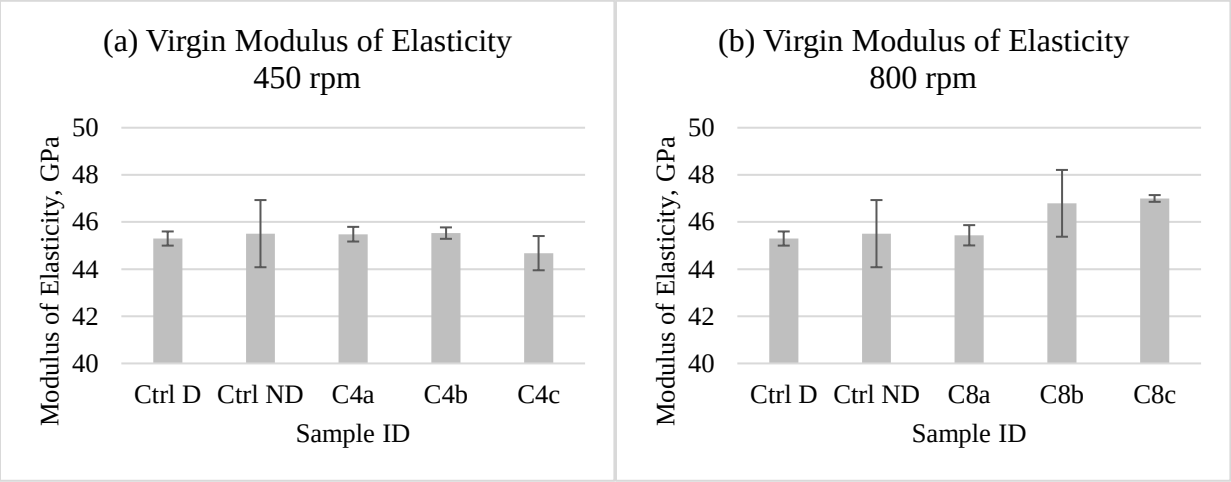

Figure 5.4. Virgin Modulus of Elasticity Variation for Microcapsule Case: (a) 450 rpm; (b) 800 rpm *(Continued).*

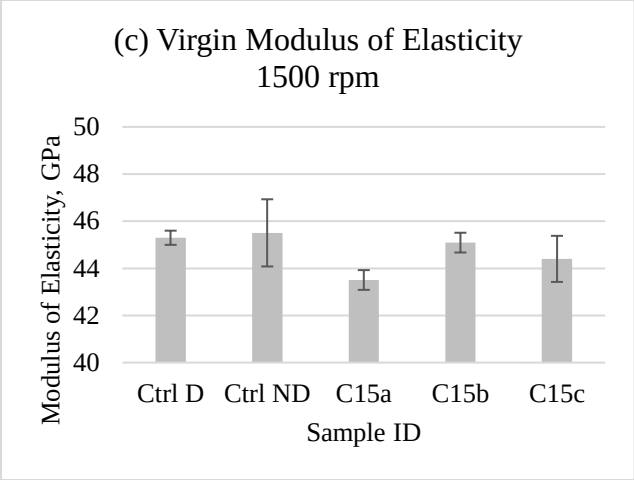

Figure 5.4. *(Continued)* Virgin Modulus of Elasticity Variation for Microcapsule Case: (c) 1500 rpm.

Damage and Healing Stages

The variation of the modulus of elasticity over time is presented in Figure 5.5. Most microcapsule containing specimens were less affected by the damage cycles than both control specimen groups. Only the sample groups C8b and C8c featured a slightly larger percentage loss in modulus than Ctrl ND, with respect to the initial virgin state. Furthermore, all specimens containing microcapsules presented a lower percentage drop in modulus than Ctrl D, thereby showcasing potentially promising mechanical properties.

After 21 days of curing, the study observed that several samples exceeded their original modulus of elasticity values after damage. In general, all samples continued to show increase in modulus of elasticity as the healing period went on. As such, it was expected that the autogenous healing capability of concrete will contribute to an increase in modulus for all samples over time under a water immersion curing regime. However, for the microcapsule-containing samples, it

was important to establish whether the autogenous healing of concrete was enhanced and affected the intrinsic mechanical properties as well.

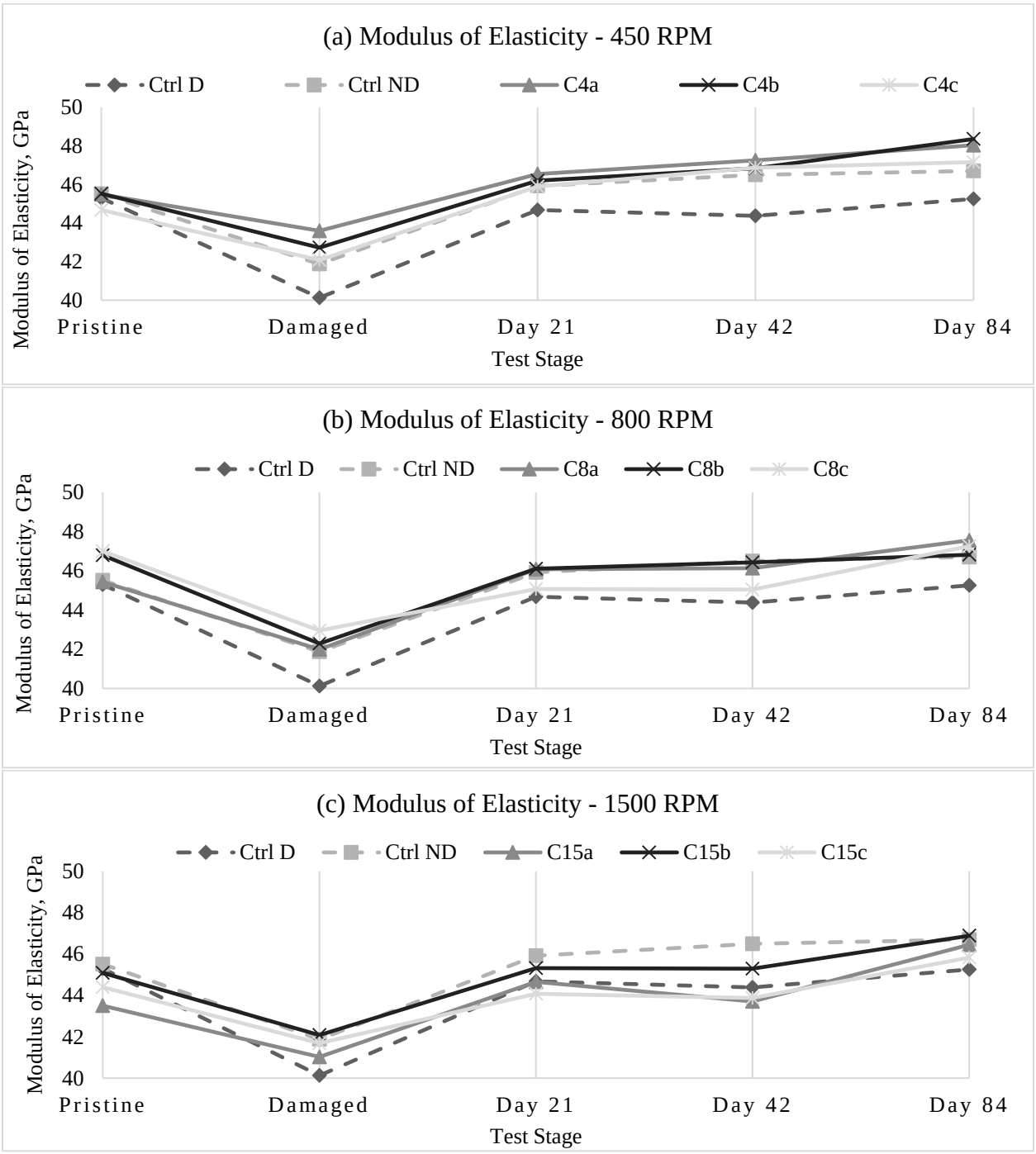

Figure 5.5. Modulus of Elasticity Variation over Time for Microcapsule Case: (a) 450 rpm; (b) 800 rpm; (c) 1500 rpm.

To establish the extent of self-healing activity, the results were normalized and expressed as a ratio, relative to the virgin modulus. The percentage decrease or increase was expressed as the ratio of the change in modulus, due to damage/recovery with respect to the virgin modulus. Hence, the net healing efficiency was established as the difference between the percentage increase in modulus due to healing and the percentage decrease in modulus due to damage. This is expressed in the following equations:

$$\% \text{ Decrease in Mod} = \frac{\text{Virgin Mod.-Damaged Mod.}}{\text{Virgin Mod.}} \times 100 \quad (1)$$

$$\% \text{ Increase in Mod.} = \frac{\text{X-Day Mod.-Damaged Mod.}}{\text{Virgin Mod.}} \times 100 \quad (2)$$

$$\text{Net Healing, \%} = \text{Increase in Mod.} - \text{Decrease in Mod.} \quad (3)$$

Thus, a specimen that fully recovers the modulus degradation due to damage would have a a net gain of zero percent. With this metric, the net modulus recovery is illustrated in Figure 5.6. While Figure 5.5 showed a remarkable recovery in modulus for Ctrl D, Figure 5.6 revealed that the specimens did not fully recover after 21 days of curing. Overall, the microcapsule specimens that achieved the highest healing efficiencies were C4a, C4c, and C15a. Indeed, the 450 rpm group achieved very positive results, while two of the three 800 rpm specimens displayed lower healing efficiencies than Ctrl D. Furthermore, all specimens containing the lowest microcapsule concentration yielded the highest net recovery percentages, while the highest concentrations yielded the lowest.

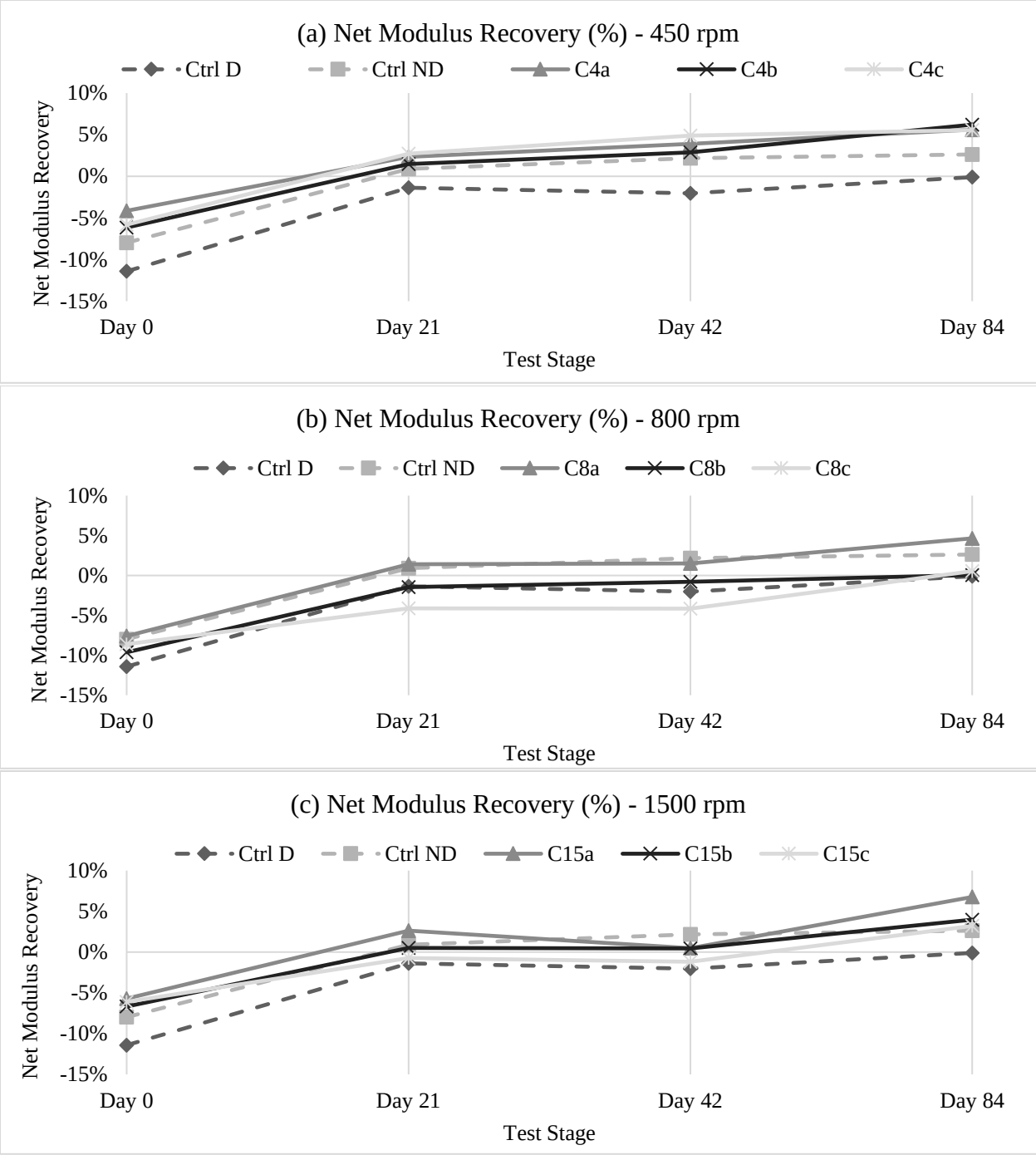

Figure 5.6. Net Modulus of Elasticity Recovery over Time for Microcapsule Case: (a) 450 rpm; (b) 800 rpm; (c) 1500 rpm.

The modulus recovery curves seemed to have a steady increase over time, albeit with a characteristic increase at the end of the healing period. Hence, at the end of the testing period, the net modulus recovery was compared for all samples after 84 days of curing as shown in Figure 5.7. The results show that virtually all microcapsule-containing specimens had a greater modulus recovery than both control specimens, except for cases C8b and C8c. In fact, Ctrl D was the only specimen group that did not surpass its pristine condition after healing, with a modulus recovery of -0.10%. Such control group was closely followed by case C8b, which achieved a modulus recovery of 0.05%. The highest net modulus recovery percentage was observed in case C15a, followed by all specimens from the 450 rpm group. Therefore, it can be inferred that the optimum microcapsule concentration lies between the 0.25% and 0.50% by weight of cement for samples exposed to axial compressive loads.

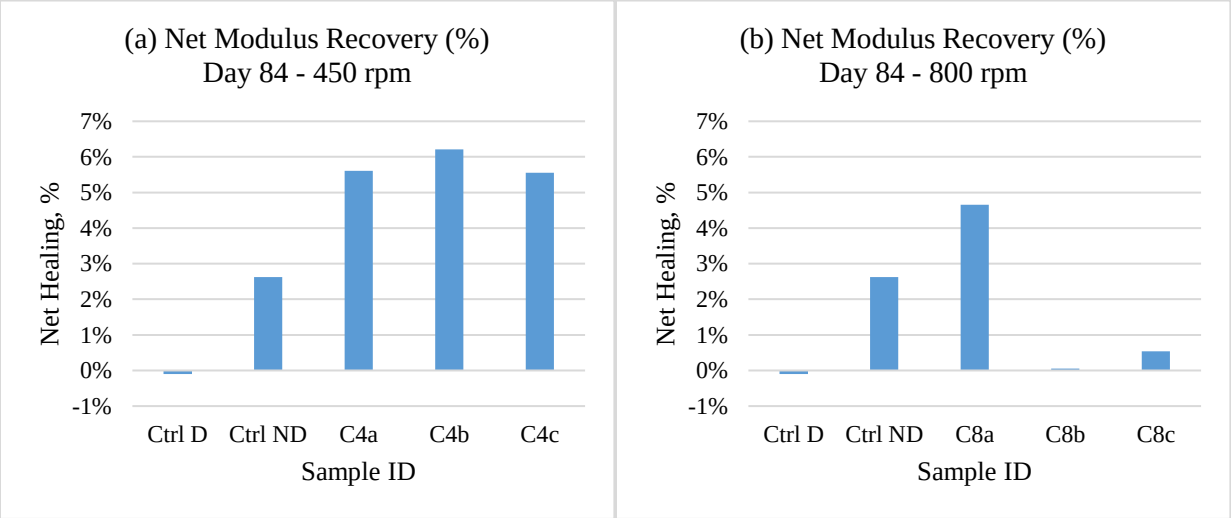

Figure 5.7. Net Modulus of Elasticity Recovery at Day 84 for Microcapsule Case: (a) 450 rpm; (b) 800 rpm *(Continued)*

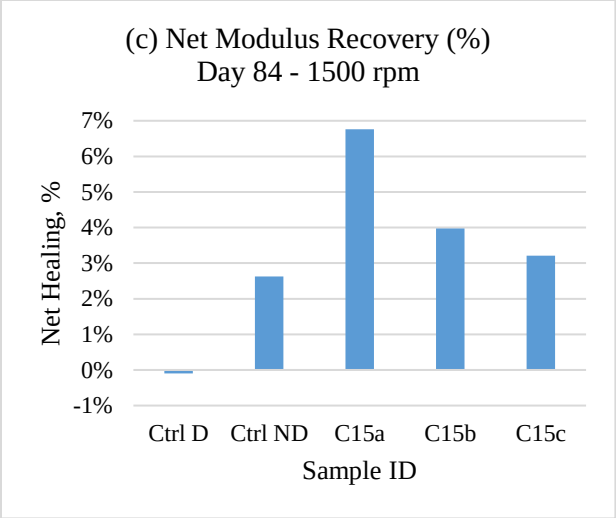

Figure 5.7. *(Continued)* Net Modulus of Elasticity Recovery at Day 84 for Microcapsule Case: (c) 1500 rpm.

5.5.4 Compressive Strength

Before Healing

Compressive strength results were compiled for the 100mm x 200mm samples in Table 5.4. Overall, the variability in strength was low, showing that the range of the compressive strength between specimens with microcapsules to be 4.1 MPa. The maximum strength was observed for the Ctrl D specimens. For the microcapsule-containing samples, the highest strength was achieved by C8a. In contrast, C15c displayed the lowest strength, while presenting the largest concentration of 1500 rpm capsules. This may be attributed to the fact that the 1500 rpm capsules tended to agglomerate more than capsules produced at 450 rpm and 800 rpm, using the new encapsulation procedure.

The corresponding compressive strength of each sample group is illustrated in Table 5.8, where the results were grouped by their respective microcapsule cases. It may be observed that a

concentration of 0.50% yielded the strongest concrete for samples containing microcapsules prepared at 450 rpm and 1500 rpm cases, respectively. In contrast, the lowest microcapsule dosage yielded higher strengths only for the 800 rpm case. Furthermore, the lowest strength was observed at the highest concentration of microcapsules for all cases.

Table 5.4. Compressive Strength Results

Sample ID	Agitation Rate, rpm	Concentration (% by weight of cement)	Avg. Compressive Strength, MPa	SD	Avg. Ultimate Load, kN	SD
Ctrl D	N/A	With Defoamer	66.1	1.18	540	9.06
Ctrl ND	N/A	No Defoamer	61.5	0.98	499	5.58
C4a	450	0.25%	59.7	1.49	490	12.00
C4b	450	0.50%	60.7	0.86	499	7.00
C4c	450	1.00%	59.4	2.39	487	18.24
C8a	800	0.25%	61.1	1.79	500	14.67
C8b	800	0.50%	60.0	1.29	493	11.66
C8c	800	1.00%	59.0	0.93	483	7.60
C15a	1500	0.25%	59.2	1.08	482	7.48
C15b	1500	0.50%	60.4	0.70	491	4.54
C15c	1500	1.00%	56.0	1.89	455	14.25

In general, Ctrl D exhibited the highest strength and was substantially stronger in compression than the other samples. In addition, the results from most microcapsule containing samples were comparable to that of Ctrl ND. To quantify the effect of microcapsule concentration on the compressive strength, a statistical analysis was conducted using Fisher's Least Square Difference (LSD) test. For the 450 rpm cases, the results showed no statistical difference between Ctrl ND and groups C4a, C4b, and C4c, while the mean compressive strength of Ctrl D remained significantly higher than all the other groups.

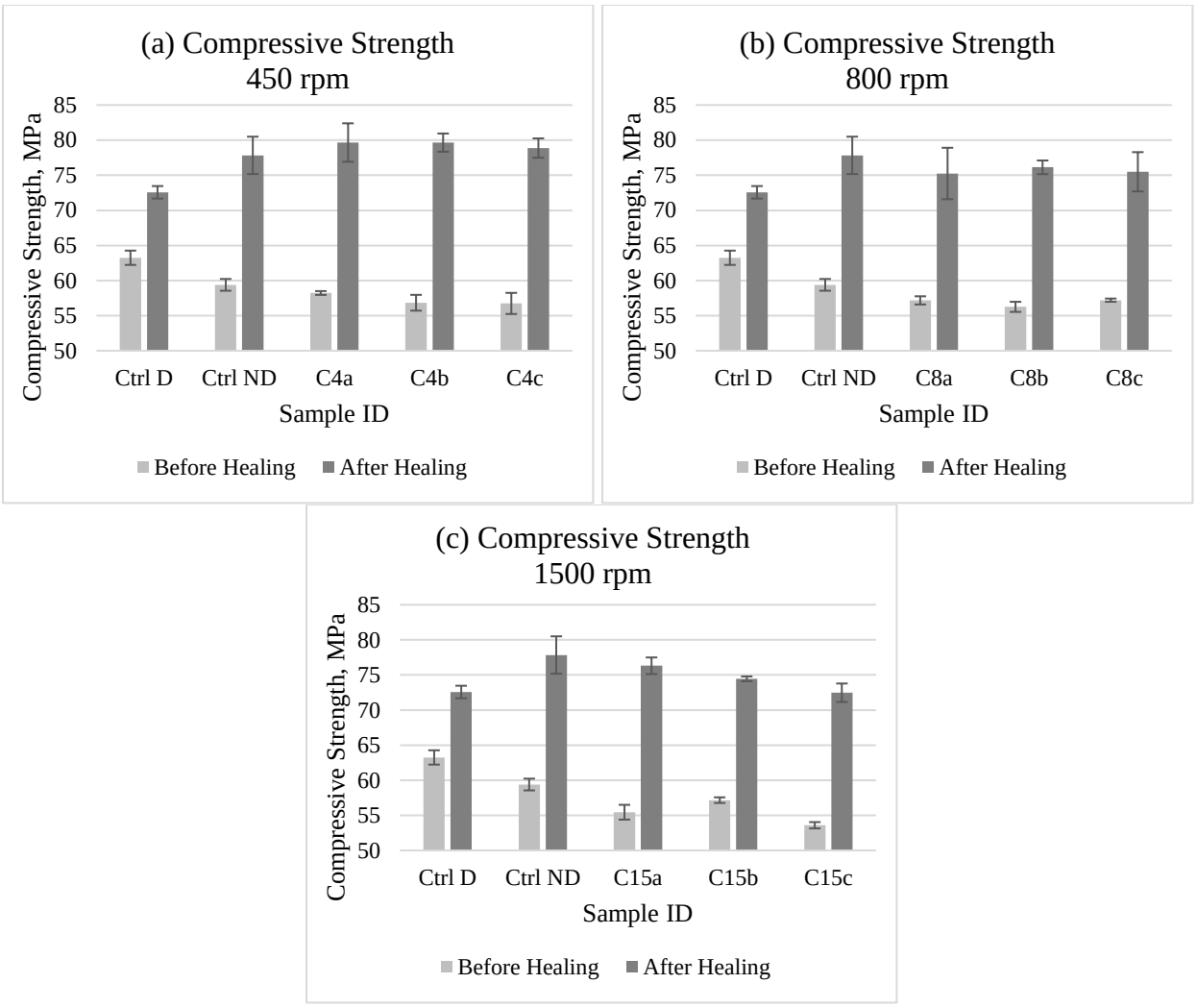

Figure 5.8. Compressive Strength Results Before and After Healing for Microcapsule Case: (a) 450 rpm; (b) 800 rpm; (c) 1500 rpm

After Healing

After all specimens were damaged and left to heal by water immersion for 86 days, compressive strength tests were conducted. The strength results before and after healing are presented in Figure 5.8. It is evident that all samples did show substantial increases in strength after damage. The strongest samples after healing were all from the 450 rpm microcapsule group, where only samples C4a, C4b, and C4c resulted in higher strengths than both control specimens. In contrast,

specimen group C15c had the lowest compressive strength values after the healing period, closely followed by the control specimen Ctrl D.

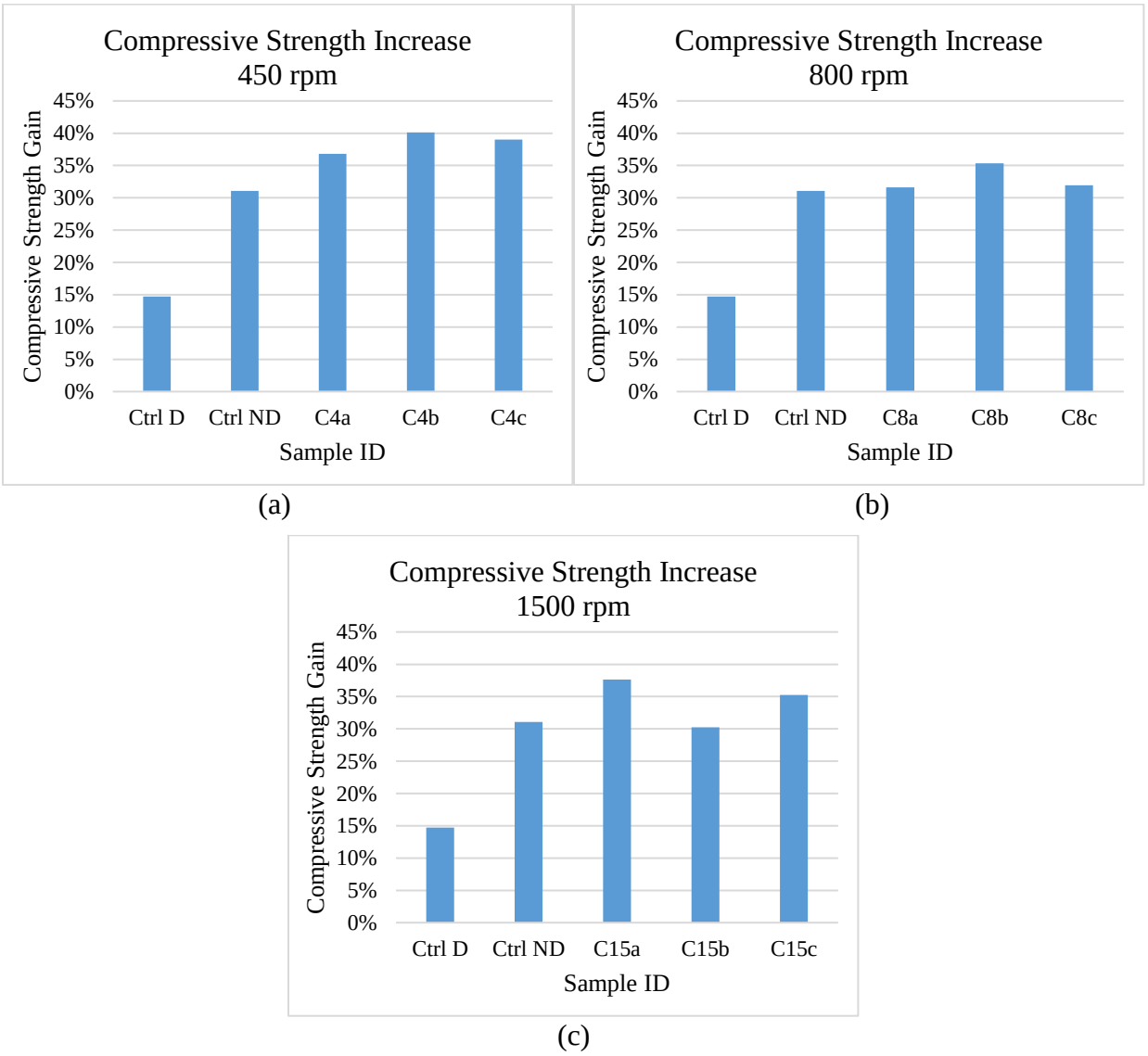

Figure 5.9. Compressive Strength Increases After Healing for Microcapsule Case: (a) 450 rpm; (b) 800 rpm; (c) 1500 rpm

It can be observed that while Ctrl D had the highest compressive strength before healing, it achieved one of the lowest strengths after healing. Therefore, it is important to measure the increases in strength relative to their initial, pristine strength values. The samples' percentage

increases in strength after healing are presented in Figure 5.9. While C15c showed the lowest strength results after healing, it is important to point out that the percentage increase is significantly higher than Ctrl D. In general, all microcapsule-containing sample groups exhibited a higher percentage increase in strength after healing than both control groups, except for C15b. Moreover, the highest increases were observed consistently from the 450 rpm specimen groups C4a, C4b, and C4c, where C4b was the highest by increasing 40% from its initial strength after damage.

5.5.5 Concrete Microstructure

The concrete microstructure was observed using the Back Scattered Electrons (BSE) mode for both control specimens Ctrl D and Ctrl ND, and the microcapsule-containing specimens C4a, C4b, C8a, C15a after 86 days of healing. In general, Figure 5.10 shows that there was a significant number of unhydrated cement particles for all observed specimens, marked by the white dots in the BSE images. This is reflective of the low water-cement ratio that was used, and thus increases the potential to promote further hydration reactions.

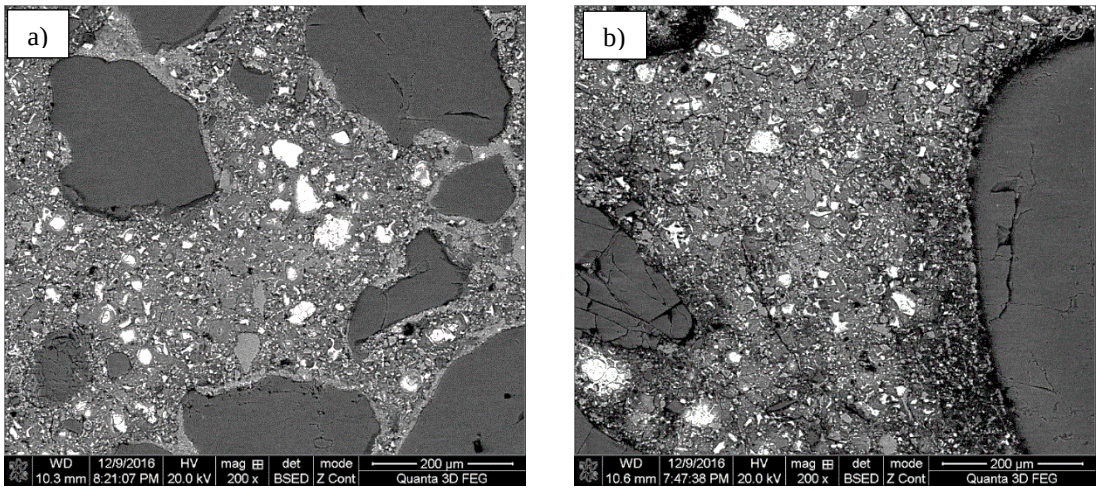

Figure 5.10. Backscattered electron images for the polished concrete microstructure for specimen groups: (a) Ctrl ND; (b) Ctrl ND. *(Continued)*

The role of the healing agent was to intensify or enhance the reaction of unhydrated cement particles, and it has demonstrated its potential with superior gains in concrete's mechanical properties after damage for most microcapsule-containing specimens. The success of the healing agent therefore greatly depends on its dispersion within the cementitious matrix, and the availability of unhydrated cement particles in the vicinity.

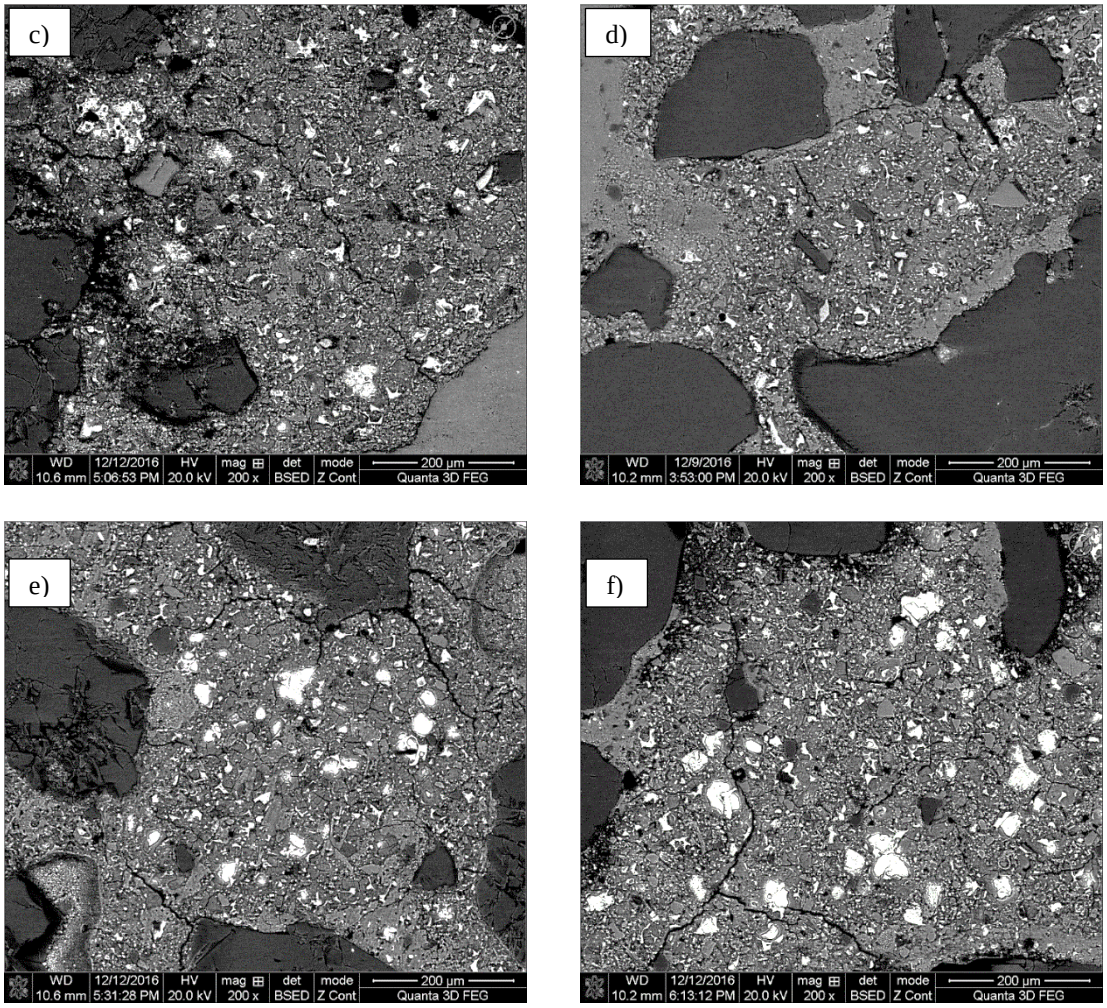

Figure 5.10. *(Continued)* Backscattered electron images for the polished concrete microstructure for specimen groups: (c) C4a; (d) C4b; (e) C8a; and (f) C15a.

The microstructure on all samples seems compact, with low voids and low porosity as shown in Figure 5.10. This also corroborates the low air content that was recorded from the concrete's fresh properties. Compared to the concrete microstructure from the authors' previous study, the porosity was substantially decreased and thus resulted in stronger specimens. Figure 5.11 shows the BSE images of the concrete microstructure from the previous study, which featured a different mix design and microcapsules developed without a Span 60 surfactant (Milla et al. 2016). In addition, the number of white spots that correspond to the unhydrated cement particles are significantly larger in quantity and size than in the authors' previous study, where a high water-cement ratio of 0.48 was used. Indeed, this increased the possibilities of the healing agent reacting with the unhydrated cement particles and thus the healing activity was successful in this study.

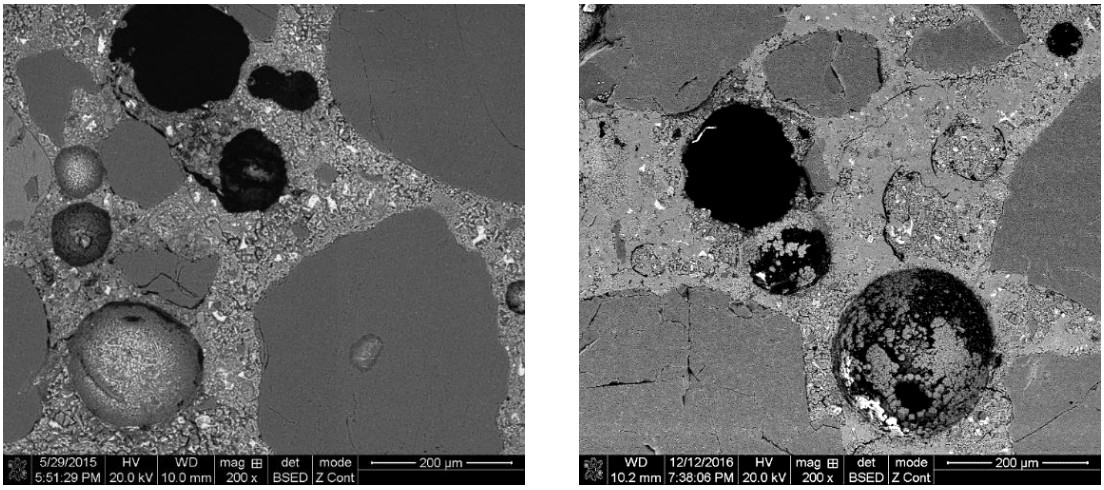

(a)

Figure 5.11. Backscattered electron images for the polished concrete microstructure for previously studied specimen groups (Milla et al. 2016): (a) 450 rpm, 1.0% *(Continued)*

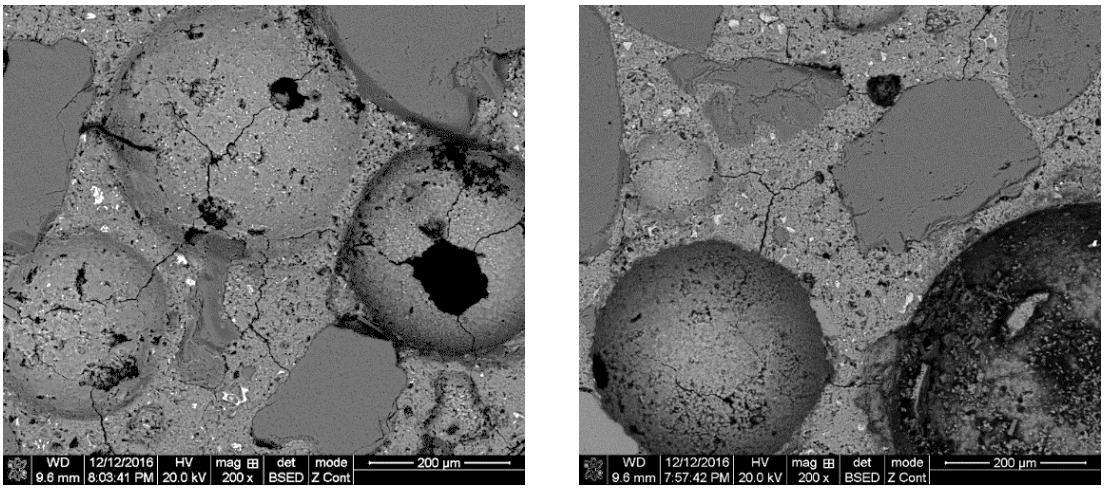

(b)

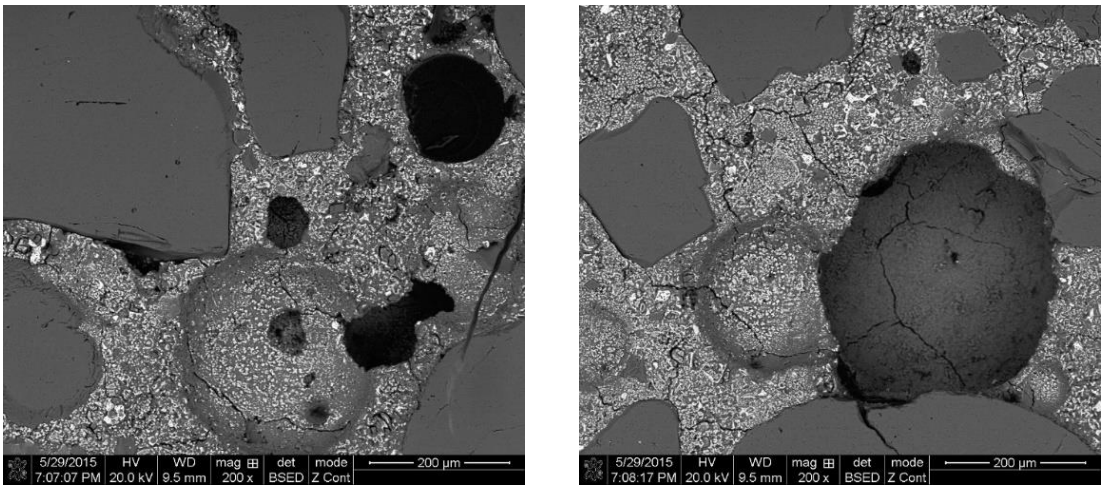

(c)

Figure 5.11. *(Continued)* Backscattered electron images for the polished concrete microstructure for previously studied specimen groups (Milla et al. 2016): (b) 800 rpm, 0.50%; and (c) 1500 rpm, 1.0%

5.6 Summary and Conclusions

The objective of this study was to evaluate the feasibility of self-healing concrete through microencapsulated calcium nitrate tetrahydrate as the healing agent, by modifying both the microencapsulation procedure and the concrete mix design adopted in previous studies. The mechanical properties of all control and microcapsule-containing specimens were evaluated

before and after damage, where the healing activity was monitored and measured periodically using the static modulus of elasticity. The success of the microcapsule technology depends on how well it increases the reaction of the exposed unhydrated cement particles with respect to the control specimens. Based on the results of the experimental program, the following may be concluded:

- The new encapsulation procedure showed a trend where lower agitation rates during synthesis produced larger microcapsules. In addition, those microcapsules synthesized at lower agitations were found to be less prone to agglomerate at the macro-level. This was due to the Span 60 emulsifier as it provided a hydrophobic coating on the microcapsule surface, which resulted in a greater attraction between the hydrophobic particles that was intensified with a larger specific surface area. Future work should focus on achieving a more uniform dispersion of microcapsules throughout the cementitious matrix.

- Both the new encapsulation procedure and a modified mix design that included a defoaming agent resulted in strong mechanical properties comparable to the control group that had no defoaming agent admixed. The lower microcapsule concentrations of 0.25% and 0.50% yielded higher strengths in compression. In contrast, microcapsule dosage of 1.00% yielded the weakest samples for all cases.

- Two of the three weakest samples in compression were from the microcapsules prepared at 1500 rpm. This may be attributed to the fact that the 1500 rpm capsules were more difficult to disperse during mixing.

- The compressive strength results after healing show that virtually all microcapsule-containing specimens resulted in a higher percentage strength gain than both controls,

relative to their initial strength, where the 450 rpm group had the highest increases from the experimental matrix. Ctrl D exhibited the lowest increase in strength, while Ctrl ND had a more significant increase, albeit smaller than the microcapsule-containing specimens (except for C15b).

- The variability of the pristine modulus of elasticity values between the control groups and the microcapsule containing specimens was minimal. In addition, most microcapsule-containing specimens were less affected by the damage cycles than both control specimen groups.
- After 21 days of healing, the modulus of elasticity values showed a significant recovery from the damaged state for all samples. However, the microcapsule-containing specimens from the 450 rpm consistently exhibited a larger net modulus recovery than both control specimens. At the end of the healing period, the largest net modulus recovery was observed for sample C15a, followed by all three 450 rpm sample groups - C4a, C4b, and C4c.

5.7 Acknowledgments

The authors would like to acknowledge the financial support through a grant from Qatar National Research Foundation (QNRF)/ National Priorities Research Program (NPRP) as well as the laboratory support from Louisiana Transportation Research Center (LTRC).

5.8 References

ACI Committee 301 (1991). "Proposed revision of: Guide to durable concrete." *Materials Journal*, 88(5).

Alexandridou, S., and Kiparissides, C. (1994). "Production of oil-containing polyterephthalamide microcapsules by interfacial polymerization. An experimental investigation of the effect of process variables on the microcapsule size distribution." *Journal of Microencapsulation*, Taylor & Francis, 11(6), 603–614.

ASCE. (2013). *2013 Report Card for America's Infrastructure*. American Society of Civil Engineers, Reston, VA.

Brown, E. N. (2003). "In situ poly (urea-formaldehyde) microencapsulation of dicyclopentadiene." 20(6), 719–730.

Dong, B., Fang, G., Ding, W., Liu, Y., Zhang, J., Han, N., and Xing, F. (2016). "Self-healing features in cementitious material with urea – formaldehyde / epoxy microcapsules." *Construction and Building Materials*, Elsevier Ltd, 106, 608–617.

Edvardsen, C. (1999). "Water Permeability and Autogenous Healing of Cracks in Concrete." *Materials Journal*, 96(4).

Gilford, J., Hassan, M., Rupnow, T., Barbato, M., Okeil, A., and Asadi, S. (2013). "Dicyclopentadiene and Sodium Silicate Microencapsulation for Self-Healing of Concrete." *Journal of Materials in Civil Engineering*, American Society of Civil Engineers, 26(5), 886–896.

Hassan, M. M., Milla, J., Rupnow, T., Al-Ansari, M., and Daly, W. H. (2016). "Microencapsulation of Calcium Nitrate for Concrete Applications." *Transportation Research Record: Journal of the Transportation Research Board*, Transportation Research Board, 2577, 8–16.

Hilloulin, B., Tittelboom, K. Van, Gruyaert, E., Belie, N. De, and Loukili, A. (2015). "Cement & Concrete Composites Design of polymeric capsules for self-healing concrete." *Cement and Concrete Composites*, Elsevier Ltd, 55, 298–307.

Justnes, H. (2003). "Explanation of Long-Term Compressive Strength of Concrete Caused by the Set Accelerator Calcium Nitrate." *11th International Congress on the Chemistry of Cement (ICCC)*, Durban, South Africa, 475–484.

Justnes, H. (2010). "Calcium nitrate as a multi-functional concrete admixture." *Concrete (London)*, 44(1), 34–36.

Kanellopoulos, A., and Giannaros, P. (2016). "The effect of varying volume fraction of microcapsules on fresh , mechanical and self-healing properties of mortars." *Construction and Building Materials*, The Authors, 122, 577–593.

Karagöl, F., Demirboğa, R., Kaygusuz, M. A., Yadollahi, M. M., and Polat, R. (2013). "The influence of calcium nitrate as antifreeze admixture on the compressive strength of concrete exposed to low temperatures." *Cold Regions Science and Technology*, 89, 30–35.

Li, V. C., and Herbert, E. (2012). "Robust Self-Healing Concrete for Sustainable Infrastructure." *Journal of Advanced Concrete Technology*, 10(6), 207–218.

Lv, L., Yang, Z., Chen, G., Zhu, G., Han, N., Schlangen, E., and Xing, F. (2016). "Synthesis and characterization of a new polymeric microcapsule and feasibility investigation in self-healing cementitious materials." 105, 487–495.

Maes, M., Van Tittelboom, K., and De Belie, N. (2014). "The efficiency of self-healing cementitious materials by means of encapsulated polyurethane in chloride containing environments." *Construction and Building Materials*, Elsevier Ltd, 71, 528–537.

Milla, J., Hassan, M. M., Rupnow, T., Al-Ansari, M., and Arce, G. (2016). "Effect of Self-Healing Calcium Nitrate Microcapsules on Concrete Properties." *Transportation Research Record: Journal of the Transportation Research Board*, Transportation Research Board, 2577, 69–77.

Övez, B., Çitak, B., Öztemel, D., Balbaş, A., Peker, S., and Çakir, Ş. (1997). "Variation of droplet sizes during the formation of microcapsules from emulsions." *Journal of Microencapsulation*, Taylor & Francis, 14(4), 489–499.

Pelletier, M. M., Brown, R., Shukla, A., and Bose, A. (2010). "Self-healing concrete with a microencapsulated healing agent." *University of Rhode Island, Kingston,USA*, (C).

Ramachandran, V. S. (1996). *Concrete Admixtures Handbook*. William Andrew Publishing, Park Ridge, NJ.

Van Tittelboom, K., and De Belie, N. (2013). *Self-healing in cementitious materials-a review*. *Materials*.

Van Tittelboom, K., De Belie, N., Van Loo, D., and Jacobs, P. (2011). "Self-healing efficiency of cementitious materials containing tubular capsules filled with healing agent." *Cement and Concrete Composites*, Elsevier Ltd, 33(4), 497–505.

Wang, J. Y., Soens, H., Verstraete, W., and De Belie, N. (2014). "Self-healing concrete by use of microencapsulated bacterial spores." *Cement and Concrete Research*, Elsevier Ltd, 56, 139–152.

White, S. R., Sottos, N. R., Geubelle, P. H., Moore, J. S., Kessler, M. R., Sriram, S. R., Brown, E. N., and Viswanathan, S. (2001). "Autonomic healing of polymer composites." *Nature*, Macmillian Magazines Ltd., 409(6822), 794–797.

Wu, M., Johannesson, B., and Geiker, M. (2012). "A review: Self-healing in cementitious materials and engineered cementitious composite as a self-healing material." *Construction and Building Materials*, Elsevier Ltd, 28(1), 571–583.

Yang, Z., Hollar, J., He, X., and Shi, X. (2011). “A self-healing cementitious composite using oil core/silica gel shell microcapsules.” *Cement and Concrete Composites*, Elsevier Ltd, 33(4), 506–512.

Zivica, V., and Bajza, A. (2001). “Acidic attack of cement based materials ҭ a review . Part 1 . Principle of acidic attack.”

Zwaag, S. van der. (2007). *Self Healing Materials An Alternative Approach to 20 Centuries of Materials Science. Igarss 2014*.

CHAPTER 6

EXAMINATION OF THE CRACK-REPAIR EFFICIENCY OF STEEL FIBER REINFORCED CONCRETE BEAMS WITH SELF-HEALING PROPERTIES

6.1 Introduction

Concrete is one of the most widely used construction materials, accounting for approximately 3.4% of the world's CO_2 emissions (Hanle 2006)(EPA 2010). Its popularity stems from its low cost, robust compressive strength, and durability. However, concrete can also be susceptible to cracking due to its low tensile strength (Mehta and Monteiro 2006). Without adequate repair and maintenance, concrete cracks could compromise the performance of reinforced concrete structures if the steel reinforcement is exposed hazardous environments. The current budgeted maintenance and repairs are insufficient to address the nation's infrastructure deterioration, where the Federal Highway Administration has identified a $836 billion backlog of investment needs in bridges and highways (FHWA 2015).

In the United States, a 2017 Bridge Report found that there are 56,000 structurally deficient bridges, where 1,900 of those are from the Interstate Highway System. In Louisiana, 15% of the state's bridges are classified as functionally obsolete (ARTBA 2017). Similarly, approximately 25,000 of Canada's 75,000 highway bridges have been deemed structurally deficient with a short remaining service life (NRC 2013). To address these challenges, concrete materials need to be redesigned to promote durability and require minimal maintenance and repairs. Over the past years, self-healing concrete has been proposed through several approaches to autonomously repair cracks, including engineered cementitious composites (ECCs), crystalline admixtures, microencapsulated healing agents, and bacterial concrete (Dry 1994,

2001; Kanellopoulos and Giannaros 2016; Li and Herbert 2012; Roig-Flores et al. 2015; Van Tittelboom and De Belie 2013; Wiktor and Jonkers 2011; Yang et al. 2009).

Self-healing concrete by microencapsulated healing agents has the advantage of providing a localized response during a cracking event given that the microcapsules are uniformly dispersed throughout the cementitious matrix. Depending on the healing agent selected, an environmental stimulus may or may not be needed to form a new crack-sealing product (Wu et al. 2012a). Studies have shown that the key factors for a successful application of self-healing concrete by microencapsulation are: (a) the viscosity of the healing agent; (b) a high probability of rupturing microcapsules during a cracking event; (c) the bond strength between the microcapsule and the cementitious matrix; (d) a robust microcapsule shell that can withstand the mixing process (Dry 1994; Van Tittelboom and De Belie 2013).

In this study, self-healing concrete was investigated through microencapsulated calcium nitrate tetrahydrate. Calcium nitrate hydrate was selected as the healing agent due to its low cost and its ability to react with the cementitious matrix. In a cracking event, the surrounding microcapsules are expected to rupture and release the healing agent that would react mainly with the unhydrated cement particles exposed at the crack surfaces. In the presence of moisture, calcium nitrate would react with unhydrated cement particles to form hydroxy nitrate salts that promote the densification of cement and contribute to the formation of calcium silicate hydrate. Moreover, calcium nitrate would also react directly with the cementitious matrix in the presence of moisture to produce calcium hydroxide and calcium carbonate, where the latter is produced by increasing the saturation index of calcite (Arce et al. 2016; Karagöl et al. 2013; Ramachandran 1996).

6.2 Background

Concrete materials have a unique, intrinsic capability to seal hairline fractures in the presence of moisture. This phenomenon is known as the autogenous healing capability of concrete, and it can occur through the continued hydration of unhydrated cement particles, and most commonly through the formation of calcium carbonate by reacting with water and the carbon dioxide in the atmosphere (Hearn 1998; Wu et al. 2012a).

However, the autogenous healing capability is limited up to 100-micron crack widths in the presence of moisture. In addition, the smaller cracks tend to heal significantly faster than larger cracks (Edvardsen 1999; Reinhardt and Jooss 2003). For this reason, researchers aim to promote a reliable, autonomous crack-repair of concrete by either: (a) significantly limiting the crack widths to facilitate the autogenous healing mechanism; (b) enhancing its autogenous healing capability through admixtures or reactive agents; or (c) forming new products with the help of a catalyst or an environmental stimulus (Huang et al. 2016; Van Tittelboom and De Belie 2013; Wu et al. 2012b).

With the use of microcapsules, a healing agent could potentially be stored for a long period and only be used when needed (i.e. during cracking) to avoid premature reactions within the cementitious matrix. Recent investigations on self-healing concrete by microencapsulated healing agents have focused on finding the optimal healing agent and concentration of microcapsules to be added by weight of cement. The healing agents studied include chemicals that can directly react with the cementitious matrix (e.g. sodium silicate) and those that need an embedded catalyst to trigger polymerization at room temperature, such as dicyclopentadiene and epoxy (Gilford et al. 2013; Kanellopoulos and Giannaros 2016; Lv et al. 2016; Mostavi et al. 2015; Pelletier et al. 2010; Wang et al. 2014; Yang et al. 2011).

With respect to the quantification of self-healing processes, Wiktor monitored the progression of the bacterial concrete's autonomous crack-repair over a period of 100 days by taking linear measurements of the crack widths at regular 0.4 mm intervals along the length of the crack. It is important to note that the crack width measurements were taken at the exact locations every week in order to normalize the results as a percentage of crack closure (Wiktor and Jonkers 2011). In addition, the healing products were characterized using the Fourier-Transform Infrared (FT-IR) spectra due to their crystalline nature. The results showed the healing product was composed of calcite and aragonite (Wiktor and Jonkers 2011).

Arce et al. evaluated the self-healing performance of microencapsulated calcium nitrate by measuring the crack areas crack before and after healing. The results were then presented as a percentage of healing with respect to the initial crack area. The healing products obtained were characterized using an environmental scanning electron microscope (ESEM) with energy dispersive spectroscopy (EDS) capabilities. Subsequently, atomic ratio plots of Aluminum/Calcium versus Silica/Calcium to verify the presence of Calcium Silica Hydrate (CSH) particles and calcium rich crystals (Arce et al. 2016).

6.3 Objective

The main objective of this study was to quantify the self-healing efficiency of a calcium nitrate tetrahydrate healing agent in steel-fiber reinforced concrete beams over time. This investigation is focused on finding the optimum crack-repair performance by evaluating the effect of the microcapsule size, microcapsule concentration (by weight of cement), and microcapsule shell properties. The results of this study addressed the potential crack-width limitations, and the self-healing performance over time under a curing regime with tap-water immersion.

6.4 Experimental Program

6.4.1 Microcapsule Preparation

The microencapsulation procedures used in this study aimed to synthesize two slightly different microcapsule shell properties to assess their effects on the performance and compatibility with concrete. The preparation procedure for microcapsules carrying calcium nitrate was based on the authors' previous study (Hassan and Milla 2016; Milla et al. 2016). In the investigation, the mechanical properties of concrete deteriorated significantly as the microcapsule concentration was increased. This drop in performance was due to the presence of sulfonic acid on the microcapsule shell that acidified the concrete mixing water.

To address the acidification of the mixing water, certain modifications were made to the microencapsulation procedure. In the first case, the microcapsules were synthesized under the same production parameters outlined in a previous study (Hassan and Milla 2016; Milla et al. 2016), with the addition of a de-ionized (DI) water bath on the newly formed capsules to neutralize the traces of sulfonic acid on the microcapsule surface. The microcapsules were subsequently recovered with a coarse-fritted vacuum filter. In the second case, the procedure was altered by minimizing the sulfonic acid catalyst used, while adding a Span 60 surfactant to stabilize the emulsion. In addition, the newly formed microcapsules were rinsed with DI water and subsequently retrieved through vacuum filtration. The details of the second encapsulation process was outlined in the authors' recent study (Milla et al. 2017).

Given that the agitation rates during synthesis control the average microcapsule diameter (Brown et al. 2003; Dietrich 1989), the agitation rates of 800 rpm and 1500 rpm for were used for both microcapsule types. The average microcapsule diameters are shown in Table 6.1, where at least 250 diameter measurements were taken for each case, based on the findings of the

authors' recent studies (Hassan and Milla 2016; Milla et al. 2016, 2017). The capsules produced with a Span 60 emulsifier (Sorbitan monostearate) were referred as 'SP', while the capsules produced without the Span 60 emulsifier are referred as 'OG'.

Table 6.1. Specimen details and average microcapsule diameters.

Sample ID	Concentration (by weight of cement)	Agitation Rate (rpm)	Average Microcapsule Size (μm)
Ctrl D	Control (With Defoamer)	N/A	N/A
Ctrl ND	Control (No Defoamer)	N/A	
SP 800, 0.50%	0.50%	800	50
SP 800, 0.75%	0.75%	800	
SP 1500, 0.50%	0.50%	1500	22
SP 1500, 0.75%	0.75%	1500	
OG 800, 0.50%	0.50%	800	59
OG 800, 0.75%	0.75%	800	
OG 1500, 0.50%	0.50%	1500	45
OG 1500, 0.75%	0.75%	1500	

6.4.2 Concrete Mix Design

In this study, the concrete beams were expected to be damaged to induce exterior cracks without breaking. Given that concrete is brittle and weak in its tensile strength, it was necessary to add reinforcements to add ductility. Hence, one-inch steel fibers (kindly supplied by D&C Supply Co., Inc.) were added to each specimen group. Typically, manufacturers recommend adding 30 kg/m^3 to 60 kg/m^3 of fibers to provide an adequate reinforcement to concrete. Limestone was used as a coarse aggregate with a maximum aggregate size of 19 mm, while sand was used as the fine aggregate with a maximum particle size of 4.76 mm. The mixing sequence followed ASTM C 192 standard.

A low water-cement ratio was desirable given that a calcium nitrate healing agent is more likely to enhance the autogenous healing capacity in concrete when more unhydrated cement nuclei are exposed in the crack surfaces. For this reason, a water-cement ratio of 0.405 was used with the super plasticizer Adva 195 to ensure workability. In addition, a defoamer supplied by Evonik Industries was used to counter air content increase observed previously when combining microcapsules with a super plasticizer. It is important to note that two different types of control specimens were used in this study. Ctrl D was admixed with a defoamer while Ctrl ND was not. This was done to evaluate whether the defoaming agent used for the microcapsule-containing specimens affected the healing efficiency. The concrete mix design details are provided in Table 6.2.

Table 6.2. Concrete Mix Design

Material Description	Proportions (kg/m^3)
Aggregate 1: Sand, Dennis Mills, LA	791
Aggregate 2: #67 Limestone, Martin Marietta	1116
Cement: Holcim Type I	326
Water: Mixing water	132
1” Steel Fibers	30
Air (%)	5.0%
Admixture 1: Adva 195 (ml/100kg)	455
Admixture 2: Microcapsules* (%)	0.25, 0.50, and 1.00
Admixture 3: TEGO Antifoam MR 1015* (%)	0.12

* By weight of cement

Fresh Concrete Properties

The slump and air content was measured per ASTM standards C231 and C143, respectively.

6.4.3 Quantification of Self-Healing Performance

Concrete Cracking

Concrete beams with dimensions of 100 mm x 100 mm x 350 mm were used in this study, where each specimen group consisted of three replicas that were all damaged to induce cracking. After the cast samples were cured for 28 days in a 95% relative humidity room, the beams were oven-dried for 3 days at 60 °C and subsequently subjected to a three-point bending test to induce cracks, using the MTS 322 Test Frame. A strain-controlled load application at a rate of 0.02 mm/min was used to prevent failure and ensure that the test can be stopped immediately after a sudden change in displacement is detected.

Curing Regime

The curing regime selected was tap water immersion at room temperature to enable healing. The tap water was replaced at Day 7, 21, and 42. All samples were oven-dried for 3 days at 60 °C prior to observation to simulate the effect of wet-dry cycles.

Crack Measurements

The self-healing efficiency was monitored over time with a stereo microscope Leica MZ75 with a Nikon Digital Sight DS-Fi2 camera attached. The images taken from each crack were stitched with Microsoft's Image Composite Editor program, and the crack widths were measured linearly with the ImageJ image processing program. The specimens were observed after healing at 7, 21, and 42 days.

6.4.4 Healing Product Characterization

ESEM/EDS

After 42 days of healing, the crack areas were investigated for their healing products forming in the crack areas. Due to the sample size limitations in an electron microscope chamber, one concrete sample from each specimen group was cored with a 5 cm coring drill, and then subsequently cut with a diamond blade saw to ensure the sample size was limited to a small 5 cm x 2.5 cm cylinder.

The samples were viewed in an environmental scanning electron microscope (ESEM) at an accelerating voltage of 20 kV under the backscattered electron (BSE) imaging mode at a low vacuum, using the FEI Quanta 3D FIB apparatus. In addition, energy dispersive spectroscopy (EDS) spectrums were collected under the point analysis mode at locations where healing products had formed for characterization.

6.5 Results

6.5.1 Fresh Concrete Properties

The results from the slump and air entrainment tests are shown in Table 6.3. In general, there was minimal variability in the air content between the control groups and the microcapsule containing specimens. It can be observed that the air content was slightly greater for the OG specimen group when compared to the SP group. Nevertheless, the air content remains low for all specimens and therefore will not compromise the strength of the mix design as experienced in the author's previous study (Hassan et al. 2016). On the other hand, the addition of a defoaming

agent could compromise the performance of concrete in colder climates due to decreased freeze-thaw resistance.

With respect to slump, the addition of the steel fibers did seem to influence workability, where the mix was found to be stiffer. The decrease in workability was observed in particular for the OG specimen group. However, with the use of a concrete vibrating table the concrete mix successfully consolidated into the beam molds.

Table 6.3. Slump and Air Content

Sample ID	Agitation Rate, rpm	Concentration (% by wt. cement)	Slump, mm	Air Content, %
Ctrl D	N/A	Control (With Defoamer)	55	1.8
Ctrl ND	N/A	Control (No Defoamer)	65	1.5
SP 800, 0.50%	800	0.50%	55	2.1
SP 800, 0.75%	800	0.75%	30	2.3
SP 1500, 0.50%	1500	0.50%	15	2.8
SP 1500, 0.75%	1500	0.75%	25	2.3
OG 800, 0.50%	800	0.50%	140	1.8
OG 800, 0.75%	800	0.75%	75	1.8
OG 1500, 0.50%	1500	0.50%	100	1.8
OG 1500, 0.75%	1500	0.75%	140	1.1

6.5.2 Self-Healing Quantification

The steel fibers added substantial ductility to the concrete beams, and thus the cracks extended from the bottom of the beam towards three quarters of the beam's side lengths. Qualitatively, it was observed that the introduction of microcapsules significantly increased the autonomous crack-repair when compared to the control specimens. The healing product appeared to be of crystalline nature, thus indicating there could be calcium carbonate and calcium hydroxide present. Images comparing the cracks before and after 42 days of healing are shown in Figure 6.1.

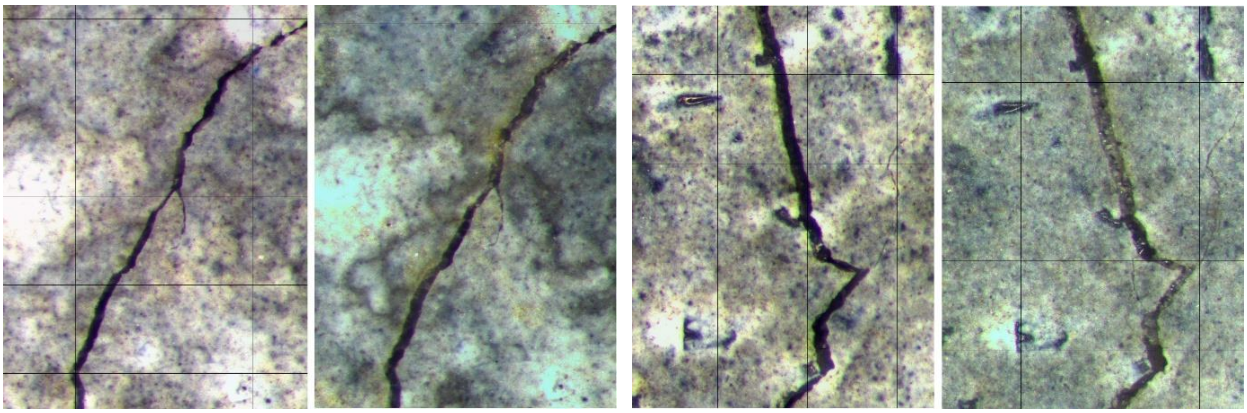

(a) Ctrl D (b) Ctrl ND

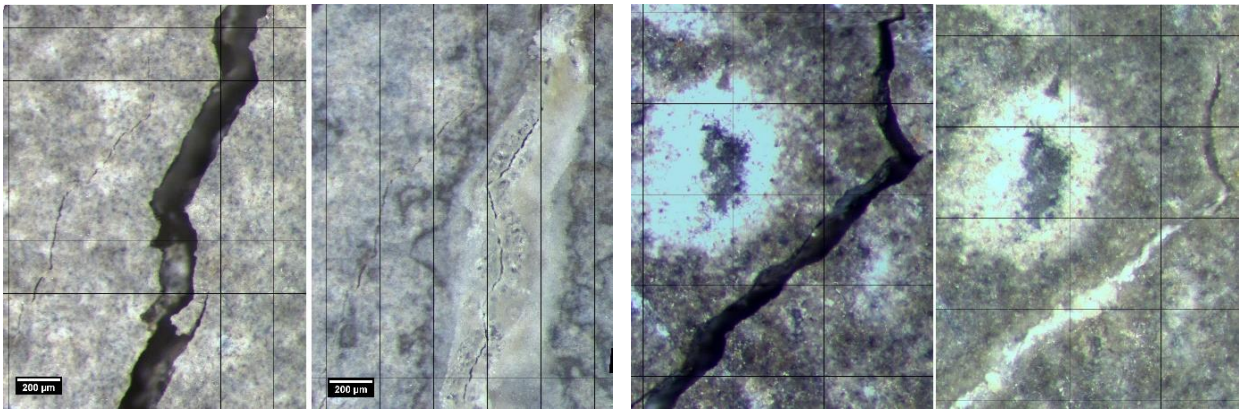

(c) SP 800, 0.50% (d) OG 800, 0.50%

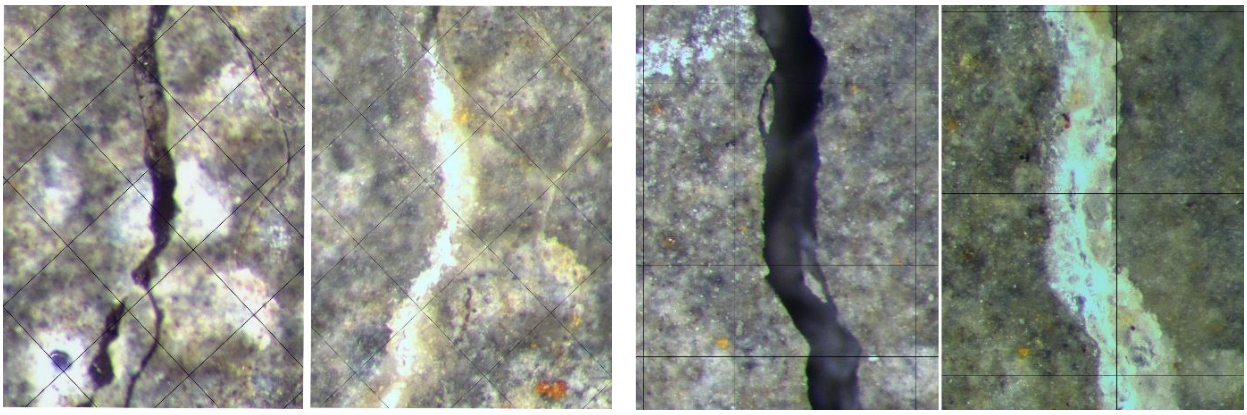

(e) SP 1500, 0.50% (f) OG 1500, 05%

Figure 6.1. Comparison of initial crack and Day 42 healing for samples: (a) Ctrl D; (b) Ctrl ND; (c) SP 800 rpm, 0.50%; (d) OG 800 rpm, 0.50%; (e) SP 1500 rpm, 0.50%; and (f) OG 1500 rpm, 0.50% (*Continued*)

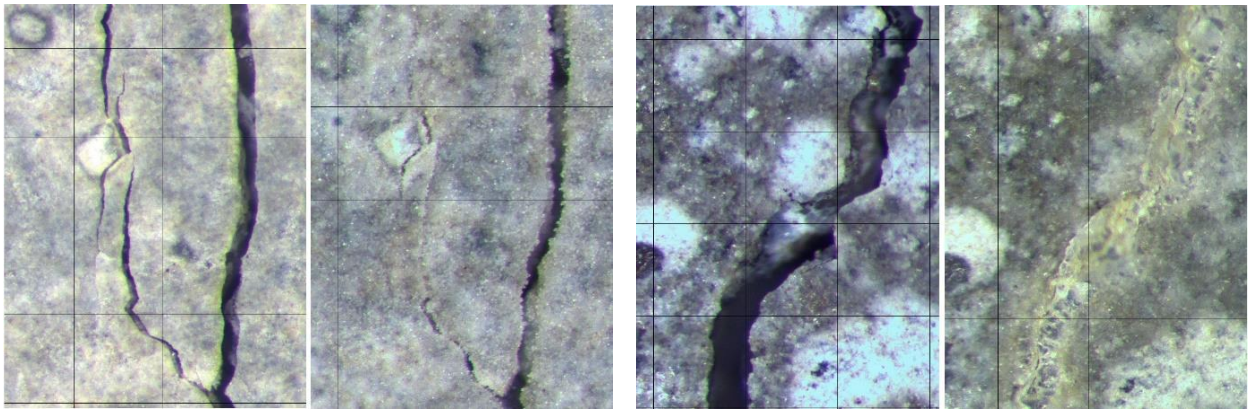

(g) SP 800, 0.75 (h) OG 800, 0.75

Figure 6.1. (*Continued*) Comparison of initial crack and Day 42 healing for samples: (g) SP 800 rpm, 0.75%; and (h) OG 800 rpm, 0.75%

Crack Measurements

For a quantitative assessment, at least 650 measurements were taken per specimen group from the side cracks that covered a variety of crack widths. The crack width measurements were taken at the exact locations before and after healing to monitor the healing progression over time. To evaluate the self-healing potential with respect to crack size, the measurements were categorized into three bins based on the initial readings before healing, from: (a) 0-25 µm; (b) 25-75 µm; and (c) 75-350 µm. This would provide insight on how the microcapsules enable healing for crack sizes beyond concrete's autogenous healing limitation.

The average crack width measurements for each specimen over time were compiled in Tables 6.4, 6.5, and 6.6 for the three crack size bins, respectively. The relatively high standard deviations shown in Table 4 are attributed to the wide range of crack widths observed in each sample, and the human error associated with taking linear measurements manually. At the 0-25 µm range, virtually all microcapsule-containing specimens decreased the average crack size over time. It is worth noting that the OG 1500 rpm cases indicated the highest crack width reduction

over time. In contrast, cases SP 1500, 0.75%, SP 800, 0.50%, and the control samples had slight increases in the mean crack widths after Day 7 and lacked considerable healing over time. It is worth noting that the wet-dry cycles may have also affected the crack widths measured.

Table 6.4. Average mean crack width measurements for the concrete beam specimens, for cracks ranging between 0-25 microns.

Sample ID	Day 0		Day 7		Day 21		Day 42	
	Mean	SD	Mean	SD	Mean	SD	Mean	SD
Ctrl D	16.7	5.3	19.6	8.1	19.0	9.1	18.9	8.8
Ctrl ND	17.5	5.1	18.3	8.3	18.8	7.8	18.4	8.2
OG 800, 0.50%	14.0	5.9	11.5	6.7	11.7	7.8	11.2	8.4
OG 800, 0.75%	13.9	6.2	9.4	7.7	10.5	8.5	9.4	9.1
OG 1500, 0.50%	15.4	5.6	11.1	8.8	7.1	7.9	6.0	7.9
OG 1500, 0.75%	14.3	5.5	9.1	8.0	9.0	7.8	7.3	7.4
SP 800, 0.50%	15.7	5.2	17.7	7.4	16.6	8.1	16.4	8.3
SP 800, 0.75%	14.5	5.7	12.9	7.7	11.4	8.2	10.2	8.4
SP 1500, 0.50%	13.6	6.1	12.1	8.1	12.1	8.4	10.7	8.9
SP 1500, 0.75%	14.4	6.0	14.9	7.8	14.9	7.9	15.7	9.0

Table 6.5 shows the results for the 25-75 μm range, where the OG specimen group generally outperformed the SP specimen group over time. The highest performing case OG 1500, 0.50% had a remarkable drop in the mean crack width, which indicates that healing took place throughout a large portion of the crack length. The control samples, however, did not show signs of healing in the 25-75 micron range either.

Table 6.5. Average mean crack width measurements for the concrete beam specimens, for cracks ranging between 25-75 microns.

Sample ID	Day 0		Day 7		Day 21		Day 42	
	Mean	SD	Mean	SD	Mean	SD	Mean	SD
Ctrl D	45.9	14.9	49.4	15.8	51.6	16.1	52.6	16.9
Ctrl ND	47.7	14.9	50.3	17.5	48.6	19.1	48.6	20.3
OG 800, 0.50%	49.0	13.7	37.3	15.5	37.2	17.7	35.4	18.1
OG 800, 0.75%	46.3	14.4	30.9	17.2	27.5	19.9	25.4	21.6
OG 1500, 0.50%	49.0	15.3	36.9	20.4	23.5	21.1	15.8	18.9
OG 1500, 0.75%	44.9	13.5	31.2	19.8	29.5	22.1	25.0	21.8
SP 800, 0.50%	47.2	14.7	48.9	17.4	42.0	20.3	40.5	21.3
SP 800, 0.75%	49.2	14.7	50.1	17.8	46.7	18.9	45.8	19.6
SP 1500, 0.50%	46.6	14.8	39.8	15.7	36.3	17.5	33.9	19.0
SP 1500, 0.75%	40.2	12.8	37.5	15.1	36.5	16.3	38.7	16.8

At the 75-350 micron range, the crack sizes were considerably large enough to limit or minimize the autogenous healing capability of concrete. In this case, the decreases in the mean crack width would be attributed to the microcapsule's healing agent reacting with the cementitious matrix. The results in Table 6 show that the mean crack width was considerably reduced in all microcapsule-containing specimens, while both control specimens resulted in larger mean crack widths and virtually no healing.

Table 6.6. Average mean crack width measurements for the concrete beam specimens, for cracks ranging between 75-350 microns *(Continued)*.

Sample ID	Day 0		Day 7		Day 21		Day 42	
	Mean	SD	Mean	SD	Mean	SD	Mean	SD
Ctrl D	110.4	29.5	113.5	29.5	118.0	30.8	119.6	30.4
Ctrl ND	104.5	27.4	110.2	27.8	108.8	29.6	112.8	30.7
OG 800, 0.50%	106.2	22.5	77.3	31.8	78.4	33.5	76.6	33.7
OG 800, 0.75%	103.8	33.5	67.9	46.7	64.5	51.6	59.9	55.7
OG 1500, 0.50%	120.7	36.5	75.7	51.6	58.2	51.3	52.8	56.2
OG 1500, 0.75%	126.3	39.1	106.0	49.2	98.0	54.4	85.7	60.1

Table 6.6. *(Continued)* Average mean crack width measurements for the concrete beam specimens, for cracks ranging between 75-350 microns.

Sample ID	Day 0		Day 7		Day 21		Day 42	
	Mean	SD	Mean	SD	Mean	SD	Mean	SD
SP 800, 0.50%	116.2	36.3	97.4	45.0	81.8	46.2	73.6	46.0
SP 800, 0.75%	97.2	16.4	92.5	16.5	80.6	21.7	82.3	21.6
SP 1500, 0.50%	119.2	34.4	90.7	40.1	84.4	47.1	83.0	48.9
SP 1500, 0.75%	87.2	16.7	82.2	14.3	81.9	21.7	77.2	24.3

Given that each specimen has its unique set of crack sizes, the results were normalized by calculating the healing efficiency using the formula below:

$$Healing\ (\%) = \frac{W_i - W_t}{W_i} \times 100$$

Where W_i is the initial crack width, and W_t is the crack width at a time *t*.

The healing efficiency distribution over time is illustrated in Figure 6.2 for the 0-25 micron range. The box and whisker plot summarizes the key features of the healing efficiency throughout the crack path, where the box outlines the interquartile range of the data, the 'X' marker the mean average, and the whiskers illustrate the standard deviations. The data points outside the standard deviations are marked as outliers, which serves as an indication that a minority of data points showed considerable healing. The standard deviations were found to be high because healing was not observed throughout the crack, thus indicating that the microcapsules were not always near the crack path.

In general, the healing efficiency increased over time for all specimens. Fisher's Least Significant Difference (LSD) test was used to analyze the effect of microcapsule type and concentration with respect to the healing efficiencies for all specimen groups. For crack sizes in

the range of 0-25 microns, virtually all microcapsule-containing specimens (except for cases SP 800, 0.50% and SP 1500, 0.75%) were found to have significantly higher healing efficiencies than the control specimens over time. The highest healing efficiencies were observed in cases OG 1500, 0.50% and OG 1500, 0.75%, averaging 64% and 52% at Day 42, respectively.

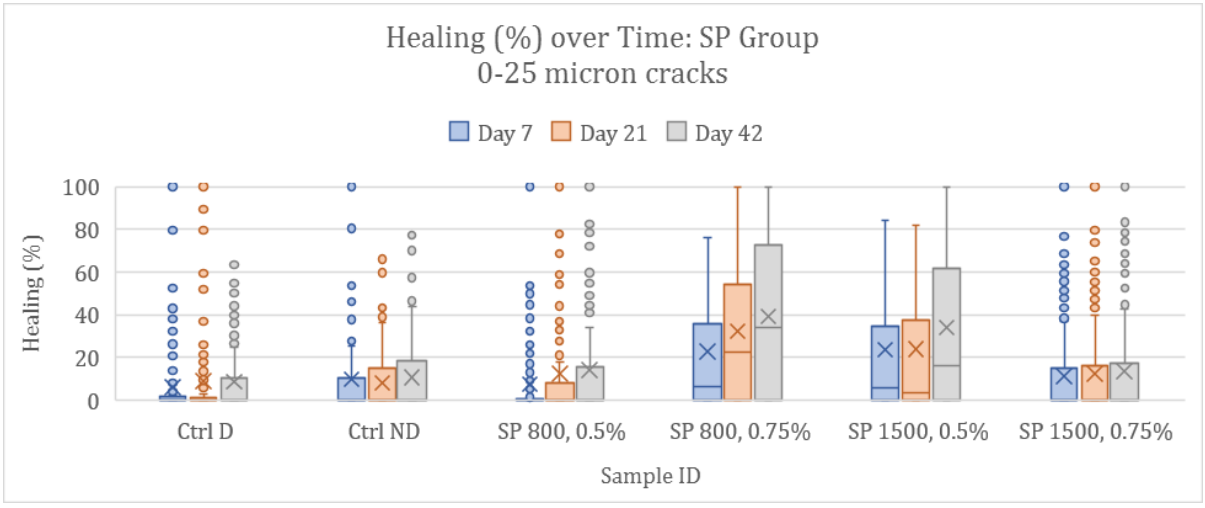

(a)

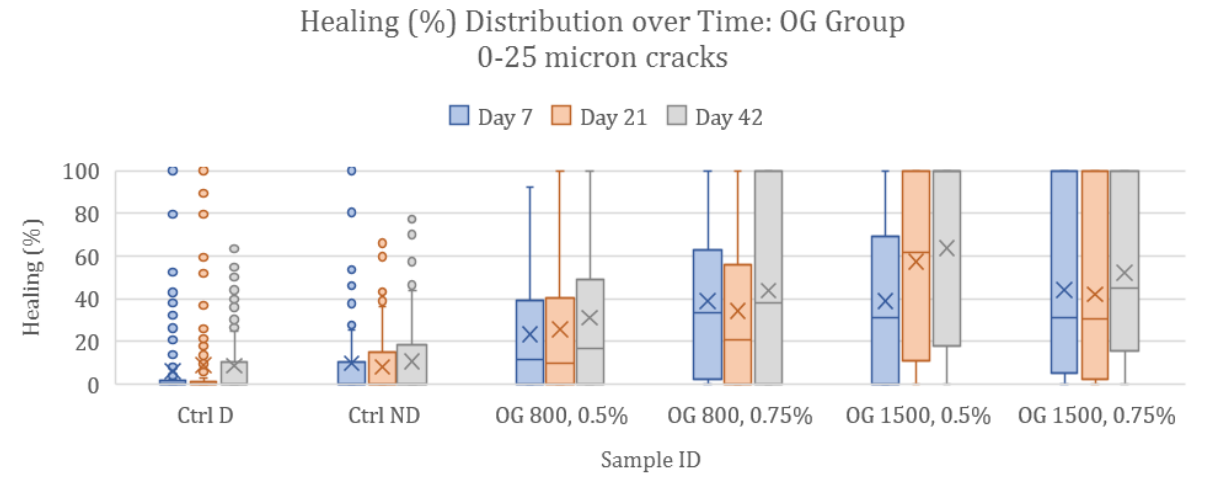

(b)

Figure 6.2. The healing efficiency distribution over time of cracks ranging from 0-25 microns, for the (a) SP specimen group; (b) OG specimen group.

For crack sizes ranging from 25-75 microns, Figure 6.3 shows the distribution of the healing efficiencies for both the OG and SP specimen groups, respectively. The distribution of the healing efficiency for the current crack sizes closely resembled that of the 0-25 micron range. Hence, the high variability reaffirms that crack-sealing occurred sporadically throughout the crack path for the microcapsule containing specimens. The control samples, however, had minimal crack-sealing and for that reason the data was more compact.

For all cases, the longer the curing time meant a higher healing efficiency, as expected. An LSD test showed clear differences between the healing performance of the microcapsule-containing specimens and the control samples at Days 7, 21, and 42. The only exception was specimen SP 800, 0.50% at Day 7, which was statistically not different from the control groups in healing at that time for the current crack size range. Furthermore, the OG specimen group outperformed the SP specimen groups when compared at the same RPM and concentration levels. The OG 1500, 0.50% case had performed consistently higher than all samples during all curing periods, and the differences between such sample and the rest is statistically significant.

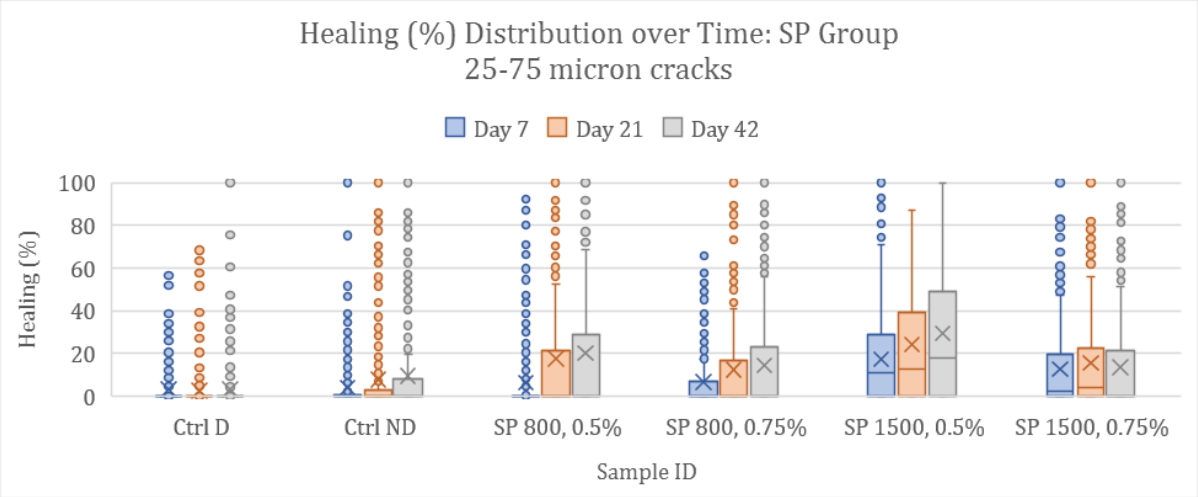

(a)

Figure 6.3. The healing efficiency distribution over time of cracks ranging from 25-75 microns, for the (a) SP specimen group. *(Continued)*

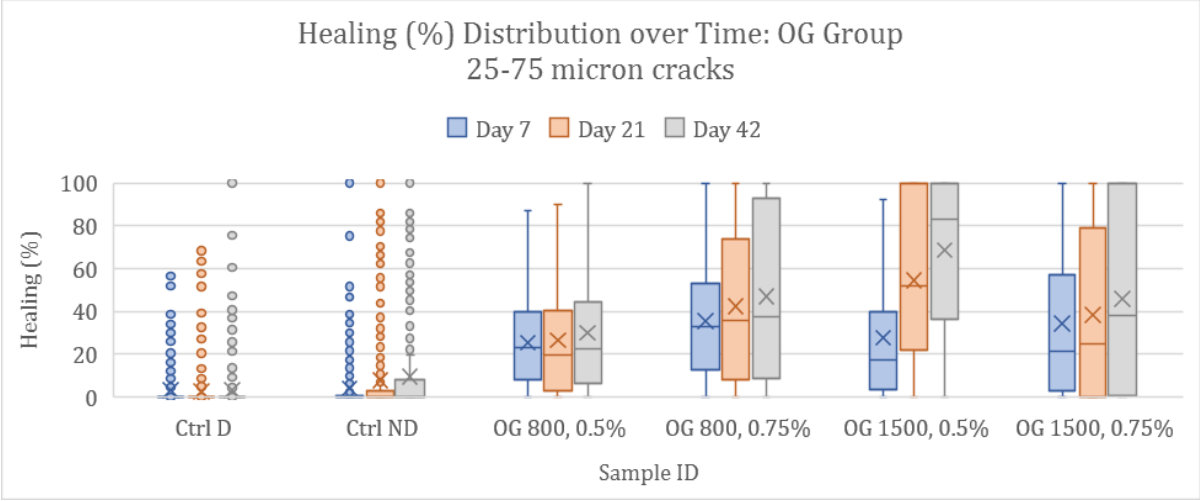

(b)

Figure 6.3. *(Continued)* The healing efficiency distribution over time of cracks ranging from 25-75 microns, for the (a) SP specimen group; (b) OG specimen group.

Lastly, Figure 6.4 shows the healing efficiency distribution over time for cracks ranging from 75-350 microns. In this size category, the control specimens consistently showed very few instances of healing, where the vast majority of the data is compact and slightly above zero. In this case, all microcapsule-containing specimens had a significantly higher efficiency than both control groups. The variability of the healing efficiency was found to be lower for most specimens due to the difficulty in completely sealing larger cracks.

A statistical analysis with an LSD test confirmed that the OG 1500, 0.50% case had a significantly higher robust healing efficiency despite the large crack sizes, followed by cases OG 800, 0.75% and OG 1500, 0.75%. The OG specimen group outperformed the SP group when compared directly with respect to the RPM and concentration (with the exception of case SP 800, 0.50% which was significantly higher than case OG 800, 0.50%). In addition, a higher

microcapsule concentration did not always increase the observed healing in any of the three crack width bins evaluated.

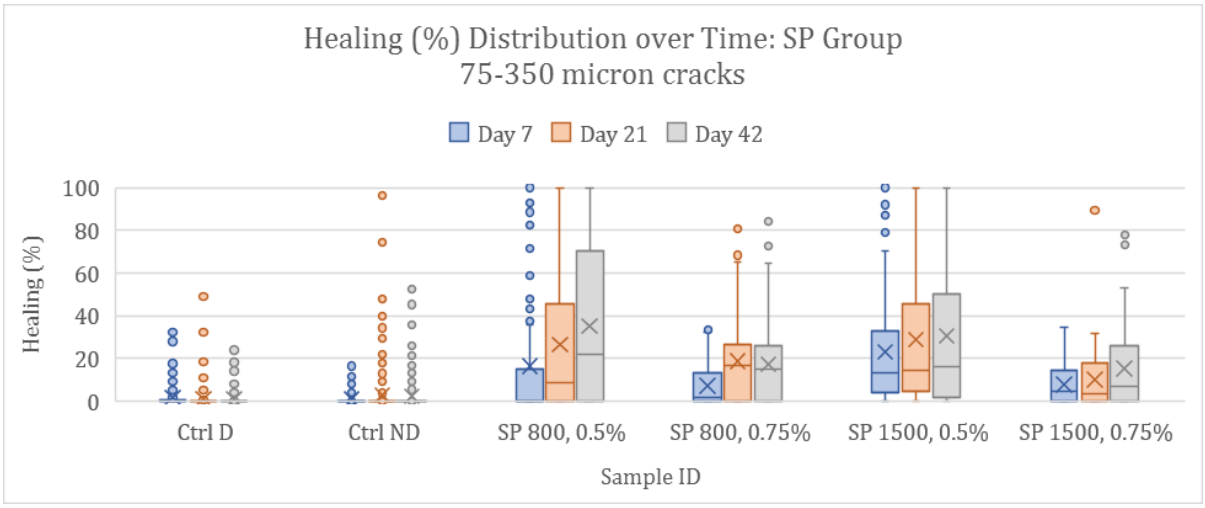

(a)

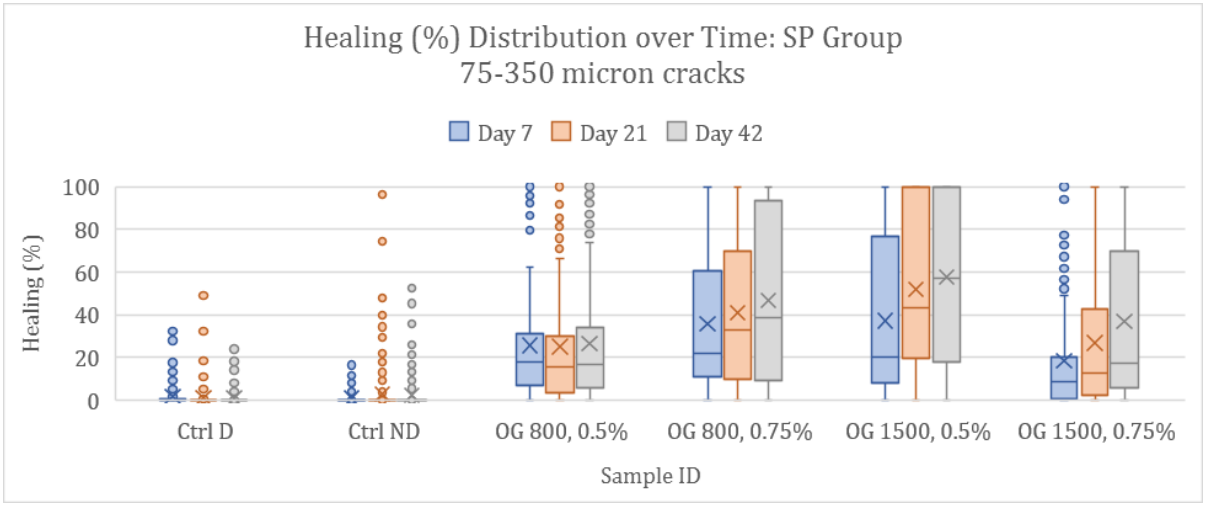

(b)

Figure 6.4. The healing efficiency distribution over time of cracks ranging from 75-350 microns, for the (a) SP specimen group; (b) OG specimen group.

Indeed, the SP microcapsules were prone to conglomerate much more than the SP microcapsules, particularly at the 1500 rpm level, which potentially resulted in a nonuniform dispersion of microcapsules within the cementitious matrix. Without adequate dispersion, not

enough microcapsules would rupture to release the required healing agent to seal the cracks. This can be attributed to the fact that the SP capsules had a hydrophobic coating that was deposited by the Span 60 emulsifier on the capsule surface. Given that larger agitation rates decrease the microcapsule size and therefore increase the specific surface area, the capsules would be more prone to agglomeration due to the hydrophobic attraction between the particles.

Crack Width Limitation

To visualize crack width limitation with respect to the microcapsule type, size, and concentration, the largest cracks that were 100% sealed were recorded over time. Figure 6.5 shows the maximum crack width sealed over time for the SP and OG specimen groups, respectively. The range of crack widths fully healed was significantly larger for several microcapsule-containing samples than the control groups. For the SP group, the samples with a 0.50% concentration had the largest crack widths healed, where the SP 800, 0.50% case peaked at 178 μm while the SP 1500, 0.50% case peaked at 176 μm. The remaining SP samples sealed cracks that were within the same order of range as the control specimens.

The OG group exhibited a much sharper contrast between the control groups and the microcapsule-containing specimens with respect to their maximum crack widths sealed. In addition, the largest crack widths fully sealed were mostly seen at Day 21. Sample OG 1500, 0.50% exhibited the highest healing potential by sealing cracks up to 290 μm long, and outperformed the other OG specimens and control samples by a substantial margin. The remaining OG specimens were found to be within the same range with respect to the maximum crack widths healed over time.

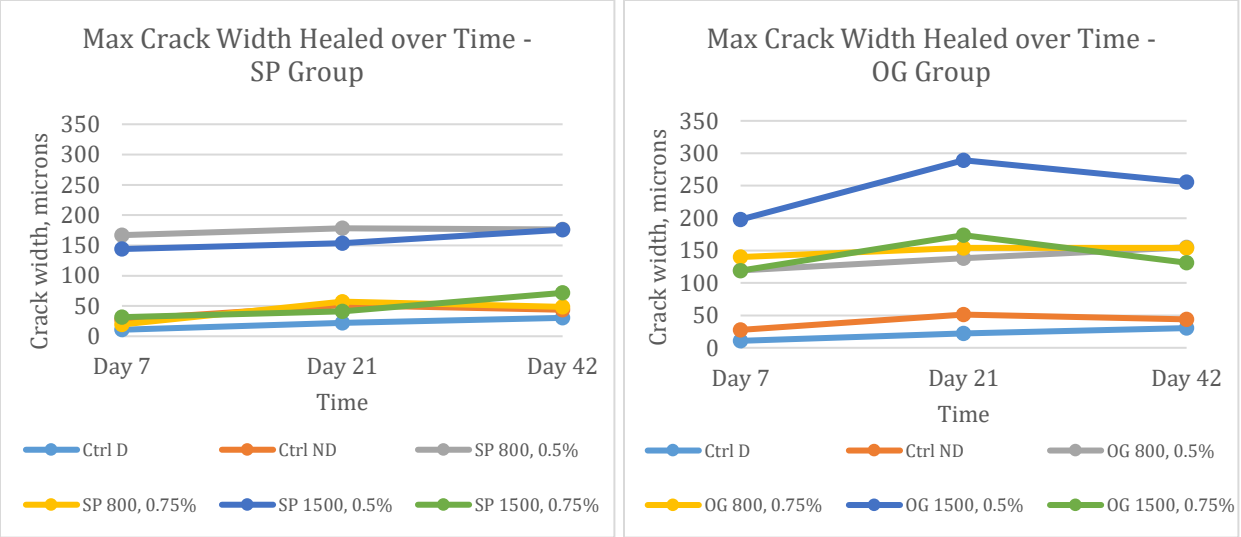

Figure 6.5. Maximum crack width healed over time for the (a) SP group; and (b) OG group.

The decrease in maximum crack width healed at day 42 could be attributed to the presence of more calcium hydroxide crystals deposited the crack surface at day 21. Since calcium hydroxide is soluble, some of the healing product could have leached and therefore affected areas that had fully sealed cracks. The extent of the calcium hydroxide leaching has been observed to be substantially low, however, particularly since the healing efficiencies did increase for all microcapsule-containing specimens over time.

6.5.3 Healing Product Characterization

SEM/EDS

The backscattered electron (BSE) images of the healing products formed at the crack surfaces are shown in Figure 6.6. The morphology of the clear majority of healing products was crystalline in nature, resembling calcite. In addition, there were clear differences between the microcapsule containing specimens and the control specimens with respect to the quantity of healing products observed.

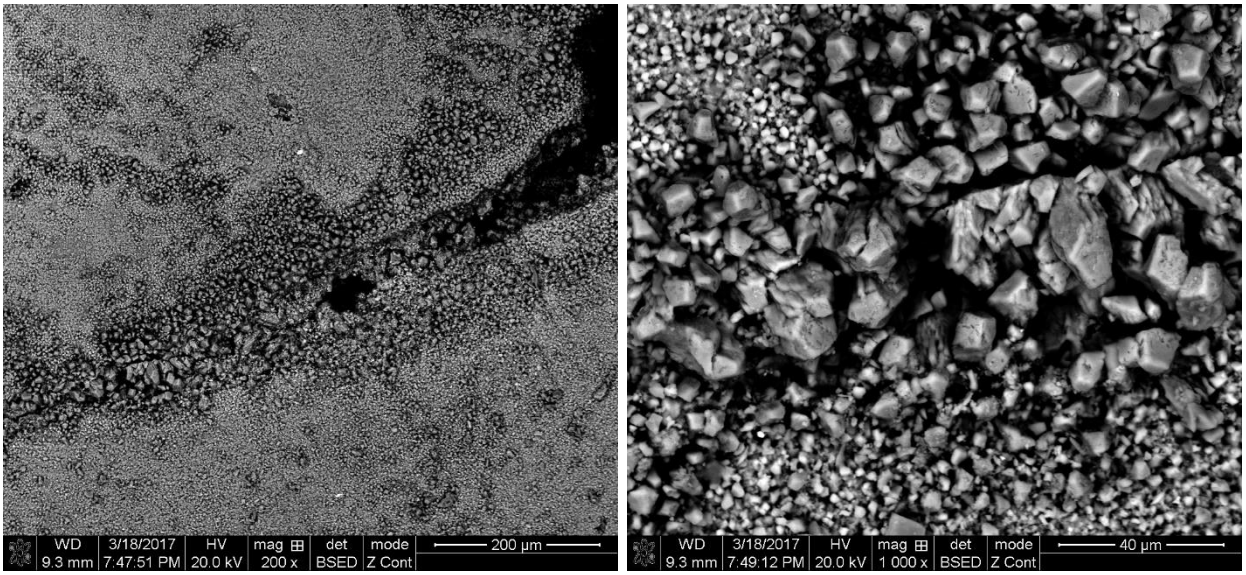

(a)

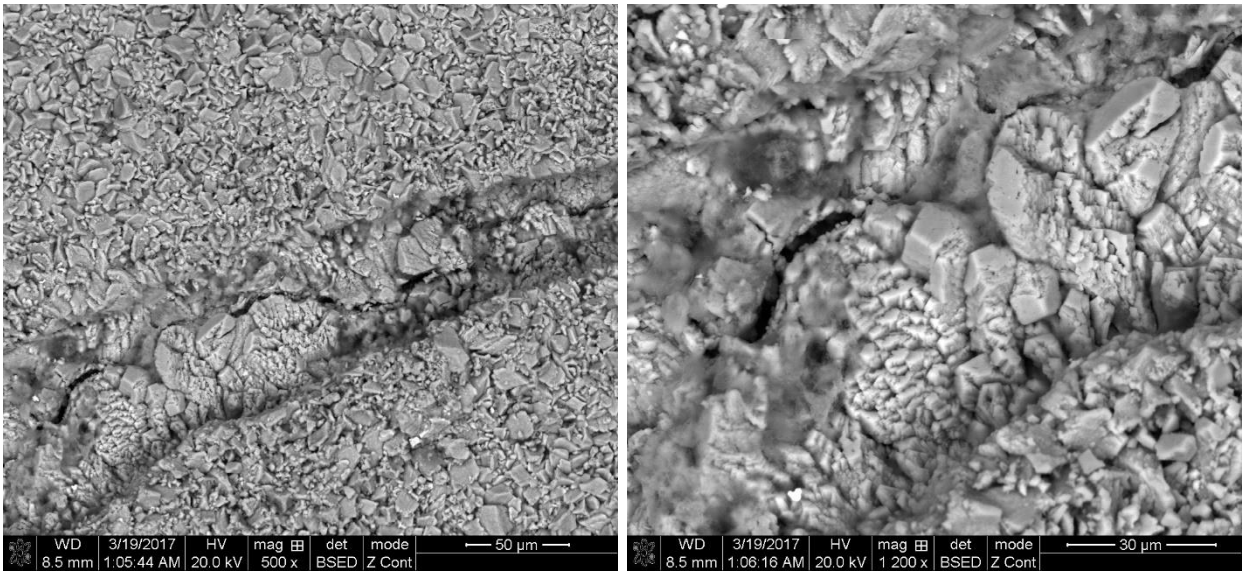

(b)

Figure 6.6. BSE images of the crack surfaces and the corresponding healing products for specimens: (a) SP 800, 0.5%; (b) OG 800, 0.5% *(Continued)*

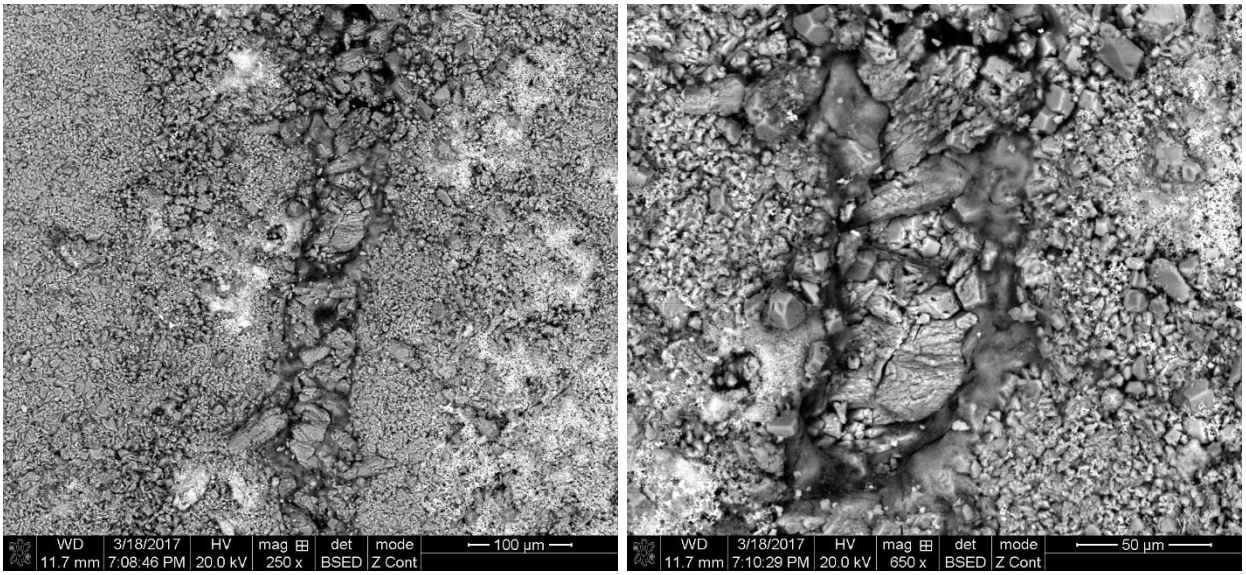

(c)

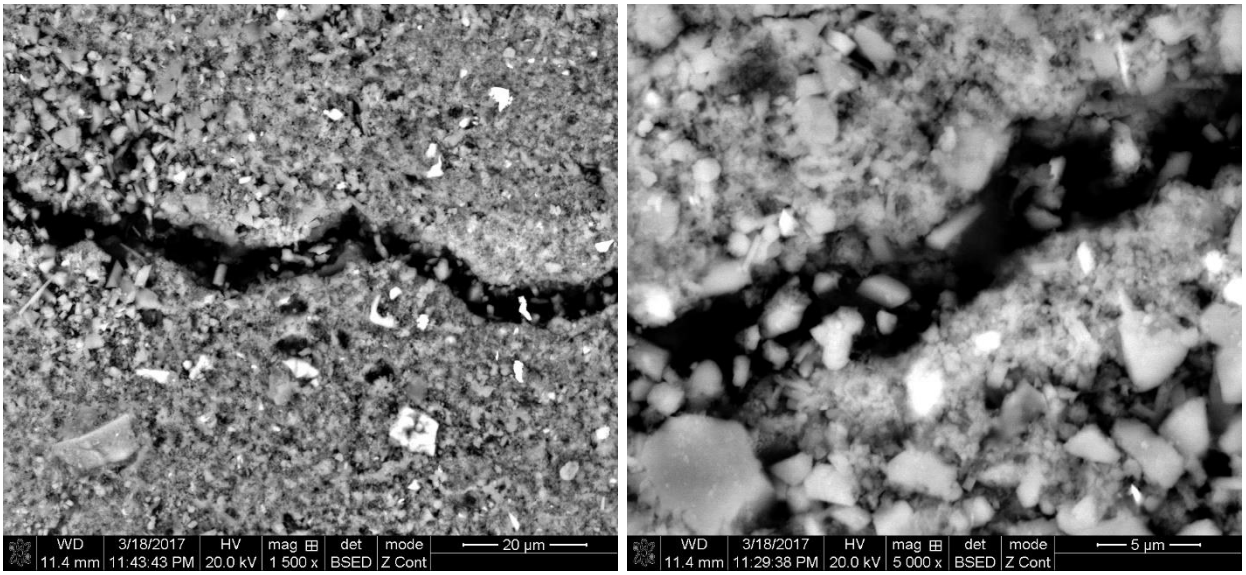

(d)

Figure 6.6. *(Continued)* BSE images of the crack surfaces and the corresponding healing products for specimens: (c) OG 1500, 0.5%; and (d) Ctrl ND.

EDS spectrums were collected at multiple spots on the crack surfaces where healing products were formed to characterize their chemical composition. At least 45 data points were collected on each sample, and the results were illustrated on an atomic ratio plot where the Al/Ca

and Si/Ca ratios were explored as shown in Figure 6.7. From both atomic ratio plots it can be observed that a clear majority of healing products are calcium-rich crystals since the data points are located near the graph's origin. This means that most of these crystals could be either calcium carbonate or calcium hydroxide. However, given that virtually all EDS data points showed significant carbon peaks, it can be inferred that most of these crystals are made of calcite crystals. However, a more substantial amount of data points was found between the CSH region and the calcium-rich crystal region for both OG and SP specimen groups, and this can be attributed to the skirt electrons that generate X-rays at points hundreds of microns away from the targeted location. Hence, in such cases the spot analysis included contributions from both CSH and calcium-rich crystals, similar to the findings reported by Arce et al. (2016).

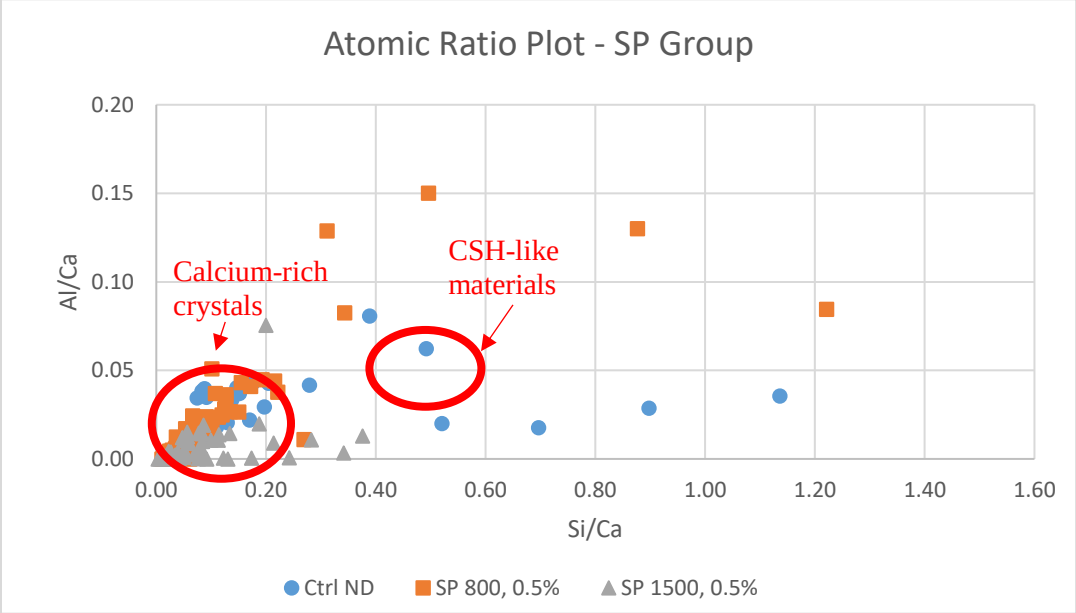

(a)

Figure 6.7. Atomic ratio plots of healing products observed at crack surfaces for (a) SP specimens *(Continued)*

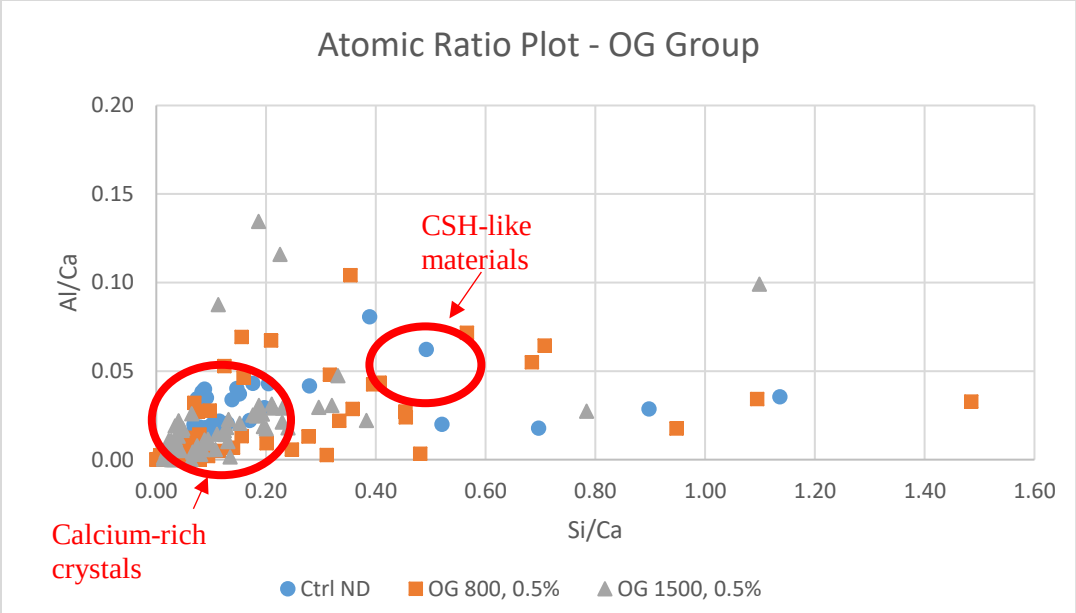

(b)

Figure 6.7. *(Continued)* Atomic ratio plots of healing products observed at crack surfaces for (b) OG specimens.

There were considerable amounts of data points located outside the CSH and calcium-rich crystal regions that can be attributed to either the silica from the sand particles (where high Si/Ca ratios were observed) or other healing products containing high alumina phases (where high Al/Ca ratios were seen) corresponding to the further hydration of exposed unhydrated cement particles in the crack surfaces.

6.6 Conclusion

Self-healing concrete through microencapsulated calcium nitrate tetrahydrate was tested for its crack-sealing efficiency in steel fiber reinforced concrete beams. The independent variables in this study were the microcapsule size, concentration (by weight of cement), and capsule shell

properties. The production parameters for the microcapsule preparation were adjusted to control the shell properties and mean particle diameter accordingly.

An atomic ratio plot of Si/Ca and Al/Ca indicated that the healing products were mostly composed of calcium-rich crystals such as calcium carbonate and calcium hydroxide. However, given that most of the EDS spectrums showed strong peaks of carbon, it can be inferred that most of these calcium-rich crystals are indeed composed of calcium carbonate. In contrast, small amounts of data points were found in the CSH-like region which thereby indicates that small amounts of calcium silicate hydrate were formed in the crack surfaces.

After monitoring the self-healing properties periodically, it was observed that all microcapsule-containing specimens had significantly higher healing efficiencies than both control groups after 21 and 42 days of healing. As the crack sizes increased, the microcapsule-containing specimens maintained a relatively high healing efficiency while the control groups resulted in progressively lower self-healing performance. Nevertheless, specimen OG 1500, 0.50% successfully sealed cracks up to 290 microns wide after a 21-day curing period.

The box and whisker plots for the three crack size categories showed high variability within the self-healing efficiency for each microcapsule-containing specimen. This was attributed to the wide range of crack sizes measured, and the sporadic healing that was observed throughout the crack path. Furthermore, the sporadic healing indicates that not enough embedded microcapsules were near the cracks, particularly for the SP specimen group. In general, the SP microcapsules were more prone to agglomeration and therefore were more difficult to disperse uniformly within the cementitious matrix. This was due to the Span 60 emulsifier in the SP group’s microcapsules which seemed to deposit a hydrophobic coating on the microcapsule

surface that promoted more agglomeration due to the hydrophobic attraction between the particles.

Based on the results presented in this study, the authors recommend further research to ensure a uniform dispersion of microcapsules within the cement matrix. Furthermore, a long-term study on self-healing would be beneficial to determine number of curing days required to achieve the full self-healing potential.

6.7 References

Arce, G. A., Hassan, M. M., Mohammad, L. N., and Rupnow, T. (2016). "Characterization of Self-Healing Processes Induced by Calcium Nitrate Microcapsules in Cement Mortar." *Journal of Materials in Civil Engineering*, 4016189.

ARTBA. (2017). "2017 Bridge Report." *American Road and Transportation Builders Association*, <http://www.artba.org/deficient-bridge-report-home/> (Feb. 3, 2017).

Brown, E. N., Kessler, M. R., Sottos, N. R., and White, S. R. (2003). "In situ poly(urea-formaldehyde) microencapsulation of dicyclopentadiene." *Journal of microencapsulation*, 20(6), 719–30.

Dietrich, K. (1989). "Amino resin microcapsules. II. Preparation and Morphology." *Acta Polymerica*, 40(4), 243–251.

Dry, C. M. (1994). "Smart multiphase composite materials that repair themselves by a release of liquids that become solids." 62–70.

Dry, C. M. (2001). "Design of self-growing, self-sensing, and self-repairing materials for engineering applications." *Proc. SPIE*.

Edvardsen, C. (1999). "Water Permeability and Autogenous Healing of Cracks in Concrete." *Materials Journal*, 96(4).

EPA. (2010). *Available and Emerging Technologies for Reducing Greenhouse Gas Emissions from the Portland Cement Industry*.

FHWA. (2015). *2015 Status of the Nation's Highways, Bridges, and Transit: Conditions & Performance*.

Gilford, J., Hassan, M., Rupnow, T., Barbato, M., Okeil, A., and Asadi, S. (2013). "Dicyclopentadiene and Sodium Silicate Microencapsulation for Self-Healing of Concrete." *Journal of Materials in Civil Engineering*, American Society of Civil Engineers, 26(5), 886–896.

Hanle, L. (2006). "Understanding CO2 emissions." *World Cement*, 37(4), 69–72.

Hassan, M. M., and Milla, J. (2016). "Microencapsulation of Calcium Nitrate for Concrete Applications." *95th Transportation Research Board Annual Meeting*, Washington D.C.

Hearn, N. (1998). "Self-sealing, autogenous healing and continued hydration: What is the difference?" *Materials and Structures*, 31(8), 563–567.

Huang, H., Ye, G., Qian, C., and Schlangen, E. (2016). "Self-healing in cementitious materials : Materials , methods and service conditions." *JMADE*, Elsevier Ltd, 92, 499–511.

Kanellopoulos, A., and Giannaros, P. (2016). “The effect of varying volume fraction of microcapsules on fresh , mechanical and self-healing properties of mortars.” *Construction and Building Materials*, The Authors, 122, 577–593.

Karagöl, F., Demirboğa, R., Kaygusuz, M. A., Yadollahi, M. M., and Polat, R. (2013). “The influence of calcium nitrate as antifreeze admixture on the compressive strength of concrete exposed to low temperatures.” *Cold Regions Science and Technology*, 89, 30–35.

Li, V. C., and Herbert, E. (2012). “Robust Self-Healing Concrete for Sustainable Infrastructure.” *Journal of Advanced Concrete Technology*, 10(6), 207–218.

Lv, L., Yang, Z., Chen, G., Zhu, G., Han, N., Schlangen, E., and Xing, F. (2016). “Synthesis and characterization of a new polymeric microcapsule and feasibility investigation in self-healing cementitious materials.” 105, 487–495.

Mehta, P. K., and Monteiro, P. J. M. (2006). *Concrete: microstructure, properties, and materials*. *Concrete*.

Milla, J., Hassan, M. M., and Rupnow, T. (2017). “Enhancing the Feasibility of Self-Healing Concrete with Microencapsulated Calcium Nitrate.” *Journal of Materials in Civil Engineering*, In Press.

Milla, J., Hassan, M. M., Rupnow, T., Al-Ansari, M., and Arce, G. (2016). “Effect of Self-Healing Calcium Nitrate Microcapsules on Concrete Properties.” *Transportation Research Record: Journal of the Transportation Research Board*, Transportation Research Board, 2577, 69–77.

Mostavi, E., Asadi, S., Asce, M., Hassan, M. M., Asce, M., and Alansari, M. (2015). “Evaluation of Self-Healing Mechanisms in Concrete with Double-Walled Sodium Silicate Microcapsules.” 27(12), 1–8.

NRC. (2013). “Critical concrete infrastructure: Extending the life of Canada’s bridge network.” *NRC (National Research Council of Canada)*, 18(1).

Pelletier, M. M., Brown, R., Shukla, A., and Bose, A. (2010). “Self-healing concrete with a microencapsulated healing agent.” *University of Rhode Island, Kingston,USA*, (C).

Ramachandran, V. S. (1996). *Concrete Admixtures Handbook*. William Andrew Publishing, Park Ridge, NJ.

Reinhardt, H. W., and Jooss, M. (2003). “Permeability and self-healing of cracked concrete as a function of temperature and crack width.” *Cement and Concrete Research*, 33(7), 981–985.

Roig-Flores, M., Moscato, S., Serna, P., and Ferrara, L. (2015). “Self-healing capability of concrete with crystalline admixtures in different environments.” *Construction and Building Materials*, Elsevier Ltd, 86, 1–11.

Van Tittelboom, K., and De Belie, N. (2013). *Self-healing in cementitious materials-a review*. *Materials*.

Wang, J. Y., Soens, H., Verstraete, W., and De Belie, N. (2014). "Self-healing concrete by use of microencapsulated bacterial spores." *Cement and Concrete Research*, Elsevier Ltd, 56, 139–152.

Wiktor, V., and Jonkers, H. M. (2011). "Quantification of crack-healing in novel bacteria-based self-healing concrete." *Cement and Concrete Composites*, Elsevier Ltd, 33(7), 763–770.

Wu, M., Johannesson, B., and Geiker, M. (2012a). "A review : Self-healing in cementitious materials and engineered cementitious composite as a self-healing material." *Construction and Building Materials*, Elsevier Ltd, 28(1), 571–583.

Wu, M., Johannesson, B., and Geiker, M. (2012b). "A review: Self-healing in cementitious materials and engineered cementitious composite as a self-healing material." *Construction and Building Materials*, Elsevier Ltd, 28(1), 571–583.

Yang, Y., Lepech, M. D., Yang, E. H., and Li, V. C. (2009). "Autogenous healing of engineered cementitious composites under wet-dry cycles." *Cement and Concrete Research*, Elsevier Ltd, 39(5), 382–390.

Yang, Z., Hollar, J., He, X., and Shi, X. (2011). "A self-healing cementitious composite using oil core/silica gel shell microcapsules." *Cement and Concrete Composites*, Elsevier Ltd, 33(4), 506–512.

CHAPTER 7

SUMMARY AND CONCLUSIONS

Self-healing concrete through microencapsulated calcium nitrate is a promising technology that could potentially address the infrastructure deterioration problem by adding durability and reducing the costly maintenance and repairs needed for concrete structures. Before this technology is to be applied on concrete infrastructure, there are several questions that needed to be answered, such as the identification of the microcapsule properties that are successfully carry the healing agent, and the effect the microcapsule size, concentration (by weight of cement), and morphology has on the intrinsic concrete material properties and self-healing potential.

To address these questions, the objectives of this study were to: (a) Develop a microencapsulation procedure for calcium nitrate as the healing agent; (b) Measure the short-term healing efficiency of the developed microcapsules in concrete; (c) Measure the long-term healing efficiency of such microcapsules in concrete.

7.1 Development of the Microencapsulation Procedure

The first part of the study was dedicated to develop a synthesis procedure for the production of urea-formaldehyde microencapsulation containing calcium nitrate and to characterize microcapsule properties such as diameter, shell thickness, and morphology of the prepared microcapsules. The production parameters investigated included the agitation rate, temperature, heating duration, and concentration of sulfonic acid for synthesis. Microencapsulation of calcium nitrate was selected given its low cost and setting accelerating effect on unhydrated cement. An economic and simple microencapsulation procedure was sought, where the production

parameters (i.e. agitation rate, temperature, heating time, sulfonic acid amount) were varied to evaluate the effects on microcapsules' morphology, size, and shell thickness.

Results indicated that the agitation rate and the temperature had a linear correlation on the microcapsule diameter and shell thickness, respectively. A higher agitation rate resulted in a smaller microcapsule diameter, while a higher temperature resulted in a thinner shell thickness from the samples observed. The morphology of all the microcapsules synthesized was virtually the same throughout the experimental matrix, which was composed of a smooth exterior surface and a rough interior surface. In addition, a broad particle size distribution was observed for all microcapsules produced. This was attributed to the type of surfactant used in the process.

7.1.1 Revisions to Encapsulation Procedure

After the microcapsules were admixed in concrete, the mechanical properties of concrete were significantly affected, where a higher concentration of capsules contributed to weaker concrete specimens. Thus, the authors investigated the factors that may have contributed to the observed strength deficiencies in concrete. One of the roots of the problems was that the microcapsules used had traces of sulfonic acid on the microcapsule surface, which acidified the concrete's mixing water. Indeed, acidic environments are detrimental to the mechanical properties of concrete.

Therefore, it was recommended that a de-ionized (DI) water bath is applied on the newly formed capsules to neutralize the traces of sulfonic acid on the microcapsule surface. The microcapsules can then be subsequently recovered with a coarse-fritted vacuum filter. Another recommendation is minimizing the sulfonic acid catalyst used, while adding another lipophilic surfactant such as Span 60 to stabilize the emulsion. In a similar fashion, the newly formed microcapsules should also be rinsed with DI water and subsequently retrieved through vacuum

filtration in this procedure. When comparing directly to the previous encapsulation procedure, the addition of a Span 60 surfactant did influence the mean microcapsule diameter.

The new encapsulation procedure with Span 60 showed a trend where lower agitation rates during synthesis produced larger microcapsules. In addition, those microcapsules synthesized at lower agitations were found to be less prone to agglomerate at the macro-level. This was due to the Span 60 emulsifier as it provided a hydrophobic coating on the microcapsule surface, which resulted in a greater attraction between the hydrophobic particles that was intensified with a larger specific surface area. Thus, the authors recommend investigating dispersing agents that will adequately break the agglomerations of microcapsules, without affecting the intrinsic material properties of both the microcapsules and the host concrete matrix.

7.2 Measuring the Short-Term Healing Efficiency

Self-healing concrete was investigated through microencapsulated calcium nitrate. The experimental matrix investigated the effect of four levels of microcapsule concentrations added in concrete (0.25%, 0.50%, 1.00%, and 2.00% by weight of cement), and three different mean microcapsule diameters (controlled by three different agitation rates – 450 rpm, 800 rpm, and 1500 rpm). The compressive strength of concrete admixed with microcapsules was tested against control specimens of the same mix design without microcapsules. Surface resistivity tests were conducted to quantify the surface permeability of the concrete specimens with and without microcapsules. The self-healing potential was measured with the modulus of elasticity test (ASTM C 469) by taking measurements before and after damage after 14 days. All specimens were incubated under water immersion after damaging at 80% of its ultimate load.

The concentration of microcapsules added, and the size of the microcapsules had a direct impact on the compressive strength of concrete. As the concentration of the microcapsules

increased, the strength of the concrete decreased. This was attributed to the increases in air content observed in concrete that were caused by the presence of microcapsules. The microcapsule size had also an effect on concrete strength. With larger microcapsules, the air content increased in the cement matrix. The surface resistivity of the virgin samples was virtually the same for the control and microcapsule-containing samples (moderate penetrability), except for the control samples and those admixed with 0.25% of microcapsules, which had a high surface penetrability. Nevertheless, the latter samples were the strongest with respect to compressive strength after damage.

With respect to the modulus of elasticity recovery, the samples containing microcapsules exhibited a higher modulus increase when compared to the 80% modulus test values. The optimal concentration of microcapsules was dependent on the sizes of the microcapsules. In general, a microcapsule concentration of 0.50% to 1.00% yielded the best results. Overall, for the short-term investigation it was found that while the microcapsules caused a decrease in concrete compressive strength, they enhanced the self-healing capability of the produced concrete.

7.3 Measuring the Long-Term Healing Efficiency

Based on the results from the short-term healing efficiency, the microcapsules proved to be significantly detrimental to the intrinsic concrete properties as the air content in the cement paste was substantially increased. Hence, factors contributing to the concrete strength deficiencies were addressed and corrected with modifications to the mix design and encapsulation procedures to evaluate the long-term healing period with respect to the mechanical properties and crack-sealing of concrete with embedded microcapsules.

The influence of the mean microcapsule diameter and microcapsule concentration parameters were studied with respect to the self-healing potential and their impact on the intrinsic concrete

properties. The microcapsule diameter was controlled by varying the agitation rate in three levels during synthesis (450 rpm, 800 rpm, and 1500 rpm), and the microcapsule concentration was varied in three levels as well (0.25%, 0.50%, and 1.00% by weight of cement). Two control specimens were used, where the control mix without a defoaming agent is referenced as 'Ctrl ND', while the control mix with a defoaming agent is noted as 'Ctrl D'.

The results showed that both the introduction of the newly developed microcapsules and a defoaming agent in the mix design were key in minimizing the air content of microcapsule-containing specimens. This resulted in strong mechanical properties comparable to the control group that had no defoaming agent admixed. The lower microcapsule concentrations of 0.25% and 0.50% yielded higher strengths in compression. In contrast, microcapsule dosage of 1.00% yielded the weakest samples for all cases. Moreover, two of the three weakest samples in compression were from the microcapsules prepared at 1500 rpm. This may be attributed to the fact that the 1500 rpm capsules were more difficult to disperse during mixing.

The compressive strength results after healing showed that virtually all microcapsule-containing specimens resulted in a higher percentage strength gain than both controls, relative to their initial strength, where the 450 rpm group had the highest increases from the experimental matrix. Ctrl D exhibited the lowest increase in strength, while Ctrl ND had a more significant increase, albeit smaller than the microcapsule-containing specimens (except for case 1500 rpm, 0.50%).

The differences in the pristine modulus of elasticity values between the control groups and the microcapsule containing specimens was minimal. In addition, most microcapsule-containing specimens were less affected by the damage cycles than both control specimen groups. After 21 days of healing, the modulus of elasticity values showed a significant recovery from the

damaged state for all samples. However, the microcapsule-containing specimens from the 450 rpm consistently exhibited a larger net modulus recovery than both control specimens. At the end of the healing period, the largest net modulus recovery was observed for sample 1500 rpm, 0.25%, followed by all three 450 rpm sample groups – 450 rpm 0.25%, 450 rpm 0.50%, and 450 rpm 1.00%.

7.3.1 Characterization of Self-Healing Processes

Self-healing concrete through microencapsulated calcium nitrate tetrahydrate was evaluated for its crack-sealing efficiency in steel fiber reinforced concrete beams. The independent variables in this study were the microcapsule size, concentration (by weight of cement), and capsule shell properties. The production parameters for the microcapsule preparation were adjusted to control the shell properties (influenced by the emulsifier selection during synthesis) and the mean microcapsule diameter (by varying the agitation rates during synthesis at 800 rpm and 1500 rpm, respectively). The influence of the microcapsule concentration on healing was investigated at two different levels: 0.50% and 0.75% by weight of cement, respectively. Two control specimens were used, where the control mix without a defoaming agent is referenced as ‘Ctrl ND’, while the control mix with a defoaming agent is noted as ‘Ctrl D’. For reference, the microcapsules produced with a Span 60 emulsifier are denoted as ‘SP’, and the microcapsules produced without a Span 60 emulsifier are referred as ‘OG’.

The crack measurements were sorted into three different size categories, with respect to the initial crack widths measured (before healing). The healing efficiencies were calculated as a percentage change relative to the initial crack width measurements, at days 7, 21, and 42, respectively. The distributions of the calculated healing efficiencies in each crack size category showed high variability for each microcapsule-containing specimen. This was attributed to the

wide range of crack sizes measured (before healing), and the sporadic healing that was observed throughout the crack path over time. The sporadic healing indicates that not enough embedded microcapsules were near the cracks, particularly for the SP specimen group. In general, the SP microcapsules were more prone to agglomeration and therefore were more difficult to disperse uniformly within the cementitious matrix. This was due to the Span 60 emulsifier in the SP group's microcapsules that seemed to deposit a hydrophobic coating on the microcapsule surface that promoted more agglomeration due to the hydrophobic attraction between the particles.

Despite the relatively high variabilities in the calculated self-healing efficiencies, after monitoring the self-healing properties periodically, a statistical analysis determined that all microcapsule-containing specimens had significantly higher healing efficiencies than both control groups after 21 and 42 days of healing. For the group of larger initial crack sizes, the microcapsule-containing specimens maintained a relatively high healing efficiency while the control groups resulted in progressively lower self-healing performance. Nevertheless, specimen OG 1500, 0.50% successfully sealed cracks up to 290 microns wide after a 21-day curing period.

At the end of the healing period, cracked concrete samples were viewed in an environmental scanning electron microscope (ESEM) under the backscattered electron (BSE) imaging mode to collect Energy Dispersive Spectroscopy (EDS) spectrums of potential healing products. The point analysis mode was used at locations where healing products had formed for characterization to plot the atomic ratios of Si/Ca and Al/Ca. The results showed that a clear majority of the healing products were calcium-rich crystals. The presence of carbon on most of these spectrums corroborated that most of these healing products were composed of calcium carbonate crystals. In contrast, minimal points were found on the calcium silicate hydrate regions within the atomic ratio plots.

7.4 Future Work

The results of this project lead to future research opportunities, including:

- Identification of a dispersing agent that will adequately spread the microcapsules uniformly throughout the cementitious matrix, without compromising the intrinsic material properties of concrete
- Identification of an admixture or mix design that adequately controls the increases in air content associated with the introduction of microcapsules in a manner that is suitable for cold environments.
- The influence of the water-cement ratio on the self-healing performance.
- The overall environmental impact from cradle-to-grave of self-healing concrete by microencapsulated calcium nitrate.
- The level of healing observed in a different curing regime.
- A life-cycle cost assessment of using this technology.
- The use of a different healing agent to compare efficiencies.
- The use of nanocapsules and their effects on the intrinsic concrete properties and self-healing potential.
- The potential of calcium nitrate microcapsules with respect to corrosion inhibition.

APPENDIX A
COPYRIGHT

Dear Jose Milla:

The Transportation Research Board grants permission to use your paper, "Microencapsulation of Calcium Nitrate for Concrete Applications," coauthored with M. M. Hassan, T. Rupnow, M. Al-Ansari, and W. H. Daly in your dissertation, as identified in your request of April 6, 2017, subject to the following conditions:

1. Please cite the publication in *Transportation Research Record: Journal of the Transportation Research Board*, No. 2577, pp. 8–16, 2016.
   DOI: http://dx.doi.org/10.3141/2577-02.

2. Please acknowledge that the material from your paper is reproduced with permission of the Transportation Research Board.

3. None of this material may be presented to imply endorsement by TRB of a product, method, practice, or policy.

The Transportation Research Board grants permission to use your paper, "Effect of Self-Healing Calcium Nitrate Microcapsule on Concrete Properties," coauthored with M. M. Hassan, T. Rupnow, M. Al-Ansari, and G. Arce in your dissertation, as identified in your request of April 6, 2017, subject to the following conditions:

1. Please cite the publication in *Transportation Research Record: Journal of the Transportation Research Board*, No. 2577, pp. 69–77, 2016.
   DOI: http://dx.doi.org/10.3141/2577-09.

2. Please acknowledge that the material from your paper is reproduced with permission of the Transportation Research Board.

3. None of this material may be presented to imply endorsement by TRB of a product, method, practice, or policy.

Every success with your dissertation. Please let me know if you have any questions.

Sincerely,

Javy Awan
Director of Publications
Transportation Research Board

VITA

Jose Eduardo Milla, a native of San Salvador, El Salvador, received his bachelor's degree at the University of New Orleans in 2013. Thereafter, he worked as a summer intern for Ben C. Gerwick, Inc. and joined Louisiana State University in August 2013 to pursue a Master of Science in Engineering Science degree, which eventually led to the pursuit of a Doctorate of Philosophy degree in Engineering Science. His research interests include infrastructure condition assessments, innovative construction materials, and sustainability in engineering.